INVESTIGATIONS OF SINGLET OXYGEN-MEDIATED AMINO ACID, PEPTIDE AND PROTEIN OXIDATION

by

ADAM WRIGHT

A thesis submitted in fulfilment of the requirements
for the award of the degree of
Doctor of Philosophy,
University of Sydney, 2002.

DECLARATION

The work contained in this thesis is original research conducted by the author at the Heart Research Institute, Sydney, except for NMR spectroscopy, which was performed in collaboration with Dr W.A. Bubb (Department of Biochemistry, University of Sydney). It has not been submitted to any other institution for a higher degree.

Adam Wright, BMedChem (Hons)

TABLE OF CONTENTS

ACKNOWLEDGEMENTS

This thesis would not have been possible without the excellent supervision of Dr. Michael Davies. Mike's encouragement, enthusiasm and patience really kept me going. Thanks Mike.

Thanks also to my associate supervisors Dr Clare Hawkins and Prof Roger Dean. Thanks Clare for all your practical guidance and advice and thanks to Roger for interesting discussions and suggestions.

I would also like to thank Dr Bill Bubb for his collaboration with the NMR spectroscopy work and Dr Stuart Linton for assistance with the electrochemical array HPLC experiments.

Thanks also to A/Prof Roger Truscott for providing the lens protein samples.

To the members of the EPR group and all members of the HRI (especially the sports people among you) thanks for your support, friendship and making the HRI an enjoyable place to work.

I am also grateful to the University of Sydney for their provision of an Australian Postgraduate Award and the HRI for other financial support.

Finally a thank you to my family, especially Dave, Kerry and Sharon for their continued support and to Tori for her confidence in me and her patience, especially during the thesis writing period.

ABSTRACT

Singlet oxygen ($^1\Delta_g$ O_2, or $^1O_2$) is generated *in vivo* by a number of enzymatic systems as well as by UV or visible light in the presence of a suitable photosensitiser. Proteins are major targets for $^1O_2$ as a result of their high abundance and rapid rate of reaction. Under physiological conditions the reactions of $^1O_2$ with proteins are belived to be mediated via oxidation of five susceptible residues – His, Trp, Tyr, Met and Cys.

Exposure of Tyr to $^1O_2$, generated by photochemical or chemical methods, leads to the formation of Tyr-derived peroxides. Similar peroxides are generated on Tyr model compounds and Tyr-containing peptides and proteins. The yield of these species is enhanced in D_2O and decreased in the presence of azide consistent with a $^1O_2$-mediated process. These peroxides are relatively stable at 4 °C, and in the absence of reductants, however, their decay is enhanced at higher temperatures or in the presence of both one- and two-electron reducing species.

NMR and mass spectrometric analysis of reaction mixtures or peroxides separated by HPLC are consistent with the formation of an (undetected) endoperoxide, which rapidly converts to a hydroperoxide located at the ring C1 position. Rapid intramolecular cyclisation reactions occur with free Tyr to yield an indolic hydroperoxide. However, when the α-amino nitrogen is absent or blocked, the major peroxide present is the ring opened C1 hydroperoxide, which undergoes slow decay at low temperature to the corresponding alcohol. At higher temperatures or on exposure to UV light or metal ions the rate of decay is enhanced and radical species are formed. These radicals have been characterised by EPR with spin trapping.

The intermediates of $^1O_2$-mediated Tyr oxidation are able to oxidise other peptides and proteins and are also able to undergo intermolecular Michael additions with both nitrogen and sulfur nucleophiles. Reaction with Lys side-chain nitrogens may lead to the formation of protein cross-links. The reaction with sulfur nucleophiles has been harnessed to develop a specific marker for $^1O_2$-mediated protein oxidation.

Initial studies on the $^1O_2$-mediated oxidation of His show that peroxides are formed, which can be reduced to yield radicals in similar reactions to those observed with Tyr.

Intracellular production of $^1O_2$ also leads to a slight decrease in cell viability, however when the cells are incubated after $^1O_2$ production has ceased, cell death increases with time. Protein-derived peroxides are also produced by intracellular $^1O_2$, which can be reduced by metal ions to yield radicals that can be detected by EPR. The decay of these peroxides appears to correlate with the increased cell death noted.

These studies have characterised some of the possible products of $^1O_2$-mediated protein oxidation *in vivo*, and demonstrated that these products are potentially reactive species themselves. Further, the first specific marker for $^1O_2$-mediated protein oxidation and preliminary studies using this compound for investigating protein oxidation in the human lens is reported.

LIST OF ABBREVIATIONS

$^1O_2$	$^1\Delta_g$ excited state of molecular oxygen
8-oxodG	7,8-dihydro-8-oxo-2'-deoxyguanosine
AAPH	2,2'-azobis(amidinopropane)dihydrochloride
AHA	6-aminohexanoic acid
ANOVA	analysis of variance
AP-2	activator protein-2
ATP	adenosine triphosphate
BCA	bicinchoninic acid (4,4'-dicarboxy-2,2'-biquinoline, free acid)
BSA	bovine serum albumin
COSY	correlation spectroscopy
DBNBS	3,5-dibromo-4-nitrosobenzenesulfonic acid
DHA	dehydroascorbate
DMPO	5,5'-dimethyl-1-pyrroline-*N*-oxide
DNA	deoxyribonucleic acid
DNP	2,4-dinitrophenyl
DNPH	2,4-dinitrophenylhydrazine
DOPA	3,4-dihydroxyphenylalanine
EC	electrochemical detection
EDTA	ethylenediaminetetraacetic acid
ELISA	enzyme linked immunosorbent assay
EPR	electron paramagnetic resonance spectroscopy
ERK	extracellular signal-regulated kinase
ESI-MS	electrospray ionisation mass spectrometry
FAD(H_2)	flavin adenine dinucleotide
FOX	$FeSO_4$/xylenol orange assay for peroxides
GC/MS	gas chromatography/mass spectrometry
GRP	glucose regulated protein
HBSS	Hank's balanced salt solution
HMBC	heteronuclear multiple bond correlation
HNE	4-hydroxynonenal
HO•	hydroxyl radical

HO-1	haem oxygenase-1
HOBr	hypobromous acid
HOCl	hypochlorous acid
HOHICA	6-oxo-2,3,3a,6,7,7a-hexahydro-1H-indol-2-carboxylic acid
HPLC	high performance liquid chromatography
HPPA	3-(4-hydroxyphenyl)propionic acid
HSP	heat shock protein
HSQC	heteronuclear single quantum coherence
HUVEC	human umbilical vein endothelial cells
ICAM-1	intercellular adhesion molecule-1
JNK	c-Jun-N-terminal kinase
LDH	lactate dehydrogenase
LH	polyunsaturated fatty acid/lipid
LO•	lipid-derived alkoxyl radical
LOO•	lipid-derived peroxyl radical
LOOH	lipid-derived hydroperoxide
m/z	mass to charge ratio
MB	methylene blue
MDA	malondialdehyde
MIA	manual iodometric assay for peroxides
MNPAE	1',4'-endoperoxide of 3-(4'-methyl-1'-naphthyl)propionic acid
MPO	myeloperoxidase
mT	milli Tesla
NAD(H)	nicotinamide adenine dinucleotide
NADP(H)	nicotinamide adenine dinucleotide phosphate
NMR	nuclear magnetic resonance spectroscopy
NOESY	nuclear Overhauser enhancement spectroscopy
O_2^{-}•	superoxide radical anion
PBS	phosphate buffered saline
PDT	photodynamic therapy
PMN	polymorphonuclear leukocytes
PUFA	polyunsaturated fatty acids
R•	carbon-centred radical

RB	rose bengal
RNA	ribonucleic acid
RO•	alkoxyl radical
ROO•	peroxyl radical
ROS	reactive oxygen species
RT	retention time
SDS	sodium dodecyl sulfate
SOD	superoxide dismutase
TCA	trichloroacetic acid
TEMED	tetramethylethylenediamine
TFA	trifluoroacetic acid
TLC	thin layer chromatography
TOCSY	total correlation spectroscopy
UV	ultraviolet

LIST OF TABLES

LIST OF SCHEMES

LIST OF FIGURES

PUBLICATIONS ARISING FORM THIS THESIS

RESEARCH PAPERS

Wright, A., Hawkins, C.L. and Davies, M.J. (2000)
Singlet Oxygen-Mediated Protein Oxidation: Evidence for the Formation of Reactive Peroxides.
Redox Report; 5(2/3); 159-161.

Wright, A., Bubb, W.A., Hawkins, C.L. and Davies, M.J. (2002)
Singlet Oxygen-Mediated Protein Oxidation: Evidence for the Formation of Reactive Side-Chain Peroxides on Tyrosine Residues.
Photochemistry and Photobiology; Manuscript under review

Wright, A., Hawkins, C.L. and Davies, M.J. (2002)
$^1O_2$-Mediated Formation of Protein-Derived Peroxides in Viable Cells
Biochemical Journal; Submitted

CONFERENCE PRESENTATIONS

Wright, A., Hawkins, C.L., Bubb, W.A. and Davies, M.J.
Singlet Oxygen-Mediated Damage to Tyr and Tyr Containing Peptides and Proteins.
Redox processes in Chemistry, Biology and Medicine. Sydney, Australia, 2001.
Poster presentation. Awarded a poster prize for this presentation.

Wright, A., Hawkins, C.L., Bubb, W.A., Dean, R.T. and Davies, M.J.
Singlet Oxygen-Induced Damage to Amino Acids, Peptides and Proteins: Formation of Short-Lived Peroxides and Identification of Products.
10th Biennial Meeting of the Society for Free Radical Research International. Kyoto, Japan, 2000.
Oral presentation. Awarded Young Investigators Award (International) by the Society for Free Radical Research and a National Heart Foundation travel grant to attend this conference.

Wright A, Hawkins C.L., and Davies M.J.

Towards a specific marker for singlet oxygen protein oxidation.

Oxidative Pathways in Health and Disease, Sydney, Australia, 1999.

Poster presentation.

Davies M.J., Hawkins C.L. and Wright A.

Singlet Oxygen-Induced Protein Oxidation: Generation of Long-lived Reactive Peroxides and Free Radicals.

13th International Congress on Photobiology and 28th Annual Meeting of the American Society for Photobiology. San Francisco, USA, 2000.

Wright A, Hawkins C.L., and Davies M.J.

SFRR Europe Summer Meeting. Dresden, Germany, 1999.

CHAPTER 1 - INTRODUCTION

1.1 GENERAL INTRODUCTION

Oxygen is a very important element in biology. It is required for the synthesis of all major bio-molecules and is the final oxidant on the pathways of oxidative phosphorylation and energy transduction [1]. Perhaps fortunately, oxygen *per se* is not very reactive with common biological substrates. However, oxygen can become activated by a number of routes and be transformed to much more powerful oxidants. The species thus formed are often termed reactive oxygen species (ROS) [2]. This family includes radical species such as the hydroxyl radical (HO•), the superoxide radical anion (O_2^{-}•), as well as peroxyl (ROO•) and alkoxyl (RO•) radicals. Non-radical species such as hydrogen peroxide (H_2O_2), ozone (O_3), singlet oxygen ($^1O_2$) and hypochlorous acid (HOCl) are also included in this group [2].

Proteins fulfil the most diverse range of roles of any molecule in biology. They are involved in cellular and extracellular structural functions, they act as transcription factors, play a role in cellular signal transduction (on both the signal and receptor sides), and perform enzymatic functions. As they have such diverse and important roles, it is not surprising that proteins are by far the most abundant biological molecules.

Recently it has become obvious that the oxidative modification of proteins is an important event in normal metabolism and in various pathologies, and oxidised proteins have been identified in a number of diseased tissues [3]. Whether protein oxidation is a cause or consequence of disease is still a matter of debate. In order to study such phenomena, it has been necessary to identify attributes of an oxidised protein that are not present in the native forms. Generic effects of protein oxidation include protein fragmentation and aggregation. Specific chemical changes to the protein, with products that are easily detected, have also been identified. General biomarkers of oxidative stress are known and include the formation of carbonyl groups on bulk protein. More specific products of protein oxidation are also known, such as 3,4-dihydroxyphenylalanine (DOPA), 3-nitrotyrosine, 3-chlorotyrosine, 3,5-dichlorotyrosine, *N*-formylkynureneine and derivatives, and many others [4].

This thesis will concentrate on the oxidation of amino acids and proteins by molecular oxygen in the first excited singlet state ($^1\Delta_g$), often abbreviated as $^1O_2$. This oxidant is known to react with proteins at a high rate, although the mechanisms and products of such reactions are not fully elucidated. The experiments described within

this thesis aimed to investigate the $^1O_2$-mediated oxidation of amino acids, particularly Tyr, by identification of the products and intermediates of this reaction. Radical species derived from the metal ion reduction of intermediate peroxide species were also investigated. The reactions of intermediates formed during $^1O_2$-mediated Tyr oxidation, with proteins and their role in $^1O_2$-mediated protein cross-linking, have been studied.

Further experiments on peptides and proteins containing Tyr have lead to the isolation and identification of a novel biomarker specific for $^1O_2$-mediated Tyr oxidation. This new biomarker has been used to analyse biological samples for $^1O_2$-mediated protein oxidation. Evidence for the formation of protein-derived peroxidic species within cells, as a result of RB photo-oxidation, is presented. The effect of $^1O_2$ generation and the formation of $^1O_2$-derived protein peroxides on cell viability has also been investigated.

1.2 OXYGEN

1.2.1 HISTORY OF OXYGEN

The fact that air itself is not an elementary substance was not realised until the late 18th century. In 1775 Joseph Priestley, an English clergyman and natural philosopher, published results suggesting that atmospheric air was actually a mixture of substances [5]. Before this time it had been known that different types of air existed and these types of air had different properties. Priestley reported that on the 1st August 1774 he succeeded in extracting air from *mercurius calcinatus per se* (HgO) by heating [5]. He found that the gas produced allowed a candle to burn with a 'remarkably vigorous flame'. Priestley performed similar experiments with other materials, some of which produced analogous gases. After many months of experimenting with this gas, Priestley concluded that it was a new type of air and of higher quality than normal atmospheric air [5].

At about the same time, Antoine Lavoisier was conducting similar experiments as Priestley. During early 1775, Lavoisier also heated *mercurius calcinatus per se* and collected the gas produced. The results of his experiments with this gas were similar to those of Priestley [6]. Lavoisier concluded that this air was 'even more pure than the air in which we live' [6]. Lavoisier extended the work of Priestley and is generally believed to be the person responsible for the idea that

common air is a mixture of gases. In a paper dealing with this 'eminently respirable air' as an acidifying principle, the term *principe oxygine* (from the Greek, *oxus* meaning acid and *gennao* meaning I beget) was coined by Lavoisier. [6]

1.2.2 Importance of Oxygen

Since the early studies of Priestley, Laviosier and many others, oxygen has become the focus of much scientific endeavour. It is now known that oxygen is the element of atomic number 8 and is usually found it is diatomic state, O_2. The natural isotopes known are oxygen-16 (99.759 %) oxygen-17 (0.037 %) and oxygen-18 (0.204 %) [7]. Oxygen can form compounds with all elements except helium, neon, argon and (probably) krypton [8]. Oxygen is one of the most important elements playing key roles in the geology, chemistry, and biology of the natural world. Oxygen is also a very important element industrially [7].

Most biological systems are dependant on oxygen, as it is the ultimate oxidant on the energy transduction pathway, a process that liberates a large amount of free energy [1, 7, 8].

1.2.3 Reactivity of Oxygen

Oxygen is known to react with nearly all known elements [8]. These reactions mostly take place at elevated temperatures even though they have negative enthalpies of reaction under standard conditions. As an example, the enthalpy of formation of water (ΔH_f^o) is –486 kJ mol^{-1} indicating that this reaction is favoured thermodynamically and should proceed spontaneously. However if oxygen gas and hydrogen gas are mixed at 1 atm pressure no reaction will occur due to the high activation energy of this process [8]. The reaction will occur if energy is added in the form of a spark or flame, or if a catalyst such as platinum is added to the system. The energy barrier arises from the spin conservation law. This energy barrier is crucial to the understanding of oxygen-mediated processes and the requirement for oxygen activation.

Hund's law states that the ground state electron configuration of an atom corresponds to the orbital occupancy that gives the highest spin multiplicity [8]. The spin multiplicity M is equal to 2S + 1 where S is 0.5 for each unpaired electron in the molecule. Atomic oxygen (O: $1s^2 2s^2 2p^4$) has four electrons in the outer most 2p orbitals that can be arranged in three non-degenerate ways (Figure 1.1) [8].

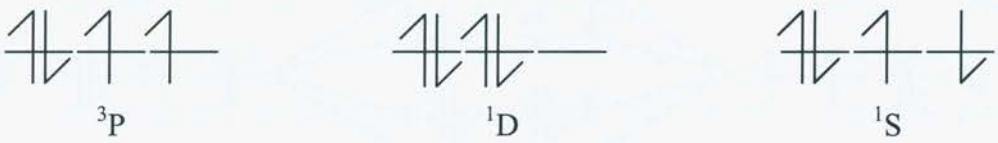

Figure 1.1; The three possible electron configurations in the partially filled 2p orbitals of atomic oxygen [8].

The use of Hund's rule shows that the first of these configurations is the ground state as it has spin multiplicity of 3 compared to 1 for the other two configurations. This first state is known as the triplet P state (^3P). The two remaining states are singlet (i.e. M=1). Hund's second law states that when multiplicity is equal, the configuration with the highest total orbital angular momentum will have the lower energy. Therefore, the ^1D state is the second state and the ^1S is the highest energy state of atomic oxygen [8].

The diatomic oxygen molecule can be analysed in a comparable fashion. Its sixteen electrons are arranged in the following configuration; $(\sigma_{1s})^2(\sigma_{1s}^*)^2(\sigma_{2s})^2(\sigma_{2s}^*)^2(\sigma_{2p})^2(\pi_{2p})^4(\pi_{2p}^*)^2$ [8]. As with atomic oxygen, the highest orbital- π_{2p}^* - is only half filled and has three possible arrangements of electrons (Figure 1.2). This configuration shows that there are again three non-degenerate ways of arranging these electrons, one triplet (ground state) and two singlet. These states, in order of increasing energy, are denoted $^3\Sigma_g^+$, $^1\Delta_g$ and $^1\Sigma_g^-$.

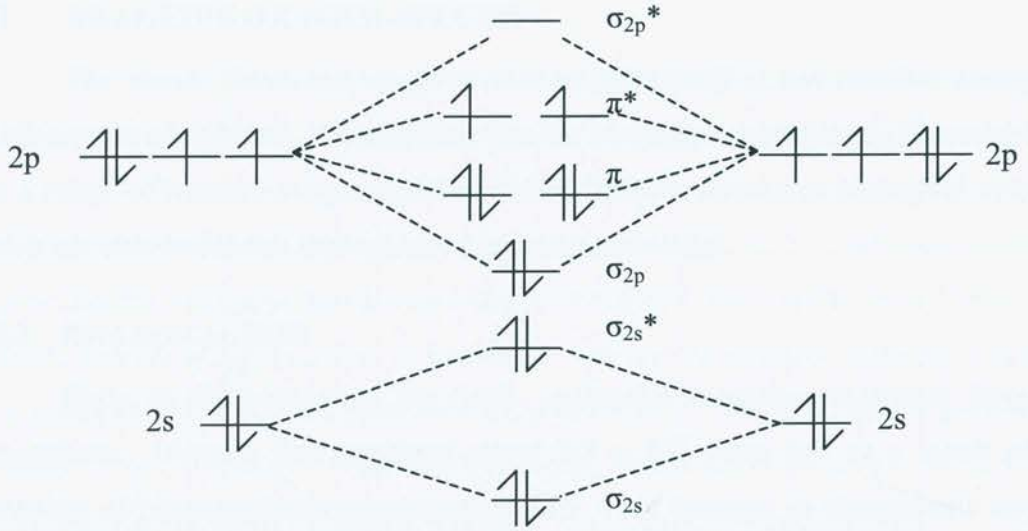

Figure 1.2; Molecular orbital diagram of the ground state of molecular oxygen [8].

The ground state of diatomic oxygen has two unpaired electrons in the outermost orbitals. A concerted reaction between a non-radical species and oxygen is unlikely to occur as most molecules have ground state singlet configurations (i.e. have no unpaired electrons) and such reactions would yield ground state singlets. Such reactions violate the principle of spin conservation, which states that the number of unpaired electrons must remain the same before and after each individual step of a reaction [8].

An alternative perspective is that for oxygen to oxidise a non-radical species it must accept two electrons. The Pauli exclusion principle states that no two electrons in an atom can have the same set of four quantum numbers. Therefore oxygen, when in the ground state, must accept electrons of opposite spin. This is unlikely to occur, as a pair of electrons in a molecule will not have two such electrons, again because it violates the Pauli principle [8].

From either of these explanations it is clear that ground state oxygen suffers a 'spin-restriction' and its reactions are slow even when thermodynamically favourable. To overcome the spin-restriction, oxygen can become activated by the addition of one or more electrons or by rearrangement of the outer most electrons so that the spin-restriction is lifted.

1.3 REACTIVE OXYGEN SPECIES

The above discussion suggests that oxygen itself is not reactive enough to oxidise most compounds. This is also true for biological compounds, however there are a range of reactive oxygen species (ROS) that are formed in biological systems, which are able to oxidise biologically important molecules.

1.3.2 BIOLOGICAL ROS

Early in the history of the Earth, molecular oxygen was absent from the atmosphere. Oxygen first appeared about 2.5 x 10^9 years ago as a result of the evolution of photosynthetic cyanobacteria [2]. This increase in atmospheric oxygen led to the formation of the stratospheric ozone layer. Molecular oxygen and ozone combined to filter out much of the solar UV radiation, which played a major part in allowing organisms to venture onto land, but oxygen itself must have put these initial organisms under much stress [2].

Present day anaerobic organisms have adapted to increased oxygen levels generally by restricting themselves to environments that are oxygen-free. Aerobic organisms have taken advantage of oxygen and now it is an indispensable part of life for animal, plant and most bacterial forms of life [2].

Mammalian mitochondria now use oxygen as the final oxidant on the pathways of energy transduction (Section 1.2.2). Mitochondria make over 80 % of the adenosine triphosphate (ATP, the energy 'currency' of the cell) required by mammalian cells and the lethal effect of inhibiting ATP production by agents such as cyanide, are well known and demonstrate its importance [2].

Oxygen does still have detrimental effects on aerobic organisms. This phenomenon, known as oxygen toxicity, can be demonstrated in most classes of aerobic organisms [2]. Originally, it was suggested that oxygen toxicity arose from the inhibition of enzymes by molecular oxygen, but this has since been shown to be of limited importance. Since 1954, the prevailing theory has been that most of the damaging effects of oxygen can be attributed to the formation of oxygen free radicals [9], which has been further refined to include other ROS [2].

Various ROS are formed *in vivo*, some of the most important being $O_2^{-}\bullet$, HO•, alkoxyl and peroxyl radicals and $^1O_2$ [2].

1.3.2a Superoxide Radical

$O_2^{-}\cdot$ can be formed by reduction of molecular oxygen. The extra electron is added into the π^* orbital thus reducing the bond order of the molecule from 2 to 1.5. $O_2^{-}\cdot$ can be formed by a number of chemical and biochemical processes. The reduction reaction normally requires a strong reductant such as a semiquinone or carbon dioxide radical anion (formate anion), or can be catalysed by metal ions. This formate radical anion reaction is frequently utilised in radiation chemistry studies. The radiolysis of water produces solvated electrons, H$\cdot$ and HO$\cdot$. In the presence of formate, $CO_2^{-}\cdot$ is formed during the radiolysis, which reduces oxygen to $O_2^{-}\cdot$. The solvated electrons and H$\cdot$ also react directly with oxygen to yield $O_2^{-}\cdot$ [10].

$O_2^{-}\cdot$ can also be produced photochemically. This process involves the photolysis of H_2O_2 yielding HO$\cdot$, which reacts with H_2O_2 to yield $O_2^{-}\cdot$. Photo-excited triplet flavin systems quenched with O_2 are another photochemical source of $O_2^{-}\cdot$ as well as $^1O_2$ [10].

$O_2^{-}\cdot$ salts, such as potassium superoxide, are slightly soluble in organic solvents. Solubility can be enhanced by the use of crown ethers, such as dicyclohexyl-18-crown-6. In very dry organic solutions this $O_2^{-}\cdot$ is stable and can be used to investigate the reaction of another compound added to the organic phase or mixed with an aqueous solution of a compound (e.g. in stopped flow experiments) [10].

Recently azo compounds, e.g. SOTS-1 have been developed which can be decomposed by heat or light to yield $O_2^{-}\cdot$ [11].

In experimental biological chemistry, a major route of $O_2^{-}\cdot$ production is by the use of xanthine oxidase. This enzyme catalyses the oxidation of both hypoxanthine and xanthine to uric acid, while reducing oxygen to $O_2^{-}\cdot$. Other substrates may also be used including acetaldehyde (ethanal) [10].

$O_2^{-}\cdot$ production is nearly ubiquitous in aerobic organisms as a result of the use of oxygen as the terminal electron acceptor in mitochondrial electron transport chains. These processes are very efficient at reducing O_2 to H_2O by a four-electron mechanism, although there does appear to be a continual leakage of electrons to oxygen giving rise to a constant intracellular flux of $O_2^{-}\cdot$. Due to this low level, but continuous, production, $O_2^{-}\cdot$ is thought to be the most abundant free radical in biological systems [2].

Despite this prevalence, $O_2^{-}\bullet$ is a relatively unreactive radical species at physiological pH (pK_a of $O_2^{-}\bullet$ is 4.8). A major reaction of $O_2^{-}\bullet$ is the single electron reduction of high-oxidation state metal ions. This is an important reaction as it allows the recycling of higher valence metal ions to lower oxidation states. The reduction of Fe^{3+} to Fe^{2+} during the Haber-Weiss reaction (Section 1.3.3) and the reduction of Cu^{2+} to Cu^{+} during the catalytic action of superoxide dismutase are important examples of this type of reaction [2].

$O_2^{-}\bullet$ is a weak oxidant and as such only reacts with relatively easily oxidised compounds, e.g. ascorbate. This reaction is relatively slow (~1.5×10^5 M^{-1} s^{-1}) and therefore is of questionable biological significance [2].

Peroxynitrite is a powerful oxidising species that can be formed by the reaction of $O_2^{-}\bullet$ with nitric oxide ($NO\bullet$) [3].

$$NO\bullet + O_2^{-}\bullet \rightarrow ONOO^{-} \qquad k \sim 7 \times 10^9\ M^{-1}\ s^{-1} \qquad (1.1)$$

Another major reaction of $O_2^{-}\bullet$ is dismutation to H_2O_2, a reaction that is likely to be a major source of cellular H_2O_2. This reaction is often represented as [2];

$$O_2^{-}\bullet + O_2^{-}\bullet + 2\ H^{+} \rightarrow H_2O_2 + O_2 \qquad (1.2)$$

However, the likelihood of four molecules colliding simultaneously is very low, meaning that the dismutation reaction is probably preceded by the protonation of $O_2^{-}\bullet$ followed by reaction of $HO_2\bullet$ with $O_2^{-}\bullet$, or by the action of superoxide dismutase enzymes (see Section 1.3.5) [2].

$$HO_2\bullet + O_2^{-}\bullet + H^{+} \rightarrow H_2O_2 + O_2 \qquad k_2 = 9.7 \times 10^7\ M^{-1}\ s^{-1} \qquad (1.3)$$

$$HO_2\bullet + HO_2\bullet \rightarrow H_2O_2 + O_2 \qquad k_2 = 8.3 \times 10^5\ M^{-1}\ s^{-1} \qquad (1.4)$$

Under physiological conditions, direct reaction of $O_2^{-}\bullet$ with biomolecules such as DNA, lipids and proteins does not appear to be a major process. The direct reactions observed are very specific cases and often involve reaction with other radicals (e.g. $NO\bullet$) or protein-bound metal ions. Therefore the major cellular consequence of $O_2^{-}\bullet$ production seems to be its ability to generate more reactive oxygen species such as H_2O_2, and peroxynitrite.

1.3.2b Hydroxyl Radical

In contrast to $O_2^{-}\cdot$, HO• is a very potent oxidant reacting indiscriminately with most substrates at, or near, diffusion controlled rates. HO• can be generated by sonolytic, radiochemical, photochemical and chemical means.

Exposure of water to ultrasound (MHz range) leads to the formation, growth and collapse of gas bubbles, an event known as acoustic cavitation [12]. Transient cavitations collapse to form 'hot spots' in which temperatures of several thousand Kelvin and pressures of hundreds of atmospheres exist. These extreme conditions lead to the homolytic fission of water producing H• and HO•. Interest in sonolysis chemistry is primarily motivated by the clinical use of ultrasound and also by its use in synthetic chemistry. It is not certain whether production of radical species occurs during medical diagnostic imaging but it has been shown that radicals are formed in the *in vitro* ultrasonolysis of human amniotic fluid [12].

Exposure of water to ionising radiation (e.g. γ-rays, X-rays, high energy electrons) leads to the formation of HO•, hydrated electrons and H•. A very clean source of HO• can be obtained by exposing water to high energy radiation in the presence of nitrous oxide (N_2O) [10].

$$e^{-}_{(aq)} + H_2O + N_2O \rightarrow HO\cdot + HO^{-} + N_2 \qquad (1.5)$$

UV photolysis of H_2O_2 produces HO•, but this then reacts with H_2O_2 to yield $HO_2\cdot/O_2^{-}\cdot$ in the absence of other substrates. Vacuum UV photolysis of water also produces HO• in alkaline solutions saturated with N_2O. The H-atoms formed are converted to HO• by the following reactions [10];

$$H_2O + h\upsilon \rightarrow H\cdot + HO\cdot \qquad (1.6)$$

$$H\cdot + HO^{-} \rightarrow e^{-}_{(aq)} + H_2O \qquad (1.7)$$

$$e^{-}_{(aq)} + H_2O + N_2O \rightarrow HO\cdot + HO^{-} + N_2 \qquad (1.8)$$

A major chemical source of HO• is obtained *via* the reduction of H_2O_2 by ferrous ions, a reaction known as the Fenton reaction. This type of reaction was first described in the late 19th century by Fenton [13]. It is now known that other metal ions, such as Cu^{+}, can catalyse similar reactions, although there still remains some controversy about the actual mechanism of the reaction and whether other oxidants are produced. The overall reaction is usually represented thus [10];

$Fe^{2+} + H_2O_2 \rightarrow Fe^{3+} + HO\bullet + HO^-$ (1.9)

$Fe^{2+} + HO\bullet \rightarrow Fe^{3+} + HO^-$ (1.10)

A related reaction, known as the Superoxide Driven Fenton Reaction (SDFR), was postulated after the observation that HO• scavengers inhibited some $O_2^{-}\bullet$ dependant reactions. Initially it was proposed that $O_2^{-}\bullet$ and H_2O_2 react to form HO• by the following overall reaction [14];

$H_2O_2 + O_2^{-}\bullet \rightarrow O_2 + HO\bullet + HO^-$ (1.11)

This reaction, also known as the Haber-Weiss reaction after its proposers, has since been found to proceed with a very low rate constant in aqueous conditions [12]. However, this reaction is catalysed by transition metal ions (e.g. Fe^{3+} or Cu^{2+}) which results in significant yields of HO• [14].

$Fe^{3+} + O_2^{-}\bullet \rightarrow Fe^{2+} + O_2$ (1.12)

$Fe^{2+} + H_2O_2 \rightarrow HO\bullet + HO^- + Fe^{3+}$ (1.13)

HO• is a highly reactive oxidant, reacting with a range of biological molecules including proteins, nucleic acids, lipids and carbohydrates at essentially diffusion controlled rates [12]. As proteins often bind metal ions HO• damage can occur at specific sites via Fenton-type chemistry. DNA oxidation by HO• leads to strand breakages and base modifications [15].

There are three main types of HO• reaction; addition to double bonds, hydrogen abstraction, and electron transfer. HO• reacts with double bonds to give secondary radicals, which, in turn, can lead to stable products [16].

An example of addition to double bonds is the oxidation of the DNA base thymine [16].

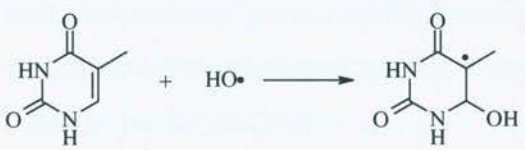

(1.14)

Hydrogen atom abstraction by HO• also leads to formation of a secondary radical that will undergo further reaction with oxygen to yield a peroxyl radical or a termination reaction with another radical species under anoxic conditions. The example of ethanol is shown below [16];

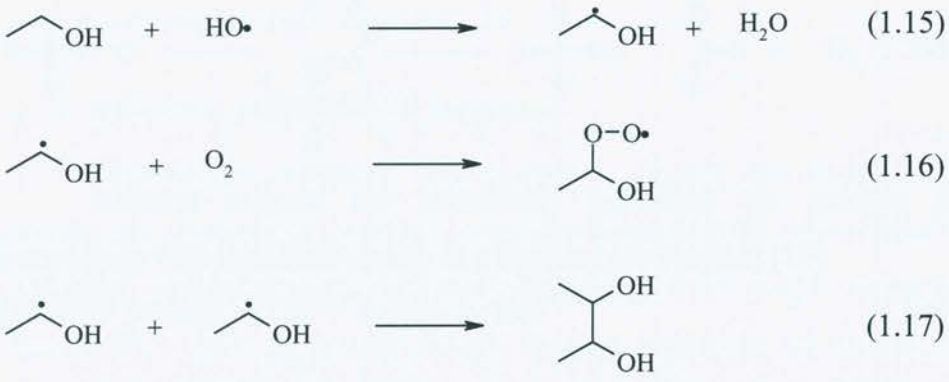

Electron transfer reactions can take place between HO• and organic or inorganic molecules. For example chloride anion is oxidised by HO• to yield Cl• [16].

1.3.2c Peroxyl and Alkoxyl Radicals

Peroxyl and alkoxyl radicals can be generated chemically, photochemically and radiolytically [10].

Peroxyl radicals are generated chemically by reaction of carbon-centred radicals with oxygen. Most carbon-centred radicals react with oxygen at near diffusion controlled rates [10].

$$R\bullet + O_2 \rightarrow ROO\bullet \qquad (1.18)$$

Oxidised metal species can react with peroxides to yield a peroxyl radical.

$$M^{n+} + ROOH \rightarrow M^{(n-1)+} + ROO\bullet + H^+ \qquad (1.19)$$

The reaction of two peroxyl radicals can lead to the formation of an unstable tetroxide (1.20). These species can decay by a number of routes, in the case of tertiary peroxyl species two routes are possible, one giving rise to non-radical products (1.21), the other yielding alkoxyl radicals and oxygen (1.22) [17]. Another well-characterised peroxyl radical-mediated reaction is the Russell mechanism, which occurs via a six-membered transition state and yields $^1O_2$ (1.23) [18].

$$2\,ROO\bullet \rightarrow ROO\text{-}OOR \qquad (1.20)$$

$$ROO\text{-}OOR \rightarrow RO\text{-}OR + O_2 \qquad (1.21)$$

$$ROO\text{-}OOR \rightarrow 2\,RO\bullet + O_2 \qquad (1.22)$$

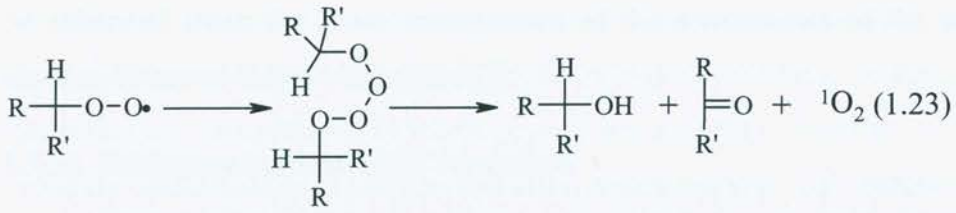

(1.23)

Alkoxyl radicals are chemically generated via reaction of peroxidic compounds with transition metals in a Fenton-type reaction [10].

$$M^{(n-1)+} + ROOH \rightarrow M^{n+} + RO\bullet + HO^- \quad (1.24)$$

Flash photolysis is the major photochemical method for alkoxyl radical production [10]. One of the most studied species is the *t*-butoxyl radical, which is generated by flash photolysis of a 1:2 mixture of benzene and di-t-butylperoxide [19].

$$(CH_3)_3CO\text{-}OC(CH_3)_3 + h\upsilon \rightarrow 2(CH_3)_3CO\bullet \quad (1.25)$$

Biological production of alkoxyl and peroxyl radicals may occur by electron transfer from complexed transition metals to peroxidic compounds by similar reactions as discussed above [10].

1.3.2d Singlet Oxygen

One further member of the ROS family is $^1O_2$. This form of molecular oxygen is activated in a manner unique from the other ROS by the arrangement of electrons in the outermost π_{2p}^* orbital. This species is the major topic of this thesis and will be discussed in greater detail in later sections (section 1.4).

1.3.3 Biological Reactions Producing ROS

1.3.3a Electron Transport Chains

Electron transport chains (Section 1.2.2) are likely to be the most important source of $O_2^{-}\bullet$, in aerobic cells. They are present in bacterial membranes, chloroplasts of plants, and in mitochondria and endoplasmic reticulum in eukaryotic cells [20].

The mitochondrial electron transport chain is a very efficient process with most of the electrons being shuttled through the entire chain to reduce O_2 to H_2O. However, a small proportion of these electrons 'leak' out of the chain and directly reduce oxygen. Under physiological conditions it has been suggested that between 1 and 3 % of oxygen reduced in mitochondria forms $O_2^{-}\bullet$. This low rate of leakage can

be enhanced when the close arrangement of the components of the mitochondrial electron transport chain is disrupted [2].

1.3.3b Radiation induced ROS formation

High-energy radiation, such as γ-rays, X-rays and high energy electrons, neutrons and α-particles, can lead to the formation of ROS intracellularly. The most significant initial reaction is the homolysis of one of the H-O bonds in water to yield H• and HO•. HO• is a very potent oxidant damaging all classes of biological molecules (Section 1.3.4). The damaging effects of ionising radiation are enhanced by the presence of oxygen. This may be due to HO• -mediated hydrogen abstraction reactions resulting in formation of biomolecule-derived radicals that undergo further reaction with O_2 to give longer-lived peroxyl radicals. Ionising radiation can also lead to the production of hydrated electrons, which, in the presence of oxygen, leads to O_2^{-}• formation.

Other, less energetic forms of radiation, such as UV and visible light, can also elicit ROS production *in vivo*. UV light is commonly subdivided into three divisions UVA (320 – 400 nm), UVB (280 – 320 nm) and UVC (230 – 280 nm). Obviously the effects of UV light are most important on the skin and the eyes. Only UVA and UVB reach the Earth's surface, as UVC, and some of the UVB, are filtered by the ozone layer [21]. UVB is of greater energy than UVA so on similar exposure, UVB will be more damaging than UVA. However, UVA penetrates the skin to a greater extent and is more abundant in sunlight, compared to UVB, suggesting that it may be the major contributor to photodamage [21]. The UV light that passes through the atmosphere is not sufficiently energetic to ionise molecules, but UVB is able to cause homolytic fission of H_2O_2 to generate HO•. Thymine and cytosine can absorb UVB, creating excited states that can react with an adjacent pyrimidine base to form cross-linked species [21]. Many of the damaging effects of UVA radiation and visible light are attributed to the production of $^1O_2$, by photosensitisation reactions, which will be discussed in section 1.4 [21, 22].

1.3.3c Metal ion catalysed production of ROS

The reduction of H_2O_2 by a reduced metal ion to afford HO• is another major source of ROS production *in vivo*. O_2^{-}• can also play a part in this reaction as it can reduce metal ions, which then react with H_2O_2 (Section 1.3.4). Pseudo-Fenton

reactions, where a metal ion reduces an organic peroxide to an alkoxyl radical, are also possible *in vivo* (Section 1.3.5). The biological relevance of these reactions is dependant on the availability of the metal ion catalysts required. The two most abundant metal ions in biological systems, which catalyse this reaction, are Fe and Cu. The availability of these ions is strictly regulated, *via* chelation, which is an important anti-oxidant defence in itself. Various proteins responsible for the sequestration of iron and copper under normal conditions include haem proteins (e.g., haemoglobin and myoglobin), transport proteins (e.g., transferrin) and intracellular storage proteins (including ferritin) [2]. The major copper storing protein is caeruloplasmin, which chelates up to 95 % of the copper present in plasma [23]. However, Fe can be released from ferritin and iron-sulfur clusters by $O_2^{-\bullet}$, and haem can be degraded by H_2O_2 to release iron. Increased levels of labile Fe have been observed in cultured cells upon oxidative stress, including exposure to H_2O_2, organic peroxides, radicals and UV light [24]. The lysis of cells can also lead to the release of metal ions, which may lead to increased ROS production in surrounding areas [24].

1.3.3d Production of ROS in the respiratory burst

Phagocytosis and the respiratory burst can contribute to ROS generation *in vivo*, but in contrast to those processes discussed above, this is a deliberate production of these reactive molecules [25]. Phagocytic cells, such as neutrophils and macrophages, are involved in the body's response to invasion by foreign organisms. Bacterial products, products of complement activation and various other chemotactic factors, activate the phagocytes to attack the invading cells. The phagocytes surround and engulf the foreign cell, cytoplasmic granules then fuse with the vacuole containing the engulfed cell and release their contents into it [26, 27].

The mechanism of killing involves the respiratory burst. This is characterised by a large increase in the amount of oxygen consumed by the phagocytic cells [27]. The enhanced respiratory activity can be triggered by opsonised bacteria or by a number of chemical stimulants; hence phagocytosis is not a pre-requisite for the respiratory burst to occur. Phagocytes are able to kill some bacterial strains in the absence of oxygen, but the majority require the presence of oxygen for effective bactericidal action. Patients who suffer chronic granulomatous disease, which arises from a genetic fault in the production of one or more of the respiratory burst components, do not possess the ability to launch the respiratory burst. These patients

often suffer from persistent infections in a variety of tissues, demonstrating the importance of the respiratory burst for host defence [25, 27].

The enhanced oxygen uptake in phagocytes undergoing the respiratory burst is due to the activation of the NADPH oxidase enzyme complex [27]. This complex uses a bound FAD^+ to oxidise NAPDH to $NADP^+$, the FADH is then oxidised by cytochrome b, and the reduced cytochrome b finally reduces oxygen to $O_2^{-}\cdot$. The complex is orientated such that the production of $O_2^{-}\cdot$ occurs either on the extracellular surface of the phagocyte or inside the phagocytic vesicle [27]. The engulfed particle is thus exposed to high flux of $O_2^{-}\cdot$, and other oxidising species. The precise mechanisms of cell killing are not certain. Thus, spontaneous dismutation of $O_2^{-}\cdot$ to H_2O_2 may kill pathogenic cells either directly or by mediating the formation of other, more potent oxidants such as HO• and HOCl. HOCl is formed by reaction of H_2O_2 with Cl^- catalysed by myeloperoxidase (MPO). In addition, $^1O_2$ formed by the reaction of H_2O_2 with HOCl may be cytotoxic. It is also possible that NO• generated by nitric oxide synthase enzymes can also react with $O_2^{-}\cdot$ to yield the powerful oxidant peroxynitrite, which may play a part in cell killing [25, 26].

1.3.3e Enzymatic ROS production

There are a variety of enzymes that produce ROS under certain circumstances in addition to the respiratory burst mentioned above. These include xanthine oxidase, lipoxygenase enzymes, and peroxidase enzymes. Lipoxygenases are non-haem, iron-containing enzymes that catalyse the oxidation of polyunsaturated lipids and fatty acids to hydroperoxides. These hydroperoxides are substrates for pathways that lead to leukotrienes and lipoxins, important signalling molecules in the immune system [28]. The hydroperoxides formed in these reactions may become substrates for metal ion catalysed reduction to alkoxyl radicals [2].

1.3.3f ROS production during reperfusion injury

Reperfusion injury (also known as reoxygenation injury) is observed after a completely or partially hypoxic (O_2-deprived) tissue is reoxygenated, usually by restoration of the blood flow. It has been observed that during a period of hypoxia, the level of ATP within the tissue decreases and the hypoxanthine concentration increases. When the tissue is reoxygenated the oxidation of hypoxanthine to uric acid

and the concurrent reduction of oxygen to $O_2^{-\bullet}$ by xanthine oxidase, has been postulated to cause tissue damage [29].

Reperfusion injury has attracted much attention from cardiologists and cardiac research scientists, as cardiac muscle is subjected to such conditions on re-establishment of blood flow after myocardial infarction. Experiments in animal models have shown that injury is observed on reperfusion of hypoxic hearts and in some cases this can be prevented by SOD, catalase and spin traps. However, most heart tissues contain low levels of xanthine oxidase, thus the importance of this enzyme in reperfusion injury has been questioned [2].

It has been suggested that ROS apart from $O_2^{-\bullet}$ could be involved in reperfusion injury. For example, experiments using rat hearts demonstrated the presence of $^1O_2$ on reperfusion using a chemical trapping method [30]. Further, it is known that reperfusion leads to enhanced infiltration of activated neutrophils, which are known to generate a host of ROS [31]. Therefore, it is likely that the tissue damage observed on reperfusion is due to a combination of a number of different ROS.

1.3.4 ROS-Mediated Damage to Biological Substrates

1.3.4a Damage to nucleic acids

DNA and RNA bases do not appear to be damaged to any appreciable extent by $O_2^{-\bullet}$ or H_2O_2 at physiological levels, although oxidation of the sugar backbone of nucleic acids can occur on reaction with H_2O_2, leading to strand breakage [15]. However, more reactive species such as $HO^\bullet$, and $^1O_2$ can cause base damage. The high reactivity of $HO^\bullet$ leads to indiscriminate oxidation of nucleotides as it reacts with purines, pyrimidines and sugars. Reaction of $HO^\bullet$ with nucleic acid bases is generally via addition reactions to the ring double bonds to give adduct radicals of the bases. Subsequent reactions of these radicals leads to the formation of a variety of products from each base [32].

$HO^\bullet$ -mediated hydrogen atom abstraction from both types of bases is also possible, resulting in formation of base-derived radicals that can participate in reactions with the sugar moiety. Peroxyl and alkoxyl radicals can also induce cleavage of the backbone of DNA molecules [33].

HO• can abstract hydrogen atoms from all five ring carbon positions in the ribose sugar to give carbon-centred radicals that react rapidly with oxygen to yield peroxyl radicals. The ultimate effect of oxidant-mediated DNA damage is determined by the position of the radical formation, with the detection of strand breaks, cross-linking, modified bases and sugars all possible [34].

In contrast to the unselective oxidation of DNA and RNA bases induced by radical species, $^1O_2$ oxidises DNA in a more specific manner, resulting in the selective oxidation of guanine bases (Section 1.5.2a).

1.3.4b Damage to lipids

Oxidative damage to lipids is mediated both by radicals and $^1O_2$. Radical-mediated peroxidation of lipids is a classical radical chain reaction. The initiation step generally involves abstraction of a *bis*-allylic hydrogen atom by HO•, alkoxyl radicals, peroxyl radicals or HO_2•. The non-protonated O_2^{-}• is a poor initiator of this reaction. The protonated form of O_2^{-}•, HO_2•, is formed at low pH (pKa = 4.8) and has much higher reactivity than O_2^{-}•. The uncharged nature of HO_2• is also a factor in its reactivity with lipids, as it is able to enter the hydrophobic regions of a lipid membrane. The product of the hydrogen abstraction reaction is a carbon-centred lipid-derived radical. In the presence of oxygen, this carbon-centred radical reacts rapidly to give a peroxyl radical. The propagation phase of the reaction begins when this lipid peroxyl radical abstracts another bis-allylic hydrogen atom leading to the formation of a lipid hydroperoxide and a further carbon-centred radical (Scheme 1.1). Transition metal ions are also important in lipid peroxidation. Firstly, they may be responsible for the production of the initial oxidant. Secondly, they can reduce the lipid hydroperoxides in a pseudo-Fenton reaction to yield alkoxyl radicals that can then initiate further chain reactions.

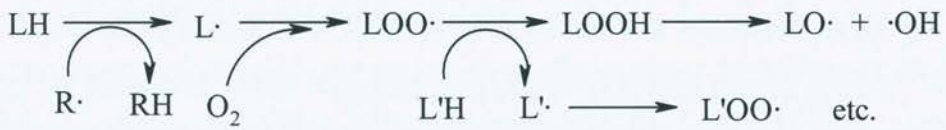

Scheme 1.1: The radical-mediated chain oxidation of lipids [35].

$^1O_2$ reacts with lipids mainly via an ene reaction to yield hydroperoxides (Section 1.5.2b). These hydroperoxides can be reduced by metal ions to initiate lipid peroxidation chain reactions similar to the radical-initiated reactions.

Cholesterol is also a target for oxidative modification. Radical-mediated oxidation yields a complex mixture of products including 7α- and 7β-hydroperoxides, and the corresponding alcohols, 7-keto derivatives, epoxy derivatives of cholesterol and many others.

$^1O_2$-mediated oxidation of cholesterol yields a less complex spectrum of products (Section 1.5.2b). The three products formed are the 5α, 6α, and 6β hydroperoxides of cholesterol, which are specific $^1O_2$-mediated oxidation products and are often employed as biomarkers for this process (Section 1.7.1 and also 1.5.2b) [36].

1.3.4c Damage to proteins

The oxidation of proteins *in vivo*, can be mediated by most ROS with the exception of H_2O_2 and $O_2^{-\bullet}$. These latter oxidants generally only oxidise proteins in the presence of accessible free thiol groups. The consequences of protein oxidation depend on the nature of the oxidant, but can include side-chain modification including carbonyl formation, backbone fragmentation and aggregation.

The $HO^\bullet$ -mediated oxidation of proteins has been studied in some detail. This highly oxidising species can react with proteins by hydrogen abstraction (1.26), or by addition, to result in the formation of protein-derived, carbon-centred radicals. Under physiological conditions these initial radicals rapidly react with oxygen to yield peroxyl radicals (1.18). The protein peroxyl radicals can then abstract another hydrogen atom to yield a hydroperoxide and another radical species (1.27). Protein hydroperoxides can be reduced by one-electron reductants yielding alkoxyl radicals (1.24), or by two electron reductants to give an alcohol (reviewed in [37]). These reactions are known to occur with aliphatic amino acid side chains such as Val, Leu and Lys. The alcohols derived from these side-chains provide useful markers for oxidative damage to proteins and have been detected on proteins extracted from diseased tissues (Section 1.7.3).

$$R\text{-}H + HO^{\bullet} \rightarrow R^{\bullet} + H_2O \quad (1.26)$$

$$R'\text{-}H + ROO^{\bullet} \rightarrow R'^{\bullet} + ROOH \quad (1.27)$$

HO•-mediated hydroxylation reactions occur with Phe and Tyr residues, and lead to the formation of *ortho*- and *meta*-Tyr, and 3,4-dihydroxyphenylalanine (DOPA) respectively [37, 38].

Sulfur containing side-chains (i.e. Cys and Met) are also susceptible to oxidation by most ROS, yielding disulfides or sulfoxides [2]. His is also oxidised by ROS yielding a range of products, including 2-oxohistidine. These amino acids are often critical residues in the active sites of enzymes and thus their oxidation can lead to enzyme inactivation [2].

1.3.4d Damage to carbohydrates

Carbohydrates including monosaccharides, polymeric species and protein-saccharide complexes (such as proteoglycans) are all susceptible to oxidation by ROS, especially HO• [15]. The abstraction of a hydrogen atom by HO• leads to the formation of a carbon-centred radical. Oxygen reacts with these radicals at near diffusion controlled rates, to yield peroxyl radicals, which can undergo rearrangement reactions leading to fragmentation, or can react with other species to yield hydroperoxides [15].

Carbohydrate oxidation is thought to be important in some disease states. Radical-mediated oxidation of carbohydrates has been shown to reduce the viscosity of synovial fluid, increase matrix degradation and lead to the fragmentation of extracellular proteoglycans, which may have implications in rheumatoid arthritis [39].

1.3.5 Biological Defence Mechanisms Against ROS

Defence against ROS-mediated injury *in vivo* is accomplished by the use of both enzymatic and non-enzymatic processes.

Enzymatic mechanisms of antioxidant defence have evolved among aerobic organisms. There are three major classes of enzymes, catalases, superoxide dismutases and peroxidases.

Catalases are haem-containing enzymes found in most aerobic organisms and a few anaerobes. Catalase is expressed in all major organs in animals, but is especially concentrated in the liver. H_2O_2 is directly decomposed by catalase forming

water and ground state oxygen. The mechanism of catalase involves two steps as shown (rates are shown for rat liver catalase [40]);

$$\text{Catalase-Fe(III)} + H_2O_2 \rightarrow \text{compound I} + H_2O \qquad k = 1.7 \times 10^7\ M^{-1}\ s^{-1} \qquad (1.28)$$

$$\text{Compound I} + H_2O_2 \rightarrow \text{catalase-Fe(III)} + H_2O + O_2 \qquad k = 2.6 \times 10^7\ M^{-1}\ s^{-1} \qquad (1.29)$$

SOD enzymes are present in all aerobic organisms. Three major forms of SOD are known, the Cu/Zn SOD, Mn SOD and Fe SOD. Cu/Zn SOD is present in virtually all eukaryotic cells. In animal cells it is predominantly located in the cytosol. Mn SOD is found in bacteria, plants, yeasts and mammals. In animal and yeast cells Mn SOD is located in the mitochondria. Fe SOD is found in bacteria, algae and higher plants. The basic reaction mechanism is similar for all three enzymes (where M = either Cu or Mn or Fe);

$$\text{Enzyme-}M^{n+} + O_2^{-}\bullet \rightarrow \text{Enzyme-}M^{(n-1)+} + O_2 \qquad (1.30)$$

$$\text{Enzyme-}M^{(n-1)+} + O_2^{-}\bullet + 2H^+ \rightarrow \text{Enzyme-}M^{n+} + H_2O_2 \qquad (1.31)$$

The best characterised peroxidase enzymes are the selenium-containing glutathione peroxidases. These enzymes use the reduced form of glutathione to catalyse the reduction of peroxide species to their corresponding alcohols. The peroxide species is not limited to H_2O_2, indeed lipid hydroperoxides, cholesterol 7β-hydroperoxide (at a low rate) and synthetic peroxides, such as cumene and *t*-butyl hydroperoxide, can also be reduced by this system. The selenium atom in the active site is essential to the catalytic mechanism of glutathione peroxidase [2];

$$\text{Protein-Se} + ROOH + H^+ \rightarrow ROH + \text{protein-SeOH} \qquad (1.32)$$

$$\text{Protein-SeOH} + GSH \rightarrow H_2O + \text{protein-Se-SG} \qquad (1.33)$$

$$\text{Protein-Se-SG} + GSH \rightarrow \text{protein-Se-GSSG} \rightarrow \text{protein-Se} + H^+ + GSSG \qquad (1.34)$$

Oxidised glutathione can be recycled enzymatically by glutathione reductase, the reduction is driven by the oxidation of NADPH.

Many other peroxidase enzymes are known, they all function as antioxidants by removing H_2O_2 and hence the potential for HO• production. However, some of

these enzymes, such as MPO and eosinophil peroxidase, generate potentially oxidising species themselves (Section 1.6.1a).

Many small molecules also have antioxidant functions. They are usually easily oxidised compounds, which can react with an oxidant to form a less reactive product. Classic examples of low molecular weight antioxidants include dietary vitamins, such as ascorbate (vitamin C), tocopherols (vitamin E), tocotrienols, glutathione, carotenoids (including vitamin A), polyphenolics derived from plants, bilirubin and reduced coenzyme Q (ubiquinol). These compounds may be broadly divided by their hydrophilic or hydrophobic nature, and hence which areas of the cell they are likely to be found in. For example, α-tocopherol is an important low molecular weight compound for the prevention of lipid peroxidation, whereas ascorbate is a water-soluble compound that can scavenge a range of oxidants as well as acting as a cofactor for several enzymes. These antioxidants can also act in synergy, for example ascorbate may reduce the α-tocopheryl radical, back to α-tocopherol [2].

It should be noted that both ascorbate and tocopherol are known to act as pro-oxidants under certain conditions. For example, it has been shown *in vitro*, that ascorbate can reduce oxidised metal ions (e.g. Fe^{3+} to Fe^{2+}), which are effective at catalysing the reduction of peroxides by metal ions, although the *in vivo* relevance of this is debatable. Tocopherols can accelerate lipid peroxidation in a process known as tocopherol-mediated peroxidation. This occurs when tocopherol facilitates the transfer of radicals from the aqueous phase into LDL particles and then act as a chain-carrying species by oxidising lipids [41].

Antioxidants capable of scavenging $^1O_2$ *in vivo* include carotenoids (α- and β-carotene, lycopene, lutein, and zeaxanthin; k_2 ca. 1×10^{10} M^{-1} s^{-1}), ascorbate (k_2 8.3×10^6 M^{-1} s^{-1}), α-tocopherol (k_2 2.3×10^8 M^{-1} s^{-1}) and glutathione (2.4×10^6 M^{-1} s^{-1}) [42].

1.4 SINGLET OXYGEN

1.4.1 INTRODUCTION

The first report of a reaction mediated by $^1O_2$ appears to have been made by Fritzsche in 1867 [43]. It was reported that naphthacene reacted in the presence of light and oxygen to yield a product that could regenerate naphthacene when heated. The identity of the reactive oxygen species involved in this reaction was not known at the time, and in fact the role of $^1O_2$ in such reactions was not established until 1972 [44]. The naphthacene oxidation product was confirmed to be endoperoxide in 1976 [43].

Evidence for the formation of a more reactive state of oxygen was not reported until the 1930's [45]. Since this time, however, many advances into the nature and reactions of $^1O_2$ have been made, stimulated by the role of this activated state of molecular oxygen in synthetic chemistry, photochemistry, and biochemistry.

Ground state oxygen ($^3O_2$) suffers from a spin-restriction (Section 1.2.3) which renders it a relatively poor oxidant. This spin-restriction can be lifted by rearrangement of the electrons within the outer most molecular orbitals. The addition of 96.3 kJ or 157 kJ of energy to oxygen can yield the two singlet states – $^1\Delta_g$ and $^1\Sigma_g^+$ respectively. The $^1\Sigma_g^+$ state rapidly decays to $^1\Delta_g$ and therefore is not thought to play a signifiant part in $^1O_2$-mediated processes. However, $^1\Delta_g$ is relatively long-lived (~ 4 μs in water, [46]) as the transition $^1\Delta_g \rightarrow {}^3\Sigma_g$ is spin-forbidden. Thus, it is the $^1\Delta_g$ state that is normally referred to by the term singlet oxygen, $^1O_2$.

Although the $^1\Delta_g$ state O_2 is much longer lived than the $^1\Sigma_g^+$ state, it is rapidly deactivated in solution by transferring excess energy to the solvent via vibrations. Thus, the lifetime of $^1O_2$ is very solvent dependent. Solvents with high vibrational frequencies provide the most efficient relaxation to the ground state. Water has a very high vibrational frequency (strong OH vibration near 3600 cm^{-1}) and therefore the $^1O_2$ lifetime is quite short in water. Solvents with CH groups (~3000 cm^{-1}) are also very efficient. Replacement of the hydrogens with deuterons decreases the quenching rate of the solvent due to lower frequency vibrations (e.g. lifetime in H_2O 4 μs, in D_2O 62 μs). Organic solvents with no hydrogens (or deuterons) offer the longest lifetimes for $^1O_2$ [46].

1.4.2 SOURCES OF SINGLET OXYGEN

Sources of $^1O_2$ can be divided into two major groups, photochemical and chemical (i.e. not involving light).

The first major method discovered for generating $^1O_2$ was the reaction between sodium hypochlorite and H_2O_2, which produces $^1O_2$ in near quantitative yield [46]. However, this reaction is not always suitable for experimental use as both hypochlorite and H_2O_2 are potential oxidising species. This reaction may be an important source of $^1O_2$ *in vivo*, as it has been suggested that the H_2O_2 produced by NADPH oxidase and hypochlorite produced by MPO, may react to generate $^1O_2$ in the phagosome (see Section 1.6.1a)

The disproportionation of H_2O_2 to yield $^1O_2$ can be catalysed by molybdate (MoO_4^{2-}) ions in basic solution [47]. The initial reaction between H_2O_2 and MoO_4^{2-}, yields diperoxomolybdate, MoO_6^{2-} (reaction 1.35), which then reverts back to MoO_4^{2-} producing $^1O_2$ (reaction 1.36) [47].

$$2\,H_2O_2 + MoO_4^{2-} \rightleftharpoons 2\,H_2O + MoO_6^{2-} \qquad (1.35)$$

$$MoO_6^{2-} \longrightarrow MoO_4^{2-} + {}^1O_2 \qquad (1.36)$$

In practice the optimal conditions for this system involve the addition of aliquots of H_2O_2 to the reaction mixture, such that the concentration of H_2O_2 introduced is twice that of molybdate ions. This leads to the formation of a red solution, which is allowed to react until the solution turns yellow in colour when another aliquot of H_2O_2 is added. H_2O_2 is added in small amounts so that minimal amounts of the inactive red-brown tetraperoxomolybdate, MoO_8^{2-} are formed (reaction 1.31). For maximal yields of $^1O_2$ the reaction is performed at alkaline pH to prevent formation of the inactive acid $HMoO_6^-$ (reaction 1.36) [47].

$$MoO_6^{2-} + 2\,H_2O_2 \rightleftharpoons MoO_8^{2-} + 2\,H_2O \qquad (1.37)$$

$$MoO_6^{2-} + H_2O_2 \rightleftharpoons HMoO_6^- + HO_2^- \qquad (1.38)$$

This system is only efficient in pure water, and aqueous methanol or ethanol. Despite this, it has been used to oxidise non-water soluble organic substrates by the use of reverse (i.e. water in oil) microemulsions [48].

Another popular chemical $^1O_2$ generation system is the use of naphthalene endoperoxides. These compounds are synthesised by addition of $^1O_2$ to a naphthalene

derivative. Saito *et al.*, reported the first use of these compounds for the generation of $^1O_2$ in 1980 [49]. These researchers used low temperature methylene blue (MB) photo-oxidation (see below) to oxidise 3-4(methyl-1-naphthyl)propionic (1.1) acid to its 1,4-endoperoxide (1.2) (Scheme 1.2).

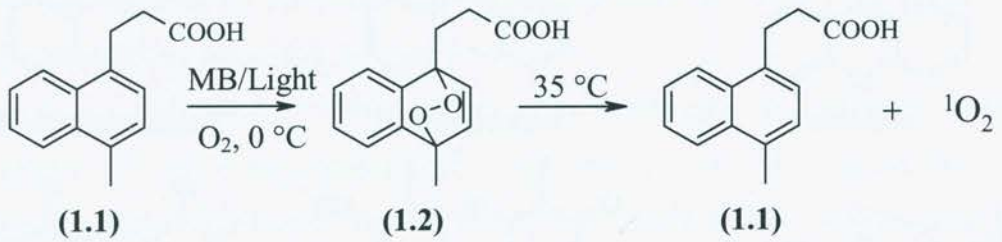

(1.1) **(1.2)** **(1.1)**

Scheme 1.2: The synthesis of a naphthalene endoperoxide and its thermal decay yielding $^1O_2$ [49].

Upon incubation at physiological temperatures, the naphthalene endoperoxide decays to yield the parent compound and a known amount of $^1O_2$. Since this early study many other naphthalene endoperoxide derivatives have been synthesised and used as sources of $^1O_2$ in chemical and biochemical studies [50].

Other, less suitable (for biochemical experiments), chemical $^1O_2$ generating systems include the decomposition of phosphite ozonides and hydrotrioxides [46].

One of the most popular methods for generating $^1O_2$ in the laboratory is by the use of photosensitisers. Photosensitisers generate $^1O_2$ by absorbing the energy from a photon ($h\nu$) of light to become an excited singlet state (^1S in Scheme 1.3). ^1S can rapidly interconvert to a triplet state (^3S), which is much longer-lived and can transfer energy to ground state oxygen ($^3O_2$). The direct activation of S to ^3S is a spin forbidden process and thus the intersystem crossing step is required.

a) absorption of light $\quad S + h\nu \longrightarrow {}^1S$

b) intersystem crossing $\quad {}^1S \longrightarrow {}^3S$

c) energy transfer $\quad {}^3S + {}^3O_2 \longrightarrow S + {}^1O_2$

Scheme 1.3: Mechanism of photosensitised $^1O_2$ generation

Each sensitiser can generate many molecules of $^1O_2$, typically 10^3 - 10^5, before being inactivated by bleaching [51]. An ever-increasing range of photosensitisers activated by both UV and visible light are available (Scheme 1.4).

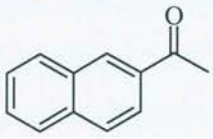

2-acetonaphthone

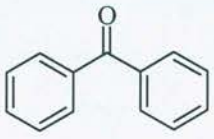

benzophenone

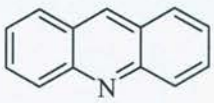

acridine

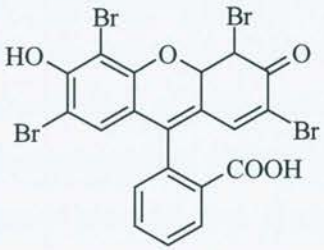

eosin

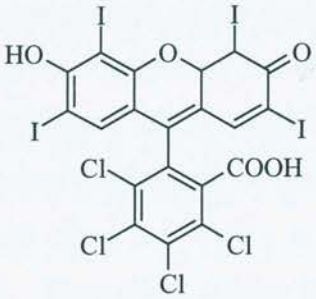

rose bengal

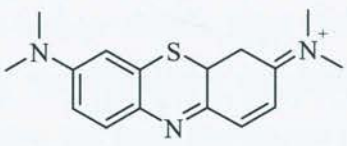

methylene blue

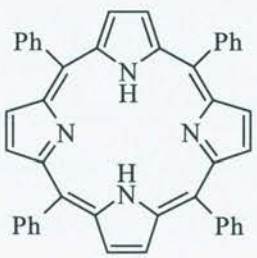

tetraphenylporphine

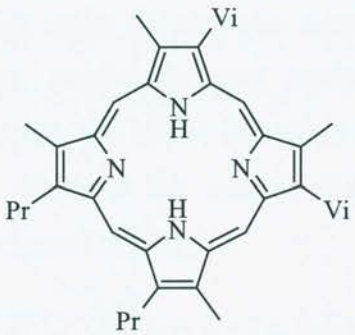

protoporphyrin IX dimethyl ester
Vi=vinyl, Pr=$CH_2CH_2CO_2CH_3$

Scheme 1.4: Some commonly used photosensitisers

Many dyes and naturally occurring compounds act as photosensitisers, including porphyrins, flavins and polyacetylenes [46]. Photosensitisation reactions producing $^1O_2$ may also be important *in vivo*, especially in areas of the body exposed to sunlight, e.g. the skin and eyes (see Section 1.6.2).

1.5 CHEMICAL REACTIONS OF $^1O_2$

1.5.1 MODES OF REACTIONS

$^1O_2$ is a highly electrophilic agent with great synthetic utility due to its ability to regio- and stereo-selectively introduce oxygen in to organic substrates. The three major reactions that $^1O_2$ participates in are the ene reaction, [4+2] cycloaddition and [2+2] cycloaddition reactions.

In the ene reaction, alkenes with allylic hydrogens are oxidised to allylic hydroperoxides with a concomitant shift of the double bond [46]. During the course of this reaction, $^1O_2$ attacks one centre of the carbon-carbon double bond with abstraction of an allylic hydrogen atom, resulting in the formation of allylic hydroperoxides [52]. The actual mechanism of the reaction has been the subject of much research and discussion since the 1940's with both stepwise and concerted reaction pathways suggested. Theoretical studies have not been able to distinguish between these possibilities, however the available experimental data favours a stepwise mechanism [43]. Various transition states for stepwise reactions have been invoked including, zwitterionic, biradical, perepoxide and exciplex formation. Presently, most experimental evidence supports the initial formation of an exciplex, prior to the formation of a perepoxide, which is the species that performs the hydrogen abstraction step (Scheme 1.5) (reviewed in [43]).

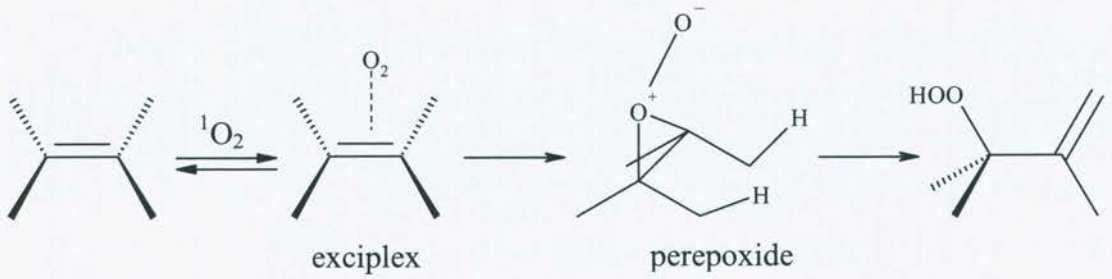

Scheme 1.5: Proposed mechanism of $^1O_2$ ene reaction with alkenes [43].

High regioselectivity can be obtained using the ene reaction. This reaction is a suprafacial process characterised by the addition of oxygen and abstraction of hydrogen from the same side of the π system, leading to the exclusive formation of the trans alkene [43, 46, 52]. This reaction was demonstrated using the chiral alkene (1.3) (Scheme 1.6) [53].

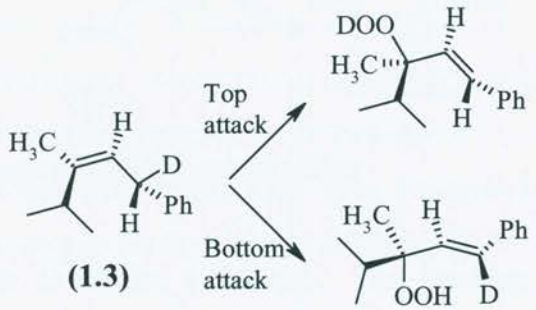

Scheme 1.6: Demonstration of the facial selectivity of the ene reaction [53].

Another factor determining the regioselectivity of the reaction is the propensity of $^1O_2$ to abstract a hydrogen atom from the most sterically hindered side of an alkene. This phenomenon has become known as the *cis* effect. For example, the methoxy group in (1.4) and (1.5) leads to reaction with, predominantly, the *cis* substituent, even when this involves the unfavourable formation of a double bond exocyclic to an already strained cycloproane ring (Scheme 1.7). The *cis* effect has also been observed in acyclic [54] and cyclic [55], aliphatic alkenes.

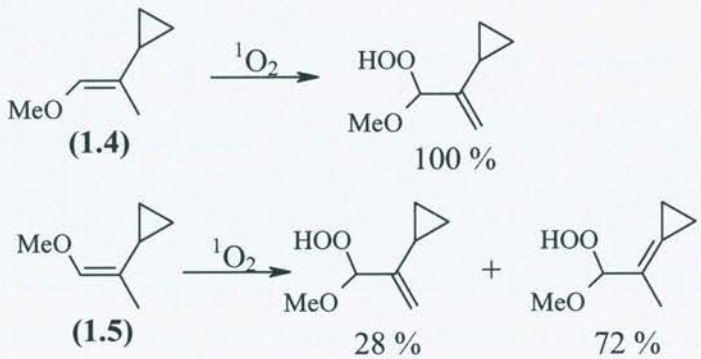

Scheme 1.7: The $^1O_2$ ene reaction *cis* effect

Regioselectivity of the ene reaction can also be influenced by the geminal effect, which leads to highly selective abstraction of allylic protons from a substituent at the α-position of an α,β-unsaturated carbonyl compound as illustrated by the oxidation of (1.6) (Scheme 1.8).

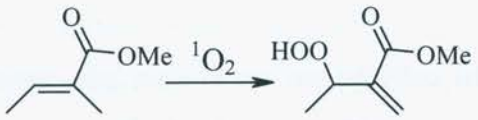

(1.6) > 97 %

Scheme 1.8: The $^1O_2$ ene reaction, geminal effect

$^1O_2$ is also able to oxidise 1,3-dienes. This reaction is very similar to the classical Diels-Alder reaction, which involves thermal reaction between 1,3-dienes and electron-deficient dienophiles (Scheme 1.9). The $^1O_2$-mediated reaction is believed to proceed via a [4+2] cycloadduct in a concerted mechanism, but other possibilities have been suggested. Gollnick and Griesbeck [56] found that *trans*, *trans*-2,4-cyclohexadiene (1.7) reacts with $^1O_2$ in a stereoselective manner to yield the cis-disubstituted endoperoxide (1.8).

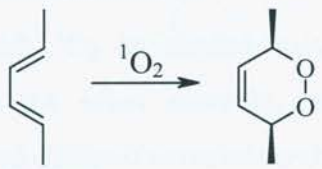

(1.7) **(1.8)**

Scheme 1.9: The $^1O_2$ [4+2] cycloaddition reaction.

Literally hundreds of these types of reactions have been reported [57] and a variety of substrates, including carbocyclic, heterocyclic and acyclic compounds, have been investigated, some examples are given below (Scheme 1.10).

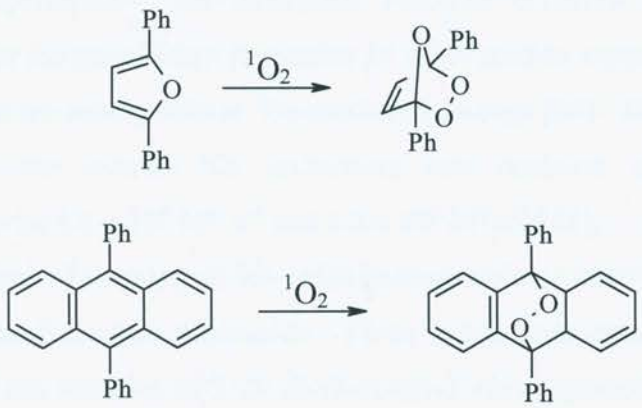

Scheme 1.10: $^1O_2$-mediated endoperoxide formation

[2+2] cycloadditions can also occur on reaction of $^1O_2$ with electron-rich substrates or with alkenes in which the competing ene reaction is structurally impossible (e.g. adamantylideneadamantane (1.9) Scheme 1.11) [58]. The products of these reactions are dioxetanes, which have been extensively studied due to their interesting ability to decompose with emission of light [46].

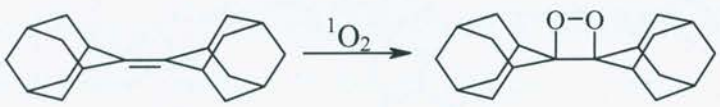

(1.9)

Scheme 1.11: The $^1O_2$ [2+2] cycloaddition reaction.

1.5.2 $^1O_2$ Reactions with Biomolecules

Biomolecules react with $^1O_2$ in similar ways to those described above, however the initial products are often unstable, especially under physiological conditions, and thus have proved difficult to isolate and characterise.

1.5.2a $^1O_2$ reaction with nucleic acids

Lutgerink *et al.*, [59] studied the $^1O_2$-mediated oxidation nucleic acids by exposing the 2'-deoxynucleoside 3'-monophosphates of adenine, cytidine, 5-methylcytidine, thymidine, guanidine, a 16-mer oligonucleotide (d-[5'-AATTCATCGATATCTA-3']), native and denatured rat kidney DNA, and single and double stranded bacteriophage DNA, to $^1O_2$ generated by the thermal dissociation of a naphthalene endoperoxide. No detectable reaction occurred with any of the nucleosides, except for guanidine. A number of other studies support the finding that only guanine bases are susceptible to $^1O_2$-mediated damage [60]. Devasagayam *et al.*, have determined the overall $^1O_2$ quenching rate constant of guanosine and deoxyguanosine to be 6.2×10^6 M^{-1} s^{-1} and 5.2×10^6 M^{-1} s^{-1} [61].

The products of reaction of $^1O_2$ with guanosine have been investigated using model compounds of the free nucleoside. Thus, it has been reported that the three main products of the reaction of 3',5'-di-*O*-acetyl-2'-deoxyguanosine (1.10) are the 4*R* and 4*S* diastereomers of 9-(3',5'-di-*O*-acetyl-2'-deoxy-β-D-*erythro*-pentofuranosyl)-4,8-dihydro-4-hydroxy-8-oxoguanine (1.11) and N-(3',5'-di-*O*-

acetyl-2'-β-D-erythro-pentofuranosyl)cyanuric acid (1.12) (Scheme 1.12) [62, 63]. These products are believed to arise from [4+2] cycloaddition yielding an endoperoxide (1.13) and a [2+2] cycloaddition yielding a dioxetane (1.14), respectively, which decay to yield the observed products [62, 63].

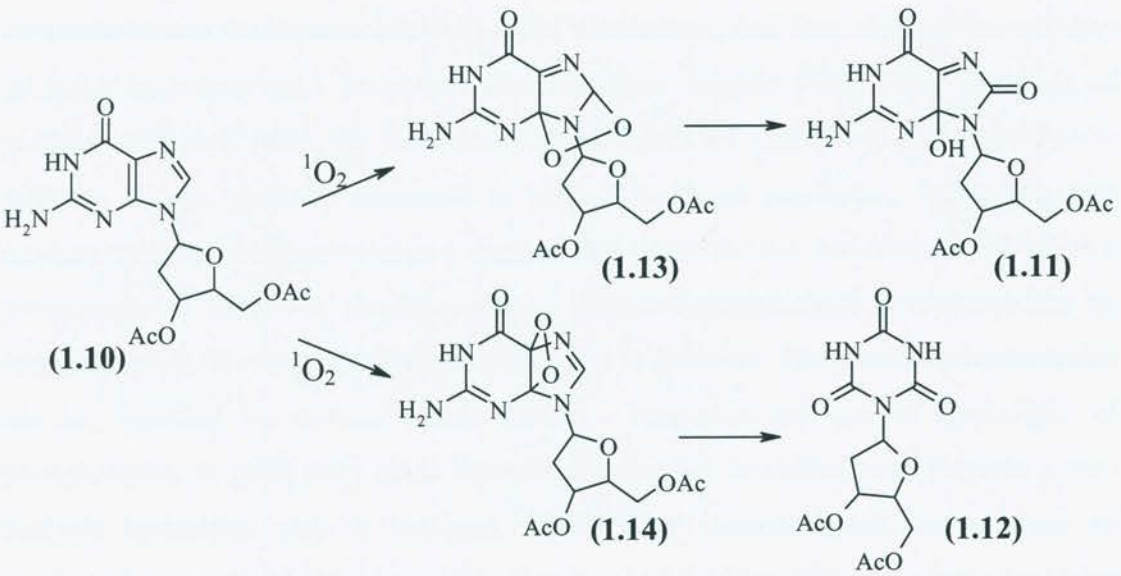

Scheme 1.12: Reactions of a guanosine derivative with $^1O_2$

Sheu and Foote [64] have used low temperature NMR to investigate the reaction further. These authors used the model compound 2',3',5'-*O*-(*tert*-butyldimethylsilyl)-8-methylguanosine and reacted this material with photochemically generated $^1O_2$ at –78 °C. NMR analysis of their reactions allowed the detection of the two diastereoisomeric endoperoxides, analogous to (1.14), which supports the previous results. However, none of the [2+2] cycloaddition product was observed under these conditions [65].

This specificity for reaction at guanine bases is characteristic of $^1O_2$, with other oxidants, notably HO•, reacting with low selectivity [66]. The reaction of $^1O_2$ with guanine yields a specific product 4-hydroxy-8-oxo-guanosine. However, this product is not useful as a diagnostic tool as it can react further to give 8-oxo-7-hydrodeoxyguanosine (also known as 8-hydroxydeoxyguanosine, abbreviated 8-oxodG), which has been detected on oxidation of DNA by a large number of species [67].

1.5.2b $^1O_2$ reactions with lipids and cholesterol

Unsaturated fatty acids react with $^1O_2$ primarily via the ene reaction, and thus yield hydroperoxides. The rate constants for such reactions are relatively low, 1.9 and 1.3 x 10^5 M^{-1} s^{-1} have been reported with the model fatty acid esters methyl linolenate and methyl linoleate respectively [68]. However, the lifetime of $^1O_2$ is extended in the non-aqueous environment found within membranes, and thus such oxidations may be more important than these low rate constants suggest [68]. The spectrum of products obtained from the $^1O_2$-mediated oxidation of membrane phospholipids is different to the products observed in radical-mediated processes, suggesting that product analysis could be used as a mechanistic probe for the involvement of $^1O_2$ in a given process. However, the separation of different phospholipid hydroperoxides by currently available chromatographic techniques is difficult. Fatty acid hydroperoxides can be resolved by reverse phase HPLC. However the use of hydrolysis of phospholipids to yield fatty acids suitable for analysis is disfavoured because a pre-analysis hydrolysis step is required, which may induce significant amounts of artefactual oxidation [69]. Recently, Stratton and Liebler [70] reported a sensitive GC/MS method, which is able to distinguish the products of linoleic acid oxidation (Scheme 1.13).

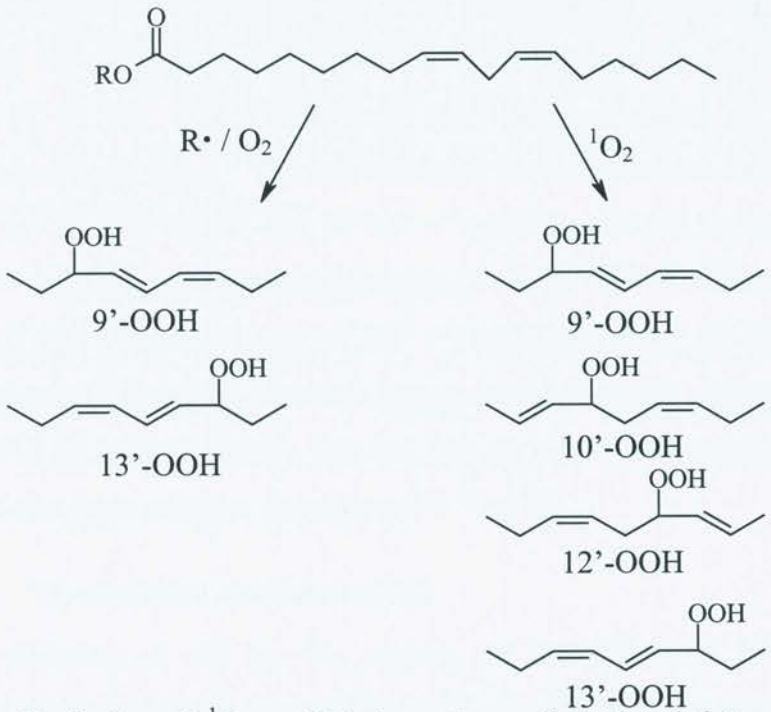

Scheme 1.13: Radical- and $^1O_2$-mediated reactions of linoleoyl fatty acid moieties [70].

Cholesterol is also oxidised by $^1O_2$ to yield hydroperoxide species with a rate constant of 6.7 x 10^4 M^{-1} s^{-1} [71]. Again this reaction yields hydroperoxides distinct from those mediated by radical processes (Scheme 1.14). Cholesterol has found favour as a mechanistic probe of lipid $^1O_2$ oxidation as its products can be readily detected (see Section 1.7.4) [36, 69].

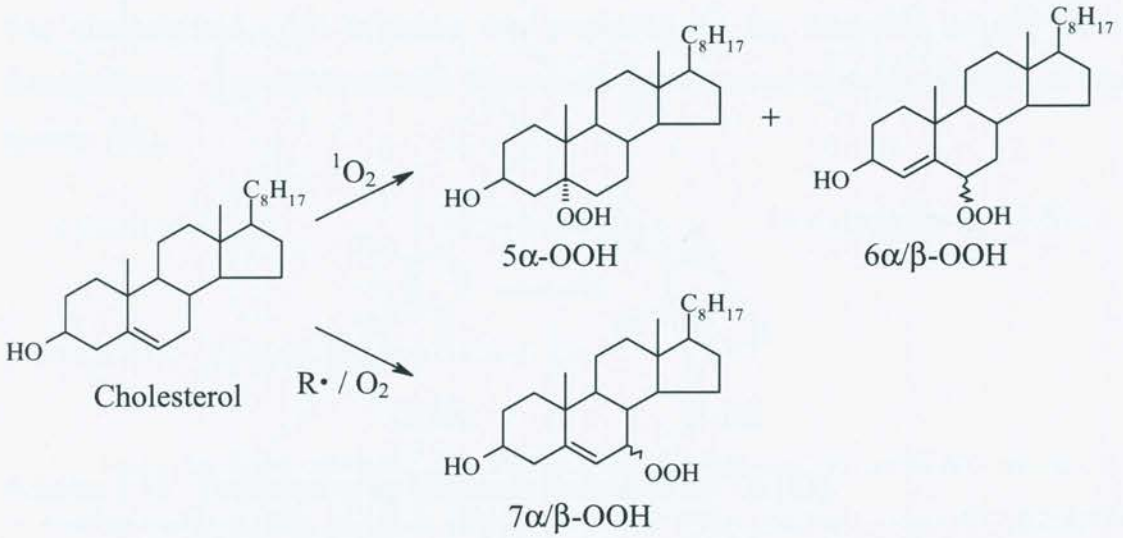

Scheme 1.14: Radical- and $^1O_2$-mediated oxidation products of cholesterol [36, 69].

1.5.2c $^1O_2$ reaction with proteins

The reactions of $^1O_2$ with proteins under physiological conditions are believed to be mediated *via* the oxidation of five amino acids residues, namely His, Trp, Tyr, Met and Cys [3, 10, 72]. These residues all react chemically with $^1O_2$, and Trp also reacts by physical quenching. The rate constants for these reactions are known; His, $k \sim 3.2 \times 10^7$ M^{-1} s^{-1} (pH 7.1), $k \sim 1 \times 10^8$ M^{-1} s^{-1} (pH > 8) and k 0.5 x 10^7 M^{-1} s^{-1} (low pH); Trp k 2-7 x 10^7 M^{-1} s^{-1} (physical quenching) 3 x 10^7 M^{-1} s^{-1} (chemical reaction); Tyr k 0.8 x 10^7 M^{-1} s^{-1}; Met k 1.6 x 10^7 M^{-1} s^{-1}; and Cys k 8.9 x 10^6 M^{-1} s^{-1} [73-80]. Under physiological pH conditions other amino acid side-chains react with $k < 0.7 \times 10^7$ M^{-1} s^{-1} [73]. At high pH, where Lys and Arg are in the deprotonated form, it has been reported that these residues also react with $^1O_2$ [81].

1.5.2c.i $^1O_2$-mediated oxidation of His

The oxidation of His by $^1O_2$ occurs via the formation of at least one endoperoxide species that may arise due to [4+2] cycloaddition reactions. Ryang and Foote [82] used low temperature photo-oxidation and NMR spectroscopy to characterise the initial products of a range of imidazoles, including His. This study

provided the first direct evidence that $^1O_2$-mediated oxidation of these compounds led to the formation of 2,5-endoperoxide products. More recently, similar techniques have been used to characterise the endoperoxide formed on $^1O_2$-mediated oxidation of a His model compound, 4,5-diphenylimidazole (1.15). Using stable isotope labelling and a combination of ^{15}N, ^{13}C and ^1H NMR at –100 °C the 2,5-endoperoxide (1.16) was characterised. No evidence was presented for the formation of any other intermediates. A complex mixture of products was observed on decomposition of this species [83].

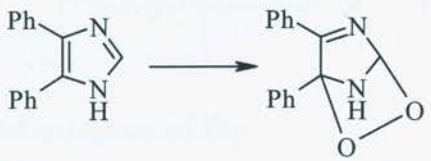

(1.15) **(1.16)**

Scheme 1.15: Oxidation of an imidazole derivative by $^1O_2$ [83].

Earlier studies (e.g. [84, 85]) showed that the initial endoperoxide formation consumed one mole of oxygen per mole of His oxidised, and that the initial endoperoxides could undergo a series of ring opening reactions consuming further oxygen. A complex mixture of products was obtained which included aspartic acid and urea [85]. The formation of these peroxides appears to occur regardless of whether the α-amino group is free or blocked, suggesting that similar reactions could take place on His residues in proteins.

1.5.2c.ii $^1O_2$-mediated oxidation of Trp

Trp is oxidised by $^1O_2$ to yield either a dioxetane across the C2-C3 bond, or a hydroperoxide at the 3 position (1.17) (Scheme 1.16). Further reactions of these intermediates yields *N*-formylkynurenine by cleavage of the C(2)-C(3) bond, or 3a-hydroxypyrroloindole by ring closure [86-91].

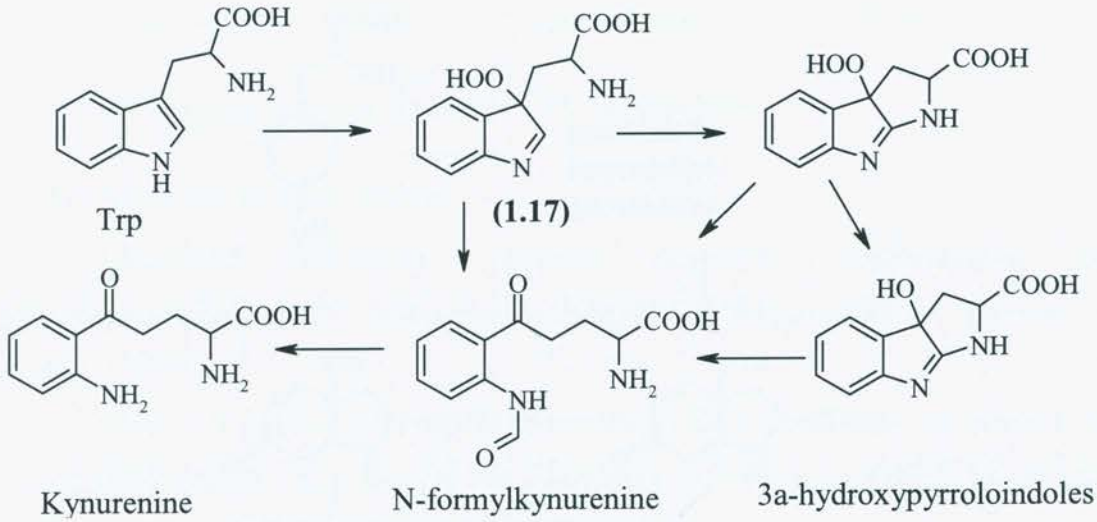

Scheme 1.16: $^1O_2$-mediated oxidation of Trp

Some of these products, i.e. *N*-formylkynurenine and kynurenine, can act as photosensitising agents, and thus the formation of these species *in vivo* may enhance further photo-oxidative processes [92-94].

1.5.2c.iii $^1O_2$-mediated oxidation of Tyr

The $^1O_2$-mediated oxidation of free Tyr has been shown to yield 3a-hydroxy-6-oxo-2,3,3a,6,7,7a-hexahydro-1H-indol-2-carboxylic acid (HOHICA) [95], which can decarboxylate under basic conditions to yield (1.18) (Scheme 1.17) [96]. It is not known whether similar species are formed in proteins, as similar reactions might be disfavoured due to the delocalisation of the α-amino nitrogen lone pair into the peptide bond. The initial intermediates formed are thought to be either endoperoxides or hydroperoxides, although the exact identity of these species has not been elucidated [95, 96].

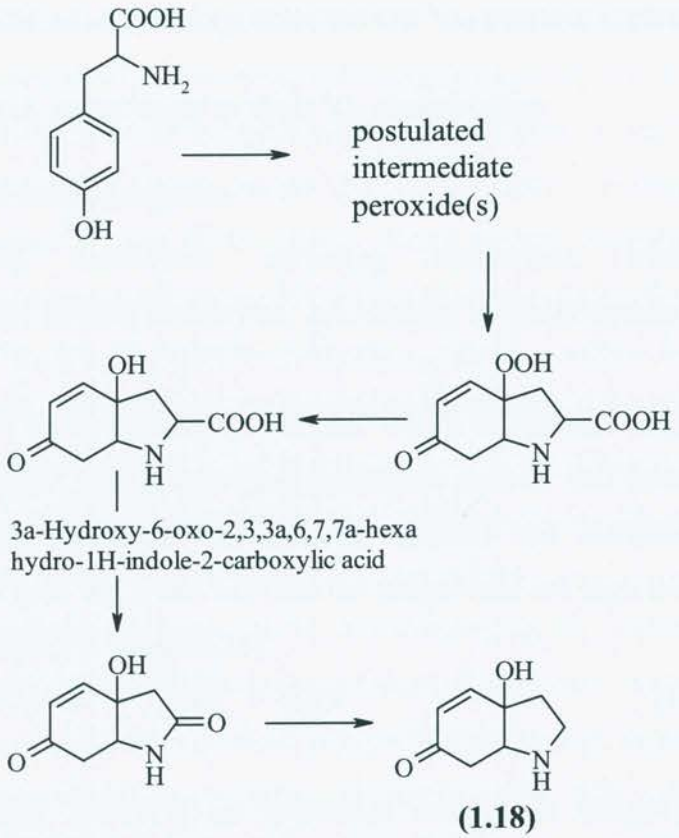

(1.18)

Scheme 1.17: The $^1O_2$-mediated oxidation of free Tyr

1.5.2c.iv $^1O_2$-mediated oxidation of Met

Met is oxidised by $^1O_2$ to yield methionine sulfoxide in a complicated mechanism that involves a zwitterionic intermediate, which undergoes subsequent reaction with the parent amino acid to yield two moles of the sulfoxide [97, 98].

$$R_2S + {}^1O_2 \longrightarrow R_2S^+OO^- \quad (1.39)$$

$$R_2S^+OO^- + R_2S \longrightarrow 2\ R_2S{=}O \quad (1.40)$$

1.5.2d.v $^1O_2$-mediated oxidation of Cys

The reactions of Cys with $^1O_2$ are the least well characterised of the five susceptible amino acids. Reaction of $^1O_2$ with free Cys has been reported to yield the disulfide in a non-quantitative manner [97]. Other products may be formed e.g., cysteic acid, although they have not been characterised. The reaction of protein-bound Cys with $^1O_2$ has not been characterised.

1.6 BIOLOGICAL CONSEQUENCES OF $^1O_2$ PRODUCTION

1.6.1 BENEFICIAL ASPECTS OF IN VIVO $^1O_2$ PRODUCTION

1.6.1a $^1O_2$ in the immune system

Specialised leukocytes, including monocytes, macrophages, and polymorphonuclear (PMN) leukocytes, are capable of phagocytosis (as discussed in Section 1.3.3d).

MPO is a haem-containing enzyme, which is released into the phagosome during phagocytosis. This enzyme has peroxidase activity and functions to generate HOCl from H_2O_2 (produced by NADPH oxidase) and chloride ions. As the concentrations of both H_2O_2 and MPO in the phagosome are high it is expected that a large amount of HOCl is formed [25].

$$H_2O_2 + Cl^- \longrightarrow OCl^- + H_2O \qquad (1.41)$$

Undoubtedly HOCl is an important oxidant in phagocytotic processes. However there are a number of other oxidants that may be produced in the phagosome. These potentially include the highly reactive HO• that could be generated by iron catalysed reduction of the H_2O_2 produced, however the amounts of redox active iron present in the phagosome is not known, and direct evidence for the production of HO• in the phagosome is scarce [25].

The production of $^1O_2$ is also suspected to occur in the phagosome by the reaction of MPO-derived HOCl and NADPH-oxidase-derived H_2O_2. Thus, in isolated MPO reactions chemical trapping studies with 2,5-diphenylfuran (although these traps are not very specific) have suggested the production of $^1O_2$. The effect of D_2O is also consistent with a role for $^1O_2$ [99]. Similar techniques have demonstrated the production of $^1O_2$ by phagocytosing neutrophils (chemical trapping with 9,10-diphenylanthracene) [100], stimulated macrophages (chemical trapping with 9,10-diphenylanthracene) [101] and in activated eosinophils (using near IR 1268 nm spectroscopy) [102]. Recent work by Tatsuzawa *et al.*, has gone as far as suggesting that $^1O_2$ is the principal oxidant in the MPO-mediated killing of bacteria in the phagosome, with the use of wild type *Escherichia coli* (*E. coli*) and lycopene-producing *E. coli*. When these *E. coli* were exposed to activated PMN, the lycopene containing transformants were more resistant to cell death than the wild type [103].

Earlier papers by this same group demonstrated that $^1O_2$ derived from naphthalene endoperoxides could lead to bacterial cell death [104, 105] and that the protection against cell death afforded by lycopene was observed when *E. coli* were exposed to $^1O_2$ and an isolated MPO system but not when either strain of E. coli was exposed to HOCl or the related oxidant HOBr [106]. These authors interpreted this result to mean that $^1O_2$ was responsible for the MPO dependant bacterial killing.

As well as its bactericidal properties, $^1O_2$ is known to be capable of inactivating viruses. Both photochemically- and chemically-generated (thermal decay of naphthalene endoperoxides) $^1O_2$ has been shown to inactivate a range of viruses (e.g. [107-110]), although these studies have concentrated on the important issue of blood product decontamination rather than *in vivo* effects.

Another interesting aspect of $^1O_2$ involvement in the immune system is the recently reported ability of antibodies to generate H_2O_2 when irradiated with UV or visible light [111, 112]. These authors propose that the energy requirement for H_2O_2 production is derived form the oxidation of water by $^1O_2$. The intermediacy of $^1O_2$ was demonstrated by the enhancing effect of D_2O and inhibitory effect of azide on the yield of H_2O_2 and by chemically generating $^1O_2$ in the absence of light. The proposition that the oxidation of water by $^1O_2$ was occurring was confirmed by the use of $H_2{}^{18}O$, and analysing the H_2O_2 produced for ^{18}O incorporation. This result, in combination with theoretical calculations, illustrated that the antibodies were catalysing the oxidation of water, using $^1O_2$ as an intermediate. Whilst this is an interesting finding it has yet to be replicated, and its biological significance has yet to be assessed.

1.6.1b Photodynamic therapy

Photodynamic therapy (PDT) is the term given to treatment of diseased tissues by the administration of a photosensitiser and light. This protocol has recently been used for the treatment of cancer and a range of other non-malignant conditions [113].

In 1900, a French neurologist named Prime, administered eosin (now known to be a photosensitiser) to patients suffering epilepsy. He noted that this treatment induced dermatitis in skin exposed to the sun (reviewed in [114]). This discovery led to the first modern medical application of a topical photosensitiser (eosin) and white light for the treatment of skin cancers, which was performed by von Tappeiner and Jesionek in 1900 [114].

Porphyrins are known to be endogenous photosensitisers, and hematoporphyrin and its derivatives were important molecules in the development of PDT. The first report in humans was by Meyer-Betz in 1913 who parenterally administered 200 mg of hematoporphyrin to himself and subsequently observed prolonged pain and swelling in light exposed areas [114]. In the 1940's it was discovered that porphyrins localised in tumours, which allowed new methods of detecting and treating tumours to be developed.

Since these early studies, significant advances have been made in PDT. Animal studies in the early 1970's demonstrated the effectiveness of hemotoporphyrin derivative against various tumours [115] and in the later 1970's human studies began [116]. Skin cancers, bladder cancers, oesophageal, lung, gynaecological, intra-ocular, brain, head, neck and rectal cancers have all been treated using hematoporphyrin derivative PDT (reviewed in [114]).

A variety of 'second-generation' photo-sensitisers have been developed recently. These aim to increase efficiency and tumour specificity and several are in clinical trials presently, including tin etioporphyrin, lutetium texaphyrin, benzoporphyrin derivative-monoacid ring A, tetra(m-hydroxyphenyl)chlorin and ALA based PDT. This latter PDT agent is the biosynthetic precursor of protoporphyrin IX [113, 114, 117].

Recent advances in laser technology have allowed the use of PDT in the treatment of deep tissues. One major application of this technique is the emergence of photoangioplasty. Along with their tumour localisation properties, hematoporphyrin derivate and Photofrin have also been found to localise in atherosclerotic plaques [118]. The texaphyrin class of compounds have had much greater success in cardiovascular PDT applications, possibly due to more selective uptake and retention of the photosensitisers and to the depth of penetration allowed by the 732 nm light used [118]. This treatment protocol has been shown to be effective in animal studies [118, 119].

1.6.2 Detrimental Aspects of *In Vivo* $^1O_2$ Production

The 'accidental' production of $^1O_2$ *in vivo* is generally a result of photosensitisation reactions. Photosensitising agents, such as porphyrins, flavins, quinones and nicotinamides, are found in the skin [120] and *N*-formylkynurenine [121] and xanthurenic acid [122] in the lens of the eye.

The biochemical consequences of $^1O_2$-mediated protein oxidation generally involve loss of function of the protein involved. Thus, nearly all enzymes investigated so far become inactivated when oxidised by $^1O_2$. Also several peptide hormones (e.g., angiotensin, insulin) exhibit loss of biological function as do some proteinaceous toxins (e.g., botulinum and tetanus toxins) [97]. *In vitro* studies have provided evidence for the formation of high molecular weight protein aggregates on $^1O_2$-mediated oxidation of proteins [123]. Some studies on photo-oxidised proteins have suggested that this cross-linking may be due to the formation of di-Tyr linkages. However, this is likely to be a radical-mediated process [72] as controlled oxidation of lens crystallin proteins by $^1O_2$ does not yield di-Tyr [124].

A series of papers by Shen *et al.*, [125-129] has investigated the photodynamic cross-linking of proteins using model compounds. Their results suggest that cross-links can be formed in dark reactions between a photooxidised residue (e.g. His, Tyr) and another residue (that may be oxidised or not) in another protein molecule.

One biological system in which protein cross-linking is likely to play a major role is cataractogenesis. The major water-soluble protein fractions of the eye lens are the crystallins. These proteins can be cross-linked by $^1O_2$-dependant processes [123, 124]. A detailed study has shown that Trp, Tyr and His residues are oxidised but it appears that only His oxidation is required for cross-link formation [124]. An interesting observation in this study is that the $^1O_2$-induced oxidation of Tyr does not yield DOPA or di-Tyr which are the oxidation products resulting from reaction with HO•. The study also reported that proteins devoid of His residues, such as melittin and bovine pancreatic trypsin inhibitor, do not form high molecular weight aggregates [124]. It is known that the loss of His and Trp residues of proteins correlates with the progressive worsening of the clinical class of cataract [130].

$^1O_2$ has been suggested to be involved with the development of many disease states including skin cancers and cataracts, but has been difficult to prove definitively. Many lines of experimental evidence have used indirect methods to suggest $^1O_2$ involvement in these processes. Recently Yamazaki *et al.*, obtained the first evidence of $^1O_2$ generation *in vivo*, by demonstrating the production of a $^1O_2$ specific cholesterol oxidation product in photo-oxidised rat skin [131]. However, this experiment used an artificial source of $^1O_2$, and as yet there is little direct evidence for $^1O_2$ production in diseased tissues.

1.6.3 $^1O_2$ AS A MODULATOR OF GENE EXPRESSION

The production of $^1O_2$ *in vivo* is known to alter the expression of a range of genes including stress proteins, early response genes, transcription factors, immunomodulatory cytokines and adhesion molecules.

The stress proteins influenced by $^1O_2$ include the heat shock proteins (HSPs), glucose regulated proteins (GRPs) and haem oxygenase-1 (HO-1). The basic heat shock response is common to all cell types and is characterised by the increased expression of specific HSPs. HSPs act as chaperone proteins that stabilise newly synthesised proteins and help repair partially denatured cell proteins [20, 132]. The induction of HSPs in response to photodynamically generated $^1O_2$ has been studied in a murine cell line [133]. Three different photosensitising agents with different subcellular localisation properties were used to demonstrate that the actual site of $^1O_2$ within the cell was important in eliciting the HSP response. Thus, photofrin II, which localises in mitochondria did not induce the HSP response, but two other photosensitisers, mono-L-asparyl-chlorin and tin etiopurpurin, which localise in the lysosomes, dramatically increased levels of HSP-70 mRNA [133].

The GRPs are another of the stress proteins that can be induced by $^1O_2$. Following cellular stress the GRPs are thought to bind and sequester improperly glycosylated, mal-folded or incompletely processed proteins in the endoplasmic reticulum [134, 135]. Photosensitised production of $^1O_2$ in a number of cell types induces a number of GRPs, with this again depending on photosensitiser localisation [136].

HO-1 is a stress protein that is upregulated by a range of cell stresses including $^1O_2$ [136]. This gene is strongly induced by UVA irradiation, and the role of $^1O_2$ in this process has been demonstrated by the use of D_2O and azide. Interestingly scavengers of other ROS, such as mannitol and dimethyl sulfoxide, had no effect on HO-1 induction [137]. The role of $^1O_2$ has been further investigated using efficient $^1O_2$ photosensitisers, such as RB [137].

The nuclear transcription factor oncogenes, *fos*, *jun* and *myc*, are also known as early response genes, as their transcriptional rate increases very rapidly when cells are stimulated by growth factors [20]. The products of these genes function as critical regulators of cell growth and differentiation, therefore mutations in these genes are likely to lead to cancerous states, hence the designation oncogene [20]. Photo-

generated $^1O_2$ has been shown to induce the accumulation of *fos* and *jun* mRNA in murine and human cell lines [138, 139].

Activator protein-2 (AP-2) is another of the nuclear transcription factors induced by $^1O_2$ production. AP-2 activation has been studied in cultured human keratinocytes exposed to UVA. The oxidant responsible for its activation was reported to be $^1O_2$, via the use of D_2O, azide and thermal decomposition of naphthalene endoperoxides. The activation of this factor by $^1O_2$ is thought to initiate a signalling cascade that is responsible for the induction of genes such as intercellular adhesion molecule-1 (ICAM-1) and HO-1 [21, 140].

The induction of mitogen-activated protein kinases (MAP kinases) by $^1O_2$ has also been investigated using both photochemically and thermally (naphthalene endoperoxide) generated $^1O_2$ [141, 142]. These studies, which used human skin fibroblasts, demonstrated that $^1O_2$ generated intracellularly activated p38 and c-Jun-N-terminal kinase (JNK), but not extracellular signal-regulated kinases (ERK). This pattern of gene activation was found to be reminiscent of that produced by UVA, but different to that produced by other UV radiation, suggesting that $^1O_2$ is the major species responsible for UVA induced gene activation [141, 142]. Various other cytokines, such as interleukins 1, 1β, 6 are also upregulated by $^1O_2$ [143].

1.6.4 The $^1O_2$-Mediated Induction of Apoptosis

Apoptosis is a strictly controlled process of programmed cell death, in which the cell becomes condensed and is then rapidly phagocytosed. It is distinguished from necrosis, the other form of cell death by this 'neat' method of death [20].

The intracellular generation of $^1O_2$ is known to bring about cell death [144]. Recent studies, mainly of PDT agents, have demonstrated that apoptosis is induced by the production of $^1O_2$ and is a major route to cell death [145]. Early studies of photodynamic induction of apoptosis showed that damage to mitochondria was important in this process and the loss of mitochondrial membrane potential, release of cytochrome *c* into the cytosol and the activation of caspase-3 were observed [146]. More recently it has been established that one of the earliest detectable effects of PDT is the selective loss of the anti-apoptotic protein bcl-2, however the pro-apoptotic protein bax is undamaged. The increased ratio of bax to bcl-2 is thought to promote apoptosis [147]. This effect was found to be common to many cell lines and may involve the cross linking of bcl-2 to other proteins [147].

1.7 BIOMARKERS OF OXIDATIVE STRESS

1.7.1 MARKERS OF LIPID AND CHOLESTEROL OXIDATION

Of the biochemical reactions of ROS, the peroxidation of lipids is probably the most extensively studied. Polyunsaturated fatty acids (PUFA) are highly susceptible to radical attack, due to the ease of abstraction of bis-allylic hydrogens by radicals and initiation of chain reactions, as discussed in section 1.3.4b. Stable products arising from lipid peroxidation include alkanes and carbonyl compounds [35].

The alkane products are generally volatile and excreted from the body in the breath. Animal studies have shown that ethene, propane, *n*-butane, *iso*-pentane, and *iso*-butane can all be analysed when exhaled by rats [148]. As the ω-3 and ω-6 PUFA are the most abundant in cell membranes, ethane and pentane are the most used of the volatile hydrocarbons for investigating lipid peroxidation. These markers have also been investigated in human subjects. For example exercise, cigarette smoking, liver diseases, cystic fibrosis, inflammatory diseases, acute myocardial infarction, Alzheimer's disease and asthma induced significant increases in one or both of these markers [35].

The F_2-isoprostanes can also be used as a marker of lipid peroxidation. These prostaglandin-like compounds are formed *in situ* by radical-mediated peroxidation of esterified arachidonic acid and subsequently released in free form, possibly by the action of phospholipases. Both gas chromatography-mass spectrometry (GC-MS) and immunological assays have been developed, but both methods require extensive sample preparation and thus the use of isoprostanes as a marker of oxidative stress is not widespread as yet. A number of *in vitro*, animal and human studies have demonstrated the potential of this technique. Thus, low density lipoprotein (LDL) treated with peroxyl radicals or peroxynitrite releases F_2-isoprostanes [149-151], and plasma levels of both free and esterified F_2-isoprostanes were found to be elevated in smokers [152].

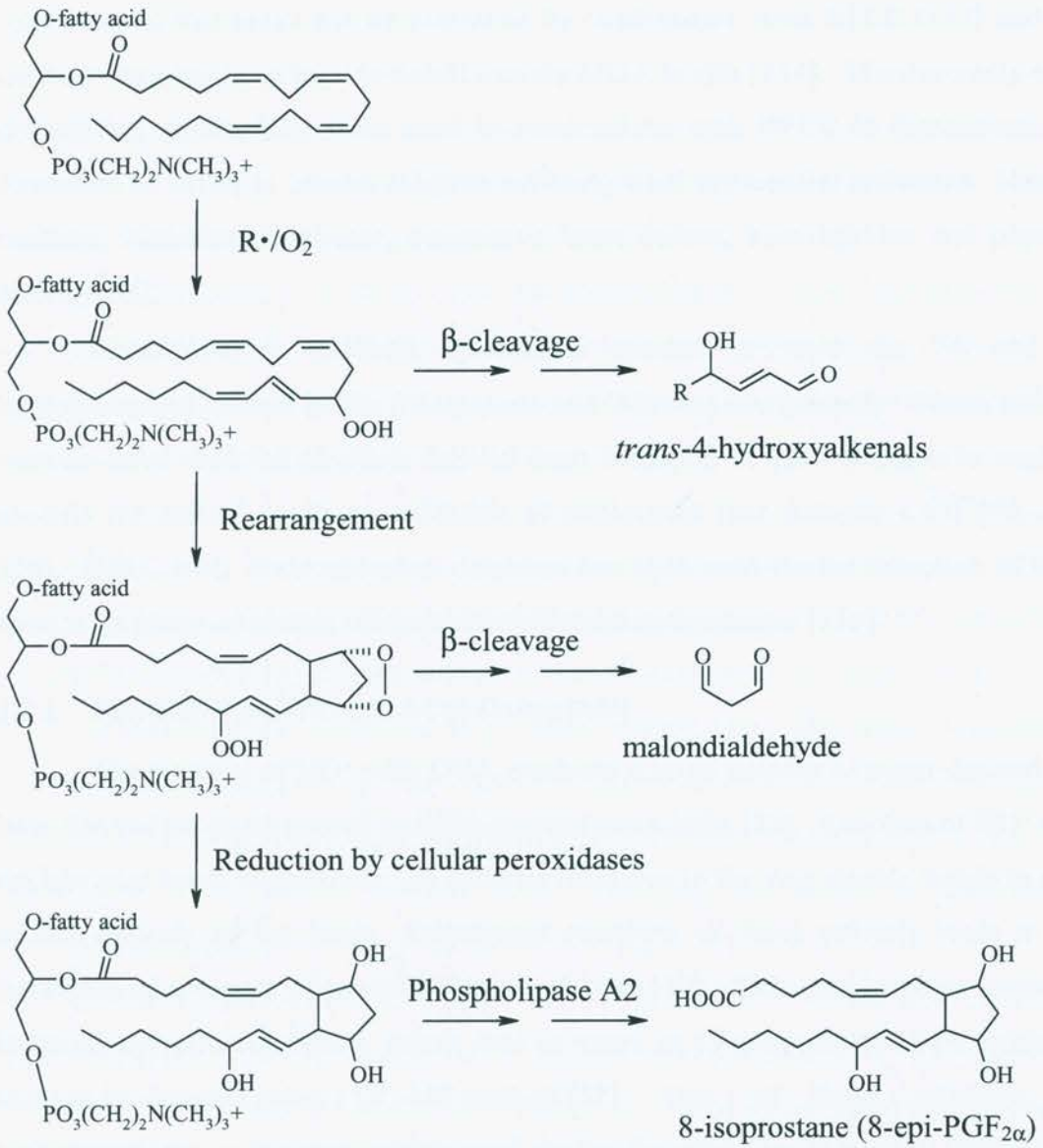

Scheme 1.18: The formation of isoprostanes on radical-mediated oxidation of lipids [35].

Aldehydic products are also produced on oxidation of fatty acids by scission, rearrangement and oxidation reactions. The major carbonyls produced by peroxidation of ω-6 fatty acids are hexanal and 4-hydroxy-2,3-*trans*-nonenal; ω-3 fatty acids produce propanol and 4-hydroxy-2,3-*trans*-hexenal [35]. The most widely used index of lipid peroxidation is the formation of malondialdehyde (MDA), which is often assayed for using the thiobarbituric acid assay. This is not a specific assay for MDA as a number of other compounds react with thiobarbituric acid, thus the results are usually expressed as thiobarbituric acid reactive substances (TBARS). The

selectivity of this assay can be improved by combination with HPLC [153] and this methodology has been used to detect urinary MDA in rats [154]. More recently other derivatising agents have been used in combination with HPLC to demonstrate the formation of MDA in human subjects suffering from myocardial infarction, diabetes mellitus, Alzheimer's disease, congestive heart failure, burn injuries and physical activity [35].

Cholesterol is oxidised by radical species to yield the 7α and 7β hydroperoxides as well as the 5,6-epoxide and 7-ketone compounds. Girotti and co-workers have used the products derived from oxidation at the 7 position as markers specific for radical mediated oxidation of cholesterol (see Scheme 1.15) [69, 155, 156]. HPLC with electrochemical detection has been used for the detection of these species on photo-oxidation of cholesterol containing liposomes [156].

1.7.2 Markers of Nucleic Acid Oxidation

The reaction of HO• with DNA produces a large number of sugar-derived and base-derived products as well as DNA-protein cross-links [32]. Reaction of HO• with nucleic acid bases is generally via addition reactions to the ring double bonds to give adduct radicals of the bases. Subsequent reactions of these radicals leads to the formation of a variety of products form each base [32]. This area has been explored in detail and a recent review article lists as many as 17 products of DNA oxidation that can be detected using a GC-MS method [32]. One of these products, 8-hydroxyguanine, is the most widely used marker for oxidative damage to DNA [157]. This product may have particular *in vivo* relevance as it is known to be mutagenic and its importance is underscored by the existence of cellular repair mechanisms for this lesion. A variety of highly sensitive assay have been developed for the detection of this product [158].

1.7.3 Markers of Protein Oxidation

Reactions of a variety of ROS with proteins are known to generate alterations to the protein backbone as well as the amino acid side-chains. The latter can act as markers of oxidant damage to proteins. The formation of protein carbonyls has been used as a general marker for oxidative damage to proteins [159]. These species have been observed to be elevated under conditions of *in vitro* oxidative stress, including exposure to iron/ascorbate [160], ionising radiation [159], $^1O_2$ [161] and ozone [162].

The carbonyl compounds formed can be assayed spectrophotometrically at 370 nm, after derivatisation with 2,4-dinitrophenylhydrazine (DNPH). It has also been found that the 2,4-dinitrophenyl (DNP) derivatives of carbonyls are immunogenic and that anti-DNP antibodies can be used for detection of protein carbonyls by Western blotting [163] and ELISA (enzyme linked immunosorbent assay) [164].

As discussed in Section 1.3.4 the reaction of HO• with both aliphatic and aromatic amino acid side-chains yields initial carbon-centred radicals formed by hydrogen abstraction, which react with oxygen to yield peroxyl radicals, hydroperoxides and alcohols [3, 4]. The peroxides formed by these reactions are not suitable as markers as they are unstable, but the alcohols derived from them have, in some cases, been characterised and used as markers of oxidative protein damage. Thus, products of Leu [165], Val [166] and Lys [167] have been detected in atherosclerotic plaques and cataractous lens at elevated levels (reviewed in [4]).

Products of the oxidation of aromatic residues have also been characterised with species such as *ortho*-Tyr and *meta*-Tyr observed on HO•-mediated oxidation of Phe, and DOPA and di-Tyr from oxidation of Tyr residues. These products have been observed in a number of human tissues, including atherosclerotic plaques and cataractous lenses [168-171].

Protein oxidation products generated by other ROS have also been identified. Thus 3-chloroTyr has been suggested as being a specific marker for HOCl-mediated protein oxidation, and 3-nitroTyr is believed to derive from protein oxidation by peroxynitrite and other nitrating species [4].

1.7.4 Markers Specific for $^1O_2$-Mediated Oxidation

The products of cholesterol oxidation by radical-mediated processes can be distinguished from those of $^1O_2$-mediated oxidation using thin layer chromatography (TLC) or HPLC with mercury cathode electrochemical detection [36]. Cholesterol has found favour as a mechanistic probe of lipid $^1O_2$ oxidation as it is a discrete chemical species and thus has a relatively simple product spectrum and does not require pre-analysis hydrolysis [36, 69]. The 5α-hydroperoxide of cholesterol is formed approximately 5 fold faster than the 6-hydroperoxides on reaction with $^1O_2$, and so it is the species generally employed as a $^1O_2$-marker. However, the slow rate of reaction of cholesterol with $^1O_2$, and the potential for rearrangement reactions of 5α-hydroperoxide to yield the 7-hydroperoxy products may be a problem associated with

this technique. Sensitive analytical techniques such as HPLC with radiometric detection or electrochemical detection may overcome the slow reactions, and the rearrangement reaction occurs at insignificant levels if the overall cholesterol loss is less than 5 %, a level that is generally the case experimentally [69]. Regardless of this the 5α-hydroperoxide of cholesterol was recently detected in the skin of rats treated with a photochemical $^1O_2$ generating system, providing the first documented direct evidence of $^1O_2$ production *in vivo* [131].

The oxidation of DNA by $^1O_2$ was discussed in section 1.5.2a. It is known that $^1O_2$ is unique in reacting with guanine bases exclusively, however other oxidants will also react with guanine. The most widely used marker for DNA oxidation is derived from this base, thus few studies that demonstrate specific $^1O_2$ oxidation have been performed. The detection of $^1O_2$ damage by monitoring the formation of 8-oxodG is complicated by the fact that this material is at least 50-times more susceptible to $^1O_2$-mediated oxidation than the parent 2'-deoxyguanosine [65]. Although this non-specificity suggests that it may not be $^1O_2$ that is responsible for the observed formation of 8-oxodG, it has recently been proven that $^1O_2$ can lead to the formation of this modified base, using an ^{18}O-labelled naphthalene endoperoxide as an intracellular source of isotope labelled $^1O_2$. An HPLC-MS/MS assay was used to demonstrate that the 8-oxodG formed also contained ^{18}O.

Currently there are no similar biomarkers for $^1O_2$-induced protein oxidation. The only assay that specifically demonstrates $^1O_2$-mediated protein oxidation is that reported by Lledias *et al.*, [172, 173] which shows that the oxidation of catalase by $^1O_2$ leads to different electrophoretic behaviour of this enzyme, which maintains its activity. These authors have suggested that similar experiments could be used to demonstrate the generation of $^1O_2$ *in vivo*.

1.8 THE AIMS OF THIS STUDY AND OUTLINE OF THIS THESIS

The investigations detailed in this thesis were performed to determine the effects of $^1O_2$ on free amino acids, peptides and on isolated and intracellular proteins. The reactions of Tyr with this activated state of oxygen were studied in detail and preliminary investigations into the $^1O_2$-mediated oxidation of His are also reported. The materials and methods employed throughout this thesis are detailed in chapter 2.

Initial studies aimed to chemically identify the intermediate products of free Tyr oxidation by $^1O_2$ (Chapter 3). It has been previously suggested that peroxides are

formed on Tyr oxidation by $^1O_2$ [95]. Thus, these experiments set out to characterise such intermediates, as well as radical species formed by the one-electron reduction of the peroxides. These studies were extended to the examination of similar reactions of Tyr residues in peptides and proteins (Chapter 4). Knowledge of the intermediates formed on $^1O_2$-mediated oxidation of Tyr suggested that some of the intermediate species would be susceptible to nucleophilic attack. Such reactions were investigated using both amine and thiol nucleophiles (Chapter 5).

$^1O_2$ is believed to be produced by activated cells of the immune system and to have cytotoxic properties. Thus, the effect of intracellularly generated $^1O_2$ on cell viability was also investigated (Chapter 6). Recently it has been shown that intracellular generation of peroxyl radicals leads to the formation of protein-derived peroxides. As $^1O_2$ is known to be generated *in vivo* and react with proteins at high rates, the formation of protein-derived peroxides on intracellular generation of $^1O_2$ and its relationship to cell viability was investigated (Chapter 6).

Preliminary results of investigations in to the $^1O_2$-mediated oxidation of His are presented in Chapter 7 and a general discussion of the results obtained is given in Chapter 8.

CHAPTER 2 - GENERAL MATERIALS AND METHODS

2.1 GENERAL INFORMATION

This chapter contains details of general materials and methods used throughout this thesis. Specific protocols and alterations are detailed in the text and relevant figure legends. All concentrations stated in the text are final concentrations unless otherwise stated.

2.2 MATERIALS

All chemicals and solvents used throughout this thesis were HPLC, ACS or AR grades and purchased from Mallinckrodt (St Louis, MO, USA), Sigma / Aldrich (St Louis, MO, USA), Merck (Darmstadt, Germany), EMScience (Gibbstown, NY, USA) or ICN (Cost Mesa, CA, USA).

The water used in all aqueous solutions and buffers was purified with a four stage Milli Q system (Millipore-Waters, Australia) equipped with a 0.2 μm pore size final filter. The pH of solutions were measured with a digital pH meter made by Hanna Instruments (Portugal) calibrated using pH 4.01, 7.00 and 10.00 standards (ICN, Costa Mesa, CA, USA).

L-Tyr, 3-(4-hydroxyphenyl)propionic acid (HPPA), *N*-acetyl Tyr, Gly-Gly-Gly, BSA, catalase, sodium molybdate, bovine γ-globulins, histone H1, sodium perchlorate and Xylenol Orange (3,3'-bis[N,N-di(carboxymethyl)-aminomethyl]-o-cresolsulfone-phthalein) were purchased from Sigma (St Louis, MO, USA). Deuterium oxide, rose bengal, were from Aldrich (St Louis, MO, USA). Gly-Tyr-Gly was obtained from Bachem (Budendorf, Switzerland). Hydrogen peroxide (30 % w/v solution) was obtained from BDH (Poole, Dorset, UK). The stable isotope labelled Tyr models, (3,5-ring-d_2)-Tyr and C(3)-d_2-Tyr were purchased from CDN (Pointe-Claire, Canada). (2,3,5,6-ring-d_4)-Tyr was supplied by Cambridge Isotope Labs (Andover, Mass, USA). Pronase (a mixture of non-specific proteases from *Streptomyces griseus*; 7000 units g^{-1}) was obtained from Roche (Mannheim, Germany).

The spin traps 2-methyl-2-nitrosopropane (MNP) and 5,5-dimethyl-1-pyrroline *N*-oxide (DMPO) were obtained from Sigma (St Louis, MO, USA). DMPO could not be used as supplied due to EPR active contaminants, thus it was purified prior to use by treatment with activated charcoal for 30 min with stirring at 4 °C in the absence of light. The charcoal was removed by filtration and the purified DMPO

stored in aliquots at – 20 °C. 3,5-dibromo-4-nitrosobenzenesulfonic acid (DBNBS) was synthesised as described previously [174].

2.3 METHODS

2.3.1 ROSE BENGAL PHOTO-OXIDATION OF AMINO ACIDS, PEPTIDES AND PROTEINS

2.5 mM solutions of substrates were prepared in water or deuterium oxide at pH / pD ca. 7. The solutions were neutralised, when necessary, with NaOH or NaOD. Solutions were photolysed, at a distance of 5 cm, using light from a Kodak S-AV 2050 slide projector (250 W bulb) filtered through a 345 nm cut-off filter. Samples contained 10 μM rose bengal (RB), were bubbled constantly with compressed air or oxygen, and were maintained at 4 °C. Sodium azide (5 mM) was added when stated. All samples were immediately treated post-photolysis with catalase (3150 units mL^{-1}, 10 mins, 22 °C) to remove photo-generated H_2O_2. This treatment has been reported previously to have no effect on the yield of organic peroxides [175].

In some experiments the removal of RB after photolysis was achieved by passage through an Acrodisc Syringe Filter (Pall Gelman) with a 0.2 μm Supor membrane; RB binds avidly to such membranes. Removal of the sensitiser was confirmed by visible spectroscopy.

2.3.2 MOLYBDATE CATALYSED DISPROPORTIONATION OF H_2O_2

2.5 mM solutions of substrate were prepared in 12.5 mM aqueous solution of Na_2MoO_4. Aliquots (60 μL) of 30 % H_2O_2 were added at 0, 1 and 10 minutes, to give a final H_2O_2 concentration of 0.31 M, and the reaction allowed to proceed for 30 minutes.

2.3.3 THERMOLYSIS OF 1',4'-ENDOPEROXIDE OF 3-(4'-METHYL-1'-NAPHTHYL)PROPIONIC ACID

2.3.3a Synthesis of 3-(4'-methyl-1'-naphthyl)propionic acid

The preparation of 3-(4'-methyl-1'-naphthyl)propionic acid was performed using published procedures [176]. A brief summary is included below.

2-(4-methyl-1-naphthylmethyl)malonic acid diethyl ester

Diethyl malonate (6 mL, 39.5 mmol, from Aldrich, St Louis, MO, USA) was added to a solution containing sodium metal (0.51 g, 22.2 mmol, from Aldrich, St Louis, MO, USA) in super dry ethanol (15 mL). This mixture was heated at reflux for 7 h following the addition of 1-chloromethyl-4-methylnaphthalene (2.5 g, 13.1 mmol, from Transworld Chemicals, Rockville, MD, USA). Water (5 mL) was added and the mixture extracted with diethyl ether. The ether extract was washed with 0.5 M sodium bicarbonate and 1 M HCl. The solution was concentrated to a volume of 10 mL on a low heat and unreacted diethyl malonate was removed by vacuum distillation at an internal pressure of 20 mbar. This resulted in the isolation of a thick yellow oil, which was carried through to the next stage without further purification.

2-(4-methyl-1-naphthylmethyl)malonic acid

The oil isolated in the previous section was dissolved in methanol (5 mL). 6 M sodium hydroxide (15 mL) was added and the mixture was heated at reflux for 2.5 h. The solution was then neutralised with 1 M HCl, and then concentrated HCl was added to the heated solution until precipitate formation was observed. Solvent was removed by filtration to yield 2-(4-methyl-1-naphthylmethyl)malonic acid (crude yield 1.5507 g, 6.86 mmol, 52 % for the above two steps).

3-(4-methyl-1-naphthyl)propionic acid

On heating 2-(4-methyl-1-naphthylmethyl)malonic acid (1.02 g, 4.5 mmol) with a heat gun, the solid melted and a gas was evolved. Heating was continued until the evolution of this gas ceased (15 min). The resulting brown solid was recrystallised from toluene to yield 3-(4-methyl-1-naphthyl)propionic acid as an off-white solid (0.7438 g, 3.5 mmol, 78 % yield). Synthesis of the desired product was confirmed using NMR, MS and UV analysis.

2.3.3b Synthesis of the 1',4'-endoperoxide of 3-(4-methyl-1-naphthyl)propionic acid

6 M sodium hydroxide was added to a suspension of 3-(4-methyl-1-naphthyl)propionic acid (8.1 mg, 38 μmol) and rose bengal (150 μmol) in water, until the starting material dissolved (pH ~ 12). Compressed air was bubbled through this solution, which was maintained at 4 °C. This solution was exposed to visible light from a Kodak S-AV 2050 slide projector (250 W bulb) filtered through a 345 nm cut-

off filter for 30 min. At intervals, samples of the reaction mixture were neutralised in borate buffer, then treated with catalase (3150 units mL^{-1}) and analysed for peroxide using the FOX assay. Generally approximately 2 mM peroxide was generated by this method, a yield of 80 %. This material was synthesised fresh for each experiment to ensure maximum peroxide yield. On incubation at 37 °C essentially all peroxide had decayed after 4 hr.

2.3.3c Use of the 1',4'-endoperoxide of 3-(4-methyl-1-naphthyl)propionic acid as a $^1O_2$ source

Tyr oxidation by this system was investigated using 0.5 mM and 1 mM substrate, which were incubated with 1 mM endoperoxide at 37 °C, pH 7.4 (borate buffer) for 24 h. BSA oxidation was investigated using 15 μM BSA and 2.5 mM naphthalene endoperoxide under the same incubation conditions.

2.3.4 Peroxide Quantification Methods

2.3.4a $FeSO_4$ / xylenol orange assay (FOX assay)

A modified version of the FOX assay reported previously [177-179] was used for the estimation of peroxide concentrations. The basis of this assay is the oxidation of Fe^{2+} to Fe^{3+}, by peroxides, in acidic solution. Fe^{3+} forms a complex with xylenol orange that can be determined spectrophotometrically at 560 nm. The reaction is initiated by addition of 50 μL of FOX reagent to 1 mL of sample. The FOX reagent consisted of 5 mM $FeSO_4$ and 2 mM xylenol orange in 0.5 M H_2SO_4. After addition of the reagent to the sample the mixtures were incubated in the absence of light for 30 min at room temperature, prior to the measurement of absorbances at 560 nm. Peroxide concentrations were calculated by comparison with a H_2O_2 (0 - 30 μM) standard curve that was prepared separately for each analysis.

The procedure for measuring peroxides derived from intracellular $^1O_2$ generation, differed slightly as the FOX reagent contained 5 mM $FeSO_4$ and 5 mM xylenol orange in 25 mM H_2SO_4 [180].

The FOX assay is a technically simple assay to perform, however the stoichiometry of the reaction varies between different peroxides. Thus, it is advantageous to calibrate this assay using another of fixed stoichiometry such as the manual iodometric assay.

2.3.4b Manual Iodometric Assay

In some cases peroxide concentrations were also determined using the manual iodometric assay as previously published [181]. The basis of this assay is the oxidation of iodide (I^-) by a peroxide to form iodine (I_2). Under acidic conditions in the presence of excess I^- the I_2 is converted to tri-iodide (I_3^-). The I_3^- is then measured spectrophotometrically at 358 nm. Samples were contained in glass HPLC vials sealed with screw caps fitted with Teflon septa. All samples were kept on ice and continuously de-oxygenated by bubbling with oxygen-free nitrogen. The reaction was initiated by the addition of 1 mL of deoxygenated 5 % (w/v) KI in methanol/acetic acid (2:1 v/v) to 200 µL of sample. The sample vials were then sealed under nitrogen and incubated in the dark at 50 °C for 15 min. After incubation 100 µL of ice-cold cadmium acetate (8 % w/v) in aqueous methanol (50 % v/v) was added to each sample to stabilise colour development, the absorbances at 358 nm were determined and compared to a H_2O_2 standard curve. As the iodide ion reacts with all peroxides with 1:1 stoichiometry, it was therefore possible to directly compare the peroxide of interest with a readily available standard peroxide such as H_2O_2.

2.3.5 Bicinchoninic Acid Assay for Protein Quantification

Protein concentrations were determined using the Bicinchoninic acid (BCA) assay as described by Smith *et al.*, [182] and Walker [183]. This assay is based on the reduction of Cu^{2+} to Cu^+ by proteins under alkaline conditions. BCA is a highly specific chromogenic reagent for Cu^+, and forms a complex that can be analysed at 562 nm. The absorbance at this wavelength is directly proportional to the protein concentration.

The assay was performed by addition of 1 mL of BCA reagent to 50 µL of sample. BCA reagent is prepared fresh daily by the mixing of 50 parts the commercially available BCA solution A (obtained from Pierce) with 1 part BCA solution B (4 % w/v $CuSO_4$). The samples were then incubated at 37 °C for 30 min and then absorbance at 562 nm was determined. The protein concentration was determined by comparison with a standard curve constructed with the protein of interest (e.g. BSA or histone H1) (0 – 1 mg mL^{-1}).

2.3.6 Chemical Modification of Protein Tyr Residues

Tyr residues on histone H1 were modified by iodination as described by Means and Feeny [184]. Histone H1 (100 mg) was reacted with iodine (9.5 mM) in the presence of potassium iodide (45 mM) at pH 9.4 (borate/carbonate buffer) and 4 °C. The reaction was allowed to proceed for 15 min after which unreacted iodine and potassium iodide were removed from the reaction mixture by dialysis against water. The extent of blocking was determined by measurement of absorbance at 312 nm.

2.3.7 Liquid Scintillation Counting

^{14}C-U-Tyr (specific activity 50 μCi mL^{-1}) was obtained from Amersham Pharmacia biotech (Sydney, Australia). All procedures involving radioactive compounds were performed whilst wearing suitable personal protective equipment and using aerosol resistant pipette tips (Molecular Bioproducts, San Diego, CA, USA). All wastes were disposed of appropriately.

^{14}C-labelled Tyr peroxides were used to investigate the binding of $^1O_2$-oxidised Tyr to proteins. Unlabelled Tyr (2.5 mM) with an additional 5.5 nmol of ^{14}C-labelled Tyr was RB photo-oxidised as described in section 2.3.1. Samples were then incubated with histone H1 (235 μM) for 24 h at 37 °C. After incubation samples were diluted to 1 mL final volume with water and TCA was added (10 % w/v) to precipitate the protein. These samples were incubated on ice for 30 min prior to centrifugation (10 000 g, 5 min). The protein pellets formed were washed with 1 mL of an ethanol-ether mixture (1:1, v/v) to remove TCA and resuspended in phosphate buffer (0.1 M, 200 μL, pH 7.4). The scintillant (5 mL, Ultima gold from Packard Instruments Company, Meriden, CT, USA) was added and the solutions mixed thoroughly. The amount of protein-bound radiolabel in each sample was determined using a Tri-Carb 2100TR liquid scintillation analyser (Packard Instruments Company, Meriden, CT, USA).

2.3.8 Cell Culture Methods

THP-1 cells, a human monocyte-like cell line, were cultured in RPMI-1640 medium (Gibco BRL, Life Technologies, Melbourne, Australia), with the addition of 10 % foetal calf serum (Gibco BRL, Life Technologies, Melbourne, Australia), 2 mM

L-glutamine (Trace Scientific, Melbourne, Australia), 100 I.U. mL^{-1} penicillin and 100 $\mu g\ mL^{-1}$ streptomycin (Sigma, St Louis, MO, USA), at 37 °C in 5 % CO_2.

Cells were prepared for experiments by washing twice with Hank's balanced salt solution (phenol-red free HBSS was used throughout, Sigma, St Louis, MO, USA). They were then incubated with HBSS containing 5 μM RB for 30 min at 37 °C in 5 % CO_2, in the absence of light. Non-RB containing control cells were treated with HBSS alone. The cells were then washed twice with HBSS, to remove extracellular RB, and resuspended in HBSS at a concentration of 4×10^6 cells mL^{-1}.

Photolyses were performed in 6 well plates with 2 mL of cell suspension per well. The light source used was a 40 W tungsten filament lamp, filtered through a 345 nm cut-off filter, which was positioned 5 cm distant from the cell suspensions. The illuminations were carried out at 4 °C, for up to 20 min.

2.3.8a Estimation of cellular viability

2.3.8a.i Ethidium Bromide release assay

Cell death was estimated by measuring the release of DNA into the medium, as a percentage of total DNA in the same number of intact cells after lysis with triton X-100, using ethidium bromide, as reported by Hawkins *et al.*, [185]. After photolysis a sample of cell suspension was taken and diluted to 2×10^6 cells mL^{-1} with HBSS. Cells were pelleted by centrifugation (5 min at 800 g). The supernatant was transferred to a clean tube and the cell pellet was lysed by addition of 1 mL of 1 % triton X-100 (Sigma, St Louis, MO, USA). 10 μL of 2.5 mM ethidium bromide was added to both supernatant and lysate samples and the fluorescence at λ_{ex} 360 nm and λ_{em} 580 nm recorded. Appropriate blanks (HBSS or triton) were subtracted and the cell death was calculated using the equation;

$$\%\,Viability = 100 - \left\{ \left[\frac{(sample - HBSS\ blank)}{(lysate - Triton\ blank)} \right] x100 \right\}$$

2.3.8a.ii Lactate dehydrogenase release assay

Initial experiments estimated cell death by monitoring the release of lactate dehydrogenase into the cell media as a percentage of the total LDH activity in the system. LDH catalyses the reduction of pyruvate to lactate using NADH as a co-factor. The substrate is added in excess so that the enzyme is the limiting reagent

and the rate of NADH loss (monitored at 340 nm) is proportional to the amount of enzyme present.

After photolysis a sample of cell suspension was taken and diluted to 1 x 10^6 cells mL^{-1} with HBSS. Cells were pelleted by centrifugation (5 min at 800 g). The supernatant was transferred to a clean tube and the cell pellet was lysed by addition of 1 mL of 0.1 % triton X-100. The LDH-catalysed reaction was initiated by addition of 200 µL of a solution containing NADH (0.15 mg mL^{-1}) and sodium pyruvate (2.5 mM) to 10 µL of both supernatant and cell lysate samples, in a 96-well plate. The absorbance at 340 nm was measured every 5 min with a plate reader (Sunrise Tecan, Instruments Chemicals and Pharmaceuticals, Milperra, Australia) and the viability calculated using the following formula;

$$\%\,Viability = \left[\frac{\Delta A_{340}\ lysate}{\Delta A_{340}\ lystae + \Delta A_{340} media}\right] - blank$$

2.3.8b Cellular protein peroxide determination

Cellular protein peroxides were determined as described by Gieseg *et al* [180]. After photolysis, proteins were precipitated from 1.5 mL of cell suspension with cold TCA (10 % w/v). Pellets were washed with 1 mL cold 10 % TCA and resuspended in 900 µL of 25 mM H_2SO_4. 50 µL of FOX reagent containing 5 mM $FeSO_4$ and 5 mM xylenol orange in 25 mM H_2SO_4, was added to the samples, which were thoroughly vortex mixed and incubated in the dark, at room temperature, for 30 min. The samples were then centrifuged to remove cellular debris and their absorbance at 560 nm was measured. Peroxide concentrations were determined by comparison to a H_2O_2 standard curve.

In some experiments the TCA precipitates were extracted with methanol (0.5 mL) and hexane (1 mL) prior to FOX analysis as above.

2.3.8c Ascorbate loading of THP-1 cells

Cells (4 x 10^6 cells mL^{-1}) were loaded with ascorbate by pre-incubation with HBSS that contained 100 µM dehydroascorbate (DHA) for 30 min. This reduced form of ascorbate is preferentially taken up by cells, via the GLUT-1 transport mechanism, and reduced intracellularly to ascorbate [186]. For the determination of intracellular ascorbate 0.5 mL samples of cell suspensions were pelleted by centrifugation (1000 g, 5 min) and the pellet extracted with 0.5 mL of ice-cold

methanol containing EDTA (1 mM). The extracts were centrifuged at 16 000 g for 2 min and the supernatants collected and stored at – 80 °C prior to analysis. The determination of ascorbate levels in these supernatants was performed using a reverse phase ODS HPLC column (Supelco, 25cm x 0.46 cm, 5 µm particle size) with electrochemical detection. The mobile phase employed was 40 mM sodium acetate, 7.5 % (v/v) methanol, 0.25 % (v/v) dodecyl-triethylammoniumphosphate and 0.45 mM EDTA, at pH 4.75 [187].

This treatment led to the intracellular ascorbate concentration increasing from undetectable levels (sensitivity limit approximately 1 pmol) to 10 nmol mg cell protein^{-1} when loading was performed in the presence of RB and to 13 nmol mg cell protein^{-1} in the absence of RB.

2.3.9 Measurement of Oxygen Uptake by THP-1 cells

Oxygen concentrations were measured using a Clark-type oxygen micro-electrode (Rank Brothers Ltd, Cambridgeshire, U.K.) with a response time of <1 s. Readings were manually recorded every 30 s. Cell suspensions (4 x 10^6 cells / mL, in HBSS, 5.5 mL) were stirred slowly and allowed to equilibrate with air at room temperature (~22 °C) and atmospheric pressure. When steady state readings were obtained the vessel was sealed and light from a 40 W tungsten filament bulb, 5 cm distant, was applied.

The electrode was calibrated by setting the maximum reading at 100 and thoroughly gassing HBSS (5.5 mL) with Ar followed by addition of sodium dithionite, to reach a minimum reading of 2.4. The readings were converted to concentrations using the difference of these two readings and the known concentration of oxygen in HBSS [188].

2.3.10 Electron Paramagnetic Resonance Spectroscopy

Radicals were detected by Electron Paramagnetic Resonance (EPR) spectroscopy using a Bruker EMX X-band spectrometer equipped with 100 kHz modulation and cylindrical ER 4103TM cavity at room temperature. Samples were contained in a flattened aqueous sample cell (WG 813SQ; Wilmad, Buena, NJ, USA). Acquisition of spectra was commenced within 2 min of initiation of each reaction unless otherwise stated.

Typical spectrometer parameters were are follows; gain 1 x 10^6; modulation amplitude 0.05 – 0.1 mT; time constant 81 ms; scan time 42 s; centre field 348 mT; field scan 8 mT; microwave power 31.7 mW, resolution 1024 points and frequency 9.76 GHz. Hyperfine coupling constants were measured directly from the field scan and confirmed by computerised simulation using WINSIM software [189].

EPR experiments involving cells were performed on cells that had been RB photo-oxidised as described in section 2.3.8. Subsequently the cells were concentrated to 40 x 10^6 cells mL^{-1} by centrifugation and resuspension in appropriate volumes of HBSS, or water (for cell lysis) before use in EPR experiments.

2.3.11 Electrospray Ionisation Mass Spectrometry

Mass spectra were recorded using a VG Platform instrument (VG Biotech, Altrincham, UK) with samples ionised using the electrospray technique in the positive mode. Data were acquired using MassLynx software (version 3.3). Samples were dissolved in 50% aqueous methanol / 1% formic acid. Solvent was delivered by a Phoenix (Fisons) syringe pump at a flow rate of 10 µl min^{-1}. 2 x 25 µL injections were made for each analysis. Dry N_2 bath gas at atmospheric pressure was used to assist in the evaporation of the electrospray droplets. The probe tip was set at 3.5 kV with 0.5 kV on the chicane counter electrode. The sampling cone was set at either 25 V or 50 V.

2.3.12 Nuclear Magnetic Resonance Spectroscopy

Nuclear magnetic resonance spectroscopy was performed in collaboration with Dr W.A. Bubb (Department of Biochemistry, University of Sydney). Spectra were recorded at a ^1H frequency of 600.14 MHz on a Bruker Avance-600 NMR spectrometer with either a triple-resonance inverse-detection, or broadband inverse-detection probe, both with triple axis field-gradients. The variable temperature unit was set at 20 °C; for Gly-Tyr-Gly reaction mixtures, experiments were also conducted with the variable temperature unit set to 5 °C. Chemical shifts are expressed relative to the internal standard sodium 2,2-dimethyl-2-silapentane sulphonate and generally represent the mid-points of cross-peaks in heteronuclear single quantum coherence (HSQC) spectra for protonated carbons, and the mid-points of cross-peaks in heteronuclear multiple bond correlation (HMBC) experiments for non-protonated carbons. All resonance assignments were supported by COSY, TOCSY, HSQC,

HMBC and NOESY data. Standard Bruker (XWIN-NMR version 2.6) pulse programs were used without modification, except for the NOESY experiments in which the HOD resonance was presaturated during the mixing time (600 ms). HSQC spectra were optimised for $^{1}J_{C,H}$ of 145 Hz and HMBC spectra for $^{n}J_{C,H}$ of 6.25 Hz.

2.3.13 High Performance Liquid Chromatography

All samples were filtered (0.45 µm filter, Pall Gellman) prior to high performance liquid chromatography (HPLC). Mobile phases were filtered (0.2 µm filter, Pall Gellman) and degassed under vacuum with sonication prior to use. Samples were injected using a SIL-10AD VP autoinjector and mobile phases were delivered at a flow rate of 1 mL min^{-1} using two LC-10AT VP pumps (Shimadzu, Kyoto, Japan). When fluorescence detection was required it was performed with a RF-10A XL fluorescence detector (Shimadzu, Kyoto, Japan).

2.3.13a Free Tyr and small model compounds

HPLC separation of non-hydrolysed Tyr and model compounds was performed using a reverse phase Zorbax column (Agilent; 25 cm x 4.6 mm, maintained at 30 °C) packed with octadecylsilanised silica (ODS), equipped with a Pelliguard guard column (2 cm, Supelco). The eluents used are detailed in relevant sections of the text and were monitored with a diode array detector (Shimadzu SPD-M10A VP) over the range 200 - 370 nm.

2.3.13b Acid catalysed gas phase hydrolysis of proteins and analysis of hydrolysis products

Gas phase hydrolysis of proteins has been widely used for the analysis of protein oxidation products e.g. [38, 165-167, 190].

After reaction, samples were aliquoted into amber hydrolysis vials (Selby Biolab, Victoria, Australia) and evaporated to dryness using a Speedivac concentrator (model SVC 200H), featuring an in-line refrigerated cold trap and a VG-5 vacuum gauge (all from Savant Instruments Inc, Farmingdale, NY, USA). Samples were then placed in a Pico-Tag reaction vessel (Waters, Rydalmere, Australia) and 1 mL of 6 M HCl and 50 µL of neat 2-mercaptoacetic acid were added, the reaction chamber, was then evacuated with a vacuum pump and incubated at 110 °C for 18 h. Samples were then evaporated using the Speedivac concentrator as above and resuspended (volumes

and solvents used are described in Chapter 5), filtered and analysed. Analyses were performed using the same column as for the non-hydrolysed samples. Eluents were monitored by both UV (SPD-10A UV-Vis detector, Shimadzu, Kyoto, Japan) and electrochemical detection (Coulochem II electrochemical detector, ESA inc., Chelmsford, MA, USA) with an in-line 5011 analytical cell (ESA inc., Chelmsford, MA, USA). Specific chromatography conditions including mobile phases and gradient programs used are detailed in relevant sections of the text.

2.3.14 Statistical Analyses

All statistical analyses were performed using GraphPad Prism software (version 3.0). Data expressed as a proportion was normalised prior to analysis by arcsine transformation. Unpaired, two-tailed t-tests were performed when only two means were to be compared. In other situations one- and two-way analysis of variance (ANOVA) was used when appropriate, with post-hoc testing as detailed in the text and figure legends.

CHAPTER 3 - FORMATION AND REACTIONS OF TYROSINE PEROXIDES FORMED BY $^1O_2$-MEDIATED OXIDATION

3.1 INTRODUCTION

Proteins are an integral component of living cells and organisms. They play diverse roles in biology ranging from the structural elements of the cytoskeleton to the myriad of enzymes, proteinaceous hormones and transcription factors. Therefore chemical processes that lead to alterations in protein structure and function can have potentially serious consequences.

$^1O_2$ is an oxidant that is produced *in vivo* and has high rates of reaction with five of the naturally occurring amino acid residues, His, Trp, Tyr, Cys, and Met as discussed in Chapter 1. The oxidation of proteins by $^1O_2$ is believed to be mediated *via* reaction with these residues in proteins.

Recently it has been realised that oxidative insults to bio-molecular targets including proteins may be important in many disease processes and the elucidation of the basic mechanisms of these processes is important in the understanding and possible prevention of these events. Therefore, we have set out to investigate the basic mechanisms of amino acid oxidation by $^1O_2$, with emphasis placed on the oxidation of free Tyr.

3.2 AMINO ACID PEROXIDES

3.2.1 THE FORMATION OF AMINO ACID PEROXIDES

The γ-radiolysis of oxygenated aqueous solutions is known to generate reactive species, predominantly the hydroxyl radical (HO•) and superoxide (O_2^{-}•) [15]. A considerable number of researchers have used this methodology to study the reactions of these species with biological molecules (reviewed by Davies and Dean [3]). As early as the 1940's, Latarjet and Loiseleur had demonstrated that the γ-radiolysis of amino acid solutions resulted in the formation of non-radical, reactive species [191]. These products were identified as a mixture of H_2O_2 and organic peroxides. Subsequent studies have demonstrated the generation of organic peroxide species upon γ-irradiation of oxygenated amino acid solutions (for example [166, 192, 193]). Product analyses have demonstrated that HO• is the major oxidant under these conditions, which is not unexpected considering the rate constants for the reaction of these radicals with amino acids (generally ~10^9 M^{-1} s^{-1} for HO• and ~10 M^{-1} s^{-1} for O_2^{-}•) [194, 195]. Gebicki and Gebicki [192] found that γ-radiolysis of solutions of the

21 common amino acids led to the formation of organic peroxides in most cases (the exceptions being Met, Ser and Thr).

The oxidation of amino acids and proteins by $^1O_2$ is also known to yield peroxide species (reviewed by Straight [97]), via the oxidation of Tyr, Trp and His residues though the exact nature of these species is poorly defined.

3.2.2 Further Reactions of Amino Acid Peroxides

The dioxygen moiety in peroxidic species contains two more electrons than the diatomic oxygen molecule. These electrons are placed in to the π^*_{2p} orbitals reducing the bond order to one [8]. Thus, the peroxide oxygen-oxygen bond is weaker than that of the dioxygen molecule. This weaker bond means that peroxides are generally unstable species and undergo a number of further reactions involving one or two electron processes. Two electron processes generally involve reduction of peroxides to their corresponding alcohols [165, 167]. One electron processes result in the cleavage of the peroxide bond and yield reactive oxygen-centred radicals; such decomposition can be catalysed by heat, transition metal ions, and light of sufficient energy [196-198].

Redox active transition metal ions have been frequently used to catalyse the decomposition of peroxide species. This type of reaction is potentially very important *in vivo*, as metal ions, particularly iron and copper, may be found in various *in vivo* situations, particularly diseased tissue [2]. Reduction by transition metal ions has been reported to induce cleavage of peroxides leading to the formation of alkoxyl radicals [197, 199]. The mechanism generally proposed for these reactions involves the reduction of a suitably labile bond A-B (e.g. peroxide bond) by a transition metal ion M^{n+}. The electron acceptor A-B forms a radical anion intermediate A^--B$^\bullet$ that rapidly dissociates to yield an anion and a radical (reaction 3.1). Amino acid (and protein) peroxides are believed to decay by a similar mechanism (reaction 3.2) [200]. Peroxides can also reduce metal ions under certain conditions (reaction 3.3), although this reaction is generally much slower than the oxidation processes [201].

$$A\text{-}B + M^{n+} \rightarrow M^{(n+1)+} + A^- + B^\bullet \quad (3.1)$$

$$ROOH + Fe^{2+} \rightarrow RO^\bullet + HO^- + Fe^{3+} \quad (3.2)$$

$$ROOH + M^{(n+1)+} \rightarrow ROO^\bullet + M^{n+} + H^+ \quad (3.3)$$

Thermal and photochemical reactions of peroxides are also thought to yield alkoxyl radicals by homolysis of the peroxide bond [196].

The radicals produced by these processes are generally very reactive species and are known to abstract hydrogens from various bio-molecular targets (reactions 3.4 and 3.5), a process that can yield further radical species.

$$RO\bullet + R'H \rightarrow R'\bullet + ROH \quad (3.4)$$

$$ROO\bullet + R'H \rightarrow R'\bullet + ROOH \quad (3.5)$$

3.2.3 The Formation and Reactions of Tyr-Derived Peroxides

The formation of Tyr-derived peroxide species has been previously reported [95, 202, 203]. Two major mechanisms of Tyr peroxide formation are known, one involves the addition of $O_2^{-}\bullet$ to the tyrosyl radical [202, 203], the other the addition of $^1O_2$ to Tyr [95].

The $O_2^{-}\bullet$ mediated formation of Tyr peroxides requires initial generation of the tyrosyl radical. This species has been generated by γ-irradiation [202], by myeloperoxidase (MPO) in the presence of $O_2^{-}\bullet$ [203] or by activated neutrophils in a MPO-dependant manner [203]. The addition of $O_2^{-}\bullet$ to the tyrosyl radical is a very rapid reaction (rate constant determined by pulse radiolysis [202] is 1.5×10^9 M^{-1} s^{-1}) with addition to either the ring 1 or 3 positions (Scheme 3.1). The production of tyrosyl radical in the absence of $O_2^{-}\bullet$ leads to the formation of di-Tyr as the major product [202].

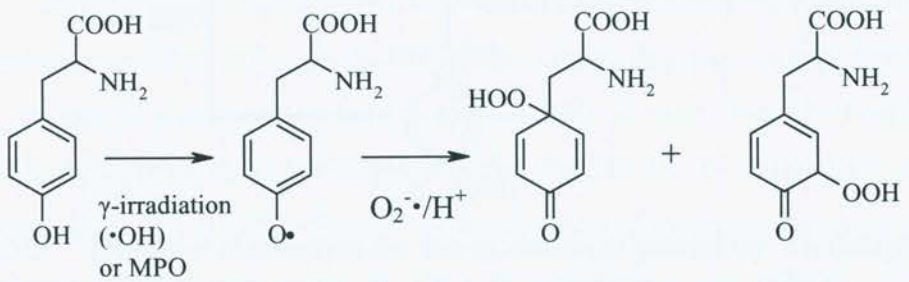

Scheme 3.1: The formation of Tyr-derived peroxide species from the reaction of the tyrosyl radical with $O_2^{-}\bullet$.

Tyr is a phenolic compound and thus the many studies of $^1O_2$-mediated phenol oxidation can be viewed as studies of a Tyr model compound. The $^1O_2$-mediated oxidation of phenolic compounds, including Tyr, have been extensively studied from

a kinetic perspective [79, 204, 205], however, the products of these reactions are not well characterised.

In 1982, $^1O_2$ was shown to chemically react with phenol (3.1) to yield 1,4-benzoquinone (3.2) [205]. This finding has been confirmed more recently [206-208]. The intermediates of this reaction have not been characterised thoroughly, although there is evidence that hydroquinone (3.3) is formed as the final intermediate prior to benzoquinone formation, especially under neutral pH conditions [205, 206]. The related compound aniline is also oxidised by $^1O_2$ to yield 4-hydroxyaniline initially, which then deaminates and subsequently forms benzoquinone [206].

Li and Hoffman [208] proposed that the initial reaction of $^1O_2$ and phenol was a [2+4] cycloaddition yielding the 1,4-endoperoxide (3.4), which could undergo an intramolecular hydrogen abstraction to yield hydroperoxycyclohexadienone (3.5). This process has been suggested to compete with solvolysis to form the di-hydroxylated product, which can then dehydrate to yield (3.5) (Scheme 3.2). Contrary to Li and Hoffman's report [208], Briviba *et al.*, detected hydroquinone as the initial product, which formed benzoquinone upon subsequent reaction [206].

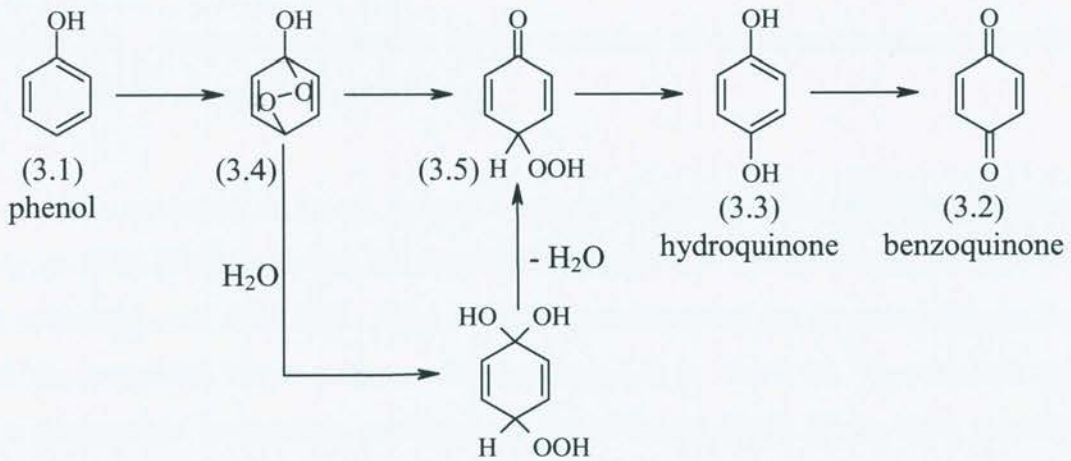

Scheme 3.2: Proposed mechanism for the oxidation of phenol by $^1O_2$ (adapted from references [205, 206, 208]).

Recently d'Alessandro *et al.*, have proposed a slightly different reaction pathway for the $^1O_2$ oxidation of phenolic compounds. Their study suggests that at high pH, where the hydroperoxide is in the anionic form, a 1,3-hydrogen shift reaction can occur between the *ortho*-hydroperoxy anion and the protonated phenol leading to

initial production of the quinone species, followed by reduction to the hydroquinone [209].

Hydroperoxide species are also produced in the $^1O_2$-mediated oxidation of substituted phenols such as 4,6-di-*tert*-butylresorcinol (3.6, R=H) [210, 211] and 3,5-di-*tert*-butylcatechol [212]. In both of these instances hydroperoxy products, analogous to the intermediate postulated by Li and Hoffman for phenol oxidation, were isolated and characterised. These authors also proposed endoperoxidic intermediates similar to Li and Hoffman, although they were not isolated (Scheme 3.3)

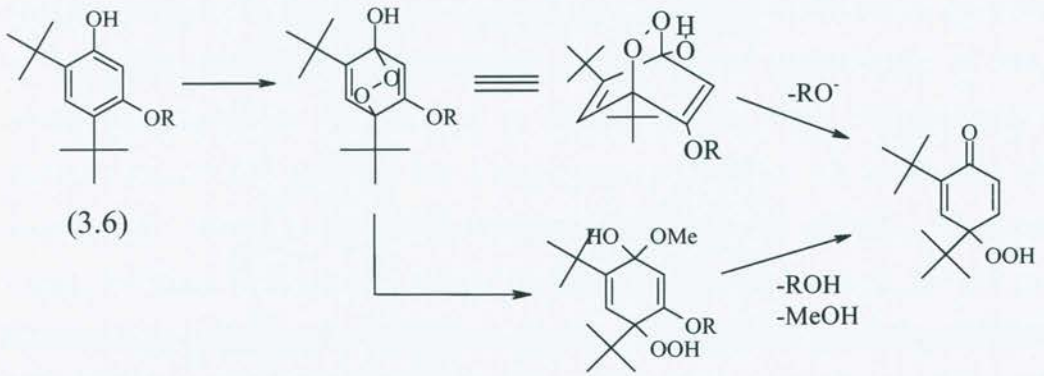

Scheme 3.3: Proposed mechanism for the oxidation of 4,6-di-tert-butylresorcinol by $^1O_2$ (adapted from references [210, 211]).

The oxidation of Tyr (3.7) by $^1O_2$ was postulated to yield peroxide species as early as 1976 [213], although the first characterisation of any peroxidic product was not published until 1995 [95]. Jin *et al.*, [95] postulated that the reaction between Tyr and $^1O_2$ proceeded via an endoperoxide species (3.8) in which the $^1O_2$ molecule acts as a dieneophile in reaction analogous to the classical [4+2] Diels-Alder reaction. This species was then postulated to undergo an intramolecular hydrogen abstraction reaction from the phenolic group to yield the hydroperoxidic species (3.9). The hydroperoxide (3.9) participates in an intramolecular Michael addition reaction to give the ring closed peroxide (3.10), which is then believed to subsequently decay to yield 3a-hydroxy-6-oxo-2,3,3a,6,7,7a-hexahydro-1*H*-indol-2-carboxylic acid (HOHICA) (3.11) which has been identified as the final product (Scheme 3.4). Endo *et al.*, found that at high pH this product decarboxylates to yield the ketolactam species (3.12) [96].

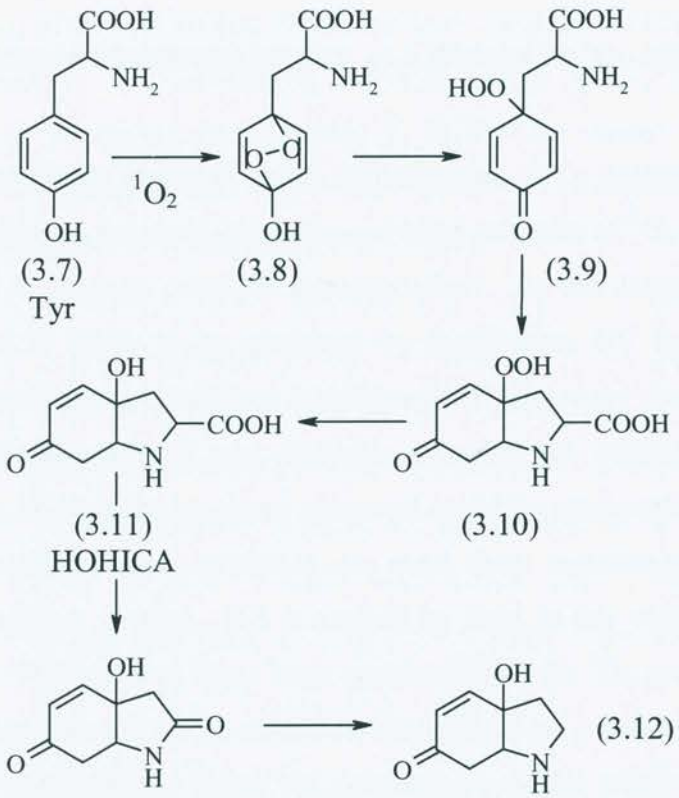

Scheme 3.4 – Proposed mechanism for the $^1O_2$-mediated oxidation of free Tyr (adapted from references [95, 96]).

3.3 AIMS

The aims of the studies reported in this chapter were to examine the formation of peroxides on Tyr after oxidation by $^1O_2$ generated by the use of rose bengal (RB) photo-sensitisation, a MoO_4^{2-} / H_2O_2 system or by the decomposition of a naphthalene endoperoxide. Peroxide formation was monitored by the ferric / xylenol orange (FOX) method, and both the peroxides and their resultant breakdown products were characterised by the use of high performance liquid chromatography (HPLC), electrospray ionisation mass spectrometry (ESI-MS) and nuclear magnetic resonance (NMR) spectroscopy. The stability of the peroxides to elevated temperature, reducing agents (both one and two electron) and light was also investigated by the FOX assay, and the formation and nature of radicals from these decay processes were investigated using electron paramagnetic resonance (EPR) spectroscopy with spin trapping.

3.4 RESULTS

3.4.1 FORMATION OF PEROXIDES ON TYR AS A RESULT OF $^1O_2$-MEDIATED OXIDATION

In order to obtain maximal yields of peroxides, a $^1O_2$ generation system was required which allowed the rapid generation of large amounts of $^1O_2$ under conditions that are unlikely to promote peroxide decomposition. As the decomposition of any peroxides formed is likely to be catalysed by metal ions, UV light and elevated temperatures, experimental conditions lacking any of these were most likely to yield positive data. Furthermore, it was desirable to avoid the addition of potentially oxidising species, so that any reactions observed could be attributed to the formation of $^1O_2$. Dye sensitised photo-oxidation can meet these requirements as long as a suitable photosensitiser is used. RB is excited by light in the visible region of the spectrum (λ_{max} = 549 nm) and has a high quantum yield for $^1O_2$ production (0.76 in water) [214]. Therefore RB photo-oxidation was considered a suitable $^1O_2$ generating system for these experiments. Other $^1O_2$ generating systems, which did not meet all of these requirements, were also investigated. The first of these systems was the MoO_4^{2-}/H_2O_2 system, which contains metal ions that may reduce peroxides, and H_2O_2, a potentially competing oxidant.

Thermal decomposition of 3-(4'-methyl-1'-naphthyl)propionic acid 1',4'-endoperoxide has also been used to generate $^1O_2$, although this was not used in these experiments as the FOX assay may not be able to readily distinguish between Tyr- or naphthalene-derived peroxides.

Initially, the formation of Tyr peroxides was investigated using the RB photochemical system. These reactions were carried out using solutions of Tyr (2.5 mM) at 4 °C, to minimise peroxide loss, with RB present at 10 μM. The visible light source used for photolysis was filtered through a 345 nm cut-off filter to avoid exposure of the samples to UV light.

Although RB is an efficient sensitiser for $^1O_2$ production, small amounts of $O_2^{-\bullet}$ are also formed during the photolysis. $O_2^{-\bullet}$ is known to spontaneously dismutate to yield H_2O_2 [2]. Thus, to ensure that the peroxides quantified were organo-peroxides rather than H_2O_2, samples were treated immediately after photo-oxidation, with catalase (3150 units mL^{-1}, 10 mins, 22 °C) to remove any photo-generated H_2O_2. This treatment does not affect the yield of organo-peroxides (Morgan, P.E., Dean,

R.T., Davies, M.J., submitted) [175]. Peroxide concentrations were estimated using the ferric oxidation of xylenol orange (FOX) assay as described in Chapter 2.

An alternative $^1O_2$ generating method using MoO_4^{2-}/H_2O_2 was also investigated. As discussed in Chapter 1 H_2O_2 can under go a catalytic disproportionation reaction to yield $^1O_2$. This reaction is catalysed by the molybdate anion, MoO_4^{2-}, as outlined in reaction 3.6 and 3.7 [47].

$$2\ H_2O_2 + MoO_4^{2-} \rightleftharpoons 2\ H_2O + MoO_6^{2-} \qquad (3.6)$$

$$MoO_6^{2-} \longrightarrow MoO_4^{2-} + {}^1O_2 \qquad (3.7)$$

Reactions were performed on Tyr solutions (2.5 mM) in Na_2MoO_4 (12.5 mM) adjusted to pH 7. The reaction was initiated by the addition of 30 % H_2O_2 (60 µL, 540 µmol) and further aliquots of H_2O_2 were added after 1 min and 10 min. Unreacted H_2O_2 was removed prior to analysis by FOX assay by treatment with catalase.

3.4.1a Results

Photolysis of Tyr with visible light ($\lambda > 345$ nm) in the presence of RB and oxygen resulted in the formation of peroxides as detected by the FOX assay. The concentration of peroxides increased in a time dependant manner over 60 min photolysis (Figure 3.1). No peroxides (< 5 µM) were detected in control samples photolysed in the absence of RB, or O_2, or in non-photolysed solutions containing all the reactants. These results demonstrate that peroxide formation is not mediated by direct photo-oxidation of Tyr, by an excited state of the photosensitiser, or by a non-photolytic reaction of Tyr with RB. However, a disadvantage of this photolytic method was that the rate of oxygenation could not be accurately controlled. This resulted in some variation in the amount of $^1O_2$ production and thus to a relatively minor degree of variability in the yield of peroxides between experiments.

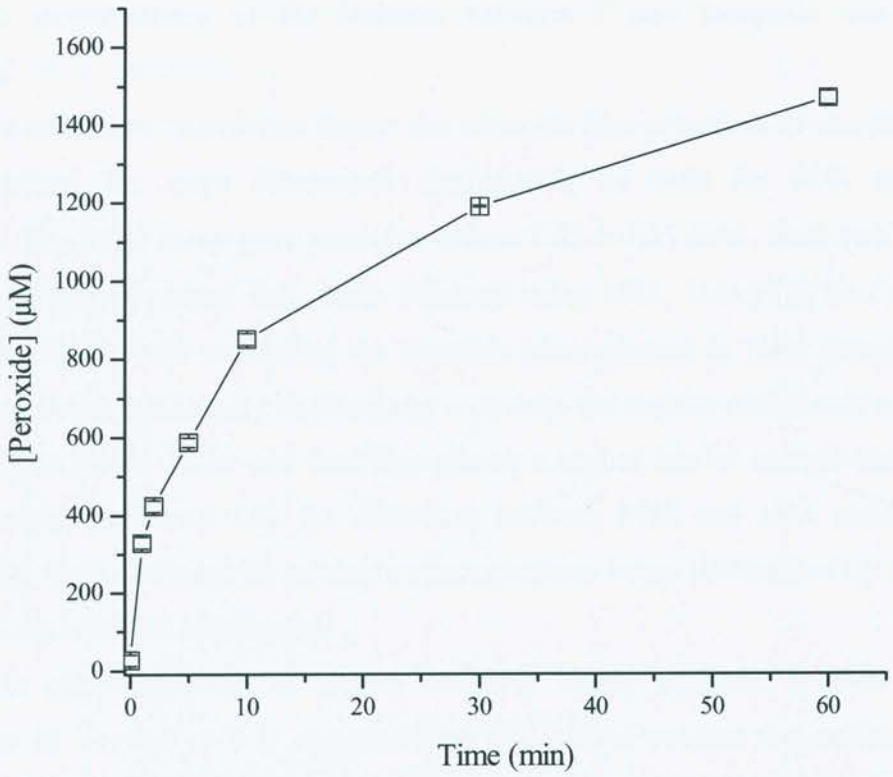

Figure 3.1: The formation of peroxides on Tyr (2.5 mM in D_2O) by visible light (λ > 345 nm) with increasing photolysis time, in the presence of oxygen and the photosensitiser RB (10 μM) at 4 °C, pH 7. Peroxide concentrations were measured using the FOX assay with H_2O_2 standards as described in Chapter 2. Data are the means (± SD) of triplicate determinations from a single experiment representative of several, as the absolute peroxide yields varied between experiments due to slight differences in oxygenation rates.

The FOX method is a technically simple and reproducible procedure, however the stoichiometry of the reaction is not always constant between different classes of peroxides. Thus, it cannot be automatically assumed that the comparison of Tyr peroxides to H_2O_2 standards yields strictly accurate results. In order to overcome this limitation a second method with a more rigorous and well-defined stoichiometry was employed. This assay is known as the manual iodometric assay (MIA) and was performed as described by Jessup *et al* [181]. As described in Chapter 2 the basis of the assay is the oxidation of iodide (I^-) by a peroxide to form iodine (I_2). Under acidic conditions, and with an excess of I^-, the I_2 is converted to tri-iodide (I_3^-), which can be measured spectrophotometrically at 358 nm. A major advantage of this assay is the

strict 1:1 stoichiometry of the reaction between I^- and inorganic and organic peroxides.

To estimate a 'correction factor' the peroxide concentrations of samples of RB photo-oxidised Tyr were determined concurrently by both the FOX and MIA methods. The FOX assay gave peroxide values 1.55 ± 0.05 (n=6, from two separate experiments) times greater than those obtained using MIA, indicating that the FOX assay was slightly over estimating the peroxide concentration in these samples. The FOX assay is less technically challenging, as it does not require completely anaerobic conditions, it is also faster and therefore allows a higher rate of sample throughput. These factors, combined with the difference between FOX and MIA results being only slight, led to subsequent peroxide concentrations being determined by the FOX assay and are reported unadjusted.

RB photo-oxidation is known to be a highly efficient method for the generation of $^1O_2$ and so it is expected that $^1O_2$ was the oxidant responsible for the formation of Tyr peroxides. Commonly the involvement of such oxidising species is investigated by the use of agents that are known to either enhance or reduce the lifetime of $^1O_2$ in solution. As discussed in chapter 1, deuterated solvents enhance the lifetime of $^1O_2$ in solution, as they have lower vibrational frequency. D_2O can enhance the lifetime of $^1O_2$ by 10-15 fold [215], thus if the formation of peroxides in these experiments is dependant on $^1O_2$ it is expected that a higher yield of peroxides will be observed in D_2O compared to H_2O. Conversely, the azide anion is a potent quencher of $^1O_2$ ($k = 5 \times 10^8\ M^{-1}\ s^{-1}$) [216] and therefore the yield of peroxides would be expected to decrease when azide is present.

Furthermore, if $^1O_2$ was the reactive species involved it might be expected that rapid depletion of the low concentration of ground state oxygen present in water might limit the peroxide yield. Therefore, experiments were carried out using pure oxygen rather than compressed air. It was expected that if the limiting reagent were oxygen then the peroxide formation would increase on saturating solutions with oxygen.

A series of experiments was performed to investigate the nature of the oxidant using the approaches outlined above. The peroxide yield was increased in the presence of D_2O, and further enhanced in D_2O under pure oxygen atmosphere (Figure 3.2). Azide was found to inhibit Tyr peroxide formation (Figure 3.2). These results

strongly suggest that $^1O_2$ is the oxidant responsible for the generation of Tyr peroxides during RB photo-oxidation.

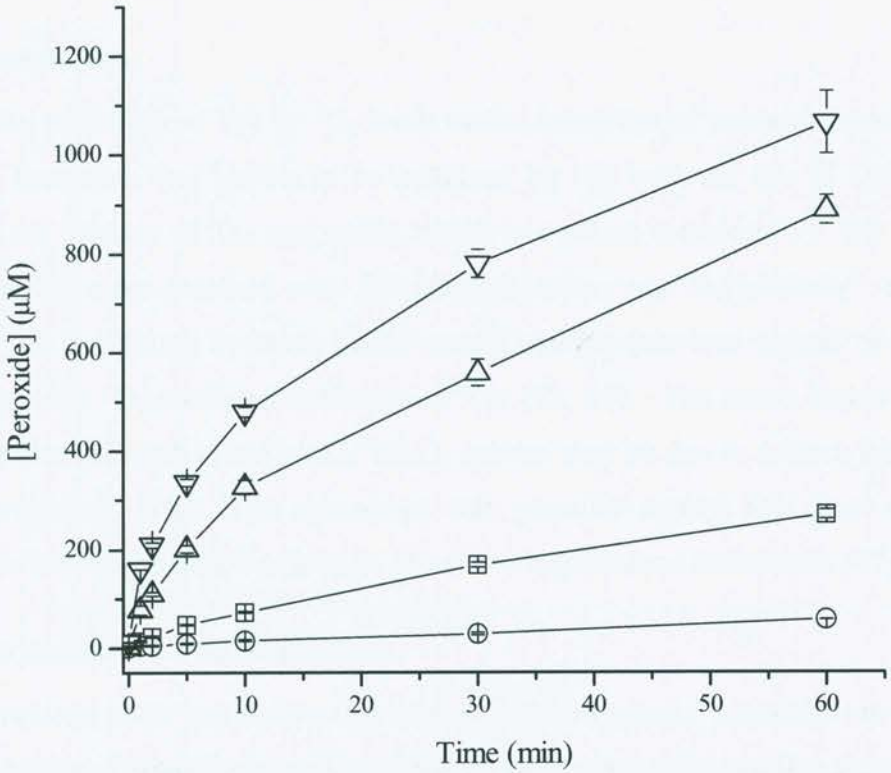

Figure 3.2: The formation of peroxides on Tyr (2.5 mM) by RB (10 μM) photo-oxidation in the presence of sodium azide (5 mM) (○), water (□), D_2O (△), or D_2O under a 100 % oxygen atmosphere (▽). Photo-oxidations were otherwise performed as described in Figure 3.1. Data are the means (± SD) of triplicate determinations from a single experiment, representative of several, as absolute peroxide yields varied between experiments due to slight differences in oxygenation rates.

To provide further evidence for $^1O_2$ intermediacy in the formation of Tyr peroxides, experiments with an alternative $^1O_2$ generating system were performed. The addition of H_2O_2 to a solution of Tyr and MoO_4^{2-} at neutral pH and 22 °C initiated the reaction. Additional aliquots were introduced after 1 and 10 min and the reaction was allowed to proceed for a total of 30 min. Catalase was used to remove excess H_2O_2 prior to FOX assay, which detected the formation of 2950 ± 30 μM peroxides (n = 6, from 2 separate experiments). Control experiments were performed which contained either H_2O_2 or MoO_4^{2-} and Tyr. In each case, after catalase treatment, relatively minor levels of peroxides were detected (10 ± 4 μM and 42 ± 5

μM respectively). This result provides further evidence for the formation of Tyr peroxides being $^1O_2$-mediated and also suggests that the presence of MoO_4^{2-} does not lead to rapid decomposition of Tyr peroxides.

3.4.1b Conclusions

The oxidation of Tyr by $^1O_2$ leads to the formation of peroxide species. The peroxide formation was shown to be mediated by $^1O_2$ with the use of D_2O, which prolongs the lifetime of $^1O_2$, and azide, which is a potent scavenger of $^1O_2$. Further, similar results were obtained with RB photochemistry and H_2O_2/MoO_4^{2-}; two very different $^1O_2$ generating systems. These results confirm previous reports of peroxide formation upon $^1O_2$-mediated oxidation of Tyr [95, 96]. The much higher yield of Tyr peroxides detected in the MoO_4^{2-}/H_2O_2 system may be due to a much higher flux of $^1O_2$ produced. This is in agreement with previous reports that have used this system for the $^1O_2$-mediated oxidation of various naphthalene derivatives [47].

3.4.2 Stability of Tyr Peroxides

Previous work has shown that amino acid and protein peroxides are unstable under a variety of conditions and can decay to yield potentially reactive species [193, 198]. In order to examine whether this was also true for these $^1O_2$-mediated, Tyr-derived peroxides the stability of these species under conditions of elevated temperature, on exposure to visible or UV light, and in the presence of added chemical reductants.

3.4.2a Loss of Tyr peroxides during incubation at elevated temperatures

Previous work has demonstrated that amino acid peroxides formed by γ-irradiation are unstable at temperatures greater than 4 °C [193, 217]. Initial studies on the stability of Tyr-derived peroxides were carried out by incubating crude photo-oxidation reaction mixtures, which contained RB and unreacted Tyr, at different temperatures. The residual concentration of Tyr peroxides was determined at various time points over 24 h.

The Tyr peroxides were found to be relatively stable when incubated, in the absence of any added agent, at 4 °C. After 24 h incubation at this temperature 20 % reduction of the initial peroxide concentration was observed (Figure 3.3). Incubation at higher temperatures resulted in more rapid loss of the peroxides, with incubation at

26 °C and 37 °C for 24 h resulting in the loss of 34 % and 77 %, respectively, of the initial peroxide concentration (Figure 3.3).

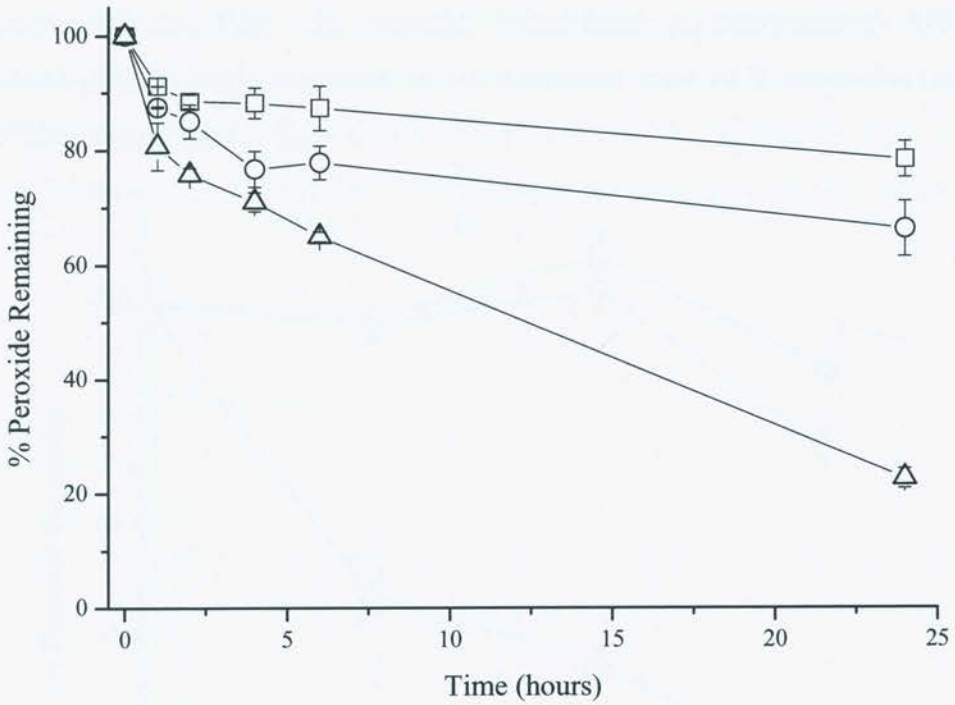

Figure 3.3: Stability of Tyr peroxides at elevated temperatures. Tyr peroxides were generated as in Figure 3.1. Crude reaction mixtures, which contain RB and unreacted Tyr as well as Tyr peroxides, were incubated in the absence of light at 4 °C (□), 26 °C (○), and 37 °C (△) for the indicted time periods before residual peroxide levels were determined as in Figure 3.1. Data are expressed as means of percentage initial peroxide concentration (n = 6, from 2 separate experiments) ± SD.

3.4.2b Photochemical stability of Tyr peroxides

Peroxide species have previously been shown to be susceptible to photochemical decay [196]. Since Tyr peroxides were formed by RB photochemistry using visible light and previously Jin *et al.*, [95] have used UV light to directly photo-oxidise Tyr, the potential for photochemical peroxide decay, which might limit the yields of peroxides detected, was investigated with solutions of Tyr peroxides.

To avoid further photosensitised reactions occurring while investigating the photochemical stability of these peroxides it was necessary to first remove RB from the reaction mixtures. This was accomplished using the filtration procedure described in Chapter 2. This treatment did not effect the initial peroxide concentration.

Solutions of Tyr peroxides, from which RB had been removed, were relatively stable on exposure to visible light when incubated at 4 °C for 90 min, with 23 %, compared to 9 %, of peroxides lost in the photolysed and non-exposed samples respectively (Figure 3.4). In contrast, broad-band (mercury-xenon) UV light irradiation led to the rapid depletion of Tyr peroxides, with 88 % peroxides lost after 90 min exposure (Figure 3.4).

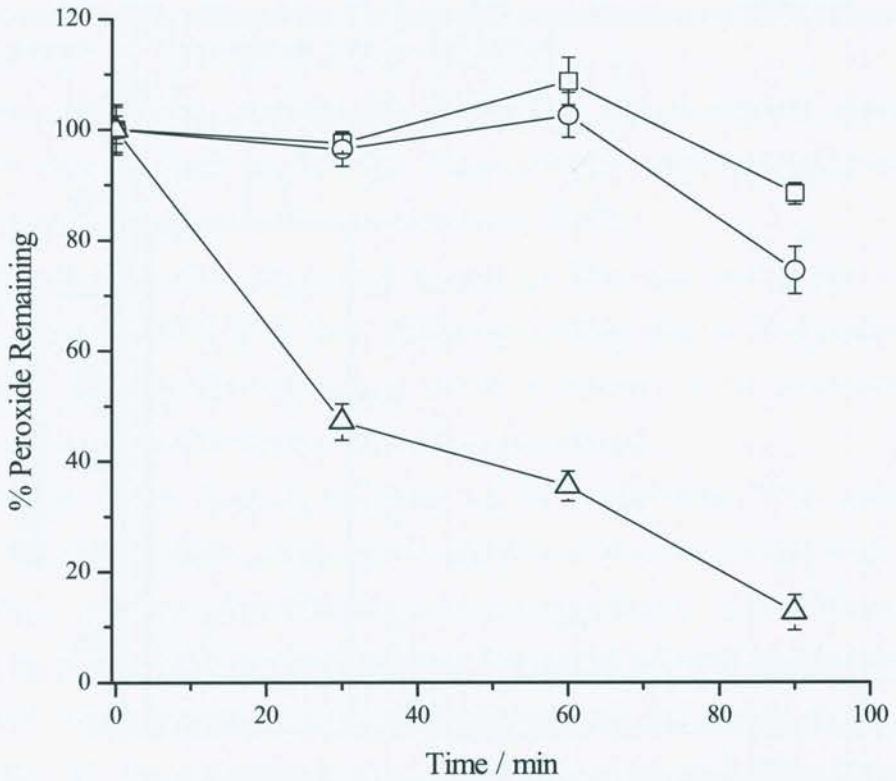

Figure 3.4: Stability of Tyr peroxides to visible and UV light. Peroxides were generated, and assayed for, as in Figure 3.1. After removal of RB by filtration (see text) Tyr peroxides were incubated at 4 °C in the absence of light (□) or exposed to visible light (○) (250 W lamp, λ >345 nm) or broad-spectrum UV light (△) (150 W mercury-xenon UV lamp). Data are expressed as means of percentage initial peroxide concentration (n = 6, from 2 separate experiments) ± SD.

3.4.2c Stability of Tyr peroxides to reductants

Peroxidic species are known to be susceptible to reduction by both one- and two- electron donors. Fe^{2+} is a well-studied one-electron reductant that has been shown to reduce amino acid hydroperoxides generated by γ-irradiation [198]. Two electron reductants are widely used in organic synthesis for the reduction of peroxides [218], and have been shown to reduce γ-irradiation generated amino acid peroxides

[165, 167]. A commonly used two-electron reductant is the borohydride anion. Thus, the capacity for reduction of Tyr peroxide by representative one- (Fe^{2+}/EDTA) and two-electron reductants ($NaBH_4$) was investigated.

As shown in Figure 3.5 pre-formed Tyr peroxides were susceptible to treatment with one- and two-electron reductants when incubated at 4 °C for 60 min. Fe^{2+}/EDTA reduced the Tyr peroxide concentration by 90 % (Figure 3.5), whereas treatment with $NaBH_4$ reduced the Tyr peroxide concentration by 95 % (Figure 3.5).

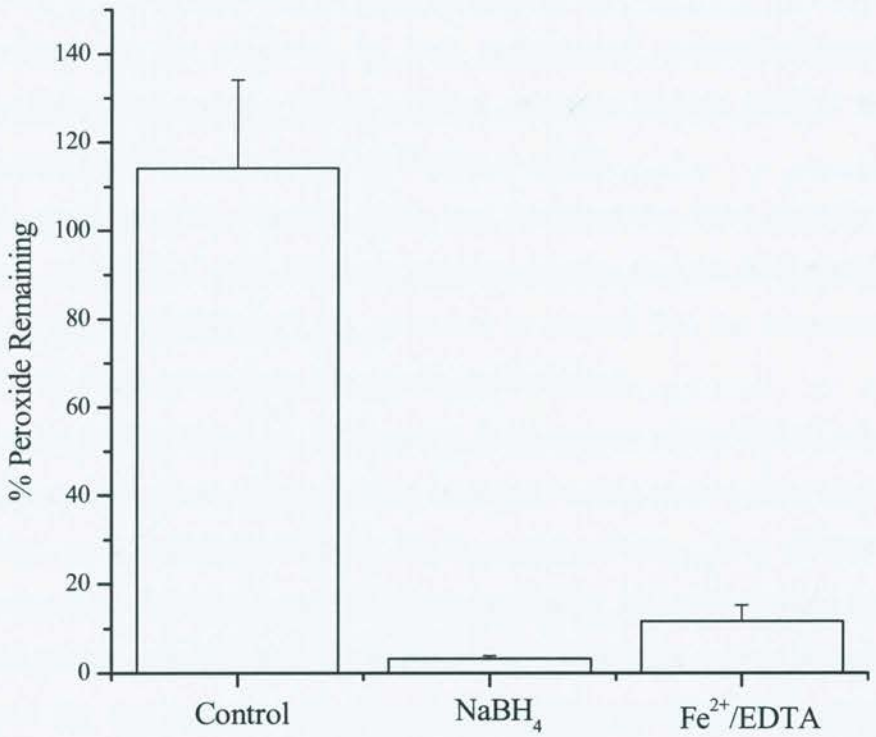

Figure 3.5: Stability of Tyr peroxides to chemical reductants. Tyr peroxides (~100 μM) were formed and assayed as in Figure 3.1. Crude reaction mixtures, which contain RB and unreacted Tyr, were incubated at 4 °C for 1 h in the presence of Fe^{2+}/EDTA (1:1 complex) or $NaBH_4$ (both 200 μM). Data are expressed as means of percentage initial peroxide concentration (n = 6, from 2 separate experiments) ± SD.

3.4.2d Conclusions

Tyr peroxides generated by $^1O_2$-mediated reactions were found to be labile to elevated temperatures, UV light and reducing species is in agreement with previous literature accounts of the decomposition of related peroxides under similar conditions [196-198].

3.4.3 Structural Characterisation of Tyr Peroxides and Further Products

The previous sections have shown that peroxide intermediates are formed upon $^1O_2$-mediated Tyr oxidation. In order to characterise the intermediates and products of these reactions further, RB photo-oxidised Tyr was analysed by HPLC, ESI-MS and 2D-NMR.

3.4.3a Analysis of $^1O_2$-oxidised Tyr by RP-HPLC

Products of Tyr oxidation by both radical and non-radical species have previously been analysed by HPLC. These products include DOPA, di-Tyr, 3-chloroTyr, and 3-nitroTyr (reviewed by Davies *et al* [4]).

The products of the reaction of $^1O_2$ and Tyr have also been partially analysed by Jin *et al.,* using HPLC [95]. These results demonstrate that the final product of Tyr oxidation by $^1O_2$ is HOHICA (3.11), as shown in scheme 3.1; the intermediates that give rise to this product however, are poorly characterised.

In their studies Jin *et al.*, [95] used a C-18 reverse phase HPLC column with water as the mobile phase. Experiments reported in this section also used reversed phase HPLC, with a slightly different C-18 packed column. Two different mobile phases were used. Initially a mobile phase containing 100 mM sodium perchlorate and 10 mM sodium phosphate buffer at pH 2.5 was used; this mobile phase system is widely used for the analysis of other Tyr oxidation products [4]. Subsequently unbuffered water was used as the mobile phase. Samples were stored at 4 °C for the shortest period possible before analysis by HPLC in an effort to minimise peroxide decay.

When RB photo-oxidised Tyr was analysed using the perchlorate containing mobile phase 3 peaks were observed with retention time (RT) of 3.2 min, 3.8 min and 14.6 min (Figure 3.6). The peak at 14.6 min is assigned to unmodified Tyr as it has the same RT as authentic Tyr and it was observed in non-photolysed control experiments. However, the two other peaks are not observed in the non-photolysed controls, suggesting that they are species generated during the reaction of $^1O_2$ with Tyr. These peaks are assigned to compounds (3.11) and (3.9), respectively, for reasons detailed below.

Over the photolysis time period the Tyr peak area decreased, whereas the peak areas of (3.9) and (3.11) increased, suggesting that they are generated from Tyr by $^1O_2$

(Figure 3.6). These new peaks had dramatically different RT to that of DOPA, a major product of HO• mediated Tyr oxidation, which elutes at 8.5 min under these HPLC conditions. It is therefore likely that $^1O_2$, and not HO•, mediates the formation of these materials.

The MoO_4^{2-}/H_2O_2 Tyr oxidation system was also investigated by HPLC. When reaction mixtures were analysed under the same HPLC conditions as above 4 peaks were observed. However, two of these eluted in the same region as (3.10) and (3.11) but were also present in control experiments, indicating that they are probably due to H_2O_2 and molybdate species. The remaining two peaks had RT matching those observed above for (3.9) and un-modified Tyr, the latter being very small. Peak (3.9) was not observed in control experiments, suggesting that similar Tyr peroxide species are generated by both $^1O_2$ generation systems. However, the presence of these additional peaks derived from the $^1O_2$ generating system precluded further analysis of the products generated with this system.

The ability of $^1O_2$ generated using the decomposition of the 1',4'-endoperoxide of 3-(4'-methyl-1'-naphthyl)propionic acid (MNPA, MNPAE for the endoperoxide) to oxidise Tyr was also investigated by HPLC. MNPA and MNPAE were synthesised and reacted with Tyr as described in Chapter 2. When analysed using the same HPLC conditions as above, control reactions containing MNPA and Tyr showed two main peaks. One eluted very early and is due to the naphthalene derivative. The other eluted at the same retention time as authentic Tyr. When reactions were performed with MNPAE, these same two peaks were observed, although the Tyr peak was slightly less intense. There was also a very small peak in the same region as (3.11) was found to elute. The small loss of Tyr suggests inefficient generation of $^1O_2$ and low yields of peroxides (although this could not be analysed), consistent with the low intensity of the product peaks. Consequently, the use of this system was not examined further.

In order to investigate whether, and which, of the species generated by $^1O_2$-mediated oxidation of Tyr are peroxides, it was decided to collect fractions from the HPLC column and analyse these for peroxide material using the FOX assay. However, as it is known that phosphate containing buffers are incompatible with this assay, a new mobile phase was developed to elute these materials. Unbuffered water was found to be suitable for this application and was adopted as employed by Jin *et al.* [95]. Under these conditions the RT of (3.9) and (3.11) are 3.3 min and 2.8 min

respectively. Peak (3.9) was found to give a positive FOX assay indicating that it is a peroxide. In contrast, peak (3.11) gave a very small absorbance in the FOX assay, which was of similar magnitude to that observed upon collection of the free Tyr peak, suggesting that peak (3.11) was not peroxidic.

The relationship between these two product peaks was further investigated by incubation of collected fractions of the peak assigned to (3.9). Re-analysis of this material by HPLC after varying periods at 37 °C, resulted in the detection of a further peak with RT 1.9 min, assigned as (3.10), with short incubation times, and increasing amounts of (3.11) after extended periods of incubation (Figure 3.7). The time course of formation and decay of these peaks is consistent with (3.9) being the precursor of (3.10) which in turn decays to (3.11). The relationship between these peaks was investigated only at a qualitative level; quantitative analysis was not possible as the peroxides are unstable and authentic standards of each of these materials were not available.

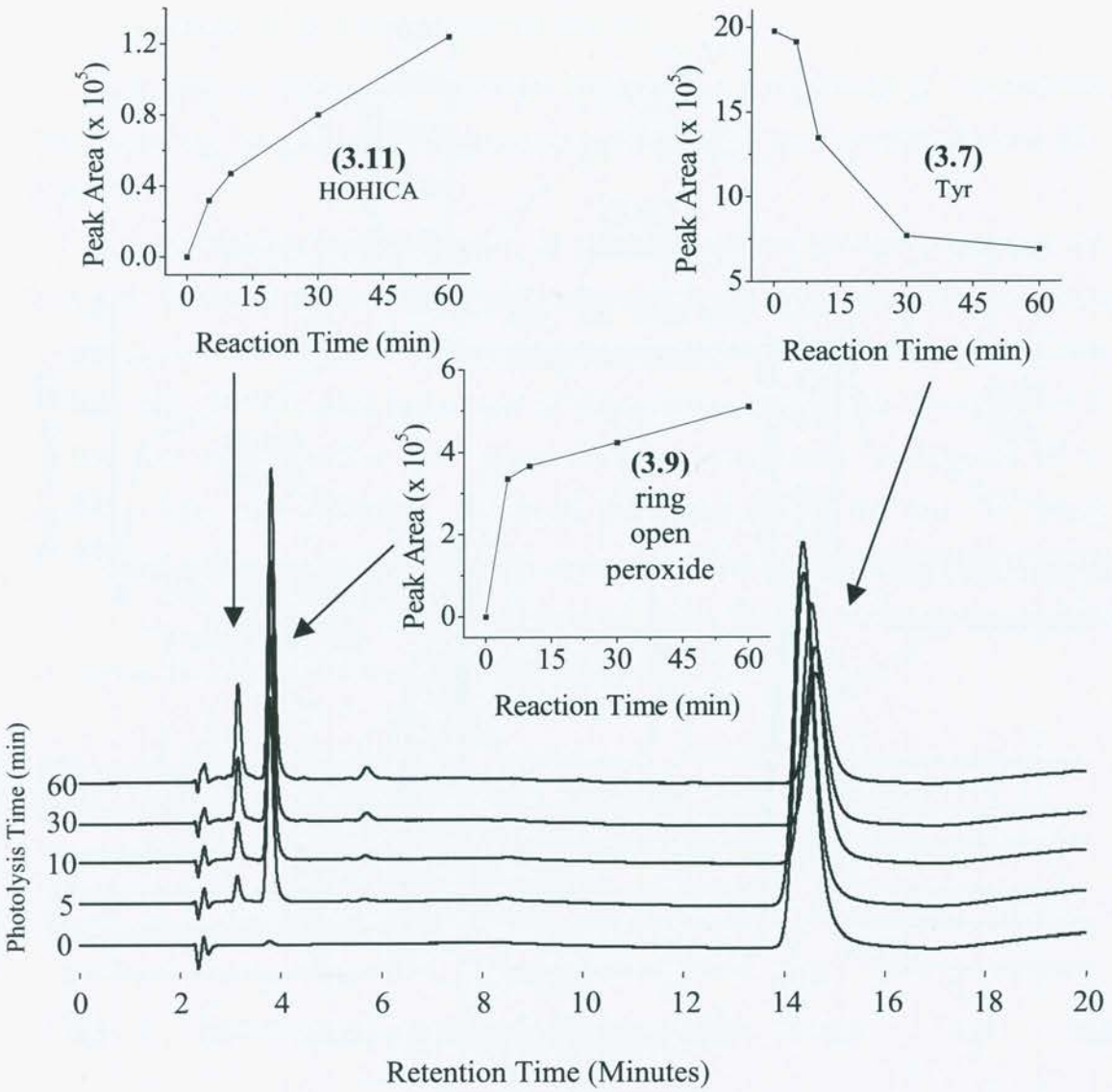

Figure 3.6: HPLC analysis of Tyr oxidation products generated on photo-oxidation of free Tyr (2.5 mM in D_2O) in the presence of oxygen and RB (10 μM). Samples were removed from the photo-oxidation reaction at the indicated times and injected (10 μL) on to a Zorbax ODS HPLC column. The mobile phase used was 100 mM sodium perchlorate in 10 mM phosphate buffer, pH 2.5. Mobile phase was eluted at a rate of 1 mL min^{-1}, and the UV absorbance of the eluent was monitored at 210 nm. Inset graphs show the kinetics of the change in peak areas over the photo-oxidation time period (1 h total).

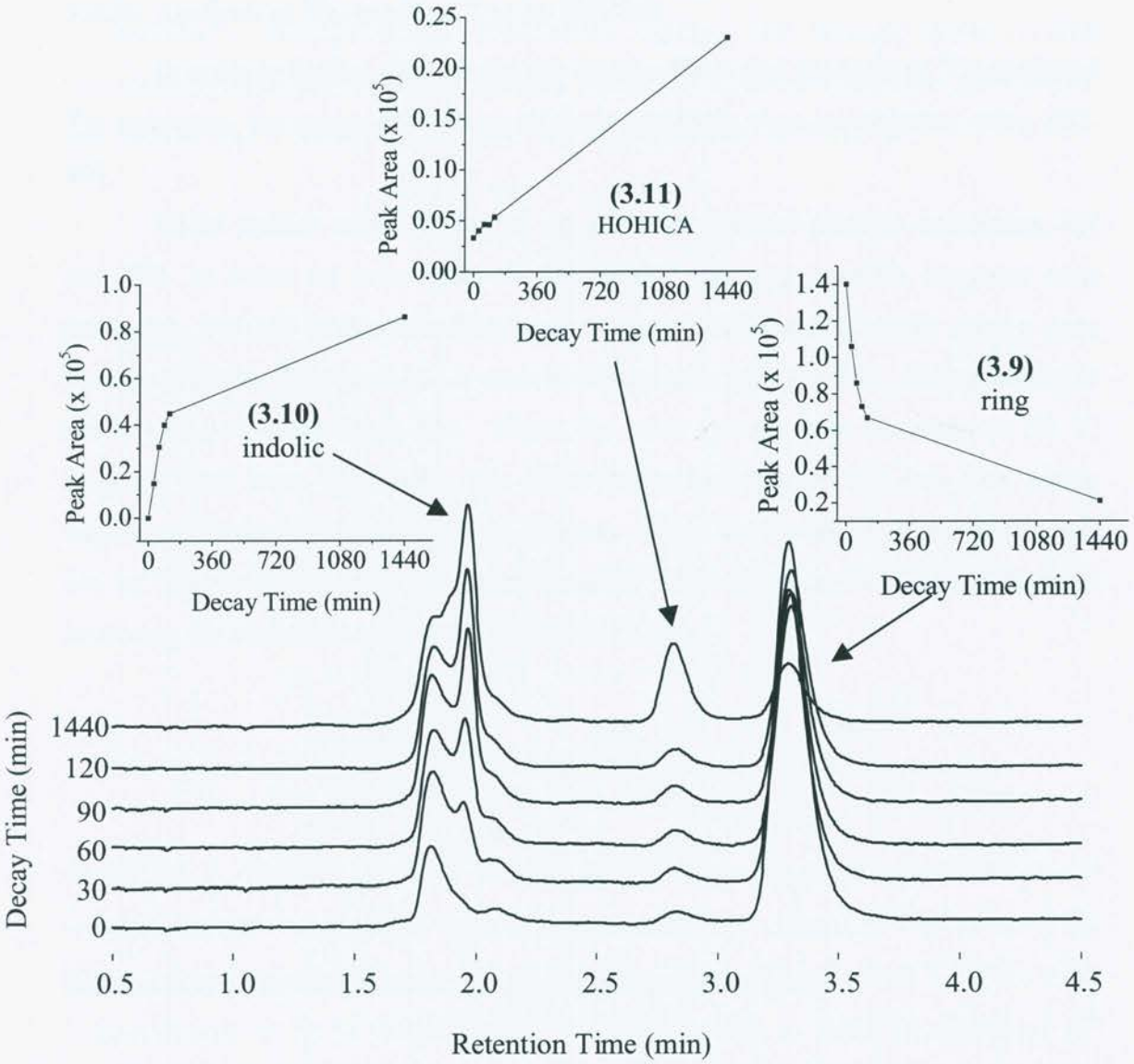

Figure 3.7: HPLC analysis of the time-dependant decay of the HPLC fraction assigned to (3.9) when incubated at 37 °C. The fraction corresponding to (3.9) was collected from HPLC immediately following photo-oxidation and incubated at 37 °C in the absence of light over 24 h. Aliquots were removed at the indicated times and re-injected on to the HPLC column. Water was used as the mobile phase and was eluted at a rate of 1 mL min^{-1}. The eluent was monitored for UV absorbance at 210 nm. Inset graphs show the kinetics of peak area change over the incubation period.

3.4.3b Analysis of $^1O_2$-oxidised Tyr by ESI-MS

In order to further characterise the intermediates and products of $^1O_2$-mediated Tyr oxidation, the molecular masses of these materials were investigated using ESI-MS.

Initial studies were performed on a non-photolysed mixture containing Tyr and RB, in order to investigate the molecular ion and possible fragment ions produced. ESI-MS of this non-photolysed mixture yielded a single peak using a cone voltage of 25 V. This peak had a mass to charge ratio (m/z) of 182, corresponding to the M+ ion of unmodified Tyr. When the cone voltage was increased to 50 V, fragment ions were observed. The major peaks had m/z of 165 and 136, which correspond to the loss of the phenol OH group and to the formation of the immonium ion of Tyr respectively. The latter product arises from a well-known reaction involving the sequential loss of H_2O and CO_2 [219].

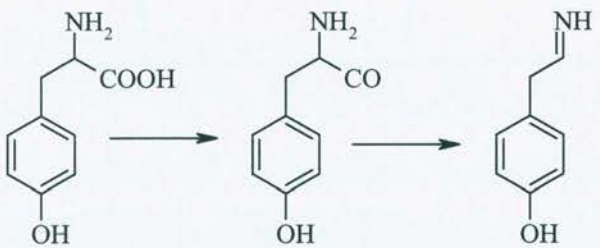

Scheme 3.5: The formation of the immonium ion of Tyr [219].

ESI-MS analysis (cone voltage 25 V) of non-fractionated RB photo-oxidation reaction mixtures yielded two major ions, one corresponding to unmodified Tyr at m/z of 182, and a further peak with m/z of 214. The latter peak was not observed in non-photolysed samples (Figure 3.8). The m/z of this peak is consistent with the addition of two oxygen atoms to the parent Tyr and agrees with earlier evidence of peroxide formation. No fragments arising from the peroxide were observed when a cone voltage of 50 V was used. The range of m/z scanned was not wide enough to observe ions corresponding to RB.

HPLC fractions of peaks (3.9) and (3.11) were also analysed by ESI-MS. The peak assigned to (3.9) gave a spectrum consisting of a single ion of m/z 214 confirming that it is a peroxide. Peak (3.11) yielded an ion with m/z 198. This molecular mass is identical to that expected for HOHICA, suggesting that the peak

assigned to (3.11) is indeed due to this material (Figure 3.9). Two other major peaks are observed in ESI-MS spectra of this HPLC fraction. The identitiy of the ion with m/z 199 is not known. The peak at 151.5 represents a loss of a fragment with m/z 46 and may be due to the loss of a formic acid fragment from HOHICA.

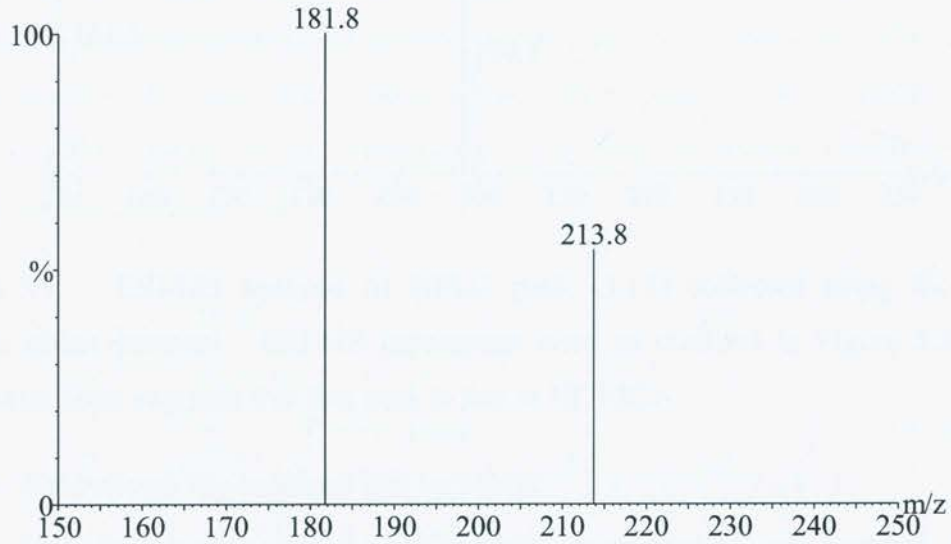

Figure 3.8: ESI-MS analysis of Tyr oxidation products generated on photo-oxidation of free Tyr (2.5 mM in D_2O) in the presence of oxygen and RB (10 μM) for 1 h. Samples were diluted with 2 % formic acid in methanol to give final concentrations of 50 % methanol and 1 % formic acid to assist ionisation of the sample. Solvent was delivered at 10 μL min^{-1} and 2 x 25 μL injections were made for each analysis. The probe tip was set at 3.5 kV with 0.5 kV on the chicane counter electrode. The sampling cone was set at 25 V. The peak at 181.8 is due to un-modified Tyr, the peak at 213.8 is due to Tyr + 32 consistent with the addition of 2 oxygen atoms to Tyr.

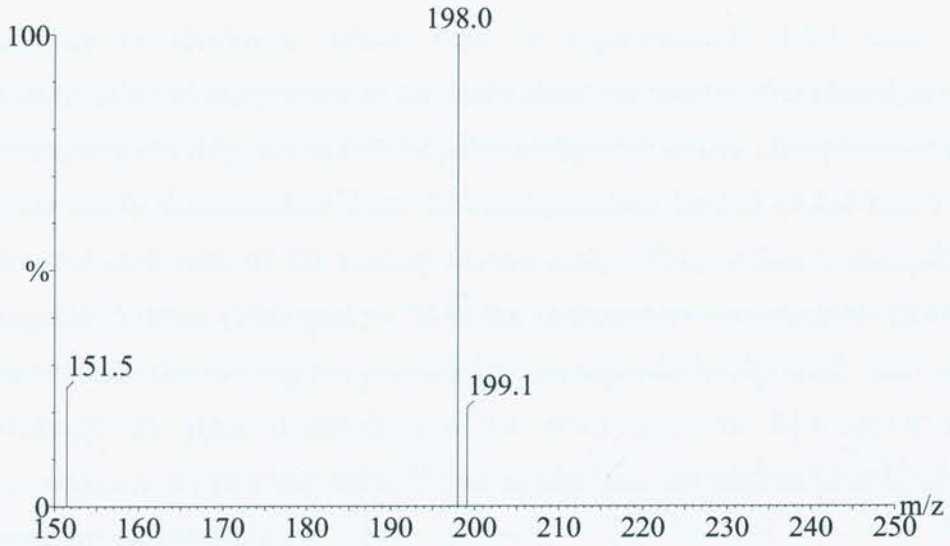

Figure 3.9: ESI-MS analysis of HPLC peak (3.11) collected using the water mobile phase protocol. ESI-MS parameters were as outlined in Figure 3.8. The molecular mass suggests that this peak is due to HOHICA.

3.4.3c Analysis of $^1O_2$-oxidised Tyr by NMR

Two-dimensional ^1H and ^{13}C NMR spectroscopy was carried out in collaboration with Dr W.A. Bubb (Department of Biochemistry, University of Sydney) and used to complete the characterisation of the intermediates and products of $^1O_2$ mediated oxidation of Tyr. Analysis was performed on non-fractionated, photolysed reaction mixtures containing RB and D_2O to enhance the yields of materials and to minimise solvent peak interference in the NMR spectra.

The NMR characteristics of Tyr are well known [220], therefore the peaks arising from un-modified Tyr in these reaction mixtures could be readily assigned. The remaining peaks in the spectra were a complex mixture that could not be immediately assigned. However, the results obtained by HPLC (Section 3.4.3a) suggested that the composition of the mixture of species would change with time on incubation at elevated temperatures and upon treatment with borohydride as a result of the interconversion of the intermediate species into their final products. Subsequent examination of such reaction mixtures might therefore allow the various species present to be identified.

Initially RB photo-oxidised mixtures were incubated at 5 °C for extended periods. Over this time the spectra simplified and comparisons with literature data

[95, 202] showed that the major species remaining were un-modified Tyr and two stereoisomers of HOHICA, which were in approximately 1.5:1 ratio. This subsequently allowed assignment of the peaks observed shortly after photolysis as two stereoisomers of the ring-closed indolic peroxide species (3.10). The peroxide species (3.10) was easily distinguished from the corresponding alcohol (3.11) based on the ^{13}C chemical shift data of the tertiary carbon atom C(3a), which is deshielded by approximately 12 ppm (90.2 ppm vs 78.1 ppm in the major stereoisomers (3.10a) and (3.11a)). Similar deshielding has previously been reported by Sy *et al.*, who reported approximately 12 ppm deshielding effect (93.3 ppm vs 81.6 ppm) of the hydroperoxide moiety of the antimalarial compound artimisinin compared to its corresponding alcohol [221].

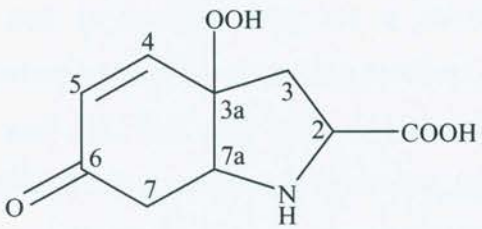

(3.10)

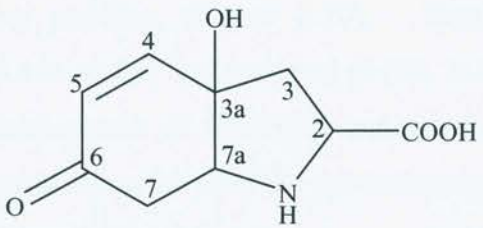

(3.11)

In order to determine the stereoisomers present in these reactions nuclear Overhauser enhancement spectroscopy (NOESY) was employed. This type of two-dimensional NMR is a very powerful tool for determining absolute stereochemistry as it detects through space interactions between protons. Unfortunately no cross-peaks involving either of the C(7) protons in (3.10) or (3.11) could be observed in NOESY spectra. This is most likely due to near complete exchange of these protons with deuterium from the solvent, rendering this position NMR silent. Non-exchangeable solvents (such as $CDCl_3$) were not investigated, as they would alter the photochemical reaction pathway. H_2O was not used, as the enhanced product yields obtained in D_2O were required for sufficient signal strength.

The second method used to deconvolute the initial spectra sought to take advantage of the reduction of the intermediate peroxides using borohydride. It was envisaged that the reduction of (3.10) would lead to the clean production of (3.11), thus simplifying the spectra. This approach should also strengthen the above

assignment of the peroxide signals, as these signals should not be observed after reduction if they are peroxidic.

NMR spectra of the borohydride reduced Tyr peroxides demonstrated that the peroxide moiety was reduced to an alcohol, and also that that the carbonyl at C(6) had been reduced to its corresponding alcohol. This procedure adds another centre of chirality to the molecule, but it appears as though the reduction proceeds in a stereospecific manner, possibly due to initial complexation of borohydride with the oxygen atom at C(3a) leading to facial stereoselectivity of the reduction [222]. Again two stereoisomers were observed in approximately 1.5:1 ratio. In this case the C(7) protons were not deuterium exchanged to the same degree and NOESY cross peaks between the proton at C(6) and the proton of the ring junction carbon C(7a) were observed. Further correlations were observed between protons on each ring in such a way that is feasible only for a *cis* ring junction (Figure 3.10). Thus, the stereochemistry of the reduction products (3.13a and b) was assigned as (2*S*, 3a*R*, 6*S*, 7a*R*) and (2*S*, 3a*S*, 6*R*, 7a*S*). As the stereoisomers of HOHICA and the indolic peroxide (3.10) were present in similar, unequal ratios the absolute stereochemistry of these species can be inferred from the reduction product data.

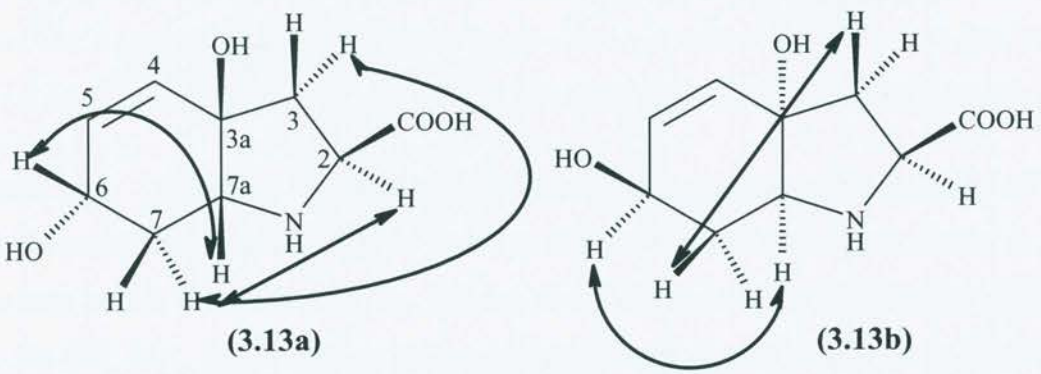

Figure 3.10: Summary of through space interactions detected by NOESY. NMR analyses were carried out on the products of free Tyr (2.5 mM in D_2O) photo-oxidation in the presence of RB (10 μM) and oxygen for 1 h. Useful NOESY spectra were only detected in samples that had been reduced by sodium borohydride prior to analysis.

The complete set of chemical shift data is summarised in Figures 3.11-3.13. Chemical shifts are expressed relative to the internal standard 2,2-dimethyl-2-

silapentane sulfonate and represent the mid-points of cross-peaks in heteronuclear single quantum coherence (HSQC) spectra for protonated carbons, and the mid-points of cross-peaks in heteronuclear multiple bond correlation (HMBC) spectra for non-protonated carbons. All assignments were supported by COSY, TOCSY, HSQC, HMBC and NOSEY data.

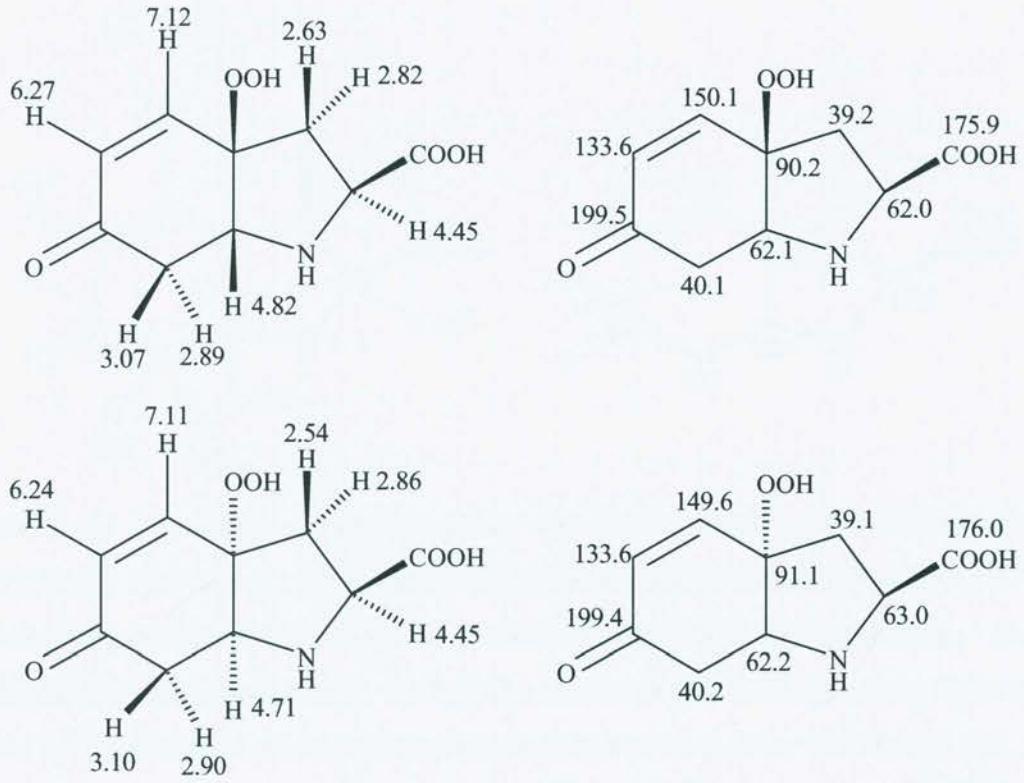

Figure 3.11: Summary of the chemical shift data for the two stereoisomers of the indolic peroxide product (3.10) of free Tyr (2.5 mM in D_2O) photo-oxidation in the presence of RB (10 μM) for 1 h. The top two structures report the data for (3.10a), i.e. the (2*S*, 3a*R*, 7a*R*) isomer. Proton chemical shift data is shown on the left and carbon chemical shifts on the right. The lower structures show proton and carbon chemical shift data for (3.11b) the (2*S*, 3a*S*, 7a*S*) isomer.

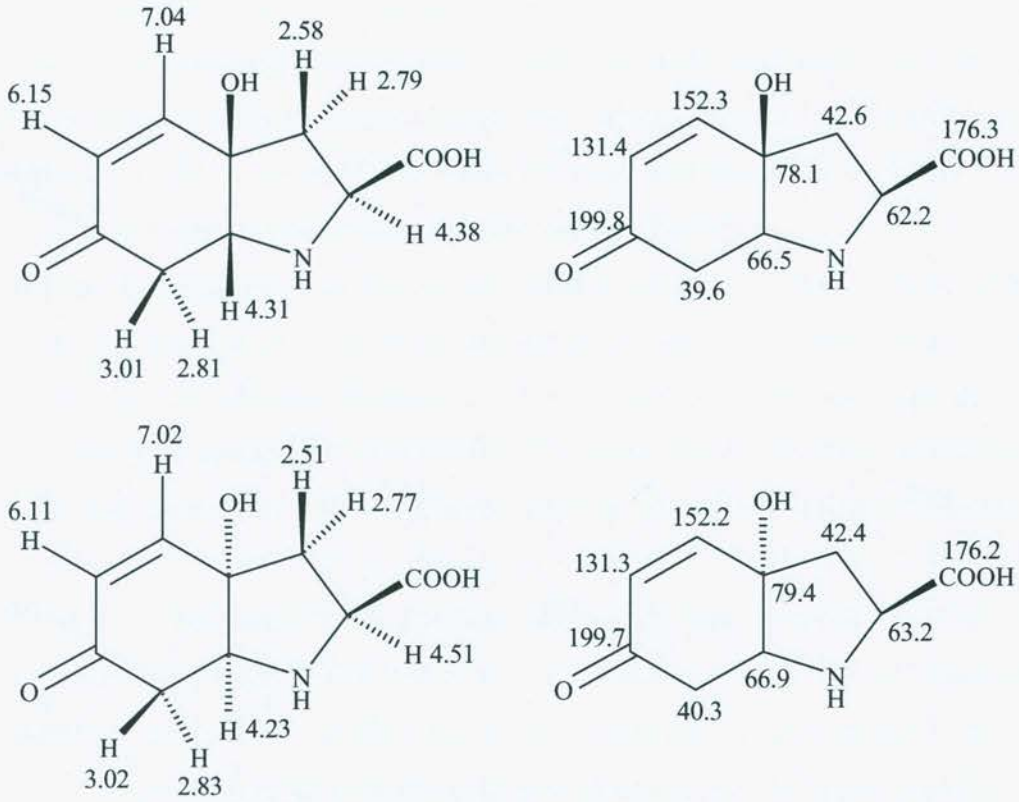

Figure 3.12: Summary of the chemical shift data for the two stereoisomers of HOHICA (3.11). Tyr photo-oxidation was performed as outlined in Figure 3.11. The top two structures report the data for (3.11a), i.e. the (2*S*, 3a*R*, 7a*R*) isomer. Proton chemical shift data is shown on the left and carbon chemical shifts on the right. The lower structures show proton and carbon chemical shift data for (3.11b) the (2*S*, 3a*S*, 7a*S*) isomer.

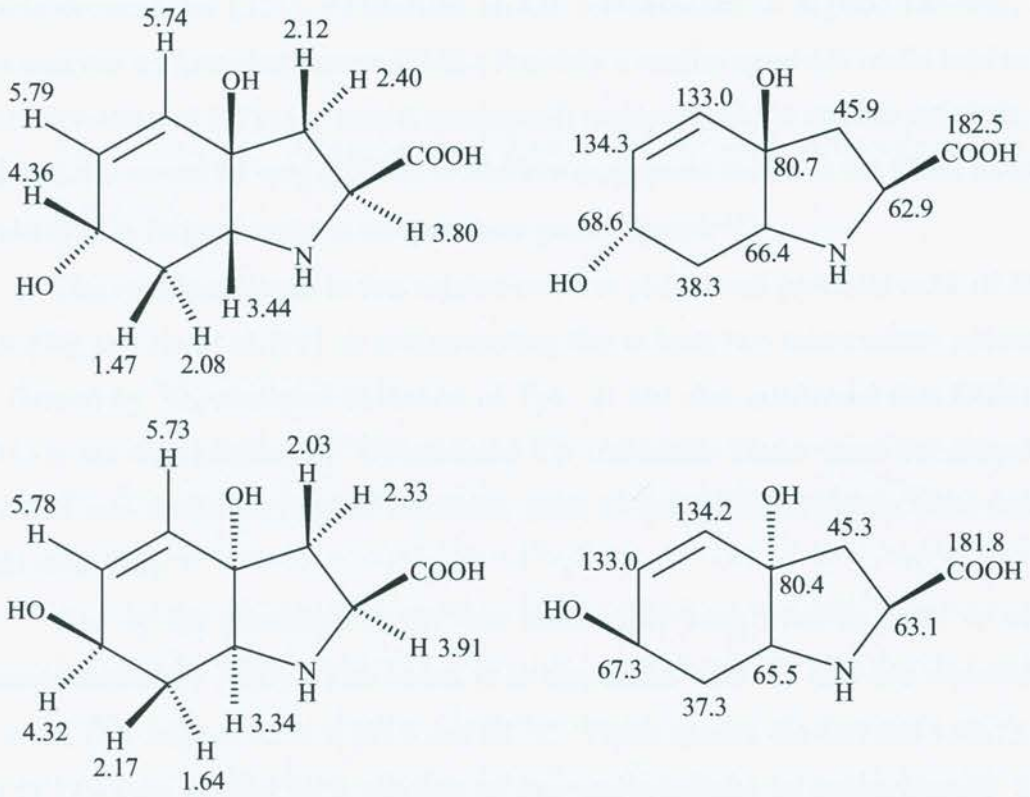

Figure 3.13: Summary of the chemical shift data for the two stereoisomers of the borohydride reduction product (3.13). Tyr photo-oxidation was performed as outlined in Figure 3.11. The top two structures report the data for (3.13a), i.e. the (2*S*, 3a*R*, 6*S*, 7a*R*) isomer. Proton chemical shift data is shown on the left and carbon chemical shifts on the right. The lower structures show proton and carbon chemical shift data for (3.13b) the (2*S*, 3a*S*, 6*S*, 7a*S*) isomer.

3.4.3d Conclusions

The results obtained in this section demonstrate that Tyr is oxidised by $^1O_2$ to yield at least two hydroperoxide species prior to its ultimate conversion to HOHICA. Little evidence for DOPA formation was obtained in agreement with previous work [95, 96, 124].

Previously it has been proposed, but not experimentally demonstrated, that the initial intermediate of $^1O_2$-mediated Tyr oxidation is the 1,4-endoperoxide (3.8) [95, 96], however no evidence for the formation of this species was observed in these experiments. This species is thought to be very short-lived and not detectable by standard techniques. Experimental evidence for endoperoxide formation has been obtained in related molecules such as analogues of histidine and analogues [82], 2-^{13}C-1,3-^{15}N-diphenylimidzole [83], guanosine derivatives [64] and 4,7-

dimethylbenzofuran [223], by reaction at low temperatures in organic solvents, and then analysis by low temperature NMR. Possibly a similar approach could lead to the future detection of a Tyr (or model compound) endoperoxide in organic solvents, but such species would be very difficult to observe in aqueous media as the NMR analysis would need to be performed at temperatures greater than 0 °C.

The results obtained in this section confirm and extend previous work of Endo *et al.*,[96] and Jin *et al.*,[95] in demonstrating that at least two intermediate peroxides are formed by $^1O_2$-mediated oxidation of Tyr. It has also confirmed that HOHICA (3.11) is the final product of $^1O_2$-mediated Tyr oxidation. Under these conditions no evidence was found for further reactions, such as the decarboxylation observed by Endo *et al.* [96].

One of the peroxides (3.10) was sufficiently long lived at 5 °C to allow characterisation by NMR. This result is in agreement with the half-life reported by Jin *et al.*, [95, 202] of 4.2 h at pH 8 and 20 °C. These spectra showed that both (3.10) and (3.11) were present as a mixture of two stereoisomers in approximately 1:1.5 ratio.

The NMR spectra of the borohydride reduction products of (3.10) could also be assigned fully. The stereochemistry of (3.10) and (3.11) could not be assigned directly due to deuterium exchange at C(7), but two stereoisomers were observed and found to be present in a similar, unequal ratio as seen with the reduction product (3.13). NOESY analysis of the reduction products assigned the stereochemistry of the ring junction as *cis*, and were used to infer the absolute stereochemistry of both (3.10) and (3.11) as (2*S*, 3a*R*, 7a*R*) and (2*S*, 3a*S*, 7a*S*).

The stereoisomerism of these species does not stem form the α-carbon as L-Tyr was used as the starting material and the conditions used should not promote racemisation. Rather, the isomerism stems from the intramolecular Michael addition (see Scheme 3.4) responsible for the formation of (3.10). The initial formation of the ring-open peroxide (3.9) results in the generation of a pro-chiral centre. During the ring closing reaction the nucleophilic amino group can attack the electrophilic α,β-unsaturated carbonyl site from either above or below. Due to the symmetry of the molecule and the fact that the amino group is tethered to the rest of the molecule only a *cis* ring junction can result, as is observed by NOESY. Endo *et al.*, also observed the *cis* junction (using circular dichroism) [96], however Jin *et al.*, reported the formation

of a *trans* junction. This assignment was based on the size of coupling constants observed in NMR spectroscopic analysis [202].

3.4.4 Free Radical Formation as a Result of Metal Ion Reduction of Tyr Peroxides

3.4.4a Background

3.4.4a.i EPR spectroscopy

Electron Paramagnetic Resonance (EPR) spectroscopy is a specific technique for the detection of paramagnetic species, such as free radicals and transition metal ions, which contain unpaired electrons. Electrons, as well as protons and certain nuclei, have a magnetic moment or spin. From quantum mechanics it is known that there are two spin states corresponding to two possible orientations in space, which are designated $\pm$ ½. In the absence of an applied magnetic field these spin states are of the same energy. However, when a magnetic field is applied the spin states diverge in energy, as one of the projections will be aligned with the direction of the magnetic field and the other, higher energy spin state will be aligned against it. The transition between these states, i.e. resonance, occurs when the equation $\Delta E = h\nu = g\beta H$ is satisfied (where h = Planck's constant, ν is the frequency of the applied energy source, g is a constant known as the g-value, β is the Bohr magneton and H (sometimes denoted B_0) is the applied magnetic field). From this equation it can be seen that the transitions will occur only at specific values of ν and H. Most commercially available EPR spectrometers employ a fixed value for ν and scan the values of H, the absorption of the microwave radiation at the different H-values constitutes the spectrum. The spectrometer used in this study employs a microwave radiation frequency of *ca.*, 9.5 GHz. The EPR spectrum of a radical species can be characterised by three parameters; the g-value, the hyperfine coupling constants and the line width.

At a fixed frequency (ν), the g-value for each radical is dependant only on H. The g-value for the free electron is 2.00232, however the g-value of a molecular electron is influenced by the nature of the neighbouring atoms. Thus changes in the in the g-value of a radical can indicate delocalisation to nearby heteroatoms.

The magnetic moment of the electron is affected by nearby magnetic nuclei, such as ^{1}H, ^{2}H, ^{13}C, and ^{14}N. The magnetic moments of these nuclei can also be aligned with or against the applied magnetic field leading to multiple transition states and thus multiple EPR signals. The distance between these states is known as the hyperfine coupling constant, and is affected by distance and orientation between the electron and nucleus. In general an EPR signal will be spilt into 2nI+1 lines by magnetic nuclei, where n is the number of nuclei and I is the nuclear spin. Thus an electron near a nitrogen atom (I = 1) will be split into 3 lines. This pattern is known as a triplet.

Observed EPR signals also reflect the mobility of radicals. When a radical is formed on a low-molecular weight species that may tumble freely in solution, sharp well-defined signals are observed. These are described as isotropic signals. If the radical is formed on a molecule with restricted rotation such as on biological macromolecules, the signal is broadened resulting in anisotropic spectra. Mobility is affected by changes in the temperature and viscosity of solutions, as well as by the molecular weight and shape of the molecules on which the radical is formed.

3.4.4a.ii Spin Trapping

Although EPR is a highly sensitive technique for the detection of radicals, these species are usually very short-lived in solution, making direct detection difficult. A technique known as spin trapping has been developed to assist in the detection of these species. Spin trapping agents generally contain nitroso or nitrone moieties, which undergo reaction with short-lived radical species producing one or more spin adducts that have greater lifetime (Scheme 3.6). Commonly used examples of nitrone and nitroso spin traps include 5,5-dimethyl-1-pyrroline-N-oxide (DMPO) and 2-methyl-2-nitrosopropane (MNP) respectively. The spin adducts formed are usually nitroxides that are resonance stabilised by delocalisation of the unpaired electron through the nitroxide functionality.

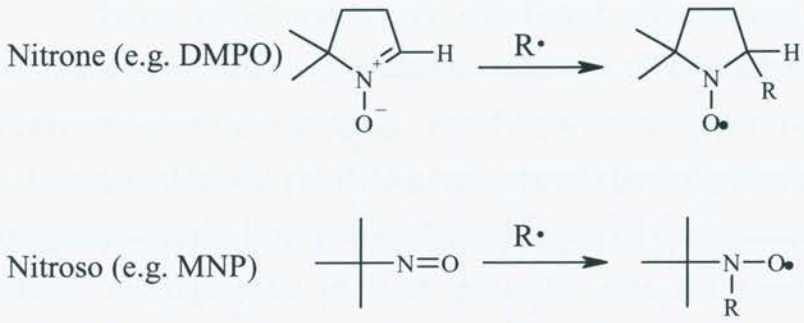

Scheme 3.6: The reactions of nitrone and nitroso spin traps.

Spectra from nitrone (e.g. DMPO) spin adducts usually consist of six lines arising from the splitting of the nitroxide nitrogen triplet into a doublet by the β-hydrogen of the spin trap. The disadvantage of these traps is that the radical of interest actually plays very little part in the hyperfine couplings observed. The size and / or electronic structure of the attached radical influences the observed spectra by affecting the conformation of the pyrrole ring (i.e. altering the dihedral angle between the orbital containing the unpaired electron and the β C-H bond), which can result in changes in the hyperfines observed [224]. This is of use when distinguishing between different types of radicals (e.g. C-centred vs O-centred or S-centred).

Spectra obtained with nitroso spin trapping (e.g. MNP) potentially yield more detailed structural information about the radical of interest as the radical is bound directly to the nitroso nitrogen (as opposed to one carbon distant in DMPO), although these traps are generally only useful for trapping carbon-centred radicals. Spectra of MNP spin adducts usually consist of a 1:1:1 triplet derived from the nitroso nitrogen, with further splittings derived from the trapped radical. The hyperfine coupling constants of these extra signals can often be used to gain diagnostic information about the initial radical.

3.4.4a.iii Radical formation from Tyr-derived peroxides

Previous sections have demonstrated that the $^1O_2$-mediated oxidation of Tyr yields peroxide species that can be decomposed by heat, UV photolysis and one- and two-electron reducing species. A large body of experimental evidence has demonstrated that radical species can be formed during such reactions [225, 226], however the formation of radicals on decomposition of $^1O_2$-derived Tyr peroxides has not been studied previously.

The aim of the next series of experiments reported was therefore to investigate the formation of radicals produced by reduction of Tyr-derived peroxides using EPR spectroscopy with spin trapping. Initial experiments demonstrated that thermal decay of these peroxides did not yield a large enough flux of radicals to be readily detected consistent with the slow rate of decomposition of these peroxides (Figure 3.3). UV induced decomposition of these peroxides was not investigated as it is well established that these spin traps are also decomposed by UV [227]. Metal ion reduction of the Tyr peroxides was therefore investigated and used throughout the following experiments.

The radicals formed were characterised using EPR spectroscopy. In order to obtain maximum information both nitrone and nitroso spin traps (i.e. DMPO and MNP) were employed in the studies reported here.

3.4.4b EPR spin trapping experiments with DMPO

Upon treatment of solutions of Tyr peroxides generated by RB photo-oxidation in H_2O (~125 μM peroxide) with thoroughly nitrogen gassed solutions of Fe^{2+}/EDTA (187.5 μM, 1:1 complex) in the presence of the nitrone spin trap DMPO (187.5 mM) complex EPR spectra were observed (Figure 3.14a). The spectra observed appear to be due to the presence of, at least, three separate radical adducts. The two major signals observed are analysed in terms of triplets of doublets with parameters of a(N) 1.60 mT, a(H) 2.41 mT and a(N) 1.54 mT, a(H) 2.06 mT (Figure 3.14 and Table 3.1), consistent with parameters previously published for carbon-centred radicals [227].

The remaining signal has been assigned to the well-characterised hydroxylated spin trap product DMPO-OH, [a(N) 1.49 mT, a(H) 1.49 mT] [227]. The equivalent nitrogen and proton coupling constants for this species collapse the expected triplet of doublet signal into a 1:2:2:1 quartet. This adduct may arise due to impurities in the spin trap preparation, low levels of Fe^{2+} autoxidation and thermal and/or photochemical reactions of DMPO. These assignments have been confirmed by computer based spectral simulation of each species separately (Figure 3.14 c,d,e) and as a mixture (Figure 3.14b).

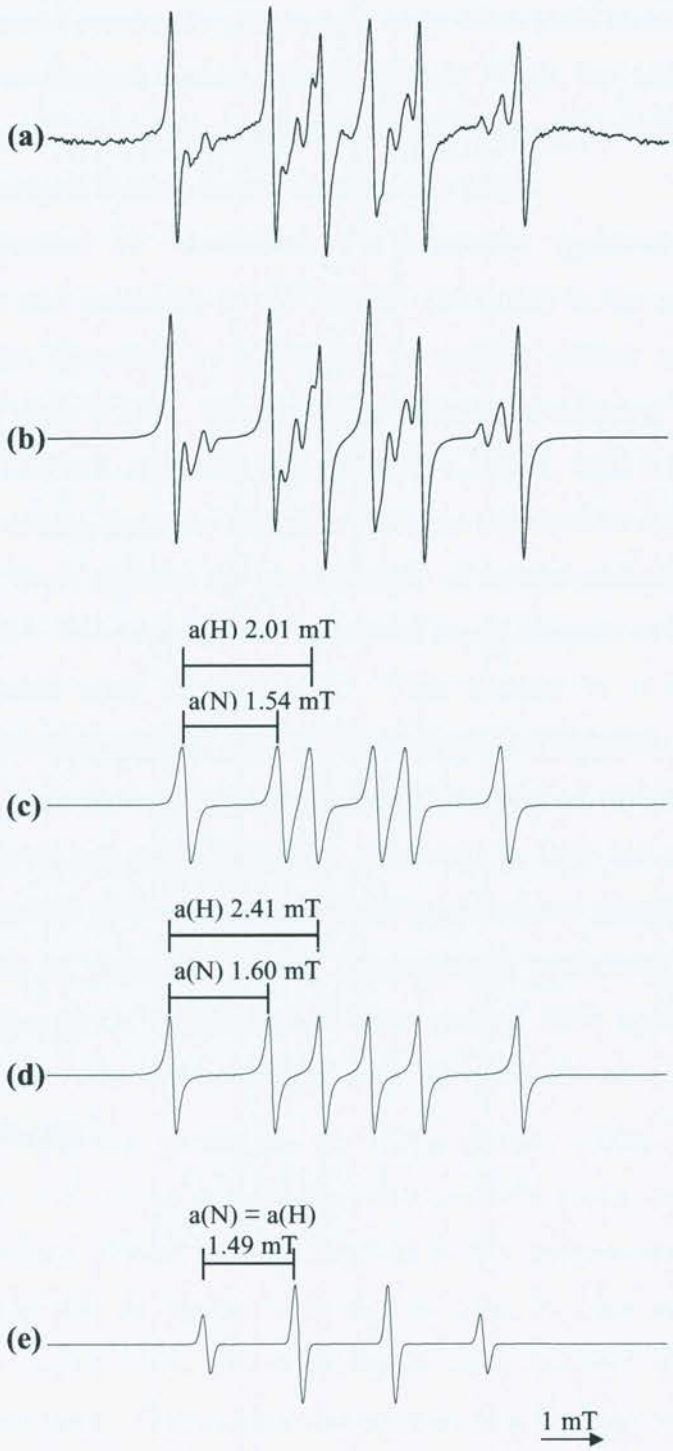

Figure 3.14: EPR spectra detected on reaction of Tyr-derived peroxides (~125 μM peroxides generated as described in Figure 3.1) with Fe^{2+}/EDTA (187.5 μM, 1:1 complex) in the presence of the spin trap DMPO (187.5 μM). (a) experimentally obtained spectrum, (b) combined computer simulation, (c)-(e) separate computer simulations of the three detected radicals using the parameters shown.

3.4.4c EPR spin trapping experiments with MNP

As discussed previously nitroso spin traps often yield more detailed structural information about trapped carbon-centred radicals. Thus, the nature of the carbon-centred adducts detected in experiments with DMPO and $^1O_2$-derived Tyr peroxides was further investigated using the nitroso spin-trap MNP.

The reduction of $^1O_2$-derived Tyr peroxides (generated by RB photo-oxidation, ~300 μM peroxide) by Fe^{2+}/EDTA (167 μM) in the presence MNP (8.3 mM) led to the detection of a number of radical adduct signals using EPR spectroscopy (Figure 3.15). These signals have been assigned to two triplets of doublets [a(N) 1.50 mT, a(H) 0.21 mT and a(N) 1.59 mT, a(H) 0.13 mT] (Table 3.1) with the triplet arising from the nitroxide nitrogen and doublet from a proton on the added radical. These features are characteristic of carbon-centred radicals of partial structure •CHRR'. Most spectra also contained small amounts of an additional sharp triplet signal with a(N) of 1.70 mT. This species is a well characterised decomposition product of MNP, di-*tert*-butyl nitroxide ((^{t}Bu)$_2$NO•, DTBN), which is known to arise from thermal or photochemical degradation of MNP [227]. Similar experiments carried out using peroxides generated in D_2O led to the detection of signals with identical parameters, but with increased signal intensity, consistent with the higher yields of peroxide present. Experiments performed on Tyr peroxides derived from the MoO_4^{2-}/H_2O_2 system also yielded EPR spectra with identical parameters. These data are consistent with the presence of a common peroxide precursor in each case.

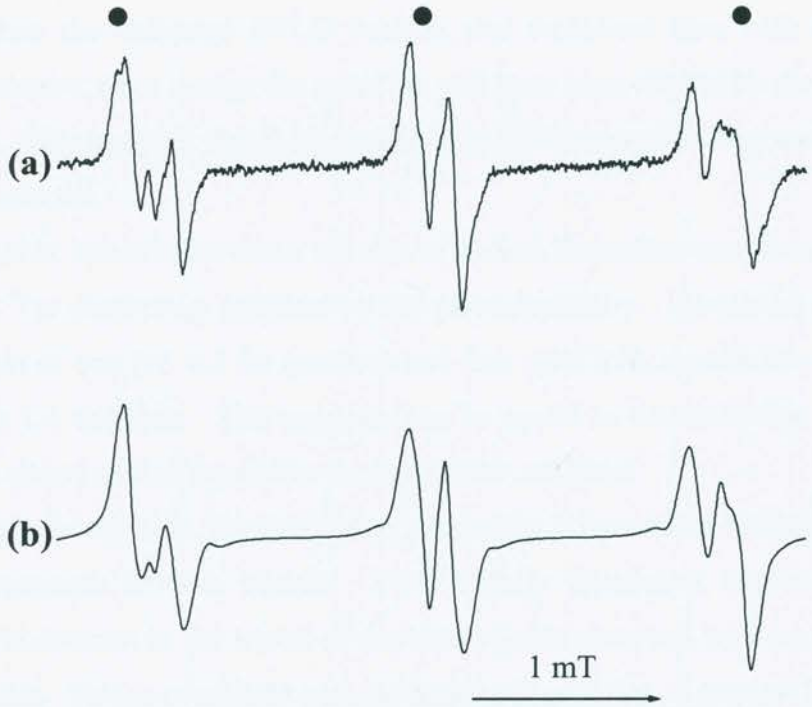

Figure 3.15: (a) EPR spectra observed on reduction of Tyr-derived peroxides (~300 μM peroxide, generated as described in Figure 1) by Fe^{2+}/EDTA (167 μM, 1:1 complex) in the presence of MNP (8.3 mM). Signals marked (●) are assigned to $(^tBu)_2NO^\bullet$ [a(N) 1.70 mT] other signals are assigned to Tyr-derived carbon-centred radicals; see text and Table 3.1. (b) Computer simulation of the spectrum in (a) using the parameters in Table 3.1.

In order to further investigate the origin of these radical species the HPLC fraction assigned to (3.9) was collected and subsequently treated with Fe^{2+}/EDTA and MNP. This fraction yielded signals identical to the unseparated reaction mixture, further suggesting that the signals were derived from $^1O_2$-derived Tyr peroxides as characterised in section 3.4.3. The same signals were observed regardless of the $^1O_2$ generating system used. These results demonstrate that the same peroxide species are produced by each $^1O_2$ generating system and that the observed radicals are obtained directly from the peroxide intermediate and not from subsequent intermolecular reactions (e.g. hydrogen abstractions from the un-modified Tyr present in the crude, un-fractionated reaction mixture). Similar experiments could not be performed with the HPLC fraction assigned to (3.10) as insufficient material was isolated.

Interestingly, the signals obtained from the MoO_4^{2-}/H_2O_2 system were more intense when the collected HPLC fraction was examined than with the complete reaction mixture, even though the peroxide will have been diluted by the fractionation procedure. This suggests that the presence of molybdate species may catalyse the loss of radical adducts.

Further information about the site of radical formation was investigated using deuterated Tyr derivatives oxidised by RB photochemistry. Deuterium atoms have a nuclear spin of one (cf. 0.5 for protons) and thus split EPR signals into 1:1:1 triplets rather than 1:1 doublets. This property can be useful in determination of the actual molecular site of radical formation on a particular substrate.

Experiments with Tyr deuterated at the ring 3,5 positions resulted in a change in the parameters of both signals. Two, slightly broadened, triplet signals were observed, in contrast to the triplet of doublets signals observed with non-labelled Tyr (Figure 3.16). This is consistent with both radicals coupling to protons (or deuterons) at the ring 3,5 positions. Extra splittings due to the deuterons were not resolved. The ratio of a(N) to a(D) is known to be 6.52 [228] thus an a(H) coupling of 0.13 mT (as observed above) would yield an a(D) of approx 0.02 mT. This is not likely to be resolved under these conditions. The use of Tyr deuterated at all available ring positions (i.e. 2,3,5,6) resulted in a similar simplification of the spectra, with a small further coupling being detected in one signal. This coupling is assigned to the deuterons at the 2,6 ring positions (Figure 3.16) (Table 3.1).

Experiments using Tyr deuterated at the C(3) (methylene, $-CH_2-$) position were also performed and yielded identical spectra to the non-labelled substrate confirming that all of the observed radicals are formed on the Tyr ring and not at the C(3) position.

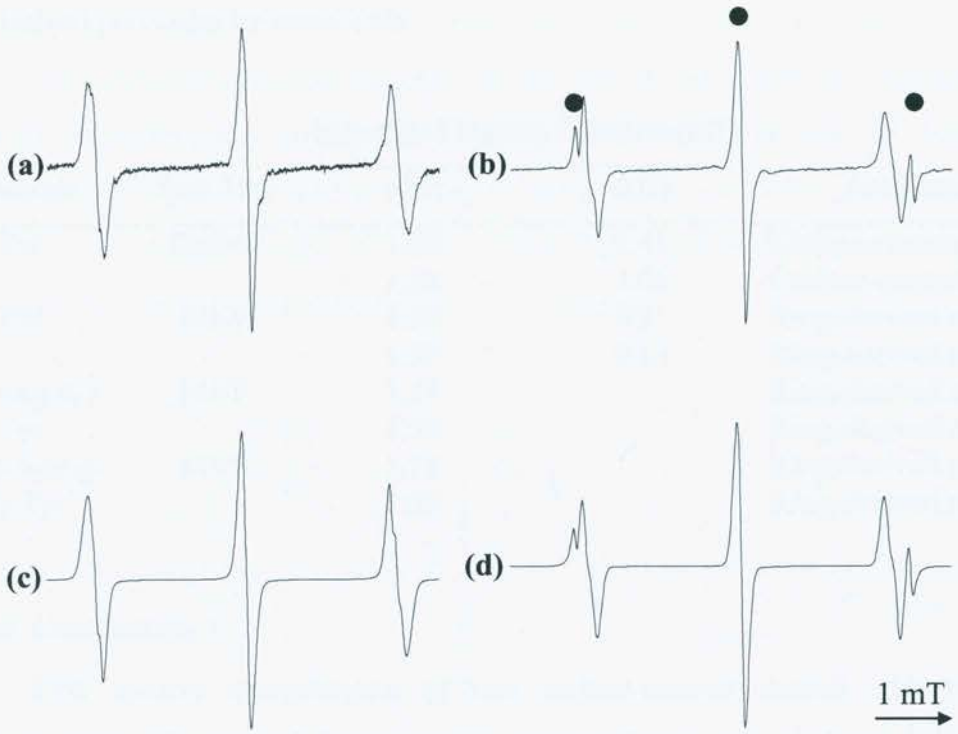

Figure 3.16: EPR spectra observed on reaction of peroxides generated on (a) 3,5-ring-d_2-Tyr and (b) 2,3,5,6-ring-d_4-Tyr with Fe^{2+}/EDTA (167 μM, 1:1 complex) in the presence of MNP. Peroxides were generated as described in Figure 3.1. Signals marked (●) are assigned to $(^tBu)_2NO^\bullet$ [a(N) 1.70 mT] other signals are assigned to Tyr-derived carbon-centred radicals. (c) and (d) are computer simulations of the spectra in (a) and (b) respectively using the parameters in Table 3.1.

Table 3.1: EPR parameters of spin trap radical adducts detected on reduction of Tyr-derived peroxides by metal ions

Substrate	Spin Trap	Hyperfine Coupling Constants (mT) a(N)	a(H)	Assignment
Tyr	DMPO	1.60	2.41	Carbon-centred radical
		1.54	2.06	Carbon-centred radical
Tyr	MNP	1.50	0.21	Ring-derived radical
		1.59	0.13	Ring-derived radical
(3,5-ring-d_2)-Tyr	MNP	1.51		Ring-derived radical
		1.59		Ring-derived radical
(2,3,5,6-ring-d_4)-Tyr	MNP	1.51		Ring-derived radical
		1.59		Ring-derived radical

3.4.4d Conclusions

EPR spectra characteristic of two carbon-centred radical adducts were observed when $^1O_2$-derived Tyr peroxides were reduced with chelated Fe^{2+} in the presence of either nitrone (DMPO) or nitroso (MNP) spin traps. Experiments with DMPO demonstrated that at least two carbon-centred radical adducts were formed under these conditions, but provided little structural information about the exact nature of these radicals. Experiments with MNP provided structural information with the location of the radical adducts demonstrated to be on the Tyr ring by the use of deuterated Tyr derivatives. Tyr deuterated at the ring 3,5 positions showed that both the radicals formed are influenced by protons (or deuterons) located at these positions and experiments with 2,3,5,6 ring-deuterated Tyr suggested that the 2,6 positions may also influence the couplings of one of the radicals. Tyr deuterated at the methylene C(3) position yielded identical spectra to the non-labelled substrate.

3.5 CONCLUSIONS

The results presented in this chapter have confirmed that $^1O_2$-mediated oxidation of Tyr leads to the formation of peroxide species (Scheme 3.7) in agreement with previously reported data [95, 96]. Peroxide formation was found to proceed in a photolysis time dependant manner and was enhanced in the presence of D_2O and suppressed by azide, suggesting that the reaction is $^1O_2$-dependant. Further confirmation of $^1O_2$-dependency was obtained in experiments using the MoO_4^{2-}/H_2O_2 $^1O_2$ generating system, which was found to oxidise Tyr to yield the same peroxide

species as RB photo-oxidation. The MoO_4^{2-}/H_2O_2 system seems to generate a yield of peroxides greater than 100 % as 2950 μM peroxides were formed from 2500 μM of Tyr. This apparent anomaly is likely to be due to the slight overestimation of peroxide concentrations by the FOX assay. The MIA was used to estimate a correction factor of 1.55. Taking this factor into account only 1903 μM Tyr peroxide was actually formed, a yield of 76 %. This high yield correlated with the large amount of Tyr consumption observed in HPLC analysis.

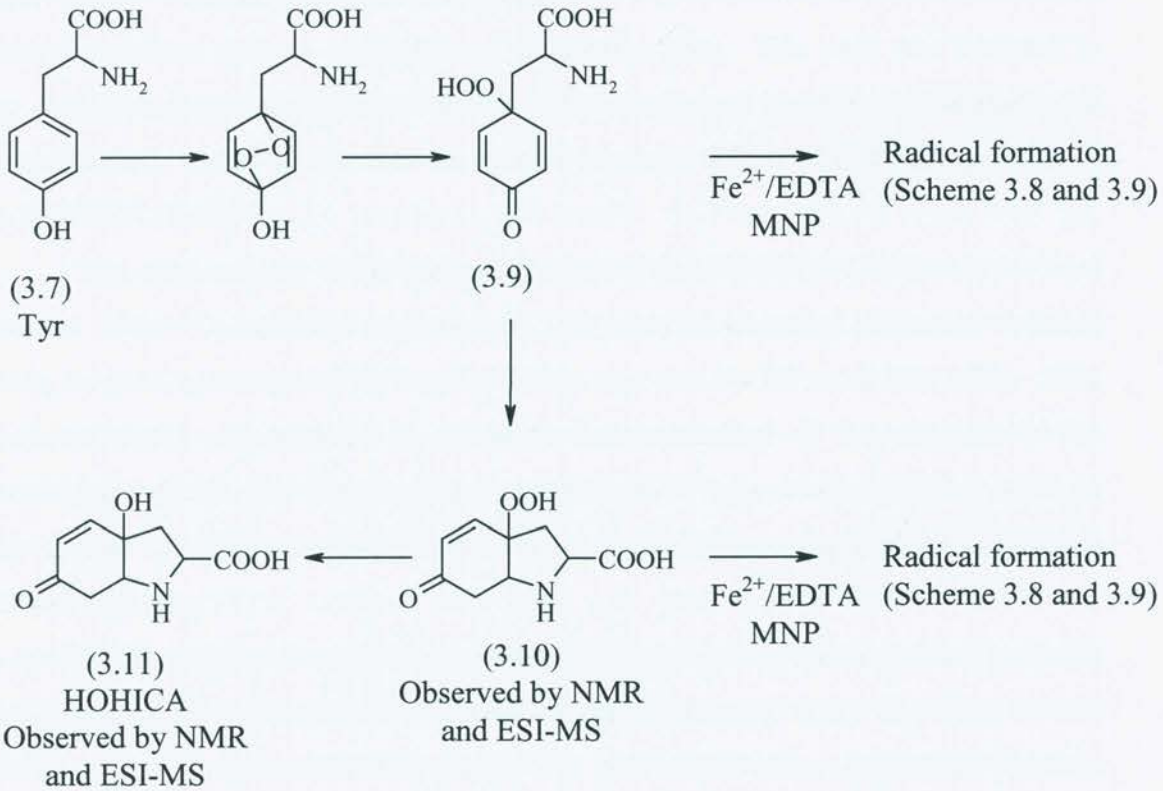

Scheme 3.7: Summary of reaction pathways observed in this chapter.

The naphthalene endoperoxide $^1O_2$ generation system was not as successful in bringing about $^1O_2$-mediated oxidation of Tyr, although very small amounts of HOHICA appeared to be generated. It was not possible to quantify the amount of $^1O_2$ produced by either RB photo-oxidation, or the MoO_4^{2-}/H_2O_2 system, and thus it was not possible to calculate the efficiency of Tyr oxidation by $^1O_2$. Thus it may be that these systems produce a much greater flux of $^1O_2$ than the decomposition of MNPAE, leading to the small amount of Tyr consumption observed using the latter method.

Tyr-derived peroxides were found to be labile to elevated temperatures, UV light and the reducing species borohydride and chelated Fe^{2+}. These results are in

agreement with previous reports of the stability of related amino acid peroxides [193, 198, 217].

Further structural characterisation of the Tyr peroxides and the products arising from their decay was carried out using HPLC, ESI-MS and 2D-NMR. Results from these experiments demonstrate that Tyr is oxidised by $^1O_2$ to yield at least two peroxide species. The initial, isolable, peroxide (3.9) was stable enough to be collected from the HPLC column and analysed by FOX assay and MS, both of which demonstrated the presence of a peroxide species. This peroxide fraction was also re-injected after various incubation times at 37 °C, which resulted in the detection of a second peak that grew in intensity over incubation time. This peak was assigned to the ring closed peroxide species (3.10). After prolonged incubation a further peak was observed, which appeared to be a stable product. MS confirmed this product to be HOHICA (3.11).

Two-dimensional NMR analysis confirmed that HOHICA (3.10) was the final product of the $^1O_2$-mediated oxidation of Tyr, with the chemical shift data obtained being in good agreement with the NMR data reported by Jin *et al.* [95, 202]. This previous work was extended to complete characterisation of the structure of the indolic peroxide (3.10). The ring open peroxide (3.9) was not observed by NMR as this species will decay to yield (3.10) over the length of time required for acquisition of the NMR data.

NMR analyses show that two stereoisomers of both of the ring closed products (3.10) and (3.11) were formed in a ratio of approximately 1:1.5. However, neither (3.10) or (3.11) yielded NOSEY spectra that could be used to assign their absolute stereochemistry. This lack of NOEs is believed to be due to near complete exchange of the C(7) proton with solvent deuterium. Photo-oxidised Tyr, which was treated with sodium borohydride prior to NMR analysis, did provide usable NOEs for this position and thus allowed complete assignment of the stereochemistry. These assignments were used to infer the absolute stereochemistry of (3.10) and (3.11).

The stereoisomers observed in the NMR experiments were not observed in HPLC experiments as their interactions with the column material would be practically identical, and therefore the two isomers will have identical RT. It may be possible to separate the stereoisomers with the use of an HPLC column packed with a chiral stationary phase, however this was not investigated in these experiments.

EPR spectra characteristic of two carbon-centred radical adducts were observed when $^1O_2$-oxidised Tyr was reduced by Fe^{2+}/EDTA complex in the presence of nitrone (DMPO) or nitroso (MNP) spin traps. DMPO experiments provided evidence for the formation of (at least) two carbon-centred radicals. MNP experiments provided structural information about the carbon-centred radicals formed. EPR spectra obtained from Tyr deuterated at the methylene C(3) position were identical to those obtained from the non-labelled substrate. This is as expected as the NMR data are consistent with the peroxides being formed on the ring C(1) position and reactions that would lead to the formation of a carbon-centred radical at C(3) are unlikely to occur.

Experiments using Tyr deuterated at the ring 3,5 and ring 2,3,5,6 positions show that the carbon-centred radicals formed are influenced by deuterons (or protons) located at the 3,5 and 2,6 positions, and suggest that both species arise from the C(3/5) ring sites. These radicals are believed to be generated via a pseudo-Fenton reaction between the peroxides and Fe^{2+}. The reduction of peroxides by transition metal ions is known to yield alkoxyl radicals, (i.e. radicals of partial structure -RO•) [197, 199, 226]. The observation of carbon-centred radicals in these experiments is rationalised by the postulated occurrence of an intramolecular epoxidation reaction between the initial (undetected) alkoxyl radical and the neighbouring double bond (Scheme 3.8). Similar reactions have been well characterised for alkoxyl radicals formed during the decomposition of unsaturated fatty acid hydroperoxides [229]. In the case of Tyr peroxides this reaction will produce a carbon-centred radical at ring position 3 (or 5) consistent with the results from the 3,5-ring-d_2-Tyr experiments. This carbon-centred radical can then be trapped by MNP yielding the radical adduct observed by EPR. This reaction was shown to occur with the ring-opened peroxide (3.9) using HPLC fractionation followed by EPR, but it is also feasible that this reaction could occur with the ring-closed peroxides (3.10), the spectra derived from these radicals are likely to be indistinguishable and indeed it is likely that the two pathways operate simultaneously (Scheme 3.8).

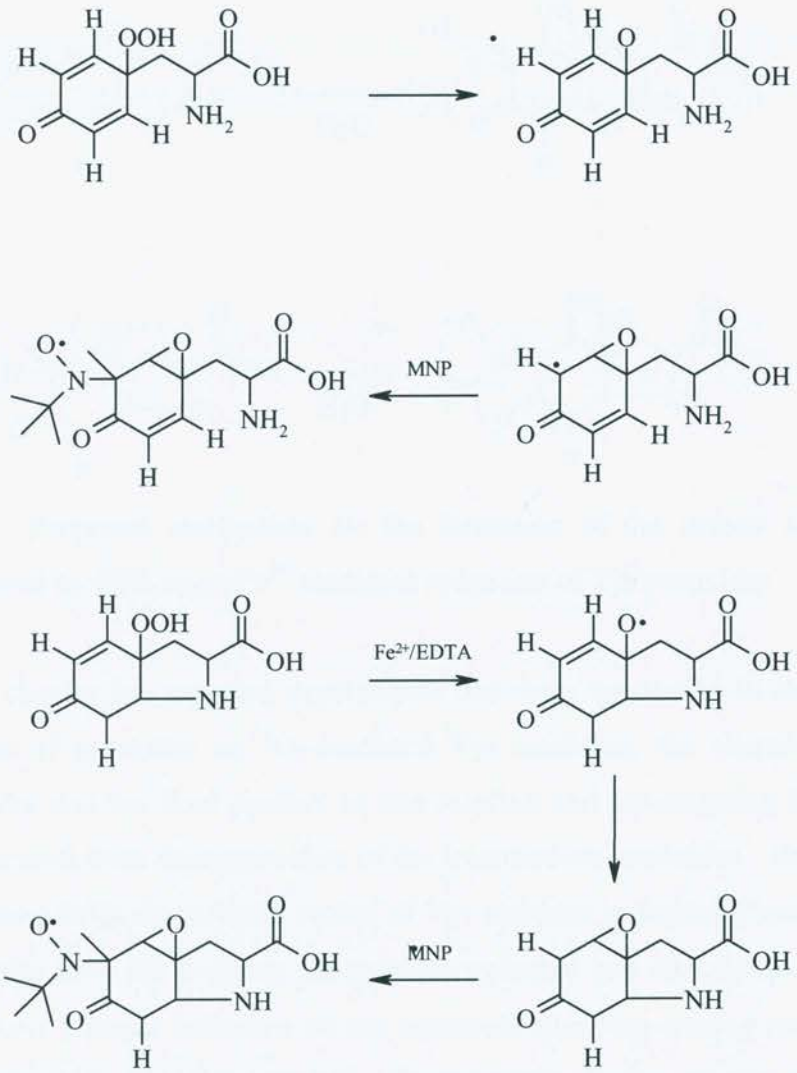

Scheme 3.8: Proposed mechanisms for the formation of one of the Tyr-peroxide derived radicals observed by EPR spin trapping

The second radical adduct observed also appears to be derived from the 3,5-position as demonstrated by the simplification of the spectra in 3,5-d_2-Tyr labelled Tyr experiments. This radical also has a small coupling to the 2,6 position as observed in the 2,3,5,6-ring deuterated Tyr experiments. This second species is thought to arise by hydrolytic cleavage of the initial epoxide ring (Scheme 3.9).

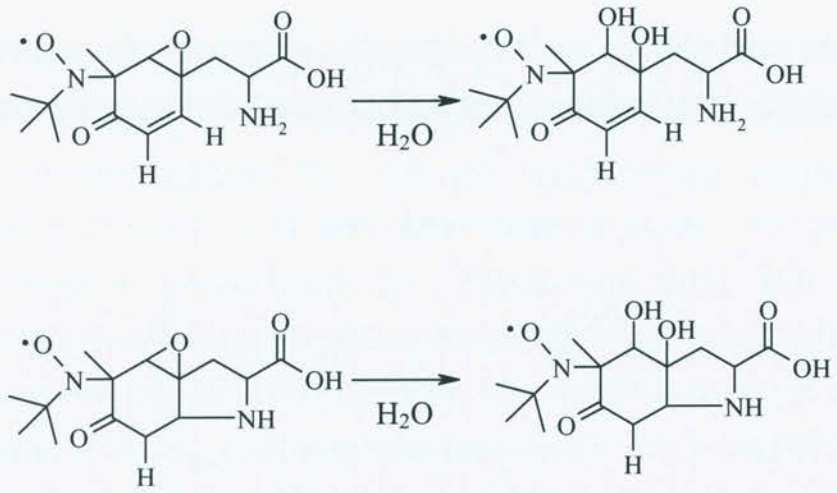

Scheme 3.9: Proposed mechanism for the formation of the second MNP radical adduct observed by EPR upon Fe^{2+} mediated reduction of Tyr peroxides

This chapter has reported experiments that were successful in demonstrating the formation of peroxides on $^1O_2$-mediated Tyr oxidation, the characterisation of these peroxides and the final product of this reaction and investigating the nature of radicals generated from decomposition of the intermediate peroxides. However, free Tyr is not necessarily an accurate model of Tyr residues in peptides and proteins as these molecules have the α-amino nitrogen incorporated into the peptide bond. This is likely to have a major influence on the intramolecular ring-closing reaction of the initial hydroperoxide (see Scheme 3.7). Consequently, further studies were carried out both with model compounds lacking this amino group, and Tyr residues incorporated into peptides and proteins. The results of these studies are described in the following chapter.

CHAPTER 4 - FORMATION AND REACTIONS OF PEPTIDE TYROSINE RESIDUE PEROXIDES GENERATED BY $^1O_2$-MEDIATED OXIDATION

4.1 INTRODUCTION

As outlined in previous chapters, Tyr residues, as well as His, Trp, Cys and Met are important targets for $^1O_2$. In the last chapter, peroxide intermediates formed on oxidation of free Tyr by $^1O_2$ were characterised, but no such work has been carried out previously on peptide-bound Tyr. Craido *et al.* [230], have examined the oxidation of di- and tri-peptides of Tyr and reported that the photosensitised oxidation of these peptides resulted in the detection of increased levels of free amine groups. This suggested that the oxidation of the Tyr residues leads to peptide bond cleavage with the release of free Tyr. However, no characterisation of intermediate peroxides or products was performed.

A major process in the conversion of Tyr through to its ultimate product HOHICA is an intramolecular Michael addition reaction involving the α-amino nitrogen atom. In a peptide or protein, this α-amino nitrogen atom will be incorporated into the peptide bond and thus will be less available for intramolecular reactions. If this is the case, it might be expected that the intermediate peroxides would be more stable and yield different products on decomposition compared to those formed on free Tyr. $^1O_2$-mediated oxidation of peptide- or protein- bound Tyr has been studied previously, although these reports mainly concentrated on kinetic aspects of the reactions rather than analysis of the products formed [79, 231].

Amino acid- and protein-derived peroxide species are known to damage other biological molecules, including low molecular weight compounds and macromolecules. Protein-derived peroxides, generated by γ-irradiation or $^1O_2$, have been shown to oxidise both free and protein thiols, in radical and non-radical mediated processes. The oxidation of protein thiols can lead to the inactivation of important cellular enzymes, such as glyceraldehyde 3-phosphate dehydrogenase (GADPH) and glutathione reductase (GR) [175]. It is also known that anti-oxidant compounds, such as ascorbate and glutathione, reduce $^1O_2$-derived protein peroxides [175]. Gebicki *et al.*, have observed the formation of protein-DNA cross-linked species on reaction of protein peroxides, generated by γ-irradiation, with DNA [232]. The mechanism of this reaction was investigated further by Luxford and co-workers who showed that radicals derived from protein peroxides could mediate single and double strand cleavage, the formation of DNA-protein adducts, and mutagenic base oxidation products [193, 217]. These studies suggest that protein-derived peroxides

may have important biological roles.

Thus, the $^1O_2$-mediated oxidation of Tyr as a residue of peptides was examined, to assist in identification of intermediate peroxides formed and to examine the final products of this reaction in a more biologically relevant context.

4.2 AIMS

The aims of the studies presented in this chapter were to extend the previous studies of $^1O_2$-mediated oxidation of free Tyr to investigate similar reactions with peptide- and protein-bound Tyr residues, using model compounds and small peptides. $^1O_2$ was generated using either rose bengal (RB) photo-oxidation, a MoO_4^{2-} / H_2O_2 system or by the decomposition of a naphthalene endoperoxide. The formation of peroxides was monitored by FOX assay, and both the peroxides and their decomposition products were characterised using high performance liquid chromatography (HPLC), electrospray ionisation (ESI) mass spectrometry (MS) and nuclear magnetic resonance (NMR) spectroscopy. The stability of peroxides formed was investigated under a variety of conditions and the formation of radicals from peroxides examined using electron paramagnetic resonance (EPR) spectroscopy with spin trapping. EPR was also used to investigate the ability of radicals derived from Gly-Tyr-Gly peroxides to transfer radical damage to other peptides and proteins.

4.2.1 Model Compounds, Peptides and Proteins Used in this Study

In the studies reported in this chapter a number of derivatives of Tyr (4.1) and model compounds were investigated. These included 3-(4-hydroxyphenyl)propionic acid (HPPA) (4.2), *N*-acetyl Tyr (4.3), and the peptide Gly-Tyr-Gly (4.4). HPPA was chosen as it lacks the α-amino group of Tyr and thus cannot undergo the Michael addition observed with $^1O_2$-oxidised Tyr. *N*-acetyl Tyr was investigated, as it is the simplest analogue of Tyr where the α-amino group is blocked by a peptide bond. The peptide Gly-Tyr-Gly was examined because it is a model for Tyr as a protein residue and it contains no other $^1O_2$-reactive residues. Photo-oxidations were carried out using 2.5 mM solutions of these substrates at neutral pH, in the presence of O_2 and 10 μM RB. The H_2O_2 / MoO_4^{2-} and naphthalene endoperoxide systems were also used to generate $^1O_2$ in some cases.

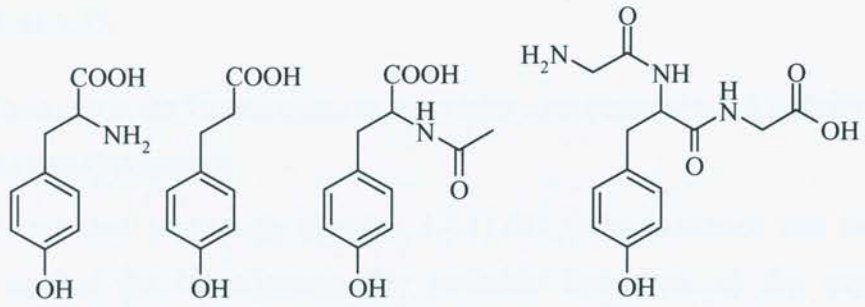

(4.1) **(4.2)** **(4.3)** **(4.4)**

The proteins used in this study include bovine serum albumin (BSA) (75 μM) and histone H1 (470 μM). BSA was used as a general protein model as it contains all of the common amino acids, and is commercially available in high purity. Histone H1 contains none of the $^1O_2$ reactive residues (Trp, Tyr, His, Cys, Met; see Chapter 1) except for a single Tyr that is near to the surface of the globular structure.

The RB photosensitised oxidation of HPPA has been studied previously by Saito *et al.*, although their studies were carried out at alkaline pH [233, 234]. These authors found that the product of this reaction was a quinol species (4.6) and postulated that a peroxidic intermediate (4.5) was the initial species generated in the reaction. No product-based studies of $^1O_2$-mediated oxidation of the other Tyr-containing compounds have previously been reported.

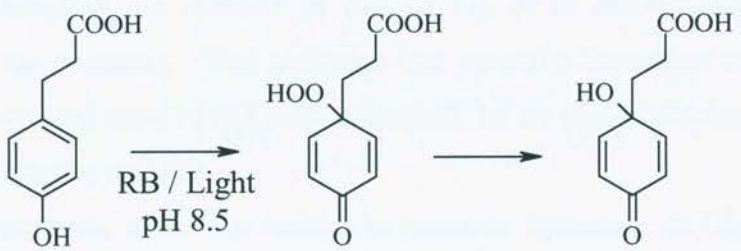

(4.2) **(4.5)** **(4.6)**

Scheme 4.1: Proposed mechanism for the photosensitised oxidation of HPPA (From references [233, 234]).

4.3 RESULTS

4.3.1 FORMATION OF PEROXIDES ON PEPTIDES AND PROTEINS AS A RESULT OF $^1O_2$-MEDIATED OXIDATION

As discussed previously (Section 3.4.1) RB photo-oxidation was found to be an ideal method for investigating Tyr peroxide formation, as the experimental conditions lacked agents which are likely to cause peroxide decomposition (e.g. transition metal ions, heat and UV light; see Chapter 3). This method was also used for the generation of $^1O_2$ in the following experiments. In some cases the MoO_4^{2-}/H_2O_2 system and the thermal decomposition of 3-(4'-methyl-1'-naphthyl)propionic acid 1',4'-endoperoxide (MNPAE) were also investigated.

4.3.1a Results

Photolysis of HPPA, *N*-acetyl Tyr and Gly-Tyr-Gly (2.5 mM, pH 7) with visible light ($\lambda > 345$ nm) in the presence of RB (10 μM) and O_2 resulted in the formation of peroxides as detected by the FOX assay. The concentration of peroxides increased in a photolysis time dependant manner over 60 min (Figure 4.1). Samples were treated with catalase (3150 units mL^{-1}, 10 mins, 22 °C) prior to FOX assay to ensure that any H_2O_2 produced in the reaction did not interfere with the determination of organoperoxides. Low levels of peroxides were detected (< 10 μM) in control samples photolysed in the absence of RB, or O_2, or in non-photolysed solutions containing all the reactants. This indicates that peroxide formation is not mediated either by an activated state of the photosensitiser, or by non-photochemical reaction between the substrates and RB.

The importance of the Tyr residue in peroxide formation on Gly-Tyr-Gly was investigated by photolysing Gly-Gly-Gly with RB. This resulted in the detection of negligible levels of peroxides (<10 μM) suggesting that the Tyr residue is the site of peroxide formation.

RB has been shown previously (see Chapters 1 and 3) to be an efficient photo-sensitiser for $^1O_2$ production. Experiments with D_2O and azide were used to demonstrate that the RB photo-oxidation of free Tyr was mediated by $^1O_2$ (Section 3.4.1). Thus, it was expected that $^1O_2$ was also the oxidant responsible for the formation of peroxides on these model compounds. To confirm this supposition, RB photolysis experiments using D_2O and azide were performed with Gly-Tyr-Gly.

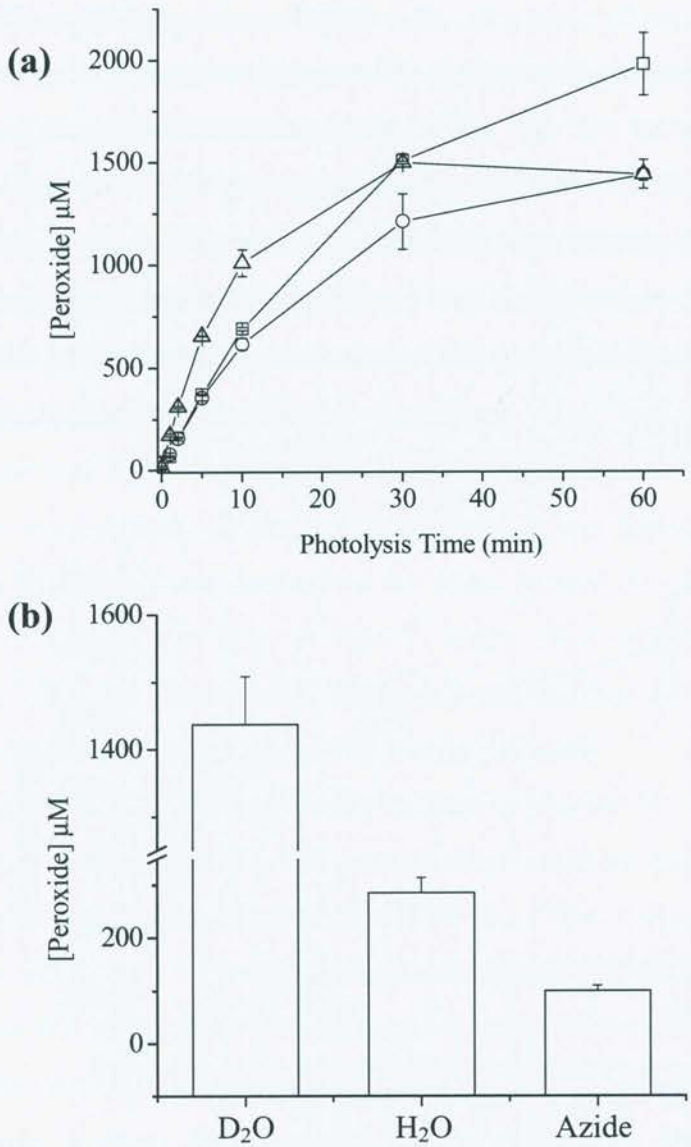

Figure 4.1: (a) The formation of peroxides on HPPA (□), *N*-Acetyl Tyr (○), Gly-Tyr-Gly (△) (all 2.5 mM in D_2O, pH 7) by visible light ($\lambda > 345$ nm) in the presence of O_2 and the photosensitiser RB (10 µM) at 4 °C. (b) Comparison of Gly-Tyr-Gly peroxide formation in of D_2O, water or the presence azide (5 mM) after 1 h RB photolysis. Peroxide concentrations were measured using the FOX assay with H_2O_2 standards as described in Chapter 2. Data are the means (± SD) of triplicate determinations from a single experiment representative of several, as the absolute peroxide yields varied between experiments due to slight differences in oxygenation rates.

As expected, peroxide formation was enhanced when photolysis was performed in D_2O and inhibited when 5 mM azide was included consistent with peroxide formation being due to a $^1O_2$-mediated process (Figure 4.1).

As peroxide formation was observed on these model compounds and peptides, RB photolysis of the proteins BSA and histone H1 was also investigated. Peroxide formation was observed on RB photolysis of BSA (75 μM) and the concentration of these species was found to increase with photolysis time (Figure 4.2). The yield of peroxides was enhanced when the photolysis was performed in D_2O (Figure 4.2). Histone H1 (470 μM) yielded approximately 260 μM peroxides after 60 min RB photolysis (in H_2O) under similar reactions conditions.

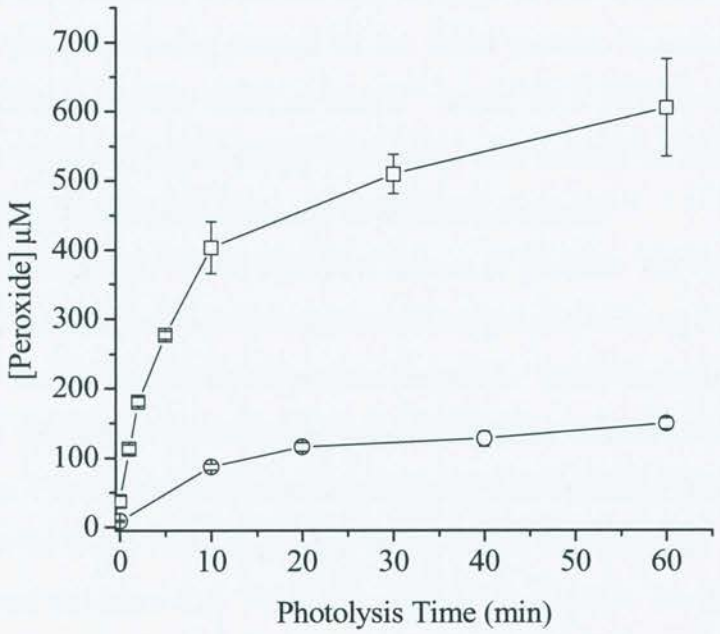

Figure 4.2: The formation of peroxides by RB photolysis of BSA (75 μM) in water (○) or D_2O (□). Photolysis conditions and peroxide determinations were as described in Figure 4.1. Data are the means (± SD) of triplicate determinations from a single experiment representative of several, as the absolute peroxide yields varied between experiments due to slight differences in oxygenation rates.

The effects of azide and D_2O on peroxide formation suggest that the formation of these species on the model compounds, peptides and proteins is mediated by $^1O_2$. Further evidence for the involvement of $^1O_2$ in the formation of protein peroxides was sought in experiments using the alternative $^1O_2$ generation systems MoO_4^{2-}/H_2O_2 and thermal decomposition of MNPAE, to oxidise BSA.

The addition of H_2O_2 (3 aliquots of 540 μmol at 0, 1 and 10 min) to a solution of BSA (75 μM) and MoO_4^{2-} (12.5 mM) at pH 7.4 (100 mM phosphate buffer) was used to generate $^1O_2$ to oxidise BSA. After 30 min reaction, unreacted H_2O_2, as well as phosphate buffer, which is incompatible with the FOX assay, was removed by gel filtration using a PD-10 column eluted with water. The high molecular weight fraction was collected and analysed for peroxides. Formation of 250 ± 10 μM (n=6 from 2 separate experiments) peroxides was detected in this fraction by FOX assay, consistent with peroxides being formed on the intact protein. In control experiments that contained BSA and either H_2O_2 or MoO_4^{2-} alone, 10 ± 10 μM and 20 ± 20 μM peroxides were detected respectively, indicating that neither of these reagents in isolation led to significant concentrations of protein peroxides.

Although the MoO_4^{2-}/H_2O_2 system is known to produce $^1O_2$ very cleanly [47], it was important to demonstrate that other oxidants, possibly arising from H_2O_2, were not responsible for the formation of protein peroxides. Thus, experiments with D_2O and azide were performed in a similar fashion to those described previously. As shown in Figure 4.3, the yield of protein peroxides was enhanced when the reaction was carried out in D_2O, and suppressed when azide was present. These results provide additional evidence that $^1O_2$ is the oxidant responsible for the formation of these protein peroxides.

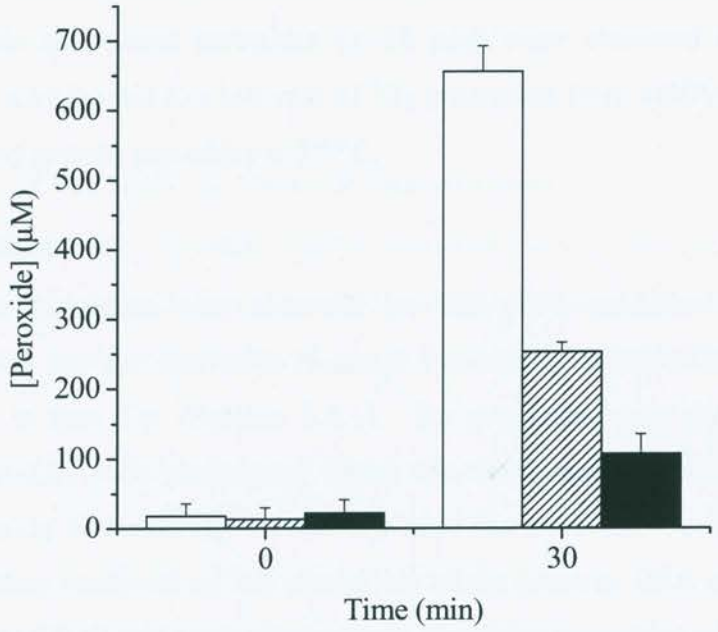

Figure 4.3: The formation of peroxides on BSA (75 μM) treated with the MoO_4^{2-} /H_2O_2 system. Reactions were performed at 22 °C in 12.5 mM MoO_4^{2-} at pH 7.4 in D_2O (open bars), H_2O (stippled bars), or in the presence of azide (5 mM) (black bars). The reaction was initiated by the addition of H_2O_2 (540 μmol). Further aliquots of H_2O_2 were added after 1 and 10 min, thus 1.62 mmol of H_2O_2 were added in total. The reaction was allowed to proceed for 30 min. Peroxide concentrations were measured using the FOX assay with H_2O_2 standards after gel filtration using a PD-10 column to remove unreacted H_2O_2. Data are expressed as means (n = 6 from 2 separate experiments) ± SD.

The second alternative $^1O_2$ source used to oxidise BSA was the thermal decomposition of MNPAE (synthesised as described in Chapter 2). This system was not suitable for monitoring the formation of peroxides on free Tyr as the FOX assay could not distinguish between the peroxides formed on Tyr from those derived from MNPAE. The high molecular weight of BSA allows separation of the protein from MNPAE and thus should allow quantification of any peroxides formed on BSA. Thus, BSA (15 μM) was incubated in a solution of MNPAE (2.5 mM) at 37 °C for various periods between 30 min and 24 hr. After incubation, the reaction mixtures were separated by gel filtration using a PD-10 column and the protein-containing fraction analysed for peroxides. This treatment ensured that only protein-derived

peroxides, and not those derived from the naphthalene derivative were quantified. Negligible levels of protein peroxides (< 10 μM) were observed in all of these reactions. This may be due to a low rate of $^1O_2$ generation from MNPAE, or the rapid decomposition of protein peroxides at 37 °C.

4.3.1b Conclusions

Peroxide formation was observed on RB photo-oxidation of the model compound HPPA, the Tyr derivative *N*-acetyl Tyr and the peptide Gly-Tyr-Gly in a similar fashion to free Tyr (Section 3.4.1). No peroxides were formed when the peptide Gly-Gly-Gly was photolysed under the same conditions, indicating that peroxide formation is occurring on the Tyr side-chain of Gly-Tyr-Gly. Peroxide formation was also observed on RB photolysis of the proteins BSA and histone H1. Experiments using D_2O and azide demonstrate that these peroxides arise from a $^1O_2$-dependant process.

The oxidation of BSA was studied further with two alternative $^1O_2$ generation systems. The high molecular weight of BSA was advantageous in these experiments as it made the separation of the protein from the low molecular weight components of both $^1O_2$ generating systems possible. Thus, it was demonstrated that the MoO_4^{2-} /H_2O_2 oxidised BSA to yield protein-bound peroxide species. D_2O and azide experiments provided evidence that these peroxides are due to the generation of $^1O_2$ by this system. The thermal decomposition of MNPAE is reported to yield $^1O_2$ [104], however low levels of peroxide formation were observed when BSA was incubated with MNPAE. To decompose MNPAE the incubations are carried out at 37 °C. The rate of protein peroxide decomposition at this temperature may be similar to the rate of their formation, thereby accounting for the lack of peroxides detected in these experiments.

4.3.2 Stability of Peptide and Protein Peroxides

Previously it was demonstrated that the peroxides formed upon $^1O_2$-mediated oxidation of free Tyr were reduced by thermal, photochemical and chemical reactions (Section 3.4.2). Peptide- and protein-derived peroxides formed via HO• attack have also been shown previously to be unstable under similar conditions [192, 193, 198, 217]. In order to investigate the stability of peroxides formed by $^1O_2$-mediated oxidation of these model compounds, peptide-bound Tyr residues, and intact proteins,

samples of these peroxides, generated as described in section 4.3.1, were incubated under various conditions and changes in the peroxide concentrations assessed using the FOX assay.

4.3.2a Stability of Peroxides to Elevated Temperatures

The stability of Gly-Tyr-Gly, HPPA, *N*-acetyl Tyr and BSA peroxides formed as a result of RB photo-oxidation was investigated by incubating samples at various temperatures and analysing residual peroxide concentrations after certain time periods.

Gly-Tyr-Gly peroxides were found to be very stable at 4 °C, with approximately 4 % loss after 24 hr incubation. Peroxide decay was more rapid at higher temperatures, with 25 % and 36 % of peroxides lost at 22 °C and 37 °C respectively over the same period (Figure 4.4). Peroxides formed on the other model compounds showed similar decay kinetics at 37 °C (Figure 4.5).

BSA-derived peroxides were found to have a similar stability to elevated temperatures, with 14 %, 27 %, 55 % peroxide loss at 4 °C, 22 °C and 37 °C respectively (Figure 4.6).

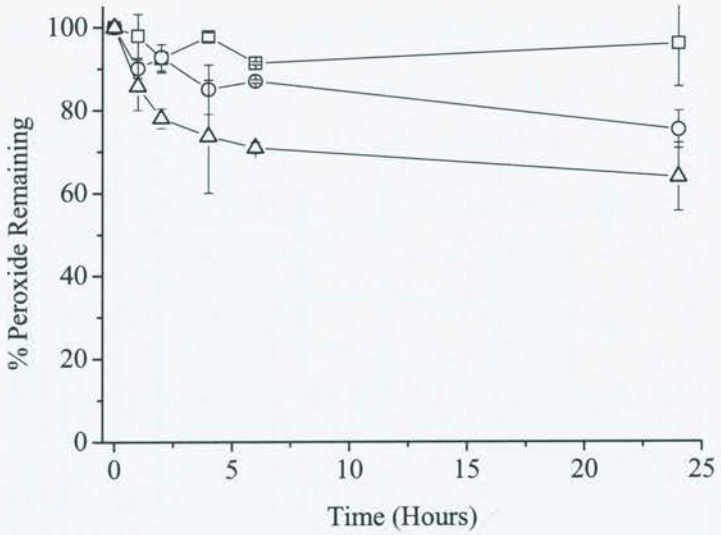

Figure 4.4: Stability of Gly-Tyr-Gly peroxides at elevated temperatures. Peroxides were formed by RB photo-oxidation as described in Figure 4.1. Crude reaction mixtures, which contain RB and unreacted Gly-Tyr-Gly as well as Gly-Tyr-Gly peroxides, were incubated in the absence of light over 24 h at 4 °C (□), 22 °C (○) and 37 °C (△) for the indicated time periods prior to the determination of residual peroxide levels as described in Figure 4.1. Data are expressed as means of percentage initial peroxide concentration (n=6, from 2 separate experiments) ± SD.

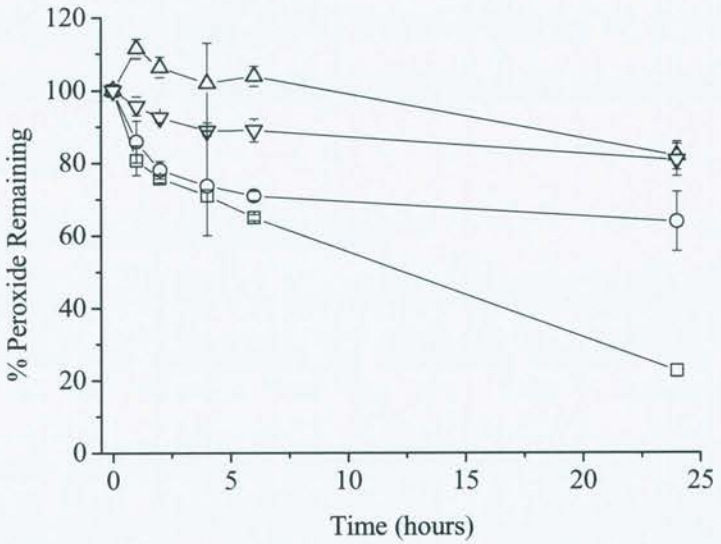

Figure 4.5: Stability of HPPA (▽), *N*-acetyl Tyr (△) and Gly-Tyr-Gly (○) peroxides at 37 °C. Peroxides were generated as outlined in Figure 4.1, incubations and peroxide determinations were performed as described in Figure 4.4. The decay kinetics of peroxides formed on free Tyr (□) peroxide decay are shown for comparison (from Figure 3.3). Data are expressed as means of percentage initial peroxide concentration (n=6, from 2 separate experiments) ± SD.

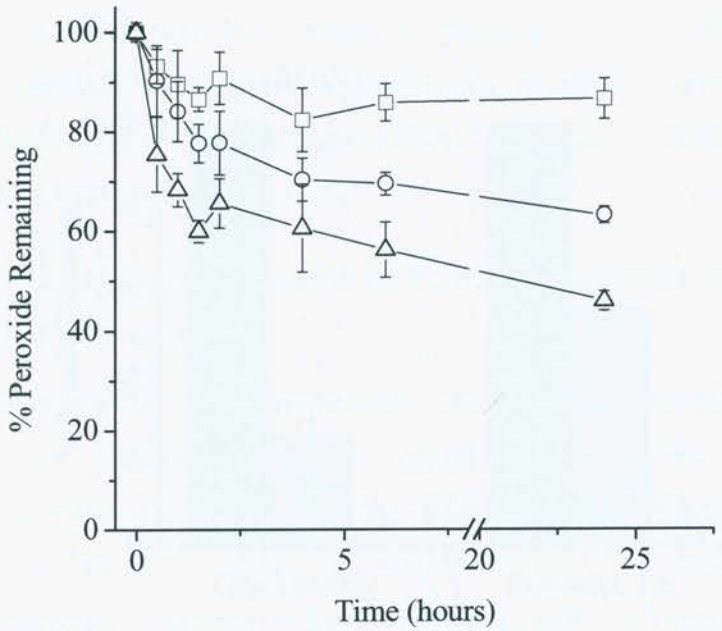

Figure 4.6: Stability of BSA peroxides at elevated temperatures. Peroxides were generated as outlined in Figure 4.1 (using 75 μM BSA), incubations and peroxide determinations were performed as described in Figure 4.4. BSA peroxides were incubated in the absence of light over 24 h at 4 °C (□), 22 °C (○) and 37 °C (△). Data are expressed as means of percentage initial peroxide concentration (n=6, from 2 separate experiments) ± SD.

4.3.2b Stability of Peroxides to Reductants

The stability of *N*-acetyl Tyr and Gly-Tyr-Gly peroxides formed as a result of RB photo-oxidation was investigated by incubating samples with Fe^{2+}/EDTA or $NaBH_4$.

A reduction in the peroxide concentration was observed when *N*-acetyl Tyr (440 μM peroxide) or Gly-Tyr-Gly (170 μM peroxide) peroxides were incubated with either Fe^{2+}/EDTA (200 μM) or $NaBH_4$ (200 μM) for one hour at 4 °C (Figure 4.7). Subsequent to Fe^{2+}/EDTA treatment, 44 % and 74 % of *N*-acetyl Tyr and Gly-Tyr-Gly peroxides respectively were reduced. As peroxides are in excess over Fe^{2+}/EDTA increased amounts of Fe^{2+}/EDTA would likely reduce the peroxide further, but this also increases the chance of Fe^{2+} autoxidation reactions (which would generate interfering H_2O_2) and hence was not investigated further. $NaBH_4$ treatment reduced

the concentration of *N*-acetyl Tyr and Gly-Tyr-Gly peroxide by 96 and 98 % respectively.

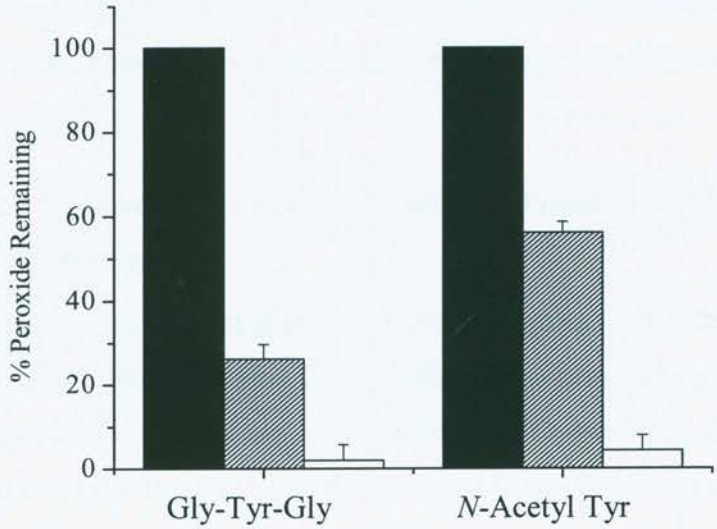

Figure 4.7: Stability of *N*-acetyl Tyr and Gly-Tyr-Gly peroxides to chemical reductants. *N*-acetyl Tyr and Gly-Tyr-Gly peroxides were incubated at 4°C for 1 h (black bars) in the presence of Fe^{2+}/EDTA (1:1 complex) (stippled bars) or $NaBH_4$ (open bars) (both reductants 200 μM). Data are expressed as means of percentage initial peroxide concentration (n = 6, from 2 separate experiments) ± SD.

4.3.2c Conclusions

Peroxides formed by RB photo-oxidation of HPPA, *N*-acetyl Tyr and Gly-Tyr-Gly were found to be susceptible to elevated temperatures and reducing species. However, the rates of peroxide decay were much slower with the model compounds and peptides than that observed with free Tyr. This is especially apparent on incubation at 37 °C, where 77 % of free Tyr-derived peroxides, compared to only 36 %, 18 % and 19 % of Gly-Tyr-Gly, *N*-acetyl Tyr and HPPA-derived peroxides respectively, had decayed after 24 hr incubation. In all of these latter peroxides, the α-amino nitrogen of Tyr is blocked or absent, suggesting a possible role for this moiety in peroxide decomposition.

The peroxides formed on *N*-blocked Tyr models were still susceptible to direct chemical reduction, as demonstrated with Fe^{2+}/EDTA and $NaBH_4$. This is as expected as most peroxides are known to be reduced by one- or two-electron reductants [165, 167, 198].

Similar losses of peroxides were observed on treatment of peroxides derived form Gly-Tyr-Gly and *N*-acetyl Tyr were treated with Fe^{2+}/EDTA. Total loss of peroxides was not observed but increased amounts of Fe^{2+}/EDTA were not investigated as, although this would likely reduce the peroxide concentration further, the chance of Fe^{2+} autoxidation reactions is also increased. $NaBH_4$ was a potent reductant of both peroxides.

4.3.3 Structural Characterisation of Peroxides Formed on Gly-Tyr-Gly and Model Compounds

The previous chapter demonstrated that peroxide species were formed on $^1O_2$-mediated oxidation of free Tyr at the ring C(1) position. The previous sections of this chapter show that peroxidic species are also formed on $^1O_2$-mediated oxidation of HPPA, *N*-acetyl Tyr and Gly-Tyr-Gly. The experiments in the following section were designed to characterise the peroxides formed on these model and peptide compounds and investigate whether there are similarities between those formed on free Tyr and those generated on model compounds, to peroxides formed on peptides containing Tyr residues. Similar studies could not be carried out on intact proteins as their large molecular size and degree of complexity makes analysis by these techniques difficult.

4.3.3a Analysis of $^1O_2$-oxidised Tyr peptide model compounds by RP-HPLC

The $^1O_2$-mediated oxidation of free Tyr has been studied by HPLC previously [95]. Results presented in the previous chapter demonstrated that two peroxidic species as well as the final product HOHICA could be detected by HPLC. In the following experiments, similar HPLC methodology was applied to investigate the $^1O_2$-mediated oxidation of HPPA, *N*-acetyl Tyr and Gly-Tyr-Gly.

Initially HPPA was analysed by reverse phase HPLC using the perchlorate containing mobile phase (100 mM sodium perchlorate, 10 mM sodium phosphate buffer, pH 2.5) used for free Tyr. Under these conditions the parent material had a retention time (RT) of 34.5 min and a further peak, which was observed only after RB photo-oxidation, eluted at 19.5 min. In contrast to the free Tyr system (see Section 3.4.3a) only a single photo-product was detected. The area of the peak corresponding to unmodified HPPA was found to decrease with increasing photolysis time, with a concomitant increase in area of the new peak (Figure 4.8). The high concentration of salts in this mobile phase made it unsuitable for experiments involving fraction

collection and analysis by MS. Thus, a second mobile phase - 0.1 % TFA in water – was developed and subsequently used for the collection of the product material for ESI-MS analysis. TFA was included in the mobile phase, as HPPA eluted very close to the void volume in initial experiments using water, thus this system was thought to be unsuitable for analysis of a (potentially) more polar product. The TFA ensured that HPPA was protonated and thus separation was on the basis of hydrophobic interactions with the column material. TFA is also volatile, making it suitable for use in ESI-MS experiments. Under these conditions the RT of the unreacted parent peak was 32.8 min and that of the product peak was 18.3 min.

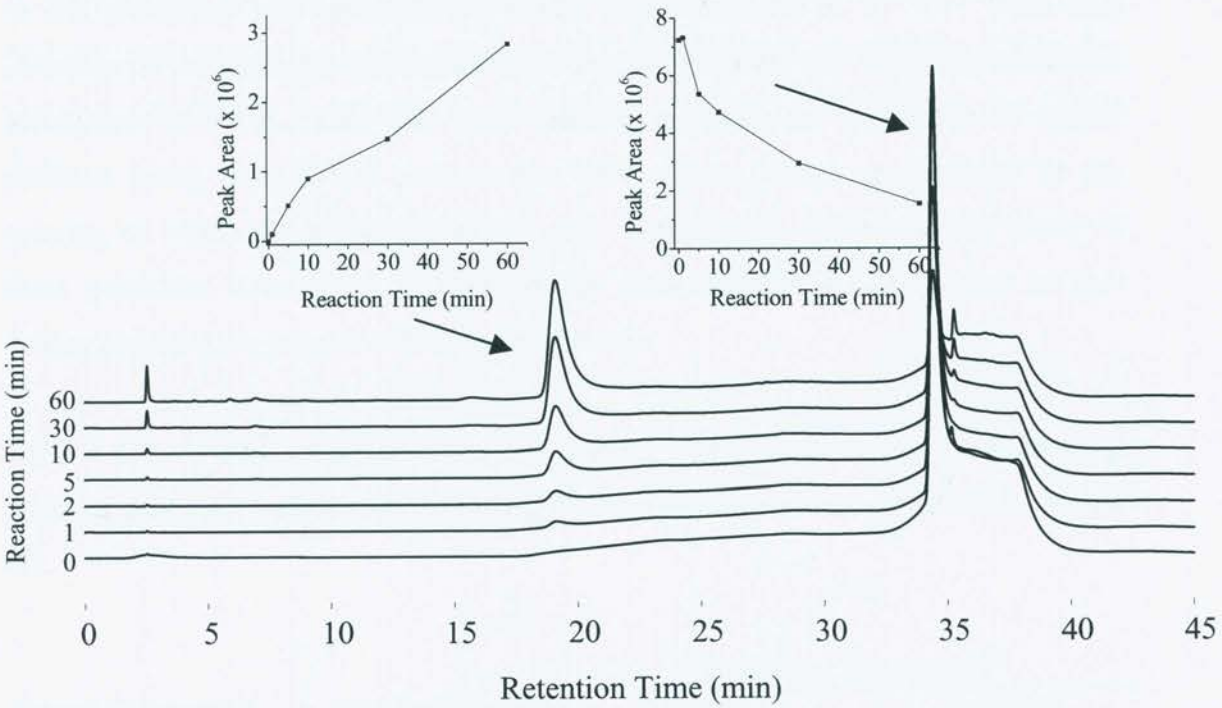

Figure 4.8: HPLC analysis of HPPA oxidation products generated on photo-oxidation of HPPA (2.5 mM, pH 7) in the presence of oxygen and RB (10 μM). Samples were removed from the photo-oxidation reaction at the indicated times and injected (10 μL) onto a Zorbax ODS column. The mobile phase used was 100 mM sodium perchlorate in 10 mM phosphate buffer, pH 2.5. Mobile phase was eluted at a rate of 1 mL min^{-1}, and the UV absorbance of the eluent was monitored at 210 nm. Inset graphs show the kinetics of the change in peak areas over the photo-oxidation time period (1 h total).

N-acetyl Tyr was analysed by reverse phase HPLC using water as the mobile phase and under these conditions the parent material had a RT of 4.5 min. When RB photo-oxidised samples were examined, a peak that was not seen in non-photolysed control experiments eluted at 2.3 min. When Gly-Tyr-Gly was analysed in a similar manner using water as the mobile phase, the parent compound eluted at 23.0 min and a single product was detected with a RT of 5.5 min. The RT of these compounds and their RB photo-oxidation products are summarised in Table 4.1.

In order to investigate the potential formation of further products (c.f. the behaviour of free Tyr reported in Section 3.4.3a), samples which had been subjected to RB photolysis and contained peroxides were incubated at 37 °C. With each substrate no evidence for the formation of further materials was obtained, even after incubation for 24 h. This does not, however, preclude the possibility of further products being formed that elute in the void volume, which are retained on the column, or which do not absorb at 210 nm. Furthermore, as the thermal decay of these peroxides were found to be relatively slow (Section 4.3.2a) it may be that further products are present at undetectable levels.

Table 4.1: HPLC characteristics of model compounds and Tyr-containing peptides analysed immediately following RB photo-oxidation as described in Figure 4.1.

		Retention Time (min)[b]	
Parent Compound	Mobile Phase	Parent	Product
HPPA	Perchlorate[a]	34.5	19.5
HPPA	0.1 % TFA	32.8	18.3
N-acetyl Tyr	Water	4.5	2.3
Gly-Tyr-Gly	Water	23.0	5.5

[a] The perchlorate mobile phase contained 100 mM sodium perchlorate, 10 mM sodium phosphate buffer, at pH 2.5.

[b] A Zorbax ODS column was used and mobile phases were eluted at a rate of 1 mL min^{-1}. Peaks were detected by monitoring the UV absorbance ($\lambda = 210$ nm) of the eluent.

4.3.3b Analysis of $^1O_2$-oxidised Tyr peptide model compounds by ESI-MS

Further investigations into the formation of peroxides upon oxidation of HPPA, *N*-acetyl Tyr and Gly-Tyr-Gly were performed using ESI-MS. Analysis of non-photolysed reaction mixtures by ESI-MS lead to the detection of the expected M+ ions of HPPA {189 (M+Na)}, *N*-acetyl Tyr {224 (M+) and 246 (M+Na)}, Gly-Tyr-Gly {296 (M+)} when the cone voltage was set to 25 V (Table 4.2). Gly-Tyr-Gly was further analysed at a cone voltage of 50 V, which lead to the observation of a number of fragments. The ions observed corresponded to M-75 (loss of Gly), M-103 (loss of $HOOCCH_2NHCO$-) and M-160 (loss of $HOOCCH_2NHCO$- and $COCH_2NH_2$). An ion with identical m/z to the latter fragment was also observed on analysis of free Tyr (Section 3.4.3b) and is assigned to the formation of the Tyr immonium ion (Table 4.2).

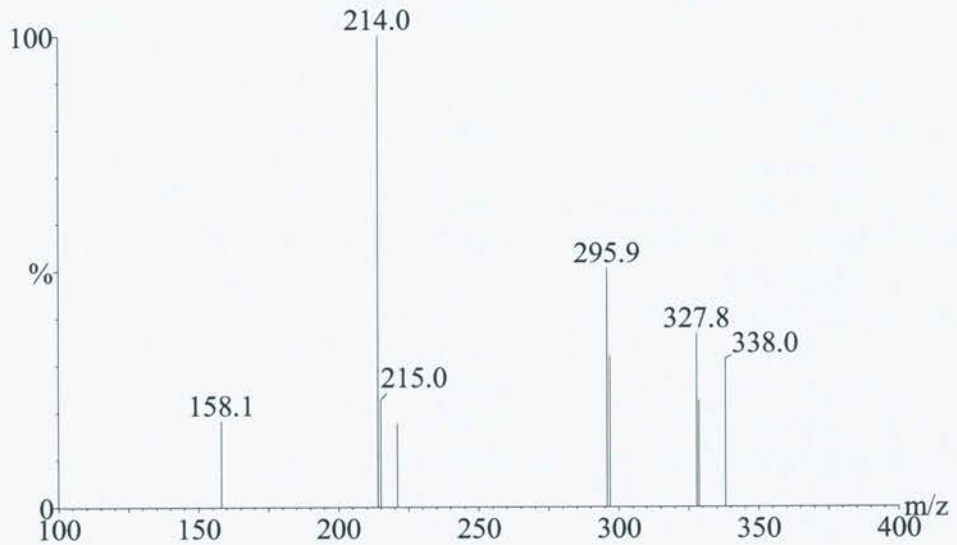

Figure 4.9: ESI-MS analysis of Gly-Tyr-Gly oxidation products generated on photo-oxidation of Gly-Tyr-Gly (2.5 mM) in the presence of oxygen and RB (10 μM) for 1 h. Samples were diluted with 2 % formic acid in methanol to give final concentrations of 50 % methanol and 1 % formic acid to assist ionisation of the sample. Solvent was delivered at 10 μL min^{-1} and 2 x 25 μL injections were made for each analysis. The probe tip was set at 3.5 kV with 0.5 kV on the chicane counter electrode. The sampling cone was set at 25 V. The peak at 296 is due to un-modified Gly-Tyr-Gly, the peak at 328 is due to Gly-Tyr-Gly + 32 consistent with the addition of 2 oxygen atoms to Tyr. The peak at 214 has not been assigned.

When reaction mixtures of HPPA, *N*-acetyl Tyr and Gly-Tyr-Gly, which had been subject to photo-oxidation (as in Section 4.3.1) were analysed by ESI-MS at a cone voltage of 25 V, ions with m/z corresponding to the unmodified parent compound and to the formation of M+32 species were observed in each case. The detection of these M+32 ions strongly suggests that 2 atoms of oxygen were added to each molecule, consistent with peroxide formation. Similar analysis of the HPLC fractions corresponding to the products generated on photo-oxidation (see section 4.3.3a) from each of these substrates yielded mass spectra with the M+32 ion as observed in the complete reaction mixture, suggesting that these materials are the peroxides detected by FOX assay of the crude reaction mixtures. As with free Tyr, no characteristic fragments of the peroxides were observed at higher cone voltages.

Table 4.2: ESI-MS characteristics of model compounds and Tyr-containing peptides RB photo-oxidised as described in Figure 4.1. Analysis was performed immediately after photolysis using a cone voltage of 25 V (unless indicated otherwise).

Compound	RB photo-oxidation (±)	m/z	Assignment
HPPA	-	188.9	HPPA M+ (+Na)
	+	188.9	HPPA M+ (+Na)
		220.8	HPPA + 32
	+[b]	220.8	HPPA + 32
N-acetyl Tyr	-	223.9	*N*-acetyl Tyr M+
	+	223.9	*N*-acetyl Tyr M+
		245.9	*N*-acetyl Tyr M+ (+Na)
		277.8	*N*-acetyl Tyr + 32 (+Na)
	+[b]	277.8	*N*-acetyl Tyr + 32 (+Na)
Gly-Tyr-Gly	-	295.9	Gly-Tyr-Gly M+
Gly-Tyr-Gly[a]	-	295.9	Gly-Tyr-Gly M+
		220.9	Loss of $COCH_2NH_2$ (i.e. loss of Gly)
		193.0	Loss of $HOOCCH_2NHCO$
		136.1	Loss of $HOOCCH_2NHCO$ and $COCH_2NH_2$ (i.e. Formation of Tyr immonium ion)
	+	295.9	Gly-Tyr-Gly M+
		327.9	Gly-Tyr-Gly + 32
	+[b]	327.9	Gly-Tyr-Gly + 32

[a] Cone Voltage 50 V.

[b] ESI-MS analysis performed on collected HPLC fractions corresponding to the products generated on RB photo-oxidation as described in Table 4.1.

4.3.3c Analysis of $^1O_2$ oxidised HPPA and Gly-Tyr-Gly by NMR

Two-dimensional NMR analyses were used to complete the characterisation of the products of $^1O_2$ oxidation of HPPA and Gly-Tyr-Gly. These experiments were performed on unfractionated, photolysed reaction mixtures containing RB, in collaboration with Dr W.A. Bubb (Department of Biochemistry, University of Sydney). These reactions were always performed at neutral pD in D_2O to enhance product yields and to minimise solvent peak interference in the NMR spectra.

NMR analysis of free Tyr (Section 3.4.3c) yielded complex spectra due to the presence of a mixture of intermediates and final products and their stereoisomers. The results presented earlier in this chapter suggest that the peroxide intermediates formed upon $^1O_2$ oxidation of HPPA and Gly-Tyr-Gly are more stable than those formed with free Tyr and therefore conversion through to final products slower. Thus, it was envisaged that less complicated NMR spectra would be observed with RB photo-oxidised HPPA and Gly-Tyr-Gly than with free Tyr.

HPPA solutions (2.5 mM) were prepared in D_2O and adjusted to pD 7 with small amounts of NaOD. The NMR characteristics of native HPPA were then determined (Figure 4.10), allowing peaks derived from unmodified HPPA to be assigned readily. Photolysis was then carried out as previously described using RB (10 μM) and visible light ($\lambda > 345$ nm). Immediate post-photolysis analyses of HPPA by NMR led to the detection of strong ^1H and ^{13}C signals that appear to be due to the presence of two species. By comparison with previous data, the minor species present was assigned as unmodified HPPA. Analysis of chemical shift data (Figure 4.10 and 4.11) and comparison with the chemical shifts of unmodified HPPA, suggests that the initial major species observed was the peroxide (4.5). The low level of parent HPPA present is consistent with the high yields peroxide detected by FOX assay (Figure 4.1) and HPLC data (Figure 4.8) described earlier. The NMR data suggest that the decomposition of the peroxide (4.5) was slow, in accord with the previous stability data (Figure 4.5). Thus after incubation at 5 °C for extended periods, slow decay of the major species was observed and signals derived from a further new species were observed. After several weeks at this temperature these signals were sufficiently intense to allow analysis and on the basis of the observed chemical shifts and splitting patterns these were assigned to the alcohol (4.6). This alcohol was readily distinguishable from the precursor peroxide on the basis of

chemical shift of the ring C(1). The chemical shift for this carbon atom in the peroxide (4.5) was 84.5; that of the corresponding carbon in the alcohol (4.6) was 72.4. This deshielding effect of the peroxide is as expected due to the higher electronegativity of this moiety compared to the alcohol. Similar deshielding effects were observed with free Tyr-derived hydroperoxides and alcohols (see Section 3.4.3c) and analogous behaviour has been reported for the peroxide artemisinin and its corresponding alcohol [221]. The alcohol (4.6) has been observed previously in RB photo-oxidation of HPPA by one-dimensional ^{1}H-NMR [233, 234]. Chemical shift data for these species are summarised in Figure 4.10 and 4.11.

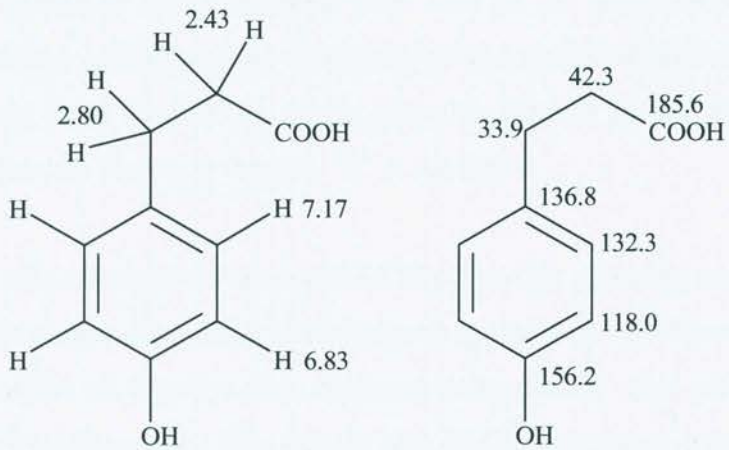

Figure 4.10: Summary of the chemical shift data for HPPA (2.5 mM in D_2O, pD 7). ^{1}H NMR data are shown at the left, ^{13}C at the right.

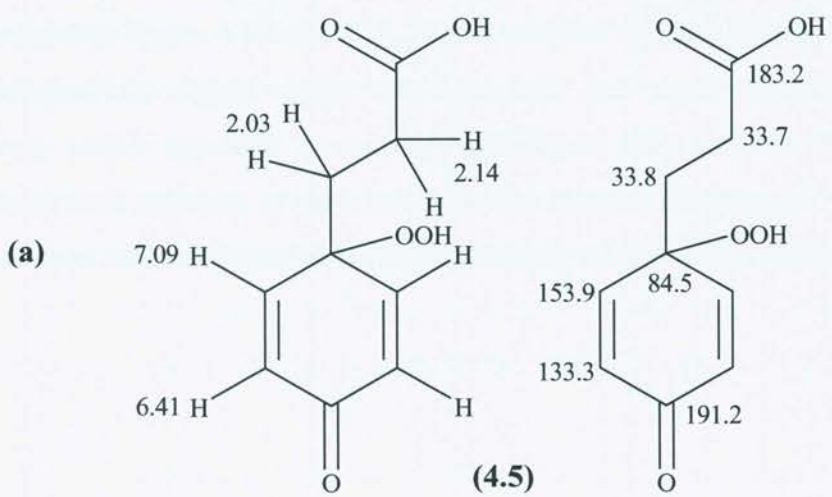

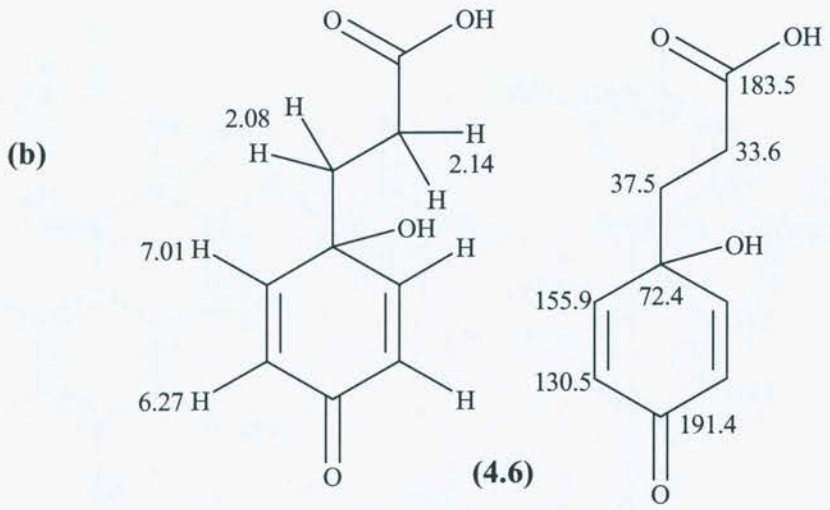

Figure 4.11: (a) Summary of the chemical shift data for the peroxide (4.5) formed on RB photo-oxidation of HPPA. (b) Summary of the chemical shift data for the alcohol (4.6) formed from slow decay of the peroxide formed by RB photolysis of HPPA. ^{1}H NMR data are shown at the left, ^{13}C at the right.

NMR data was obtained for unmodified Gly-Tyr-Gly allowing assignment of the peaks due to the parent compound in photolysed samples of Gly-Tyr-Gly. In RB photo-oxidised samples of Gly-Tyr-Gly, analysed immediately after photolysis, an additional species was observed. The signals had NMR parameters consistent with the hydroperoxide derivative (4.7) analogous to that observed with HPPA. Slow decay of this signal was observed when samples were incubated at 5 °C for several weeks, and signals corresponding to the alcohol (4.8) increased over this period. This alcohol/hydroperoxide pair displayed similar enhanced deshielding effects as observed with free Tyr and HPPA. Chemical shift data for these species are summarised in Figure 4.12 and 4.13. When samples were incubated at 20 °C, the rate of hydroperoxide signal decay was increased and more complex spectra were observed, which appeared to contain resonances from several different species. Despite several attempts at very long spectral acquisition times (> 96 h) these new features were never obtained at sufficient intensity to allow their assignment.

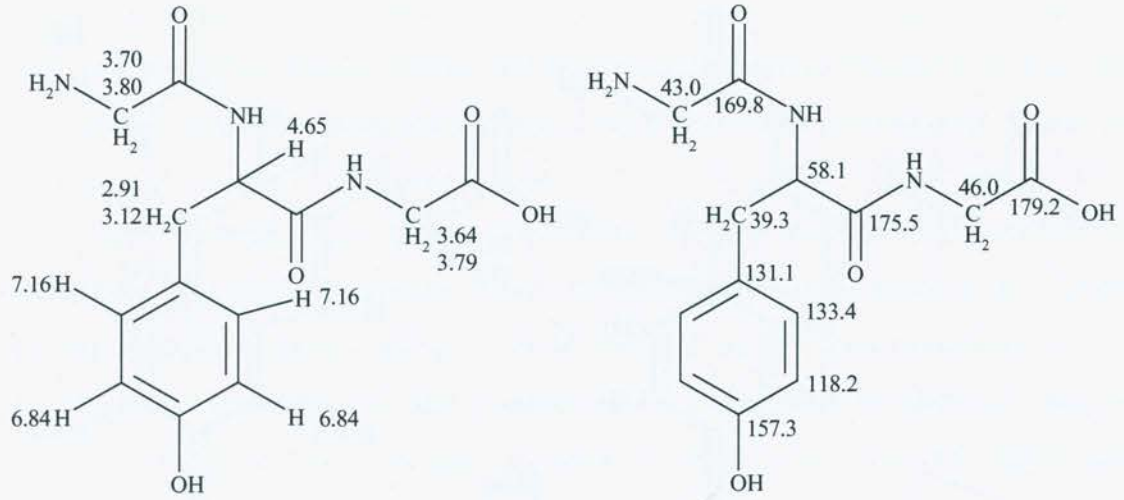

Figure 4.12: Summary of the chemical shift data for Gly-Tyr-Gly. ^{1}H NMR data are shown at the left, ^{13}C at the right.

(a)

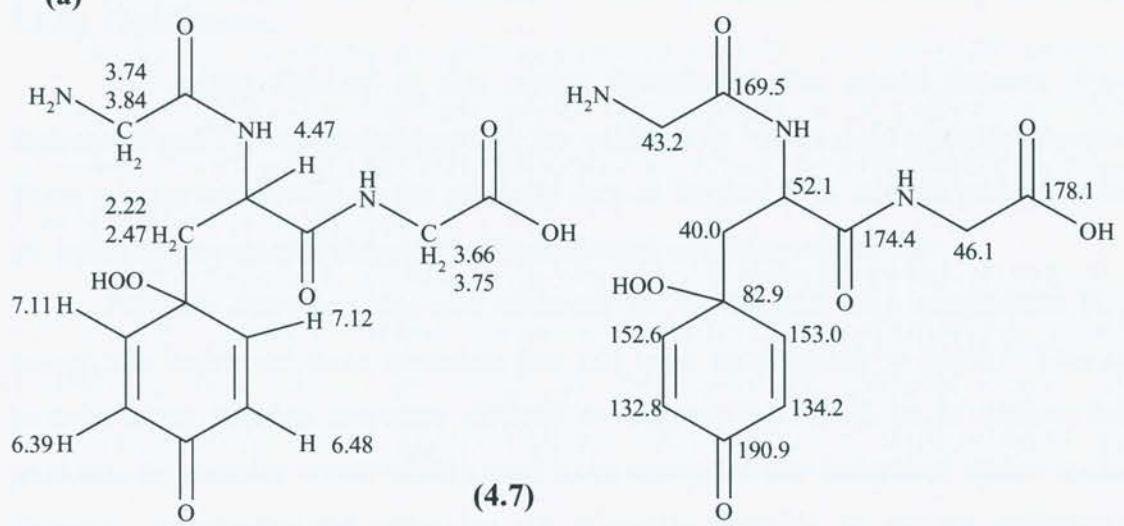

(4.7)

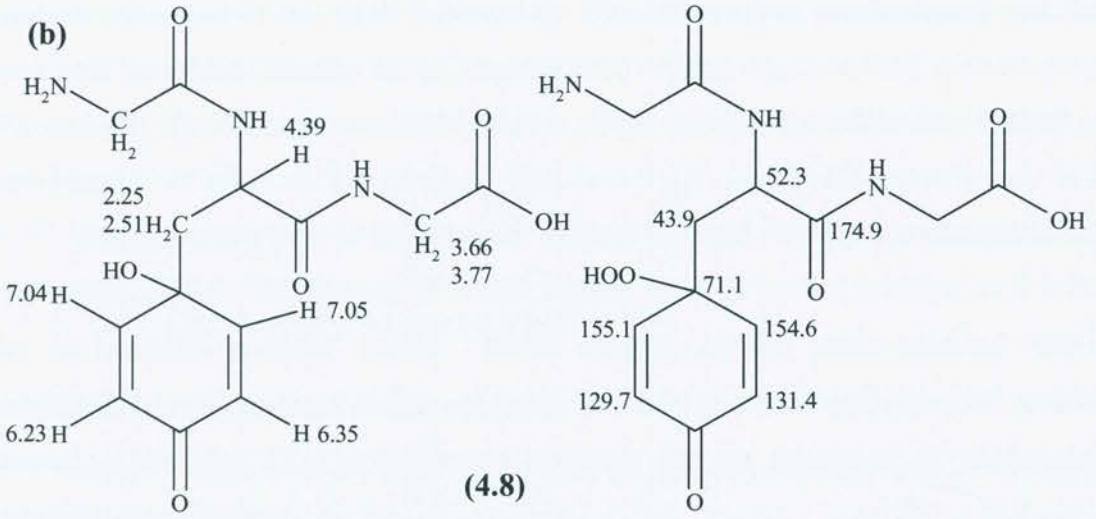

Figure 4.13: (a) Summary of the chemical shift data for the peroxide formed on RB photolysis of Gly-Tyr-Gly. ^{1}H NMR data are shown at the left, ^{13}C at the right. (b) Summary of the chemical shift data for the alcohol generated on decay of the peroxide formed by RB photolysis of Gly-Tyr-Gly. ^{1}H NMR data are shown at the left, ^{13}C at the right.

4.3.3d Conclusions

The results obtained in this section demonstrate that model phenols, Tyr-derivatives and Tyr-containing peptides are oxidised by $^{1}O_2$ to yield peroxide species. These species are formed on the aromatic ring of Tyr residues, and are analogous to the initial hydroperoxide detected in $^{1}O_2$-mediated oxidation of free Tyr.

Peroxide formation was also observed on $^{1}O_2$-oxidised BSA and histone H1, though the nature of these materials has not been investigated in depth. This is because intact proteins are more difficult to separate by HPLC, so to analyse the products, the proteins would ideally need to be converted into individual amino acids. However, protein-derived peroxides are generally unstable to protein hydrolysis conditions [166], thus the products of RB photo-oxidised proteins were not investigated by HPLC. NMR analysis of intact proteins is also generally very difficult, due to the complexity of the observed resonances and the fact that these molecules tumble (in general) slowly in solution leading to the observation of broad NMR signals. This means that the spectra are generally very difficult to assign, even using high field, two-dimensional techniques.

HPLC experiments with RB photo-oxidised HPPA demonstrated rapid loss of the starting material and the corresponding increase of a single product peak. HPLC

fraction collection of this peak followed by ESI-MS analysis demonstrated that this peak was peroxidic. Similar HPLC and ESI-MS results were obtained with *N*-acetyl Tyr and Gly-Tyr-Gly, demonstrating that a single peroxidic product was formed in both cases.

An important step in the reaction of free Tyr and $^1O_2$ was an intramolecular cyclisation. The model compound HPPA cannot undergo such a reaction as it lacks the nucleophilic α-amino group. NMR analysis of RB photo-oxidised HPPA confirmed that the product of this oxidation is a non-cyclised hydroperoxide species located at the ring C(1) position; no evidence for the formation of ring-closed peroxides was obtained.

NMR analysis of RB photo-oxidised Gly-Tyr-Gly showed that a similar non-cyclised peroxide is formed in this case. Gly-Tyr-Gly does have a nitrogen atom in an analogous position to free Tyr, but intramolecular cyclisation is not expected to be rapid in *N*-acetyl Tyr and Gly-Tyr-Gly, as the nucleophilicity of the amino group will be greatly reduced due to delocalisation of the lone pair of electrons in the peptide bond. Cyclisation may also be hindered by steric interactions. Incubation of HPPA and Gly-Tyr-Gly peroxides for extended periods at 5 °C prior to NMR analysis resulted in the detection of alcohol species with no evidence for presence cyclised products. In contrast to free Tyr, these materials appear to preferentially undergo slow conversion to the alcohol.

As these peroxides are structurally similar to the initial hydroperoxide detected with free Tyr they are also readily reduced by metal ions. As a consequence, further experiments were carried out, which are detailed in the following section, to investigate potential radical formation arising from reduction of these peroxides by Fe^{2+}.

4.3.4 Free Radical Formation as a Result of Metal Ion Reduction of Peroxides Formed on Gly-Tyr-Gly, Model Compounds and Proteins

Experiments with free Tyr (Section 3.4.4) established that peroxides formed by reaction of $^1O_2$ with free Tyr yielded carbon-centred radicals when reduced with Fe^{2+}/EDTA. MNP spin trapping, in conjunction with deuterated Tyr derivatives, was used to gain structural information about these radicals. These experiments allowed the assignment of radicals to the ring C(3)/C(5) sites. The previous sections demonstrated that similar peroxides are generated by reaction of $^1O_2$ with model

compounds and peptide-bound Tyr residues. Thus, the aim of the following series of experiments was to investigate the formation of radicals upon Fe^{2+}/EDTA reduction of peroxides formed by $^1O_2$ reaction with the Tyr model compounds HPPA, *N*-acetyl Tyr, Gly-Tyr-Gly and the proteins BSA and histone H1, using EPR spectroscopy with MNP spin trapping.

4.3.4a EPR spin trapping experiments with MNP

4.3.4a.i Small molecule experiments

Peroxides were formed by RB (10 μM) photolysis of HPPA, *N*-acetyl Tyr and Gly-Tyr-Gly (all 2.5 mM, in H_2O, pH 7) using visible light ($\lambda > 345$ nm) as described in section 4.3.1a. The peroxide containing solutions were all pre-treated with catalase (3150 units mL^{-1}, for 5 min, 22 °C) to remove any photo-generated H_2O_2.

The treatment of RB photo-oxidised solutions of HPPA (~ 1400 μM peroxide), *N*-acetyl Tyr (~ 320 μM peroxide) and Gly-Tyr-Gly (~ 140 μM peroxide) with thoroughly nitrogen gassed solutions of Fe^{2+}/EDTA (176 μM) in the presence of MNP (11.8 mM) resulted in the detection of radicals using EPR spectroscopy.

Three radical species were detected with $^1O_2$-oxidised HPPA (Figure 4.14a). These species have parameters consistent with the formation of carbon-centred radicals and are assigned as two triplet of doublet signals [radical #1;a(N) 1.53 mT, a(H) 0.21 mT and radical #2; a(N) 1.54 mT, a(H) 0.16 mT] and a triplet of doublet of doublets [radical #3; a(N) 1.53 mT, a(H) 0.22 mT, a(H) 0.08 mT]. The relative intensities of the signals observed in this system change over time. The initial triplet of doublet of doublets signal appears to decrease in intensity, whereas the other signals become more prominent with increasing incubation time at 22 °C.

To further investigate the origin of these signals, the peroxide fraction was collected from HPLC separation of RB photo-oxidised HPPA using the perchlorate system, as described in Section 4.3.3a. Reaction of this collected fraction with Fe^{2+}/EDTA in the presence of MNP, gave a single EPR signal in contrast to the experiments using the complete reaction mixture. This signal can be analysed in terms of a triplet of doublet of doublets with similar couplings to radical #3 observed in the unseparated system [a(N) 1.53 mT, a(H) 0.22 mT, a(H) 0.08 mT]. Computer simulation was used to verify the experimentally-determined coupling constants. These parameters are characteristic of a carbon-centred radical adduct which has

couplings to two non-equivalent protons. This signal decreased in intensity with time but no other signals were observed, in contrast to the previous experiments (Figure 4.14b).

The perchlorate containing mobile phase used to collect the peroxide HPLC peak is buffered at pH 2.5, thus this low pH may be responsible for the different behaviour observed in these EPR experiments. In order to examine this further, unseparated RB photo-oxidised HPPA was prepared as previously (Section 4.3.1a) and the radical adducts formed as described above. Upon subsequent adjustment of the pH by addition of a small amount of the perchlorate mobile phase, or hydrochloric acid, radical #3 was detected similar to experiments with the HPLC separated fraction. When these solutions were then neutralised (pH 7) using NaOH, the previously observed signals (radicals #1 and #2) returned and displayed similar time dependant changes.

When *N*-acetyl Tyr peroxides (~ 320 μM peroxide) were reduced with Fe^{2+}/EDTA (176 μM) in the presence of MNP (11.8 mM) signals due to the formation of three radical adducts were observed (Figure 4.15). These species were assigned as two triplet of doublet signals [a(N) 1.50 mT, a(H) 0.19 mT and a(N) 1.57 mT, a(H) 0.23 mT] and one triplet of doublet of doublets [a(N) 1.53 mT, a(H) 2.4 mT, a(H) 0.07 mT], these parameters were verified using computer-based spectral simulation (Figure 4.15). The parameters of these species are characteristic of carbon-centred radicals, and are similar to those observed in experiments with RB photo-oxidised Tyr (Section 3.4.4c). Collected HPLC fractions (using water as the mobile phase as described in Section 4.3.3c) of the peroxidic product of RB photo-oxidation of *N*-acetyl Tyr exhibited signals with identical parameters when reduced with Fe^{2+}/EDTA in the presence of MNP, suggesting that the radicals were derived directly from the peroxidic species.

Gly-Tyr-Gly peroxides (~ 140 μM peroxide) reduced with Fe^{2+}/EDTA (176 μM) in the presence of MNP (11.8 mM) also yielded two triplet of doublet signals [a(N) 1.52 mT, a(H) 0.23 mT and a(N) 1.54 mT, a(H) 0.13 mT] and a triplet of doublet of doublets [a(N) 1.55 mT, a(H) 0.21 mT, a(H) 0.07 mT) (Figure 4.16). These coupling constants were confirmed using spectral simulation (Figure 4.16). These signals are characteristic of carbon-centred radicals with similar coupling constants to those observed previously (Section 3.4.4c) in experiments with free Tyr.

Collected HPLC fractions (using water as the mobile phase as described in Section 4.3.3c) of the peroxidic product of RB photo-oxidation of Gly-Tyr-Gly were observed to give the same signals when reduced by Fe^{2+}/EDTA in the presence of MNP, suggesting that the radicals are derived directly from this peroxide.

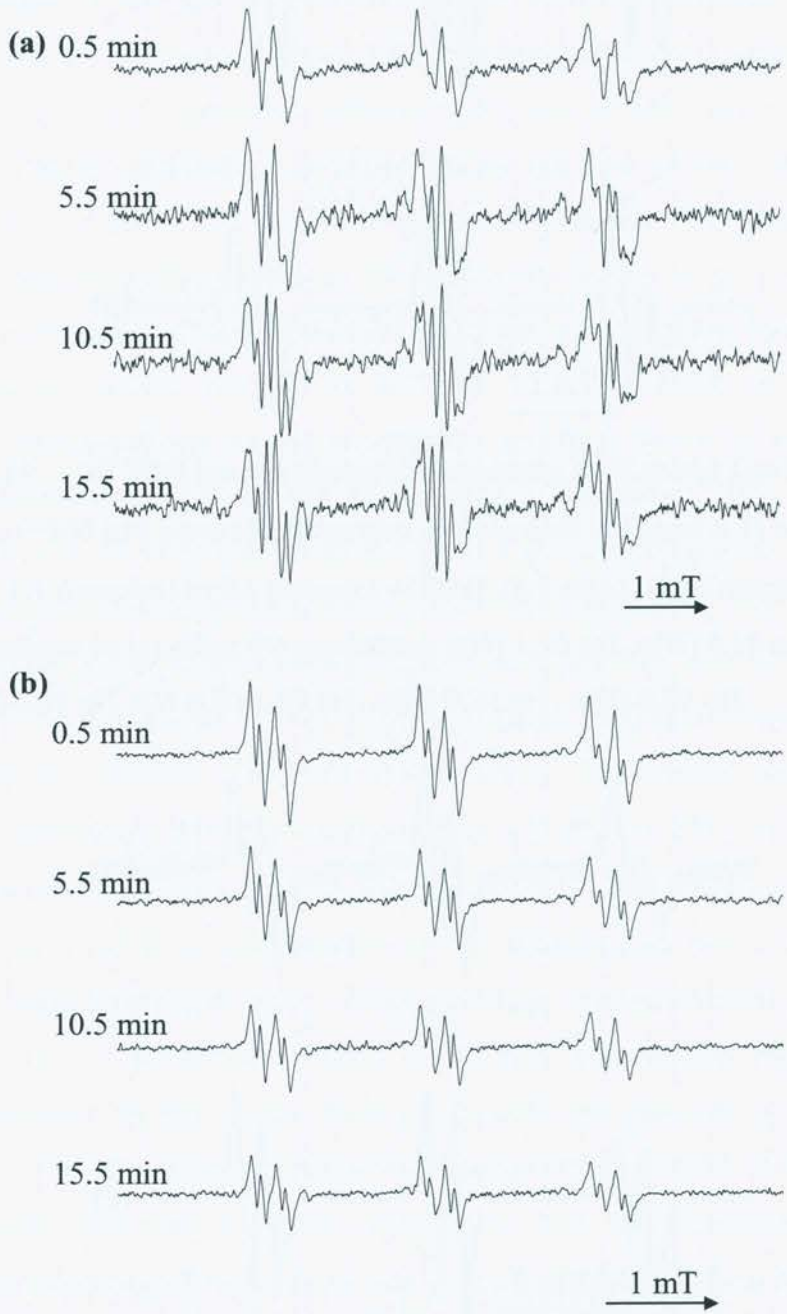

Figure 4.14: EPR spectra detected on reaction of HPPA-derived peroxides (~1400 μM peroxides generated as described in Figure 4.1) with Fe^{2+}/EDTA (176.5 μM, 1:1 complex) in the presence of MNP (11.8 mM). Times refer to time after initiation of

the reaction by addition of Fe^{2+}/EDTA. (a) Spectra acquired at pH 7, (b) spectra acquired at pH 3.

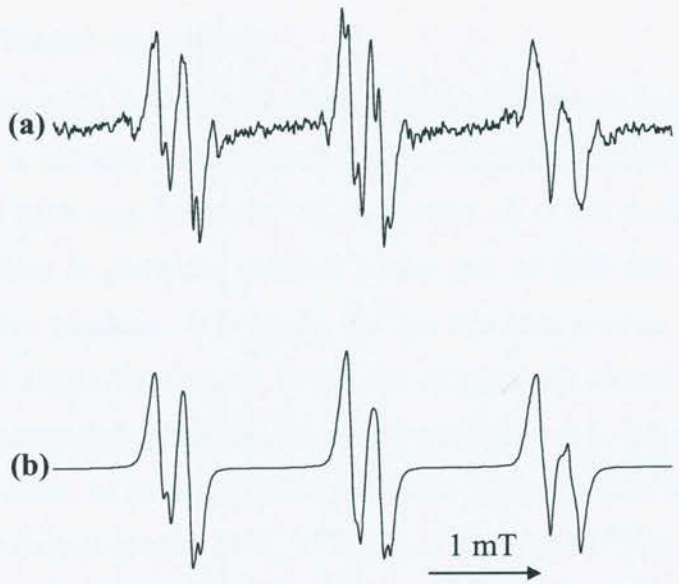

Figure 4.15: (a) EPR spectra observed on reaction of *N*-acetyl Tyr-derived peroxides (~300 μM peroxide, generated as described in Figure 4.1) with Fe^{2+}/EDTA (167 μM 1:1 complex) in the presence of MNP (8.3 mM). (b) Computer simulation of the spectrum in (a) using the parameters a(N) 1.50 mT, a(H) 0.19 mT; a(N) 1.57 mT, a(H) 0.23 mT and a(N) 1.53 mT, a(H) 0.24 mT, a(H) 0.07 mT.

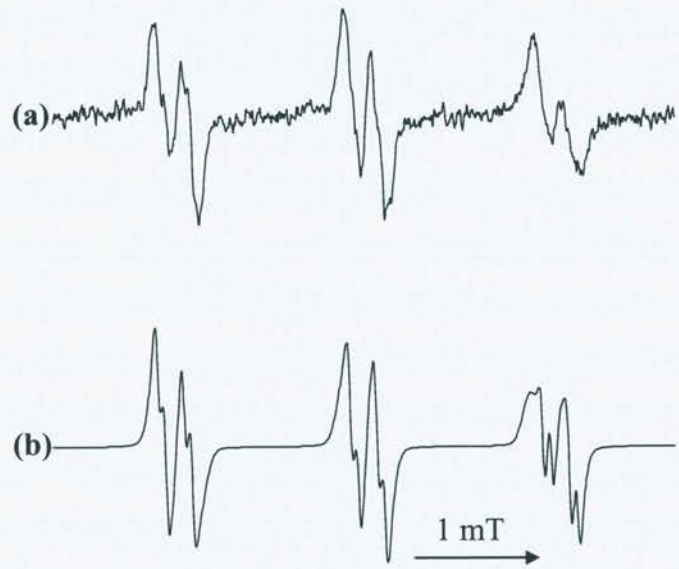

Figure 4.16: (a) EPR spectra observed on reaction of Gly-Tyr-Gly-derived peroxides (~300 μM peroxide) with Fe^{2+}/EDTA (167 μM 1:1 complex) in the presence of MNP (8.3 mM). (b) Computer simulation of the spectrum in (a) using the

parameters a(N) 1.52 mT, a(H) 0.23 mT; a(N) 1.54 mT, a(H) 0.13 mT and a(N) 1.55 mT, a(H) 0.21 mT, a(H) 0.07 mT.

4.3.4a.ii Protein experiments

In section 4.3.2, it was shown that peroxide species are formed on proteins by RB photolysis. It was also demonstrated that this peroxide formation is $^1O_2$-dependant with the use of D_2O, and the MoO_4^{2-}/H_2O_2 system. It is not possible to ascribe this peroxide formation to particular residues in the case of BSA due to the presence of other $^1O_2$ reactive residues. It is likely, but has not been proven, that in the case of histone H1, the single Tyr residue is the site of peroxide formation as none of the other residues generally regarded as $^1O_2$ reactive are present in this protein.

The reduction of protein-derived peroxides has previously been shown to yield protein-derived radical species [193, 217, 226, 235]. The EPR spectra observed are generally very broad and lacking in hyperfine couplings due to the size of the adduct and its corresponding slow rate of tumbling in solution. This anisotropic line broadening can be overcome with the use of a proteolytic enzyme, such as pronase [236]. This treatment will release smaller, more mobile, adducts from the large protein adduct, which results in the detection of sharp, isotropic EPR spectra.

In the experiments reported in this section, EPR spin trapping was used to investigate the formation of radicals on reduction of $^1O_2$-derived protein peroxides.

Treatment of RB photo-oxidised BSA (75 μM, ~ 200 μM peroxide treated with catalase (3150 units mL^{-1} 5 min, 22 °C) with Fe^{2+}/EDTA (167 μM) in the presence of MNP (8.3 mM) resulted in the detection of broad, anisotropic EPR signals, characteristic of large, slowly-tumbling, protein-derived radical adducts (Figure 4.17). A sharp triplet signal of relatively low intensity was also observed. The parameters of this signal [a(N) 1.70 mT] are identical to those observed previously for $(^tBu)_2NO\bullet$, a well-known decomposition product of MNP [227]. No signals were observed in control experiments with non-photolysed BSA. Upon proteolytic digestion of the adducts with pronase (2 units, 15 min, 37 °C), the signal was sharpened to reveal a triplet of doublets [a(N) 1.53 mT, a(H) 0.24 mT] with similar hyperfine coupling constants to those observed with Tyr and model compounds (Figure 4.17). This suggests that Tyr-derived peroxides may be involved in the formation of these radical adducts but it does not, of course, prove that this is indeed the case. Further, there are also other signals present in the spectra obtained

from the pronase digested adducts, which could be due to the formation of peroxides on other residues in the protein, for example His (see Chapter 7) and (Hawkins *et al.*,

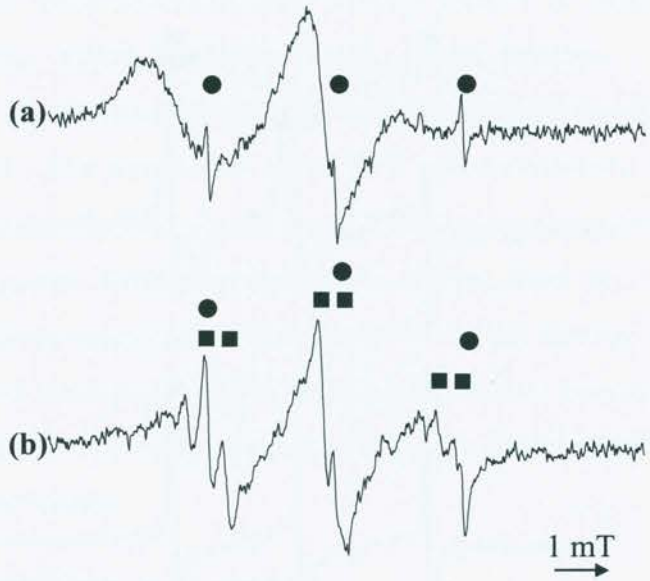

unpublished data).

Figure 4.17: (a) EPR spectra observed on reaction of BSA-derived peroxides (~ 200 μM peroxide) with Fe^{2+}/EDTA (167 μM, 1:1 complex) in the presence of MNP (8.3 mM). Signals marked (●) are assigned to $(^tBu)_2NO\cdot$ [a(N) 1.70 mT]. (b) As (a), except after incubation of the pre-formed adducts with pronase (2 units, 15 min, 37 °C). Signals that are similar to those observed with RB photo-oxidised Tyr are denoted (■) (see text for further details).

Similar results were obtained with RB photo-oxidised histone H1. In this case, the signals were not broadened to the same extent as those derived from BSA, and it was possible to identify features that have similar parameters to those previously observed in experiments with the smaller compounds (Figure 4.18) possibly due to the smaller size of this protein relative to BSA.

To further investigate the origin of the signals observed with histone H1, iodination was used to chemically block Tyr residues, as described in Chapter 2. This was achieved by reacting histone H1 with iodine in the presence of potassium iodide at pH 9.4 at 4 °C. After 15 min, unreacted iodine and potassium iodide were removed from the reaction mixture by dialysis (for further details see Chapter 2).

No signals were observed when photolysed, iodinated, histone H1 was treated with Fe^{2+}/EDTA (172.4 μM) in the presence of MNP (12.3 mM). This is consistent

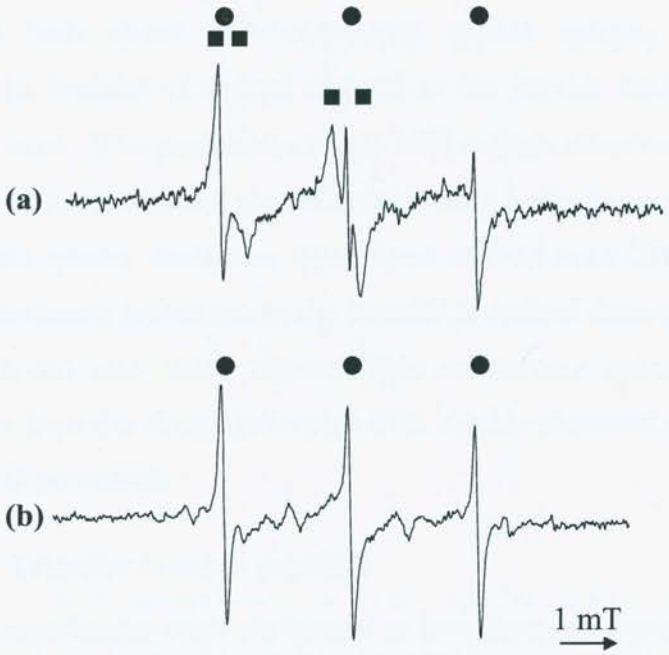

with, but does not definitively prove, that the signal seen with the native protein was Tyr-derived (Figure 4.18).

Figure 4.18: (a) EPR spectra observed on reaction of Histone H1 derived peroxides (~200 μM peroxide) with Fe^{2+}/EDTA (167 μM, 1:1 complex) in the presence of MNP (8.3 mM). Signals marked (●) are assigned to $(^tBu)_2NO^•$ [a(N) 1.70 mT]. (b) as (a) except that iodination was used to block Tyr residues prior to photo-oxidation. Signals that have similar parameters to those observed in experiments with RB photo-oxidised Tyr are denoted (■) (see text for more detail).

4.3.4b Transfer of radical damage from Gly-Tyr-Gly to other peptides and proteins

The radicals formed by metal ion reduction of Gly-Tyr-Gly-derived peroxides (Section 4.3.4a) are reactive species and hence are expected to rapidly react with other biomolecules. Proteins are highly abundant in cells and so it is likely that they may be a potential target for reaction these radicals.

The potential occurrence of such reactions was investigated by reducing the Gly-Tyr-Gly peroxides in the presence of a target peptide or protein and a spin trap.

As discussed in Chapter 1, the EPR spectra observed from particular radical adducts have characteristic coupling constants. Thus, it was expected that careful selection of target molecules for these reactions would make it possible to identify radical species derived from both initial and transferred radical species. For experiments investigating the transfer of radical damage to the peptide backbone, Gly and Ala peptides were used. The parameters of the EPR signals observed from the α-carbon radical adduct of these residues should contain both hydrogen and nitrogen couplings and should yield spectra distinctive from those derived from Gly-Tyr-Gly peroxides. Similarly, experiments investigating the transfer of radical damage from Gly-Tyr-Gly to proteins should also yield characteristic anisotropic spectra that are readily distinguishable from the sharp (isotropic) EPR signals observed on reduction of Gly-Tyr-Gly-derived peroxides.

4.3.4b.i Transfer to small peptides

Initial experiments were performed to investigate the spectra derived from the reaction of HO• with Ala-Ala and Gly-Gly-Gly, in order to provide authentic spectra of these radicals for comparison to any signals observed in the transfer experiments. Thus, Gly-Gly-Gly (57.5 mM) was reacted with HO•, generated by a Fe^{2+} (2.3 mM) / H_2O_2 (2.9 mM) system, in the presence of 3,5-dibromo-4-nitrosobenzenesulfonic acid (DBNBS) (1.15 mM) and the resulting radical adducts examined by EPR spectroscopy. This nitroso spin trap was used in preference to MNP, in these experiments, due to its solubility in water and the lack of spin trap decomposition products, which might obscure any low intensity signals generated as a result of transfer reactions. The spectra detected were consistent with the formation a carbon-centred radical adduct, which was assigned as a triplet of doublet of triplets [a(N) 1.38 mT, a(H) 0.75 mT, a(N) 0.21 mT] (Figure 4.19). These hyperfine couplings were confirmed by computer simulation. This signal is characteristic of a trapped carbon-centred radical, which has couplings to the spin trap nitrogen, an adjacent proton and a further nitrogen atom (Scheme 4.2). It is assigned to a trapped α-carbon radical, formed by H-abstraction from one of the α-carbon positions on this tri-peptide as observed previously [237].

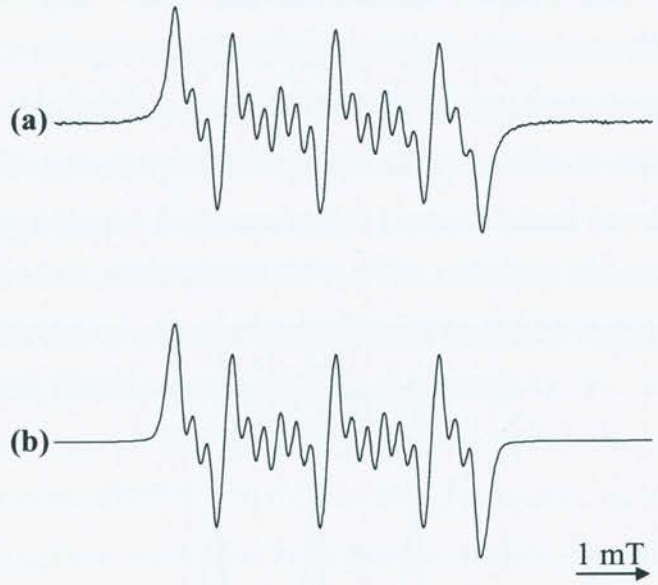

Figure 4.19: (a) EPR spectra observed on the reaction of HO• (generated using Fe^{2+} (2.3 mM) and H_2O_2 (2.9 mM)) with Gly-Gly-Gly (57.5 mM) in the presence of DBNBS (1.15 mM). (b) Computer simulation of the spectrum in (a) using the parameters a(N) 1.38 mT, a(H) 0.75 mT and a(N) 0.21 mT.

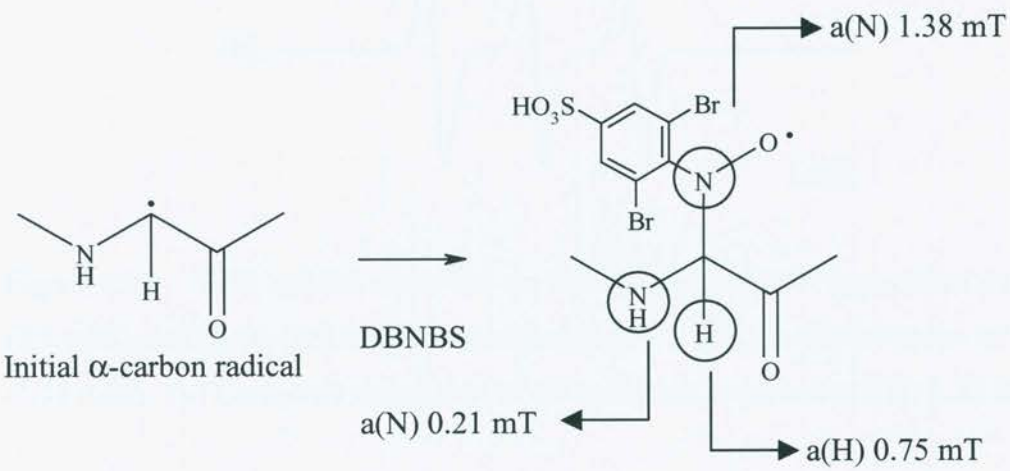

Scheme 4.2: The formation of the spin trapped α-carbon radical formed by HO• - mediated H-abstraction from Gly-Gly-Gly.

Similar experiments were carried out with Ala-Ala and resulted in the detection of one major triplet signal [a(N) 1.32 mT, confirmed by computer simulation] with a small amount of a further signal. This latter species is tentatively

assigned to either a triplet of triplets or a triplet of doublets with only the outermost features visible (Figure 4.20). The major signal is characteristic of a carbon-centred radical and has a nitrogen splitting very similar to that observed with Gly-Gly-Gly. The spectra are simplified, relative to the Gly-Gly-Gly case, as the α-carbon radical arising from hydrogen abstraction from Ala does not have an α-proton, and the extra nitrogen splitting from the backbone amide is not resolved due to steric interactions between the side chain and DBNBS [237]. The additional feature in the wings of the spectrum could be due to radicals resulting from hydrogen-atom abstraction from the methyl side-chains, but this was not investigated further.

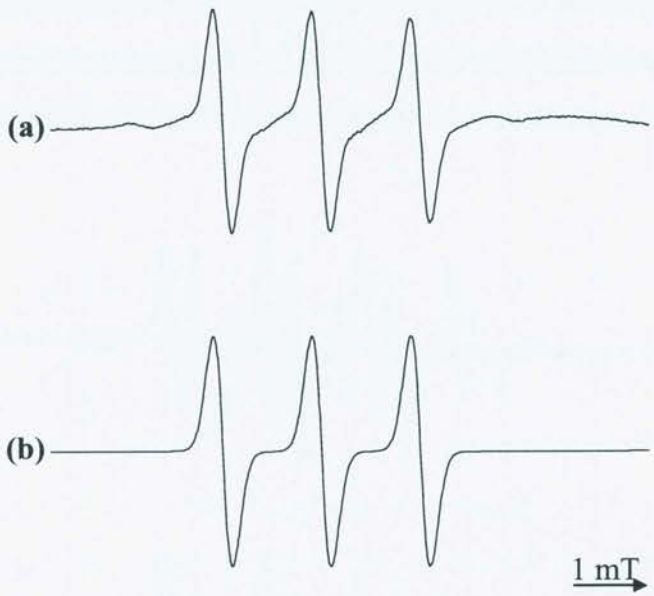

Figure 4.20: EPR spectra observed on the reaction of HO• (generated using Fe^{2+} (2.3 mM) and H_2O_2 (2.9 mM)) with Ala-Ala (57.5 mM) in the presence of DBNBS (1.15 mM). (b) Computer simulation of the spectrum in (a) using a(N) 1.32 mT.

Initial control experiments carried out with non-photolysed samples of Gly-Tyr-Gly demonstrated the formation of low concentrations of Gly-derived radical species when Fe^{2+}/EDTA was used as the radical initiator. This is consistent with an autoxidation reaction of Fe^{2+} resulting in HO• generation, in accord with previous observations [238]. It has been reported previously that Cu^{+} is less prone to autoxidation under similar conditions (Luxford, C. PhD Thesis) [239] and therefore further experiments were carried using this species as the reductant. Cu^{+} was

generated *in situ* by the sequential addition of deoxygenated solutions of Cu^{2+} (150 μM) and Ti^{3+} (100 μM). The treatment of non-oxidised Gly-Tyr-Gly (2.5 mM) with Cu^{+} in the presence of DBNBS (2 mM) and Gly-Gly-Gly (saturated solution) resulted in no detectable radical formation. The lack of signals observed showed that this system was suitable for examining radical transfer reactions mediated by Gly-Tyr-Gly peroxide-derived radicals. Control reactions performed with Ala-Ala (saturated solution) exposed to similar concentrations of non-oxidised Gly-Tyr-Gly to Cu^{+} in the presence of DBNBS gave significant amounts of the Ala-Ala α-carbon radical. In an attempt to prevent the autoxidative reactions thought to be responsible for these signals, O_2 was eliminated from the reaction mixture by bubbling the mixture of Gly-Tyr-Gly, Ala-Ala and DBNBS with O_2-free nitrogen prior to the addition of Cu^{2+} and Ti^{3+}. This approach was successful in reducing the Ala-Ala α-carbon signal down to almost undetectable levels and was subsequently used in all experiments.

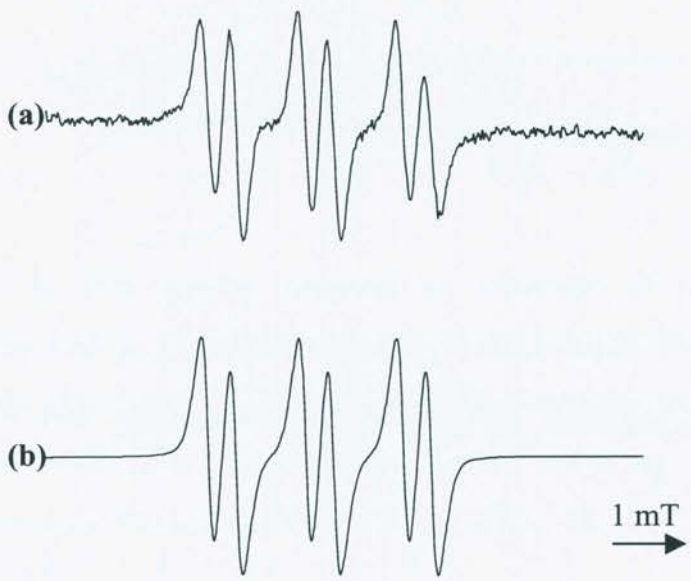

Figure 4.21: (a) EPR spectra observed on reduction of Gly-Tyr-Gly-derived peroxides (generated on 2.5 mM Gly-Tyr-Gly by RB (10 μM) photolysis for 60 min, peroxides ~600 μM) by Cu^{+} (generated by sequential addition of Cu^{2+} (150 μM) and Ti^{3+} (100 μM)) in the presence of DBNBS (2 mM). (b) Computer simulation of the spectrum in (a) using the parameters a(N) 1.31 mT and a(H) 0.38 mT.

Reaction of Gly-Tyr-Gly-derived peroxides (~ 600 μM peroxide as quantified using the FOX assay) with Cu^{+} in the presence of DBNBS led to the formation of EPR signals assigned to a triplet of doublets [a(N) 1.31 mT, a(H) 0.38 mT] (Figure 4.21). This species is characteristic of a carbon-centred radical with a coupling to a neighbouring proton, in accord with earlier experiments carried out with MNP.

When a similar reaction was performed in the presence of Gly-Gly-Gly (saturated solution) the same Gly-Tyr-Gly-derived signal was observed, although it was of much lower intensity, suggesting that some of the Gly-Tyr-Gly-derived radicals have reacted with the Gly-Gly-Gly (Figure 4.22). However, the Gly-Gly-Gly-derived radical was not observed. This may be due to a slow trapping rate or the formation of low concentrations of this radical with features obscured by the remaining Gly-Tyr-Gly-derived signal.

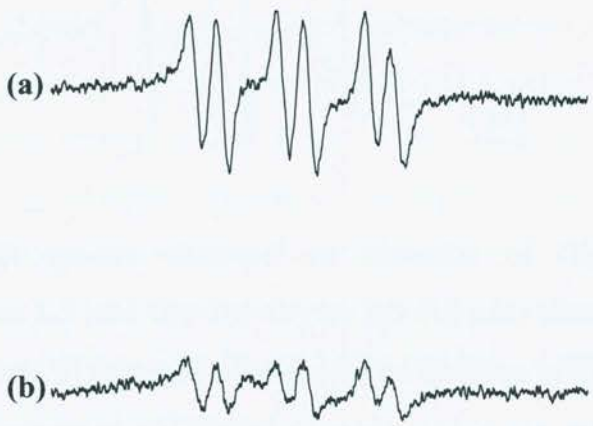

Figure 4.22: (a) EPR spectra observed on reduction of Gly-Tyr-Gly-derived peroxides (generated on 2.5 mM Gly-Tyr-Gly by RB (10 μM) photolysis for 60 min, peroxides ~600 μM) by Cu^{+} (generated by sequential addition of Cu^{2+} (150 μM) and Ti^{3+} (100 μM)) in the presence of DBNBS (2 mM). (b) as (a) with the addition of 230 μL (total reaction volume 500 μL) saturated solution of Gly-Gly-Gly.

Analogous experiments with Ala-Ala resulted in the detection of small amounts of the Gly-Tyr-Gly-derived signal and a relatively intense triplet signal, which corresponded to the Ala-derived α-carbon radical (Figure 4.23). The distortion of the spectrum that is especially noticeable on the left hand side is likely to be due to the presence of residual paramagnetic Cu^{2+}.

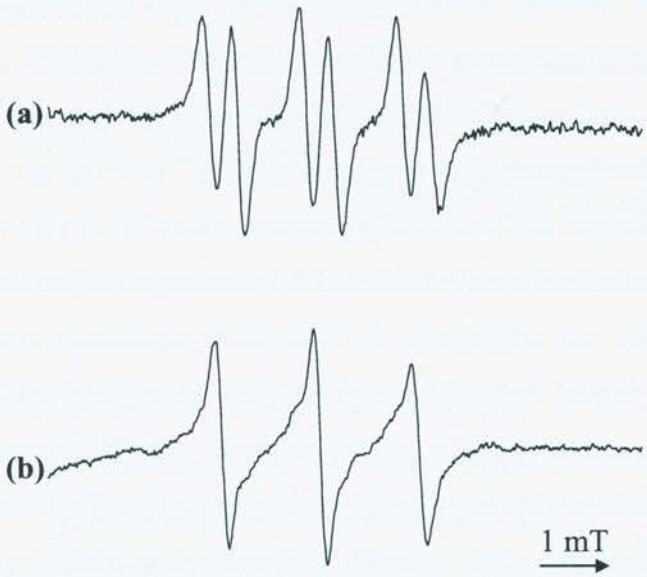

Figure 4.23: (a) EPR spectra observed on reduction of Gly-Tyr-Gly-derived peroxides (generated on 2.5 mM Gly-Tyr-Gly by RB (10 μM) photolysis for 60 min, peroxides ~600 μM) by Cu^{+} (generated by sequential addition of Cu^{2+} (150 μM) and Ti^{3+} (100 μM)) in the presence of DBNBS (2 mM). (b) as (a) with the addition of 230 μL (total volume 500 μL) saturated solution of Ala-Ala.

These results indicate that radicals formed by the reduction of Tyr-derived peroxides can react with model peptides, probably via H-abstraction, yielding α-carbon radicals.

4.3.4b.ii Transfer to proteins

The EPR spectra observed with spin trapped protein-derived radicals are usually broad and anisotropic, as shown in Section 4.3.4a.ii. Accordingly, it was expected that any radicals formed on proteins by reaction with Gly-Tyr-Gly peroxide-

derived radicals would be easily discernable when compared to the peptide-derived signals.

Initial experiments were carried out with non-oxidised Gly-Tyr-Gly and BSA (335 μM) in the presence of DBNBS and Cu^{+} (prepared as described above). This resulted in the observation of broad signals assigned to protein-derived radicals, probably arising from direct reaction of the metal ions with protein; therefore, BSA was not used in subsequent experiments.

Bovine γ-globulins were investigated, as these proteins are highly soluble in aqueous solution. Therefore, it should be possible to maximise the amount of protein present and the chances of observing protein-derived radicals. Addition of Cu^{+} (generated using the Cu^{2+}/Ti^{3+} couple as above) to a deoxygenated solution of non-oxidised Gly-Tyr-Gly (1.25 mM), bovine γ-globulins (184 mg mL^{-1}) and DBNBS (2 mM) did not result in the formation of detectable levels of radicals.

These same conditions were used to investigate the reaction between RB photo-oxidised Gly-Tyr-Gly (~ 600 μM peroxide) and bovine γ-globulins in the presence of Cu^{+} and DBNBS. Analysis of this reaction mixture by EPR led to the observation of the Gly-Tyr-Gly peroxide-derived triplet of doublets and a broad signal characteristic of a protein-derived radical (Figure 4.24). Incubation of this mixture for 2 h at 22 °C led to a decreased intensity of the triplet of doublets signal due to decay and hence the protein-derived signal could be observed more clearly (Figure 4.24). This may be due to the small molecule radicals being more likely to undergo termination reactions, as these species do not suffer the steric interference associated with protein-derived radical adducts.

In order to confirm that these signals were due to protein-derived radicals identical reaction mixtures were subjected to gel filtration. Elution of the materials from the column and collection of the protein fractions followed by EPR analysis showed a broad signal, characteristic of a protein-derived radical (Figure 4.24c).

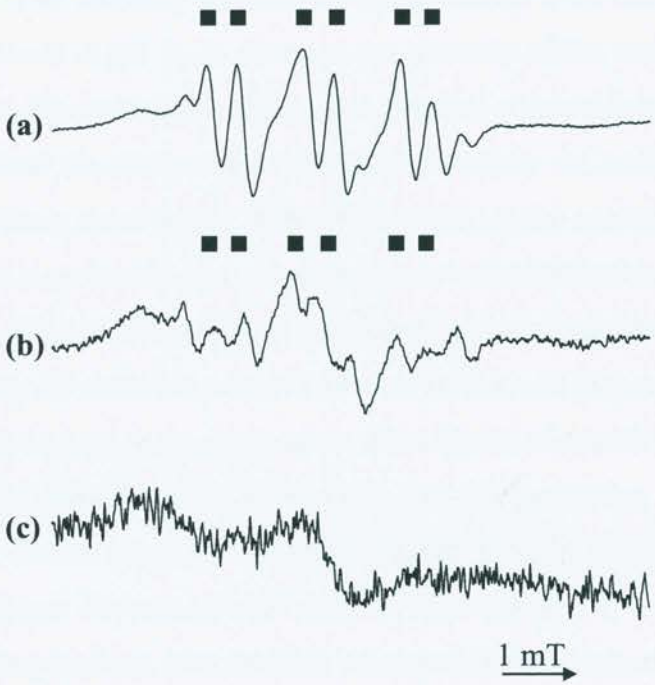

Figure 4.24: (a) EPR spectra observed on reduction of Gly-Tyr-Gly peroxides (generated on 2.5 mM Gly-Tyr-Gly by RB (10 μM) photolysis for 60 min, peroxides ~600 μM) by Cu^{+} (generated by sequential addition of Cu^{2+} (150 μM) and Ti^{3+} (100 μM)) in the presence of DBNBS (2 mM) with the addition of 230 μL bovine γ-globulins (184 mg mL^{-1}). (b) as (a) after 2 h incubation at 22 °C. (c) major protein containing fraction collected after gel filtration of (a). Features marked (■) are assigned as Gly-Tyr-Gly-derived. Note, these spectra are not presented at the same gain as the fractions eluted from the PD-10 column were diluted and also some decay of the radicals occurred during the fractionation process.

4.3.4c Conclusions

EPR spectra characteristic of three carbon-centred radicals were observed when $^{1}O_2$-derived peroxides on HPPA, *N*-acetyl Tyr and Gly-Tyr-Gly were reduced with Fe^{2+}/EDTA in the presence of MNP. In all cases, the radicals observed had very similar hyperfine coupling constants to those observed with free Tyr-derived peroxides (Section 3.4.4c). This similarity suggests that these carbon centred-radical adducts are also formed at the Tyr ring C(3) position.

EPR experiments using RB photo-oxidised HPPA revealed the formation of an triplet of doublet of doublets signal (radical #3) that was not observed in experiments

with free Tyr. The intensity of this signal decreased over time when the radical adducts were formed at pH 7. In contrast, the intensity of the remaining two adducts (radicals #1 and #2) increased. When the reaction was performed at low pH, the signal from radical #3 decreased in intensity, however no additional signals were observed under these conditions. The effect of pH on the spectra observed suggests that the different signals observed are dependant on the ionisation state of the HPPA-derived adduct. Thus at low pH it is possible that the signal observed is due to the protonated carboxylic acid (i.e. neutral) form of HPPA. At higher pH, it is likely that the anion form becomes more important. This triplet of doublet of doublets signal was also observed with *N*-acetyl Tyr and Gly-Tyr-Gly peroxides. As it was possible to use the water mobile phase system for the isolation of the peroxides in these cases, the low pH behaviour of these radicals was not investigated.

In all three systems, the reaction of peroxidic products separated by HPLC, with Fe^{2+}/EDTA in the presence of MNP yielded signals identical to those from the complete reaction mixture suggesting that the radicals are formed directly from the peroxides.

The formation of protein-derived radical species was observed with RB photo-oxidised BSA and histone H1. In the case of BSA broad anisotropic signals were observed, which are characteristic of protein-bound radical adducts [226, 235]. These adducts were digested with pronase yielding smaller, more mobile, adducts which gave sharper EPR spectra. These sharper signals were assigned to a triplet of doublets signal, which had hyperfine coupling constants similar to those observed with free Tyr and model compounds. This suggests that Tyr may be a major target of $^1O_2$-mediated oxidation of this protein under the conditions employed. Other signals were also present in these spectra, which may be due to the reduction of peroxides formed on other residues.

Similar triplet of doublet EPR signals were observed from histone H1-derived peroxides at pH 7. This triplet of doublets signal was not observed in experiments with iodinated histone H1, where the Tyr residue had been chemically blocked. This provides further evidence to support the formation of radicals centred on the protein Tyr-residue.

EPR spectra consistent with the formation of (at least) one carbon-centred radical were observed on reduction of Gly-Tyr-Gly peroxides, formed by $^1O_2$-mediated oxidation, by Cu^+ in the presence of DBNBS. These radicals have different

parameters to those observed in previous chapters; this is due to the different spin trapping agent used. However, the spectra observed with DBNBS have the same splitting pattern as the MNP adducts (i.e. triplet of doublets), suggesting that they are likely to be due to the same initial radical species.

Generation of this radical in the presence of the small peptides Gly-Gly-Gly and Ala-Ala resulted in decreased intensity of the Gly-Tyr-Gly peroxide-derived radical spectrum and the observation of additional EPR signals assigned to the α-carbon radicals formed on Gly and Ala. These results suggest that a radical, or radicals, formed from the reduction of the peroxide are able to abstract a hydrogen atom from these centres to yield the observed secondary radicals.

There are two possible mechanisms by which this hydrogen abstraction reaction may occur depending on which of the Gly-Tyr-Gly-derived radicals is involved. The proposed, but undetected, alkoxyl radical formed on reduction of the Gly-Tyr-Gly peroxide could react with the peptide to yield the observed α-carbon radical and an alcohol (4.6) (Scheme 4.3). This alcohol was characterised by NMR as a decomposition product of the Gly-Tyr-Gly-derived hydroperoxide (Section 4.3.3c).

Alternatively, the ring C(3) carbon-centred radical, formed by an intramolecular epoxidation reaction of the initial alkoxyl radical with the adjacent double bond, could also abstract a hydrogen from the target peptide, yielding the same α-carbon radical and the non-radical form of the epoxide species (Scheme 4.3b).

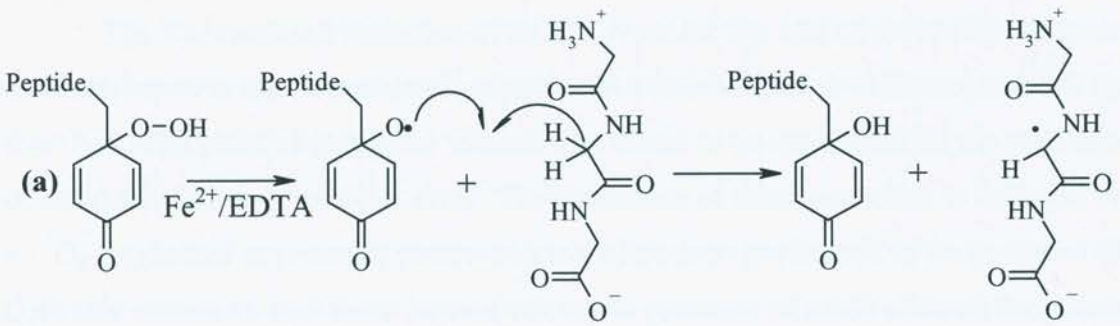

Peptide bound peroxide | Alkoxyl radical | Gly-Gly-Gly | **(4.6)** | α-carbon radical

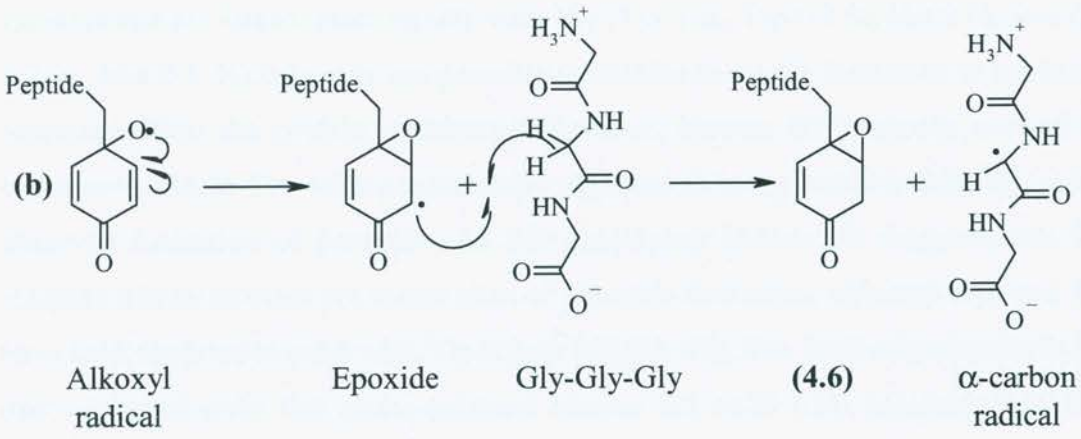

Scheme 4.3: (a) and (b) Alternative, proposed mechanisms for the production of α-carbon radicals on reaction of Gly-Tyr-Gly peroxide-derived radicals with Gly-Gly-Gly residues.

Generation of the Gly-Tyr-Gly peroxide-derived radical in the presence of bovine γ-globulins, led to the detection of broad EPR signals, characteristic of protein-derived radicals. This suggests that similar transfer reactions may occur with intact proteins. However, due to the large amount of steric crowding, it is unlikely that the Gly-Tyr-Gly peroxide-derived radical will directly abstract a hydrogen atom from an α-carbon within the protein structure and is thus expected to react with side-chains of residues found on the protein surface.

4.4 CONCLUSIONS

The $^1O_2$-mediated oxidation of HPPA, *N*-acetyl Tyr and Gly-Tyr-Gly has been shown to result in the formation of peroxides in a similar fashion to those produced on free Tyr. The yield of peroxides formed was found to be dependant on the presence of light, RB and on photolysis time. The formation of these peroxides is believed to be $^1O_2$-dependant as peroxide production in experiments performed in the presence of D_2O was enhanced, and those carried out in the presence of azide showed decreased yields of peroxides. Similar peroxides were observed using the MoO_4^{2-}/H_2O_2 $^1O_2$ generation system, providing further evidence for the role of $^1O_2$ in the generation of these peroxides.

Reaction of $^1O_2$ with both BSA and histone H1 was also found to yield peroxides. The amino acid composition of BSA is such that it contains all of the

residues that are known react rapidly with $^1O_2$ (Tyr 3 %, Trp 0.3 %, His 2 %, free Cys 0.2 %, Met 0.6 %) thus it is not possible to ascribe peroxide formation to particular residues within the protein structure. However, histone H1 has only one of the residues - a single Tyr - that are normally regarded as being reactive with $^1O_2$. The observed formation of peroxides on RB photolysed histone H1 suggests that Tyr residues within proteins are major sites of peroxide formation, although Lys and Arg have been reported to react with $^1O_2$ at high pH [81, 97]. The yield of peroxides (~260 μM) obtained from RB photo-oxidised histone H1 (470 μM) indicates that it is possible that peroxide formation is limited to the Tyr residue of this protein.

Peroxide formation was not observed on incubation of BSA with MNPAE at 37 °C. This may be associated with the low stability of protein peroxides and slow generation of $^1O_2$ in this system.

Peroxides formed on HPPA, *N*-acetyl Tyr and Gly-Tyr-Gly were found to be susceptible to elevated temperatures but were markedly more stable than free Tyr-derived peroxides. This enhanced stability is believed to be due to the blocked (or absent) nature of the α-amino groups. The decay of free Tyr peroxides (see section 3.4.2a) progressed from the ring open hydroperoxide, which undergoes an intramolecular cyclisation reaction to yield an indolic hydroperoxide species. This species decayed further to give the final alcohol product, HOHICA. The enhanced stability of peroxides derived from HPPA, *N*-acetyl Tyr and Gly-Tyr-Gly suggests that the initial ring-opened hydroperoxide is intrinsically, relatively stable. With $^1O_2$-oxidised free Tyr, the proximity of a suitable Michael donor (i.e. the α-amino group) to the α,β-unsaturated carbonyl section of the molecule makes the intramolecular cyclisation reaction a favourable, additional pathway to peroxide decay. The absence of a suitable Michael donor in HPPA, *N*-acetyl Tyr or Gly-Tyr-Gly disfavours the cyclisation reaction and hence the peroxides are more stable.

Further structural characterisation of the peroxidic products was performed using HPLC, ESI-MS and NMR. Results from these experiments demonstrate that $^1O_2$-mediated oxidation of HPPA, *N*-acetyl Tyr and Gly-Tyr-Gly results in the formation of peroxides analogous to the ring C(1) peroxide formed with free Tyr. No evidence for the formation of ring-closed, indolic peroxides was detected, but NMR analysis of oxidised HPPA and Gly-Tyr-Gly indicated that the corresponding ring C(1) alcohols (4.6) and (4.8) were formed after prolonged incubation at low

temperatures. When Gly-Tyr-Gly-derived peroxides were incubated at room temperature a complex spectrum was observed by NMR, which could not be assigned definitively as these resonances were weak. This behaviour is interpreted in terms of the presence of low concentrations of multiple products. These products may be generated as a result of radical-mediated reactions that become more important at higher temperatures.

Overall, the results in this chapter suggest that the $^1O_2$-oxidation of model compounds and Tyr in peptides occurs via a similar initial reaction. The initial peroxide intermediate in all cases is a hydroperoxide at the ring C(1) position. At this point the pathways diverge, with Tyr undergoing an intramolecular cyclisation to yield HOHICA, and the model compounds and peptide Tyr peroxides being relatively stable, but decaying slowly at low temperature to yield the analogous alcohols (Scheme 4.4). It is expected that similar species will be formed on $^1O_2$-mediated oxidation of Tyr residues in proteins, but it was not possible to characterise the products of these reactions to the same extent due to the difficulties in obtaining usable NMR spectra from entire proteins.

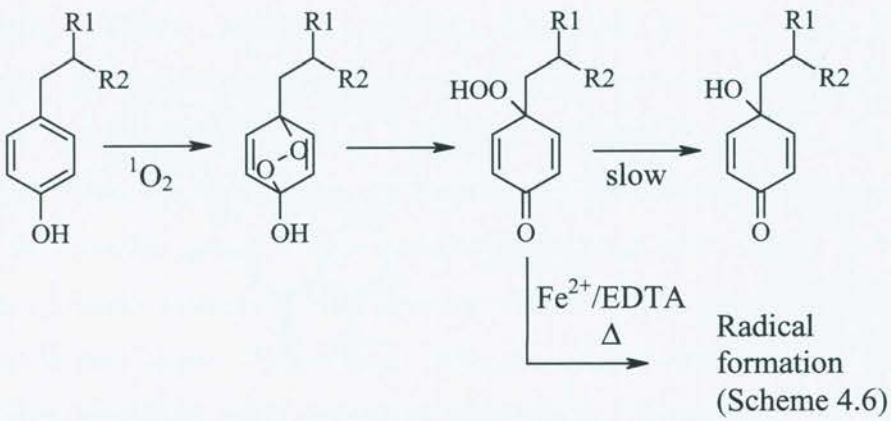

Scheme 4.4: $^1O_2$ mediated oxidation of Tyr model compounds and Tyr as a peptide residue. HPPA, R1 = H, R2 = COOH. *N*-Acetyl Tyr, R1 = $NHCOCH_3$, R2 = COOH. Gly-Tyr-Gly, R1 = N-Gly, R2 = CO-Gly.

EPR spectra characteristic of three carbon-centred radical adducts were observed when Fe^{2+}/EDTA was used to reduce $^1O_2$-oxidised HPPA, *N*-acetyl Tyr and Gly-Tyr-Gly in the presence of the nitroso spin trap MNP. The observed adducts had very similar parameters to those observed with $^1O_2$-oxidised free Tyr, hence the

radicals are assigned to carbon-centred radicals formed at the ring C(3) position of the Tyr side chain. These radicals are believed to arise from pseudo-Fenton reaction of the peroxide with Fe^{2+}/EDTA forming an (undetected) alkoxyl radical, in a manner similar to that proposed for free Tyr. This radical adds to the adjacent double bond in a reaction well-characterised for decay of lipid-derived hydroperoxides [229], forming an epoxide and a carbon-centred radical at the ring C(3) position. This radical is the initial radical observed by EPR with MNP spin trapping. The second adduct is believed to arise from hydrolysis of the epoxide ring yielding a diol species that has slightly different EPR parameters (Scheme 4.5).

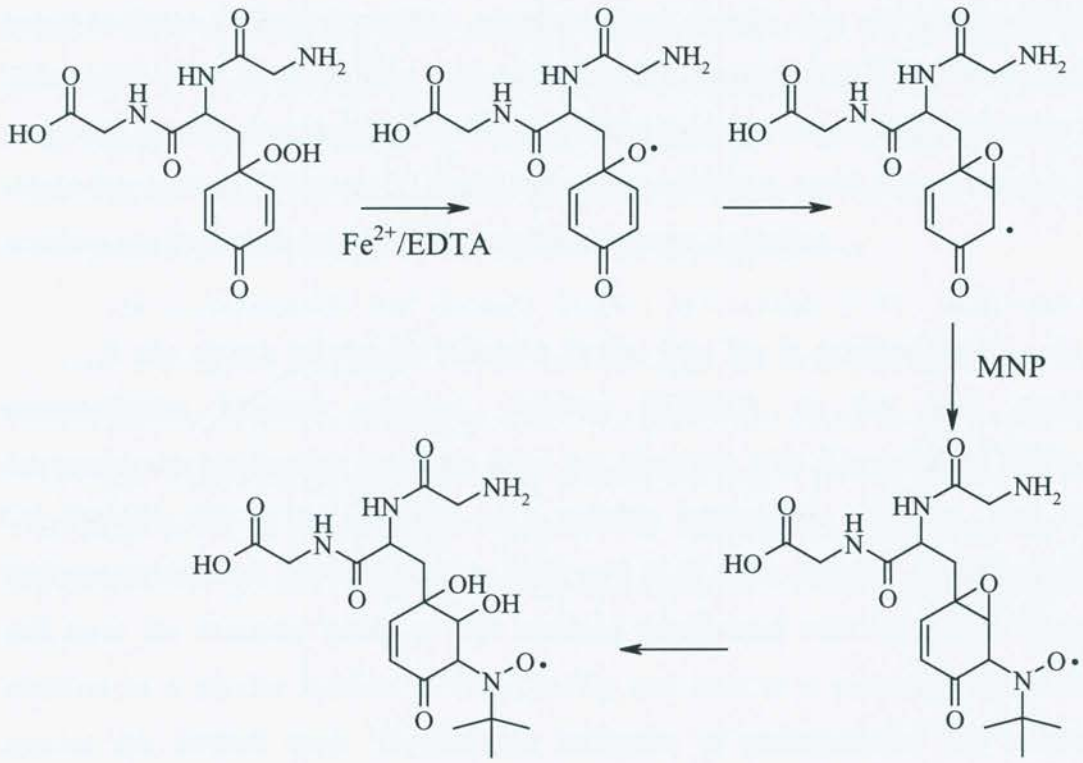

Scheme 4.5: Proposed mechanism for the formation of the Gly-Tyr-Gly peroxide-derived radical adducts observed by EPR spin trapping with MNP.

The low pH experiments with HPPA made the assignment of the triplet of doublet of triplet signal (radical #3) possible in the more physiological conditions used for the experiments with *N*-acetyl Tyr and Gly-Tyr-Gly.

EPR spectra obtained with RB photo-oxidised BSA reduced with Fe^{2+}/EDTA in the presence of MNP consist of a broad anisotropic signal, characteristic of a large,

slowly-tumbling, protein-derived radical adduct. The proteolytic digestion of this adduct with pronase afforded smaller, more mobile, adducts in which hyperfine structure could be resolved. Spectra obtained in this way showed a triplet of doublets signal with very similar hyperfine coupling constants to those observed with free Tyr and model compounds. This suggests that the radicals observed with the protein may also be formed on the ring of the Tyr side chain. Thus, Tyr residues may be important targets for reaction of $^1O_2$ with proteins.

This hypothesis was supported by the results obtained from histone H1. Spectra obtained from histone H1-derived peroxides also showed signals very similar to those observed with free Tyr and model compounds. These signals were not as broad as those derived from BSA peroxides even though they are protein-derived. This may be due to the smaller size of histone H1, compared to BSA, allowing this protein to tumble more rapidly in solution. These signals were not observed when the single Tyr residue of histone H1 was blocked by iodination, again suggesting that Tyr residues are important targets in $^1O_2$-mediated protein oxidation.

It was shown previously (Chapter 3) that free Tyr is oxidised by $^1O_2$, via an intramolecular Michael addition, yielding HOHICA as the final product. Intramolecular cyclisation reactions were not observed with $^1O_2$ oxidised HPPA or Gly-Tyr-Gly due to the absence of a suitable nucleophile. Rather, ring C(1) hydroperoxides and alcohols such as (4.7) and (4.8) were detected. Intact proteins will have the α-amino group of Tyr residues deactivated with respect to Michael addition in a similar fashion to Gly-Tyr-Gly and thus it is proposed that similar species are formed upon $^1O_2$-mediated oxidation of proteinaceous Tyr residues. However, these relatively stable peroxides arising from $^1O_2$-mediated Tyr oxidation are not likely to be inert towards further reactions, indeed they may act as initiating agents for further oxidative damage. Protein peroxides are known to be able to transfer damage to nucleic acids [193, 217] and enzymes [175]. This may occur *via* direct reaction between the peroxides and sensitive moieties of the target molecule (e.g. Cys and Met residues) or may arise from reduction of the peroxide by intracellular metal ions to free radical intermediates, which are known to be able to propagate damage to a range of biomolecules.

Further experiments were performed to investigate the ability of Tyr-derived peroxides to transfer radical damage to other peptides and proteins. Thus, it was demonstrated using EPR spectroscopy with spin trapping, that radicals formed on Tyr residues can react with Gly and Ala peptides to yield backbone α-carbon radicals, and with proteins to yield protein-derived radicals. The formation of such α-carbon radicals is a favourable process due to resonance stabilisation of the radicals by the amide and carbonyl groups [240]. The formation of the α-carbon radicals of Gly and Ala suggest that the Tyr-derived radicals are able to transfer oxidative damage to the protein backbone, which may result in protein fragmentation. However, the situation in intact proteins is likely to be complicated by the steric bulk of the amino acid side chains. Thus, it is unlikely that significant amounts of damage are transferred from the Tyr residues of one protein to the backbone of another, though this has not been investigated in any great detail. The radical formation observed on decomposition of $^1O_2$-mediated peroxides formed on proteins is expected to have important consequences for the structure and function of the damaged protein.

The hydroperoxides and alcohols detected in this study (4.5) – (4.8) have the potential for further reactions. These intermediates are α,β-unsaturated carbonyl compounds, and thus are potential Michael acceptors that could feasibly react with intracellular nucleophiles such as amine compounds (e.g. Lys side chains) or thiol compounds (e.g. Cys residues and/or glutathione). The potential involvement of such reactions in the genesis of further biological damage is the focus of the following chapter.

CHAPTER 5 - FURTHER REACTIONS OF $^1O_2$-OXIDISED TYR: DEVELOPMENT OF MARKERS OF $^1O_2$ MEDIATED PROTEIN OXIDATION

5.1 INTRODUCTION

In previous chapters the $^1O_2$-mediated oxidation of Tyr (5.1) was shown to lead to the formation of peroxide intermediates. The peroxides formed on free Tyr by RB photo-oxidation were found to be relatively unstable to incubation at 37 °C. However, $^1O_2$-derived peroxides formed on Tyr residues in the peptide Gly-Tyr-Gly were found to have higher stability. Due to the effective blocking of the α-amino and carboxylic acid moieties of Tyr by peptide bonds, the peroxides derived from Gly-Tyr-Gly are likely to be a more suitable model for the reactions that occur on $^1O_2$-mediated oxidation of Tyr residues of intact proteins. Therefore the higher stability of these peroxides may have important consequences in a physiological context.

Previously it has been thought that the oxidation of proteins rendered them more susceptible to clearance by the cell, and thus oxidised proteins were not expected to play major roles in physiological situations. However, recently it has been found that heavily oxidised proteins are actually resistant to degradation and elimination from the cell, and thus it has been speculated that these species are of greater importance than first realised [241, 242].

The decomposition products of Tyr peroxides were characterised in Chapters 3 and 4. The hydroperoxide of free Tyr (5.2) was found to undergo an intramolecular cyclisation reaction, resulting in an indolic peroxide, which further decayed to yield 3a-hydroxy-6-oxo-2,3,3a,6,7,7a-hexahydro-1H-indol-2-carboxylic acid (HOHICA) (5.3). This reaction occurs due to the presence of an α,β-unsaturated system on the six-membered ring which is susceptible to attack by a nucleophile. This reaction is an example of the well-known Michael reaction.

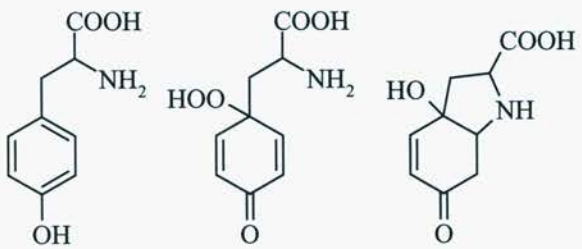

(5.1) **(5.2)** **(5.3)**

In the case of *N*-acetyl Tyr, Gly-Tyr-Gly, and presumably intact proteins, this reaction is disfavoured by the delocalisation of the nitrogen's lone pair of electrons in the peptide bond, suggesting that an intramolecular reaction is unlikely with such substrates. No ring-closed species were detected in $^1O_2$-oxidised Gly-Tyr-Gly or model compounds (Section 4.3.3c), in support of this hypothesis. The product of $^1O_2$-derived Gly-Tyr-Gly peroxide decay was found to be a cyclohexa-2,5-dienone derivative with an alcohol group centred at ring position C(1) (5.4). Thus, this product maintains the α,β-unsaturated carbonyl functionality and is still potentially available for further Michael addition reactions (e.g. with other amine groups or thiols).

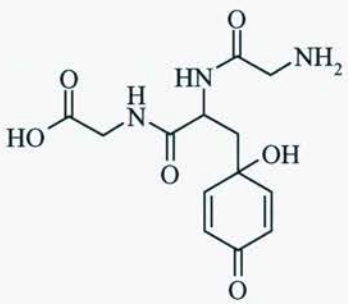

(5.4)

Examples of similar reactions are common. For example it is known that aldehyde lipid oxidation products such as 4-hydroxynonenal (HNE) and malondialdehyde (MDA) react with protein Lys, His and Cys side-chains [243]. These reactions are thought to proceed via a Michael reaction pathway. Thus, the reaction of HNE with Lys was shown to yield the addition product, however the reaction of MDA with Lys resulted in the formation of a Schiff base intermediate [244]. This difference is probably due to MDA existing predominantly as its unreactive enolate tautomer at physiological pH. HNE also readily reacts with thiol nucleophiles such as glutathione, coenzyme A, and *N*-acetyl Cys [245].

Other biochemical examples of Michael additions include: the reaction of dieneone-containing prostaglandins with thiol nucleophiles (such as glutathione) [246], acrolein reactions with protein His and Lys residues [247, 248] and reactions of thiol nucleophiles with quinones (such as the quinone of DOPA).

As both the initial hydroperoxides of $^1O_2$-mediated Tyr oxidation, and their reduction products (e.g. (5.4)), have the potential to undergo further reactions it was

decided to investigate these as they might result in the propagation or amplification of $^1O_2$-mediated peptide/protein oxidation.

5.2 AIMS

The aims of the studies presented in this chapter were to investigate the ability of the cyclohexa-2,5-dienone type products to undergo Michael reactions with biologically relevant nucleophilic nitrogen-containing compounds, such as the amine side-chain of Lys when present both on the free amino acid and as a residue in proteins. Reactions of these Tyr oxidation products with sulfur containing nucleophiles were also investigated.

5.3 RESULTS

5.3.1 REACTION OF $^1O_2$-OXIDISED TYR WITH AMINES

The peroxides derived from $^1O_2$-mediated oxidation of Tyr were found to decay at elevated temperatures (Chapter 3 and 4). It was also found that peroxides formed on the free amino acid were less stable than those derived from 3-(4-hydroxyphenyl)propionic acid (HPPA) – a Tyr model lacking the α-amino group- as well as *N*-acetyl Tyr and Gly-Tyr-Gly. The more stable peroxides were all formed on compounds that lack the (free) α-amino group, thus it was proposed that a major pathway for the loss of this peroxide is through reaction with other nucleophiles (such as amines) via Michael reactions. Such reactions might occur both intramolecularly, as observed with free Tyr, and possibly intermolecularly. In order to examine the possible occurrence of such intermolecular reactions with low molecular weight amines, $^1O_2$-derived peroxides formed on the 'non-cyclisable' model compounds HPPA (5.5), and *N*-acetyl Tyr (5.6) were incubated with Lys (5.7) and a Lys model compound, 6-aminohexanoic acid (AHA) (5.8), which lacks the α-amino group. The loss of peroxides after 24 h incubation at 37 °C was then determined using the FOX assay, as described in Chapter 2. Control experiments were also performed using free Tyr peroxides and Tyr peroxides with added amine to investigate competition between intra- and inter-molecular pathways.

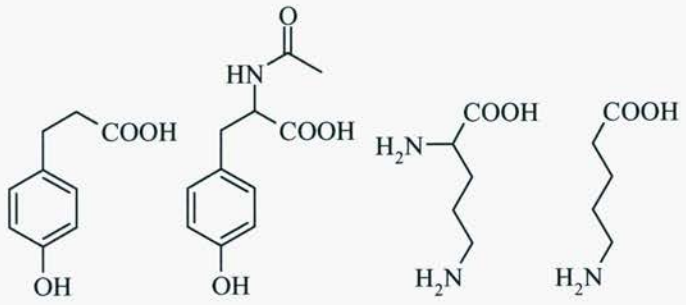

(5.5) **(5.6)** **(5.7)** **(5.8)**

5.3.1a Results

5.3.1a.i Experiments with amine-containing model compounds

Peroxides were generated using RB photochemistry as described in previous chapters. Thus HPPA (2.5 mM, pH 7) was photolysed with visible light ($\lambda > 345$ nm) at 4 °C for 60 min, in the presence of RB (10 μM). To this solution was added Lys or AHA (250 mM, pH 7) resulting in a peroxide concentration of ~ 660 μM, and the mixtures were incubated in the absence of light for 24 h at 37 °C. Control experiments were carried out with the addition of a similar amount of water. The FOX assay was used to quantify peroxide concentrations prior to and after this incubation. As shown in Figure 5.1, 65 ± 6 % of peroxides (n = 4) remained after 24 h in control samples, whereas in those containing Lys or AHA, 28 ± 4 % and 21 ± 1 % of peroxides remained, respectively. Similar results were obtained with *N*-acetyl Tyr- and Tyr- derived peroxides, although control levels of peroxide loss were higher in these cases (Figure 5.1). These results suggest that the presence of Lys and AHA enhances the rate of peroxide decomposition, possibly by an intermolecular Michael addition reaction as postulated above. Such a reaction would lead to the formation of a peroxide species analogous to the ring closed peroxide observed with free Tyr. These peroxides seem to be much less stable than the initial non-cyclised species; this may be due to the altered electron density of the peroxide bond rendering it more labile. The ability of AHA to cause similar reduction of peroxide concentrations to Lys, suggests that the major reactive species is the side-chain amine, or that both α-amino and side-chain amino group can react.

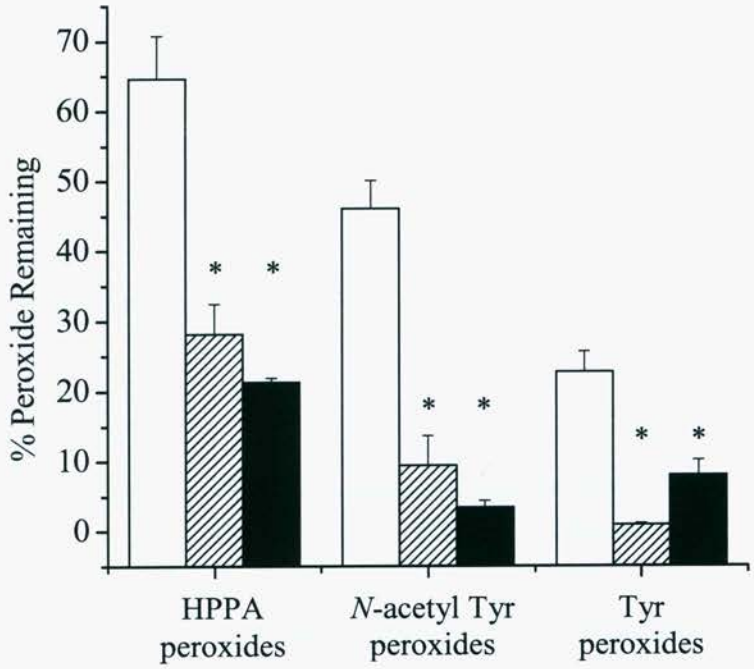

Figure 5.1: Loss of $^1O_2$-generated peroxides on incubation with Lys and AHA. Peroxides were formed by RB photolysis ($\lambda > 345$ nm) of 2.5 mM solutions of HPPA, *N*-acetyl Tyr, or Tyr at 4 °C for 60 min. Incubations were performed at 37 °C for 24 h, in the presence of added water (white bars), Lys (250 mM, stippled bars) or AHA (250 mM, black bars). The FOX assay was used to quantify peroxide concentrations prior and subsequent to incubation. All solutions were treated with catalase (3150 units mL^{-1}) prior to FOX assay to remove any photo-generated H_2O_2. Data are expressed as means ± SD (n = 4). (*) Indicates statistically significant differences from relevant controls (1-way ANOVA with Tukey's post-hoc testing).

5.3.1a.ii Experiments with Proteins

In order to determine whether similar reactions occur between proteins and Tyr-derived peroxides, experiments were carried out using the Lys-rich protein histone H1 (~ 25 % Lys by weight) and also with BSA.

After incubation of histone H1 (234 μM) with HPPA-peroxides (~ 1200 μM) for 24 h at 37 °C, 0 ± 1 % of peroxides remained, which was statistically significant from the control where 68 ± 8 % remained (n=4, two-tailed t-test p=0.000008). Similar results were obtained when Tyr-derived peroxides (~ 500 μM peroxide) were incubated with histone H1 and BSA (Figure 5.2).

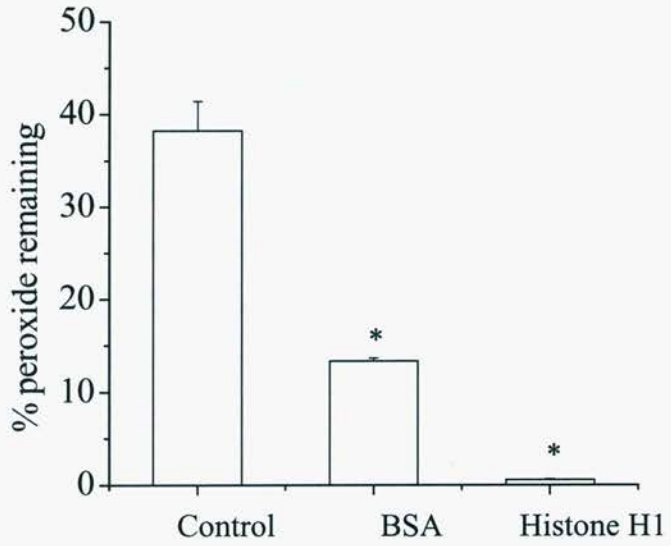

Figure 5.2: Loss of free Tyr peroxides (generated as described in Figure 5.1) on incubation with BSA (75 μM) and histone H1 (235 μM) for 24 h at 37 °C. The FOX assay was used to quantify peroxide concentrations prior and subsequent to incubation. All solutions were treated with catalase (3150 units mL^{-1}) prior to FOX assay to remove any photo-generated H_2O_2. Data are expressed as means ± SD (n = 4). (*) Indicates statistically significant differences from relevant controls (1-way ANOVA with Tukey's post-hoc testing).

These results demonstrate that the presence of histone H1 or BSA accelerates the loss of $^1O_2$-derived Tyr peroxides. In combination with the previous results it seems likely that the peroxide decay is accelerated by the formation of a covalent bond between the Tyr residue and a Lys residue, although it is possible that other residues of the protein are involved. Thus, the protein could be catalysing direct reduction of the peroxides. This may occur, with BSA, via the free Cys residue. Histone H1 does not contain Cys residues, however it is possible that other residues, such as Met or alcohol containing side-chains, may mediate this type of reaction. If direct reduction is leading to the loss of peroxides, no intermolecular adducts between Tyr and the protein will be formed. However if the Michael addition reaction is occurring the oxidised Tyr residue will become bound to the protein.

In order to investigate this further, radiolabelled Tyr peroxides (~ 800 μM peroxide), generated from ^{14}C-labelled Tyr by RB photo-oxidation were reacted with histone H1 (235 μM) and (BSA 75 μM). The use of free Tyr-derived peroxides

introduces the further complication of competing intramolecular reactions. However, free Tyr was the only radiolabelled derivative commercially available, thus it was used in subsequent experiments. The reaction mixtures were analysed by FOX assay as above, yielding similar results, and also were analysed for radioactivity bound to the protein. This was achieved by precipitating the proteins by addition of TCA (5 %), washing the pellets with ethanol:ether (1:1) and resuspending the proteins in sodium phosphate buffer (200 μL) prior to the addition of scintillation fluid (5 mL). The radioactivity associated with the protein was then determined by scintillation counting, as described in Chapter 2.

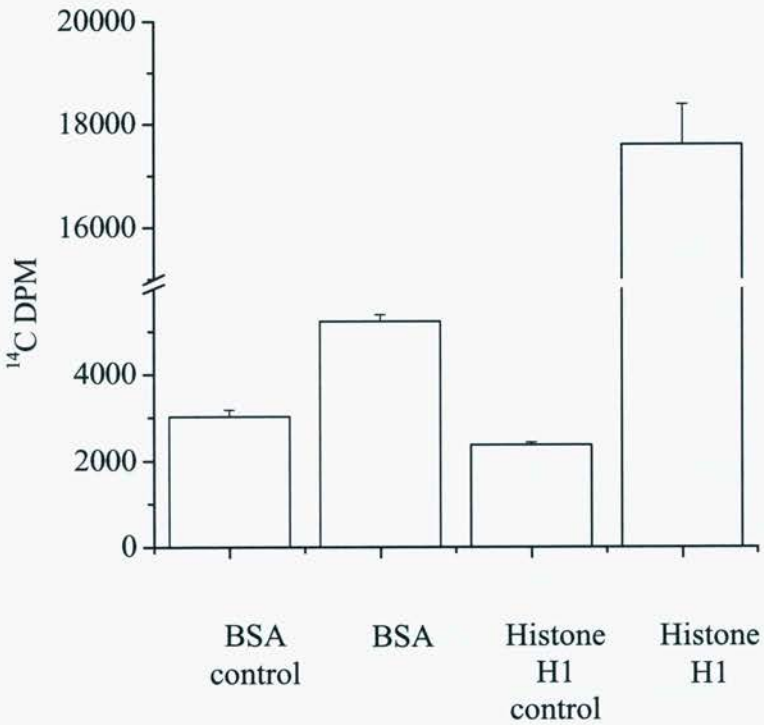

Figure 5.3: Analysis of radiolabel bound to proteins. Radiolabelled Tyr peroxides (~ 800 μM peroxide) were generated using 2.5 mM solutions of Tyr in D_2O, containing an additional 5.5 nmol of ^{14}C-labelled Tyr, by RB photo-oxidation as described in Figure 5.1. Controls were incubated with non-oxidised, labelled Tyr. The crude reaction mixture was incubated at 37 °C for 24 hr in the presence of BSA (75 μM) or histone H1 (118 μM), prior to protein precipitation (10 % w/v TCA) and analysis by liquid scintillation counting as described in Chapter 2. Data are presented as means ± SD of duplicate determinations from a single experiment (representative of several) as initial peroxide concentrations were not constant between experiments due to differences in oxygenation rates of the RB photo-oxidation.

Significantly more radiolabel was found to be associated with BSA and histone H1 when these were incubated with Tyr peroxides than with non-illuminated Tyr (Figure 5.3). This suggests that $^1O_2$-derived Tyr peroxides can react with these proteins to yield a covalently linked species. As the non-specific binding of radiolabelled Tyr is similar for BSA and histone H1, the enhanced binding of radiolabelled Tyr peroxides to histone H1 may be due to the greater number of Lys residues in this protein (25 % Lys compared to approximately 10 % in BSA).

5.3.1b Conclusions

The initial hydroperoxide intermediate of $^1O_2$-mediated Tyr oxidation was postulated in Chapter 3 to be a cyclohexadienone species, with results from HPPA and Gly-Tyr-Gly (Section 4.3.3c) supporting this hypothesis. As a result of the structure of these intermediates it would be expected that they act as Michael acceptors and react with nucleophilic agents. The reduced stability of the free Tyr-derived peroxides was thought to be due to the formation of the carbon-nitrogen bond observed in the indolic products such as (5.3) and thus it was expected that other substituents present at this position may result in overall more rapid loss of the peroxides.

It was found that reaction of $^1O_2$-derived Tyr and model compound peroxides with amine groups derived from Lys or AHA led to decreased stability of the peroxides. This is thought to arise from reaction of the nucleophilic amine with the electrophilic carbon atom present at ring position C(2) (Scheme 5.1). A similar, intramolecular, reaction is thought to be responsible for the decreased stability of the peroxides formed on free Tyr. There were no differences observed between the reactions with Lys or AHA, suggesting that the α-amino group of Lys is not required for the reaction and that similar reactions may occur when the α-amino group of Lys is unavailable for reaction due to its incorporation in to peptide bonds.

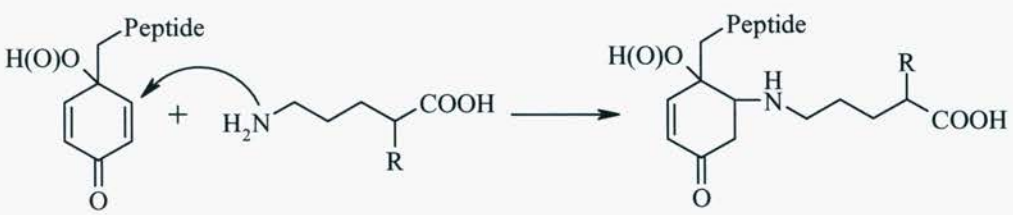

Scheme 5.1: Proposed reaction between intermediate formed by $^1O_2$-mediated oxidation of Tyr and Lys (R = NH2) or AHA (R=H).

As expected from the above results, the enhancement of Tyr and model compound peroxide decay also occurred when the reactions were performed in the presence of the Lys rich protein histone H1, and the general protein model, BSA. These experiments were extended with the use of radiolabelled Tyr peroxides. When these peroxides were incubated with histone H1 or BSA, an enhanced rate of loss of the peroxides was also observed. By use of radiolabelled Tyr in combination with liquid scintillation counting it has been possible to show that Tyr was indeed bound to the protein.

The results of this section demonstrate a possible mechanism for the $^1O_2$-dependant crosslinking of proteins that has been observed previously in *in vitro* studies and is suspected to play a role in the development of cataractous lenses [123-128, 249, 250].

5.3.2 Reaction of $^1O_2$-Oxidised Tyr With Thiols – Isolation of a Potential Marker for $^1O_2$-Mediated Protein Oxidation

The reaction of Tyr oxidation products with amine nucleophiles was observed in the previous section. Previous work [175] has shown that $^1O_2$-derived Gly-Tyr-Gly peroxides can react with thiol groups in similar ways. Thus, the incubation of Gly-Tyr-Gly derived peroxides with thiols has been shown to lead to an increased rate of peroxide loss, which is reversed when the thiol groups are blocked [175]. The thiol used can be a low molecular weight compound (e.g. glutathione) or protein-derived. When the thiol is part of an enzyme, the reaction of the Gly-Tyr-Gly peroxide with the thiol can lead to the inactivation of the enzyme [175]. The loss of peroxides may be due to two-electron reduction or Michael addition to the Tyr ring, similar to that seen with the amine compounds.

Experiments in this section focus on the reaction of the Tyr-oxidation products with thiol nucleophiles, with the aim of developing a compound to be used as a marker of $^1O_2$ mediated protein oxidation.

Generic markers of oxidative damage to proteins (such as protein carbonyls) have been in use for some time [251]. Recent technological advances in analytical science have allowed the development of techniques sensitive enough to detect compounds that are produced specifically due to a particular type of oxidative stress. A variety of such markers are now known and are derived from both aliphatic and aromatic amino acid side chains, as discussed in Chapter 1.

Studies into specific markers of $^1O_2$-mediated oxidation of proteins are not as well advanced as those for other oxidising species. This may be due to the fact that peroxide intermediates are known to be produced by most $^1O_2$ reactions with proteins. These compounds are unstable (e.g. Chapters 3 and 4), especially under high temperature conditions, which are generally used in protein hydrolysis procedures that allow the analysis of oxidation products from specific amino acids e.g. [38, 165-167, 190]. The results obtained in the previous chapters have demonstrated that relatively stable hydroperoxides are generated on $^1O_2$-mediated oxidation of Tyr residues within proteins and also that these peroxides (or the analogous alcohols) can undergo further reactions with nucleophilic agents. Thus, it seemed plausible to react such Tyr oxidation products with a nucleophile as a derivatisation reaction prior to, or during, hydrolysis. This would potentially prevent further reactions of the oxidation products and alter their properties sufficiently for straightforward detection.

The analysis of modified amino acids within proteins is generally performed after hydrolysis of the protein, so that the individual amino acids can be distinguished. This procedure allows collection of the modified amino acids for characterisation and also measurement of the parent amino acid. The later is important for quantitative work as it allows the amount of modified amino acid to be expressed per mole of parent molecule, which can be used to correct for protein lost during sample preparation. Gas phase hydrolysis of proteins usually involves incubation at 110 °C *in vacuo* for 18 hrs, in the presence of 6 M HCl and a reductant, such as phenol, 2-mercaptoethanol or 2-mercaptoacetic acid to minimise artefactual oxidations. From previous results it is expected that these thiol compound will react with oxidised Tyr residues, leading to the formation of an adduct species. If this does occur it may be a useful reaction for the detection of $^1O_2$-oxidised Tyr residues.

5.3.2a Results

5.3.2a.i Experiments with Tyr and small model compounds

Initial experiments were carried out with the simple peptide model Gly-Tyr-Gly. Thus, Gly-Tyr-Gly (2.5 mM) was oxidised by $^1O_2$ generated using visible light ($\lambda > 345$ nm) photolysis of RB (10 μM) as previously. After photolysis samples were subjected to the gas phase hydrolysis procedure outlined above and in Chapter 2.

Oxidation products of Tyr, including 3,4-dihydroxyphenylalanine (DOPA), di-

tyrosine, nitro- and chloro-Tyr have been analysed previously using HPLC (reviewed in [4]). The HPLC conditions used resulted in good separation of these analytes and thus it was decided to use similar conditions in these initial experiments. The mobile phases for these analyses were 100 mM sodium perchlorate in 10 mM sodium phosphate buffer at pH 2.5 (mobile phase A) and 80 % methanol in water (mobile phase B). The column used was a Zorbax ODS (250 x 4.6 mm, 5 μm pore size). Mobile phases were pumped at a rate of 1 mL min^{-1} and a gradient elution program was used. This program consisted of 12 min isocratic elution with 0 % B, followed by a linear increase to 20 % B over 8 min, further elution at 20 % B for 3 min before increasing to 50 % B over the next 3 min; isocratic elution at 50 % B for a further 3 min, followed by re-equilibration with 100 % A for 10 min. The eluent was monitored at 210 nm.

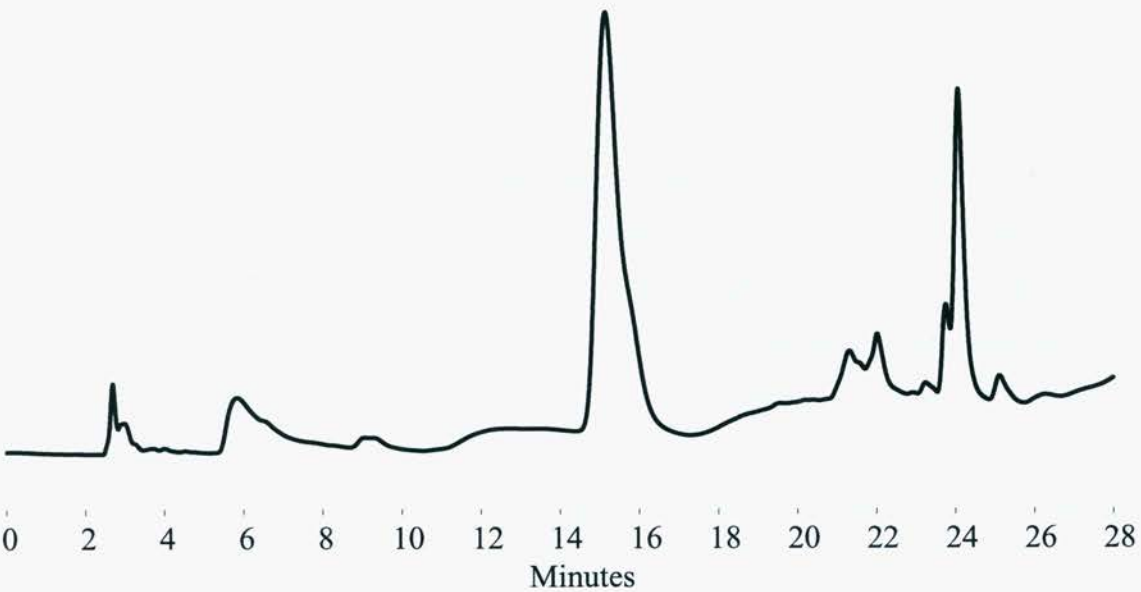

Figure 5.4: HPLC analysis of the products generated on gas phase hydrolysis of RB photo-oxidised Gly-Tyr-Gly. Photo-oxidation was performed in the presence of oxygen using a visible light source $\lambda > 345$ nm), RB (10 μM) and Tyr (2.5 mM in D_2O) at 4 °C for 60 min. After photo-oxidation samples were lyophilised and subjected to a gas phase acid catalysed hydrolysis procedure in the presence of 2-mercaptoacetic acid (700 μM), as described in Chapter 2. 10 μL samples of the hydrolysate were loaded onto a Zorbax ODS column, which was eluted at a flow rate of 1 mL min^{-1} with 100 mM sodium perchlorate, 10 mM phosphate buffer at pH 2.5 and 80 % methanol in water using a gradient program as described in the text. Peaks were identified by absorbance at 210 nm.

Using these chromatographic conditions analysis of non-photolysed Gly-Tyr-Gly solutions that had been subjected to the hydrolysis procedure, resulted in the detection of a single HPLC peak with retention time (RT) of 15 min. This co-eluted with authentic Tyr and is therefore assigned to this amino acid. When $^1O_2$-oxidised Gly-Tyr-Gly was analysed using this methodology parent Tyr was observed along with three product peaks with RT of 9, 22, and 24 min (Figure 5.4). One of these had RT identical to that of authentic DOPA under these conditions (9 min) and was therefore assigned to this material. This peak was not observed in the non-oxidised samples and therefore is likely to be a reaction product. This is consistent with the results reported in Chapter 3 where small amounts of DOPA were observed on photo-oxidation of free Tyr (Section 3.4.3a). The other two peaks were not observed with the non-oxidised samples and hence may be specific oxidation products of Tyr. The identity of these materials was subsequently explored to determine whether they might be specific products of $^1O_2$-mediated Tyr oxidation.

In order to achieve better separation of these reaction products (particularly those eluting at 22 and 24 min), which is required for efficient fraction collection and further characterisation, the gradient program was altered. After some experimentation it was found that isocratic flow of 0 % B for 12 min (unchanged), followed by a linear increase to 20 % B over 12 min, further elution at 20 % B for 4 min, increase to 50 % B over 3 min, isocratic at 50 % B for 3 min, followed by 10 min re-equilibration at 0 % B for 10 min, gave good resolution of these materials. The RT of Tyr was unchanged under these conditions (15 min), the potential marker peaks now eluted at 23 and 26 min.

To investigate whether these materials arise from oxidation of Tyr and were not products of Gly oxidation or contaminating materials, a variety of Tyr model compounds were RB photo-oxidised, hydrolysed as above and analysed using the HPLC conditions above. Thus oxidised Tyr, *N*-acetyl Tyr, Gly-Tyr and Gly-Tyr amide were all found to exhibit the new peak eluting at 26 min, but not the 23 min peak. This latter peak was thus not further investigated. In no case did the non-oxidised control experiments exhibit any peaks in this region. Similarly analysis of Gly and Gly-Gly-Gly that had been RB photolysed and hydrolysed did not show any peaks in this area of the chromatogram. This new peak was also observed in the analysis of a mixture of RB photo-oxidised Tyr and Gly-Tyr-Gly, suggesting that a

common product is being generated from both starting compounds. In contrast, studies with HPPA did not yield this peak but resulted in the detection of the parent compound with a RT of 34 min and a further peak that eluted at 38 min, suggesting that the intact α-amino acid moiety was required for the production of the new compound.

In Chapter 3 the HPLC characteristics of $^1O_2$-oxidised Tyr that had not been hydrolysed were reported (Section 3.4.3a). In these post-hydrolysis experiments no peaks corresponding to any of the peroxides or the final product HOHICA were observed, and thus these products could not be used as a marker for $^1O_2$-mediated Tyr oxidation in proteins.

The results reported above suggest that a product formed by $^1O_2$-mediated oxidation of Tyr is responsible for the peak at 26 min. The peak is also unlikely to be a non-cyclised alcohol analogous to that observed on $^1O_2$-mediated oxidation of Gly-Tyr-Gly as this species was not observed in experiments with free Tyr, but the new peak was seen with both Tyr and Gly-Tyr-Gly. Therefore it is likely that the compound corresponding to the 26 min peak is formed from further reaction(s) of the Tyr photo-oxidation products during the hydrolysis procedure. As discussed previously the intermediates of $^1O_2$-mediated Tyr oxidation are expected to be susceptible to nucleophilic addition and thus it was thought possible that the new compound might be a product of the reaction between oxidised Tyr intermediate and the 2-mercaptoacetic acid present in the hydrolysis reaction mixture. Experiments investigating this hypothesis are presented in the following section.

5.3.2a.ii Characterisation of the potential marker peak

In order to determine the molecular weight of the new compound, it was decided to collect fractions from the HPLC and analyse these using mass spectrometry (MS). The mobile phases used for HPLC previously were not suitable as they contained high concentrations of salts, which are incompatible with the MS instrument, thus a new mobile phase system was developed and utilised. This new mobile phase consisted of 0.1 % TFA in water as mobile phase A and 80 % methanol as mobile phase B. 0.1 % TFA had a similar pH to the perchlorate containing mobile phase, thus maintaining the analytes in protonated forms, ensuring that retention on the column was on the basis of hydrophobic interactions. The same gradient program was used as previously and under these conditions the peak corresponding to Tyr

eluted at 17 min and the new peak had RT of 26 min. Collected HPLC fractions of the new peak were then analysed directly by ESI-MS. However, these experiments were unsuccessful as no informative ions were observed. This is likely to be due to the small amounts of material that were collected using this method and such levels being below the sensitivity limit of the ESI-MS instrument.

In order to circumvent these problems, and in particular to obtain higher yields of material for MS analysis, the effect of redissolving the hydrolysate in a variety of solvents was investigated. Previously water had been used to redissolve the hydrolysate in the same volume as the initial sample. It was found that methanol, but not acetonitrile, ethyl acetate or acetone, was suitable for the dissolution of the hydrolysate and also that 10-fold less solvent could be used for a similar amount of material. This allowed ten times as much material to be loaded, using the same injection volume. The RT of the Tyr and putative marker peaks were unchanged under these conditions. Injection of five times the volume of sample (50 μL compared to 10 μL used previously) was used, in combination with the methanol hydrolysate solvent method, for fraction collection. Re-injection of the collected fraction revealed the presence of the new peak only, indicating that the marker compound was stable when subjected to this procedure. The accumulated fractions were subsequently combined and solvent removed under vacuum, to afford a brown solid. On re-dissolving a sample of this material in methanol, and HPLC analysis, the same new peak was observed, indicating that the collection procedure had not altered this compound.

The material obtained from the removal of solvent from 8 mL of combined HPLC fractions could be redissolved in 200 μL of methanol, an effective 40-fold concentration of this material. ESI-MS analysis of this solution revealed a base peak with m/z 272 (cone voltage 25 V) (Figure 5.5). Fragmentation could be induced by increasing the cone voltage, and when set at 75 V fragments corresponding to M-17, M-46, M-76, M-121, M-136 were observed.

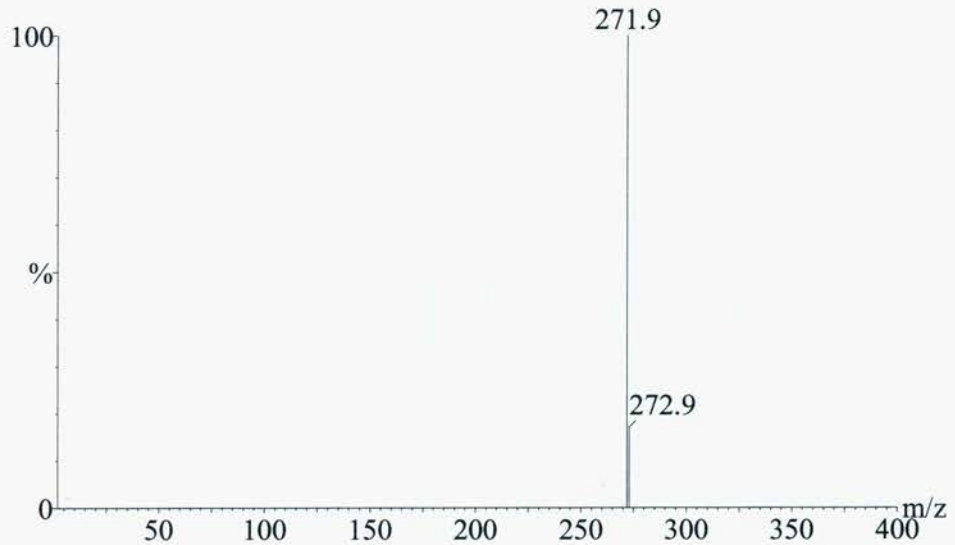

Figure 5.5: ESI-MS analysis of collected HPLC fractions of the potential marker peak. Tyr oxidation and hydrolysis were performed as described in Figure 5.1. HPLC separations used 0.1 % TFA as mobile phase 'A', and 80 % methanol as 'B', the gradient program was as described in the text. Solvent was removed from collected HPLC fractions and then re-dissolved in 200 µL of 50 % methanol and 1 % formic acid to assist ionisation of the sample. Solvent was delivered at 10 µL min^{-1} and 2 x 25 µL injections were made for each analysis. The probe tip was set at 3.5 kV with 0.5 kV on the chicane counter electrode. The sampling cone was set at 25 V.

It was hypothesised that the increased mass of this substance, relative to Tyr, could be derived from reaction with the 2-mercaptoacetic acid present in the hydrolysis procedure. This was further investigated in experiments where the hydrolysis was carried out in the absence of this thiol, and in the presence of an alternative thiol, 3-mercaptopropionic acid of higher molecular mass. When thiol compounds were excluded from the hydrolysis reaction (phenol was used as the reductant), no peaks were observed in the region of the HPLC chromatogram in which the potential marker was previously observed to elute, suggesting that the thiol compound could be playing a role in the formation of the new compound (Figure 5.6).

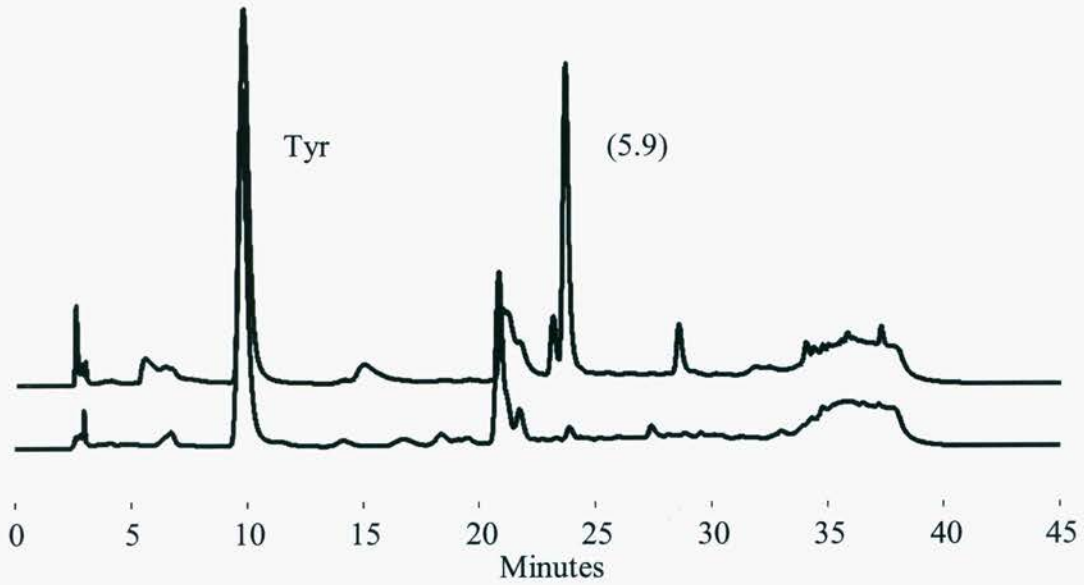

Figure 5.6: HPLC analysis of RB photo-oxidised Tyr that had been subjected to the acid-catalysed, gas phase hydrolysis procedure in the presence (top) and absence (bottom) of 2-mercaptoacetic acid. HPLC analysis was performed as described in Figure 5.4.

In contrast, when 3-mercaptopropionic acid was employed in the hydrolysis system and HPLC analysis carried out on the resulting hydrolysate a later eluting peak, with RT 29 min, compared to 26 min previously, was observed. Fraction collection, solvent removal, and ESI-MS analysis led to the detection of a base peak with m/z of 286, 14 mass units greater than that observed with 2-mercaptoacetic acid (Figure 5.7). This is consistent with the addition of a thiopropionate group to the Tyr molecule, and provides further evidence that the new peak seen with 2-mercaptoacetic acid is due to the addition of a thioacetate group to Tyr.

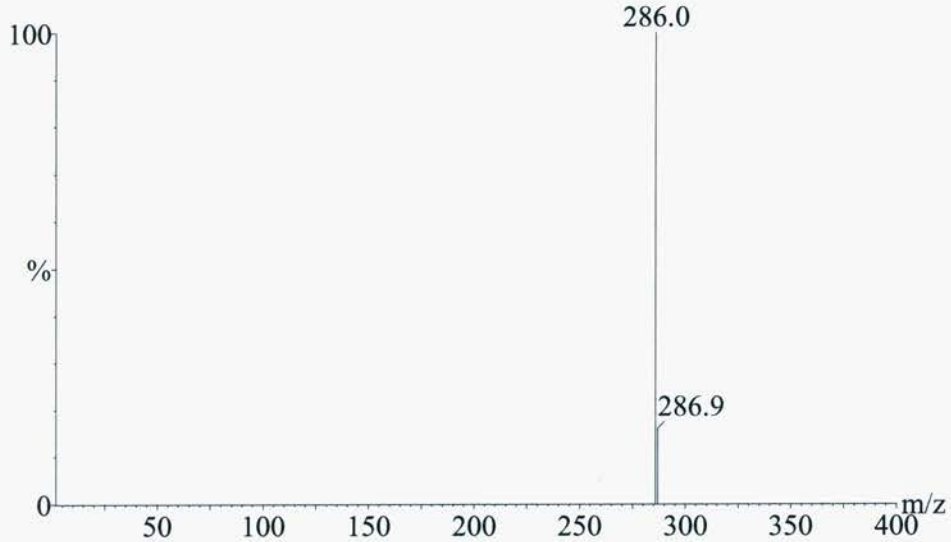

Figure 5.7: ESI-MS analysis of HPLC fractions of RB photo-oxidised Tyr hydrolysed in the presence of 3-mercaptopropionic acid. HPLC and MS were performed as described in Figure 5.5.

The product obtained from the 2-mercaptoacetic acid derivatisation was further characterised using nuclear magnetic resonance (NMR) spectroscopy, in collaboration with Dr W.A Bubb (Department of Biochemistry, University of Sydney). The spectra obtained demonstrated the presence of one compound only, which had resonances consistent with a Tyr derivative substituted at the ring C(2) position. The chemical shift of the ring C(2) atom was deshielded, suggesting that this carbon was bonded to an electronegative heteroatom. This, combined with the presence of an extra methylene unit and the ESI-MS data (above) confirm that the potential marker material is 2-amino-3-(2-carboxymethylsulfanyl-4-hydroxy-phenyl)-propionic acid (5.9). The chemical shift data of this species are summarised in Figure 5.8.

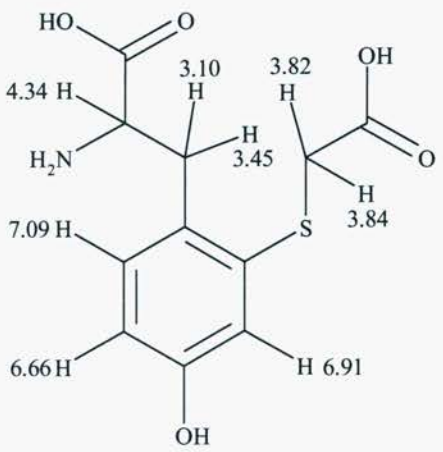

(5.9)

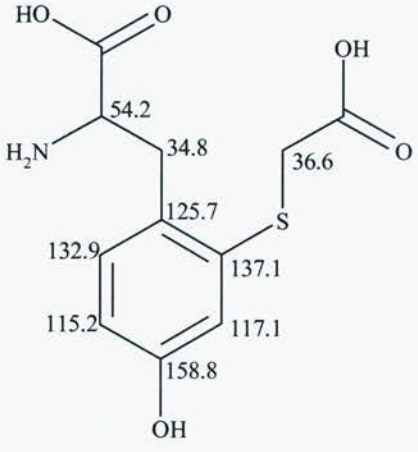

(5.9)

Figure 5.8; Summary of the chemical shift data of the HPLC purified potential marker compound (5.9), ^{1}H NMR data are shown on the left, ^{13}C on the right.

This structure agrees with the MS data obtained previously and also allows the assignment of the fragments observed when the cone voltage was set to 75 V. The assignments are as follows; M-17, loss of OH; M-46, loss of COOH; M-76 loss of -$CH(NH_2)COOH$; M-121, M-76 with loss of COOH; and M-136, loss of COOH and SCH_2COOH).

5.3.2a.iii Investigation of the mechanism of formation of 2-amino-3-(2-carboxymethylsulfanyl-4-hydroxyphenyl)propionic acid

To investigate the mechanism of formation of (5.9) and in particular to determine which of the intermediates formed during Tyr oxidation give rise to (5.9), a series of experiments was planned in which $^{1}O_2$-oxidised Gly-Tyr-Gly was exposed to various conditions of temperature, prior to hydrolysis and analysis by HPLC. Further experiments used collected fractions of HOHICA (5.3) – the product of free Tyr oxidation by $^{1}O_2$ - which were subjected to acid hydrolysis. HPLC and ESI-MS, without prior HPLC fractionation, were also used to analyse RB photo-oxidised HPPA that had been exposed to the hydrolysis conditions.

Gly-Tyr-Gly (2.5 mM) was reacted with $^{1}O_2$, generated using RB (10 μM) photo-oxidation, as described in Chapter 2. Samples of the photolysis reaction mixture were kept at –80 °C, or incubated at 4 °C, 37 °C and 60 °C for 72 h prior to lyophilization and hydrolysis. The HPLC results from these samples were compared

to those obtained from freshly photolysed Gly-Tyr-Gly and freshly photolysed Gly-Tyr-Gly that had been snap frozen (in liquid nitrogen) and subsequently thawed. These conditions were chosen to simulate possible storage procedures of more complex samples prior to hydrolysis and analysis. The peak corresponding to (5.9) was observed at similar intensity in all cases (Figure 5.9).

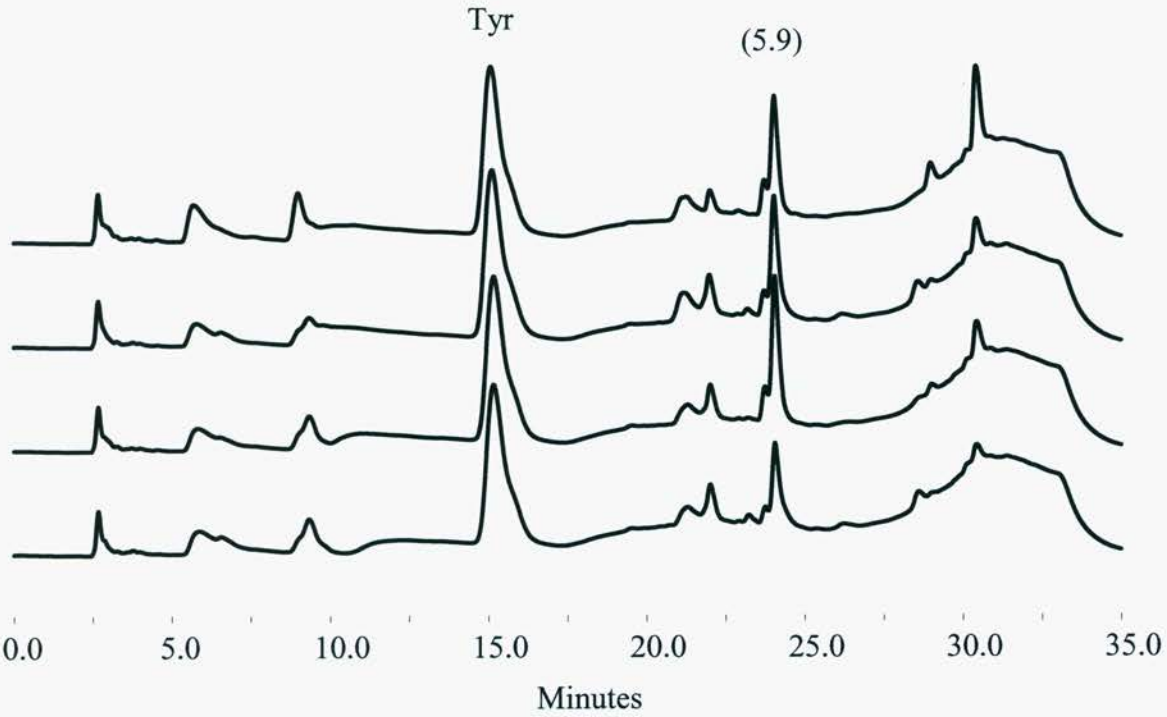

Figure 5.9: HPLC analysis of RB photolysed, hydrolysed Gly-Tyr-Gly that had been stored at –80 °C (bottom), or incubated at 4 °C, 37 °C, or 60 °C (top) for 72 hr prior to acid-catalysed, gas phase hydrolysis in the presence of 2-mercaptoacetic acid. HPLC was performed as described in Figure 5.4.

In accordance with the data presented in Chapter 4 incubation at 60 °C for 72 hr is likely to lead to the decay of the peroxides formed on by $^1O_2$-mediated oxidation of Tyr. However, it is likely that significant amounts of peroxide remain in the samples kept at – 80 and 4 °C. These results imply that formation of (5.9) can occur when peroxides are present, but that their presence is not necessary for it to take place. If peroxides are present at the beginning of the lyophilization and hydrolysis procedure, they are not likely to survive it due the 18 h incubation at 110 °C that is part of the process. Thus, it is not surprising that (5.9) formation can occur in the absence of Tyr peroxides.

The results obtained in Chapter 4 suggest that the major species present after incubation at 110 °C for 18 h is likely to be the non-cyclised alcohol analogous to (5.4). This type of structure is thought to be available for nucleophilic attack at the ring C(2) position, and thus it was hypothesised that this reaction is leading to the formation of (5.9). To test this hypothesis samples of HOHICA, which had been previously isolated by HPLC, and RB photo-oxidised HPPA were prepared and analysed after exposure to the hydrolysis procedure. HPPA was chosen as a model for the non-cyclised peroxides as intramolecular Michael additions are not possible with this substrate due to the lack of an α-amino group.

HPLC analysis of the hydrolysate from isolated HOHICA lead to the observation of the peak assigned as (5.9), as well as a small amount of Tyr. Analysis of the HPPA reaction led to the detection of one major peak (RT 38 min) and a small amount of the parent compound (RT 34 min). The major peak was not observed in non-oxidised samples, suggesting that it is a product of the reaction. Unlike the Tyr-derived products, the presence of this new peak did not depend on the presence or absence of thiols in the hydrolysis reaction (Figure 5.10). This result indicates that these agents are not involved in this reaction. Analysis of the complete reaction mixture after hydrolysis using ESI-MS led to the observation of two ions of m/z 189 and 205, which correspond to the (sodium adducts of) parent HPPA and an M + 16 peak (Figure 5.11). Based on previous NMR results (Section 4.3.3c) this latter peak is assigned as the molecular ion of 3-(1-hydroxy-4-oxo-cyclohexa-2,5-dienyl)propionic acid (5.10) which was observed as the decay product of the hydroperoxide formed on $^1O_2$-mediated HPPA oxidation (Chapter 4).

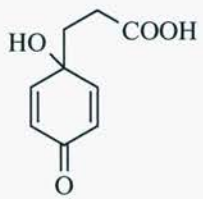

(5.10)

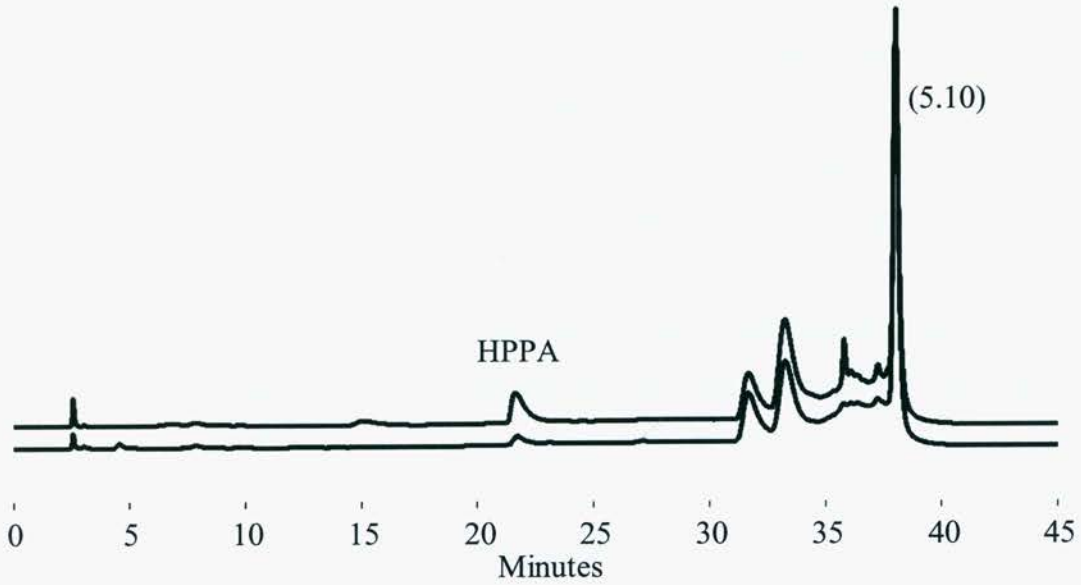

Figure 5.10: Analysis of RB photolysed HPPA that was subjected to hydrolysis conditions in the presence (top) and absence (bottom) of 2-mercaptoacetic acid. Hydrolysis and HPLC analysis were performed as described in figure 5.4.

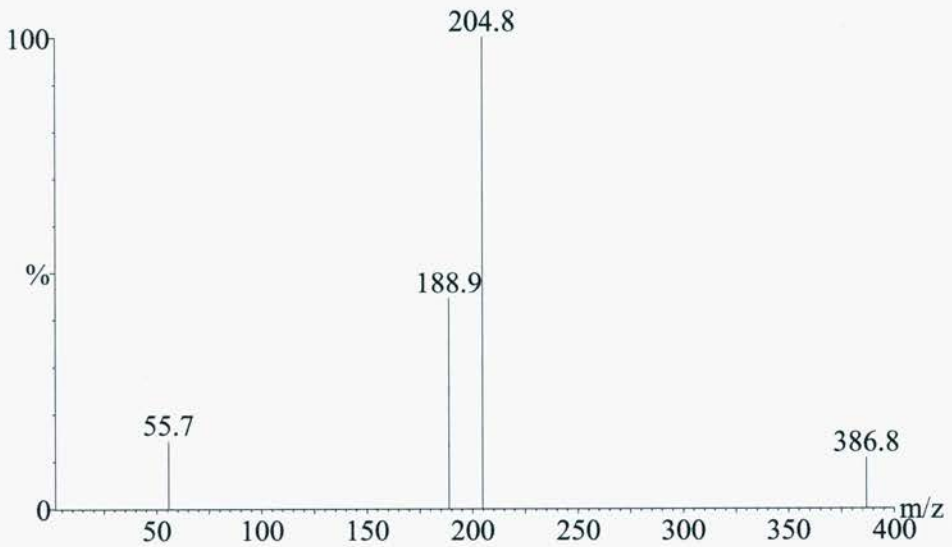

Figure 5.11: ESI-MS analysis of RB photolysed and hydrolysed HPPA without HPLC separation. ESI-MS was performed as described in Figure 5.5.

The combination of these results suggests that (5.9) can be formed from HOHICA and not from non-cyclised alcohols such as (5.4) as demonstrated by the results obtained with $^1O_2$-oxidised HPPA. However, (5.9) is clearly formed from $^1O_2$-oxidised Gly-Tyr-Gly and from $^1O_2$-oxidised proteins (see below). Possible explanations for these seemingly contradictory results include: i) that HPPA may react in a different manner from peptide Tyr residues and thus may not be a good model for this reaction; ii) that on hydrolysis of Gly-Tyr-Gly HOHICA may be formed by intramolecular reaction and this then subsequently reacts with 2-mercaptoacetic acid (Scheme 5.2); or iii) that a cyclisation reaction does take place in the intact peptide or protein, yielding HOHICA on hydrolysis, which is then derivatised by 2-mercaptoacetic acid (Scheme 5.3), however this is not supported by NMR results reported in Chapter 4, in which no cyclized products were observed (Section 4.3.3c).

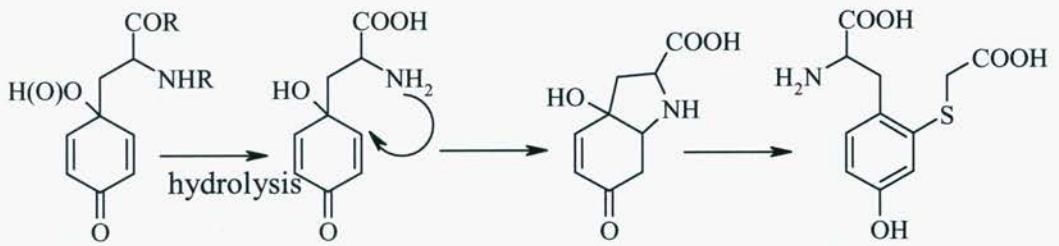

Scheme 5.2: Possible reaction mechanism for the formation of (5.9) from $^1O_2$-oxidised Tyr residues.

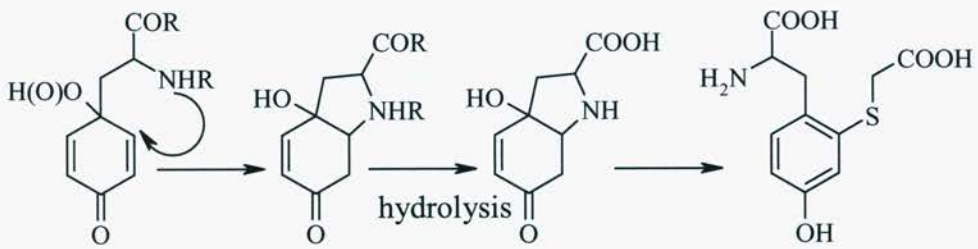

Scheme 5.3: Alternative mechanism for the formation of (5.9) from $^1O_2$-oxidised Tyr residues.

5.3.2a.iv Experiments with $^1O_2$-oxidised proteins

The potential marker compound observed in the previous section was intended to be used as a marker of $^1O_2$-mediated protein oxidation. Therefore the methodology developed above was used to analyse $^1O_2$-oxidised proteins.

BSA (75 μM), ribonuclease A (RNase A, 73 μM) and insulin (porcine, 175 μM) were photo-oxidised with visible light (λ > 345 nm) in the presence of RB (10 μM) at 4 °C for 60 min and 240 min and subsequently hydrolysed in the presence of 2-mercaptoacetic acid and analysed by HPLC.

The area of the Tyr peak was observed to decrease over the photolysis time period, and the formation of a peak at a similar RT (26.5 min) to that previously observed for the putative marker compound was observed in all cases. This peak increased with photolysis time, but was generally of low intensity. In addition to this material peaks with identical RT to authentic di-Tyr were also observed in the non-oxidised controls for each protein, this presumably arises during the initial commercial isolation process. In the case of RNase A, a slight increase in di-Tyr was observed over the photolysis timecourse.

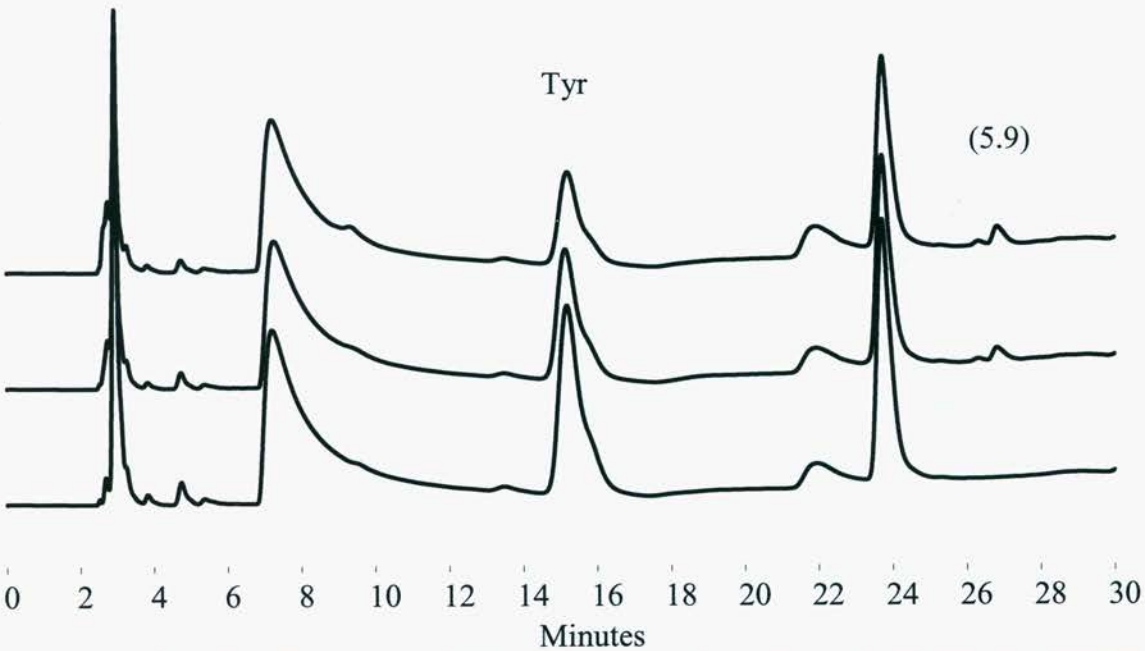

Figure 5.12: HPLC analysis of RB photo-oxidised and hydrolysed insulin. Insulin (175 μM) was RB photo-oxidised as described in Figure 5.4 for 0 min (bottom), 60 min and 240 min (top), prior to lyophilization and hydrolysis as described in Figure 5.4.

These results demonstrated that the putative marker compound was formed, and could be detected, on $^1O_2$-oxidised proteins, however the peaks were of very low intensity and thus may not be suitable for the analysis of $^1O_2$-oxidised proteins in more complicated analyses, such as tissue samples. The enhancement of sensitivity of this method is discussed in Section 5.3.3.

5.3.2b Conclusions

The gas phase, acid-catalysed hydrolysis of Tyr, Tyr-containing peptides and Tyr-containing proteins in the presence of 2-mercaptoacetic acid was found to yield (5.9). This product could be detected by HPLC with detection at 210 nm, and was observed with a variety of RB photo-oxidised Tyr-containing peptides and proteins. In no case was (5.9) detected in control experiments on non-oxidised substrates. This material was isolated using repetitive HPLC fractionation and characterised by ESI-MS and NMR.

(5.9) could be observed on $^1O_2$-oxidised proteins, however the intensity of this peak was quite small and it was expected that the system used for detecting this potential $^1O_2$-oxidation marker in the preceding experiments would not be suitable for the analysis of more complicated biological samples where there would be many more materials present which absorb in the UV region. Further experiments were performed, as described in the next section, which aimed to develop more sensitive methodology for the detection of (5.9).

5.3.3 Enhanced Sensitivity for the Detection of $^1O_2$-Mediated Tyr Oxidation Products and its Use in Biological Samples

The results presented in Section 5.3.3a.ii, demonstrated that (5.9) was generated, and could be detected, on hydrolysis of $^1O_2$-oxidised proteins. However the sensitivity of the detection method used was very low. Thus, the aim of the following series of experiments was to develop a more sensitive method of detecting the products of $^1O_2$-mediated protein oxidation.

5.3.3a Results

Fluorescent tagging and electrochemical detection were the two methods of enhancing sensitivity of the assay investigated, as these methods are generally both more selective and sensitive for suitable analytes.

5.3.3a.i Investigations of fluorescent tagging with OPA

Conversions of amino acids into species with high extinction coefficients at longer wavelengths or fluorescent derivatives are common methods of carrying out amino acid analysis. Early experiments used reagents such as ninhydrin, which reacts with most amino acids to yield a blue coloured product. More recently fluorescent compounds have been used to assist in the detection of amino acids, including 9-fluorenylmethyl chloroformate (FMOC) and ophthaldialdehyde (OPA). These compounds have been used previously for the detection of amino acid oxidation products including 3-hydroxylysine [167] and valine and leucine alcohols respectively [252].

OPA tagging was attempted initially, as similar procedures were well established in the laboratory and the derivatisation reaction could be carried out automatically using the Shimadzu SIL-10 VP auto-injector. It was expected that OPA would derivatise (5.9) as this agent reacts with the free amino group of amino acids, and it was shown previously that this group is intact in (5.9).

The HPLC conditions used for this analysis were similar to those published previously by Fu *et al.* [190]. The mobile phases consisted of methanol, tetrahydrofuran and 20 mM sodium acetate in 20:2.5:77.5 ratio for mobile phase A, and 80:2.5:17.5 for mobile phase B. The column (Supelco C18 150 x 4.6 mm, 5 μm particle size) was eluted at a rate of 1 mL min^{-1} using a gradient elution program, which consisted of 0 % B for the first 2 min, followed by a linear increase to 30 % B over the next 18 min, an increase to 60 % B over the next 10 min, a further increase to 100 % B over 5 min, isocratic at 100 % B for the next 5 min, followed by re-equilibration at 0 % B for 5 min..

The use of OPA to derivatise (5.9) was initially investigated by reacting a sample of (5.9), collected from previous experiments, with OPA (using the auto-injector) and analysing the products by HPLC. This resulted in the detection of a peak with RT of 5.5 min. Chromatograms of a non-fractionated, but hydrolysed, RB photolysis reaction mixture (*N*-acetyl Tyr was used in this case) derivatised with OPA exhibited two major peaks, with RT 5.5 min and 16.5 min (Figure 5.13). The former is identical to the RT observed for the purified (5.9) peak, the latter is identical to that observed for OPA derivatised Tyr.

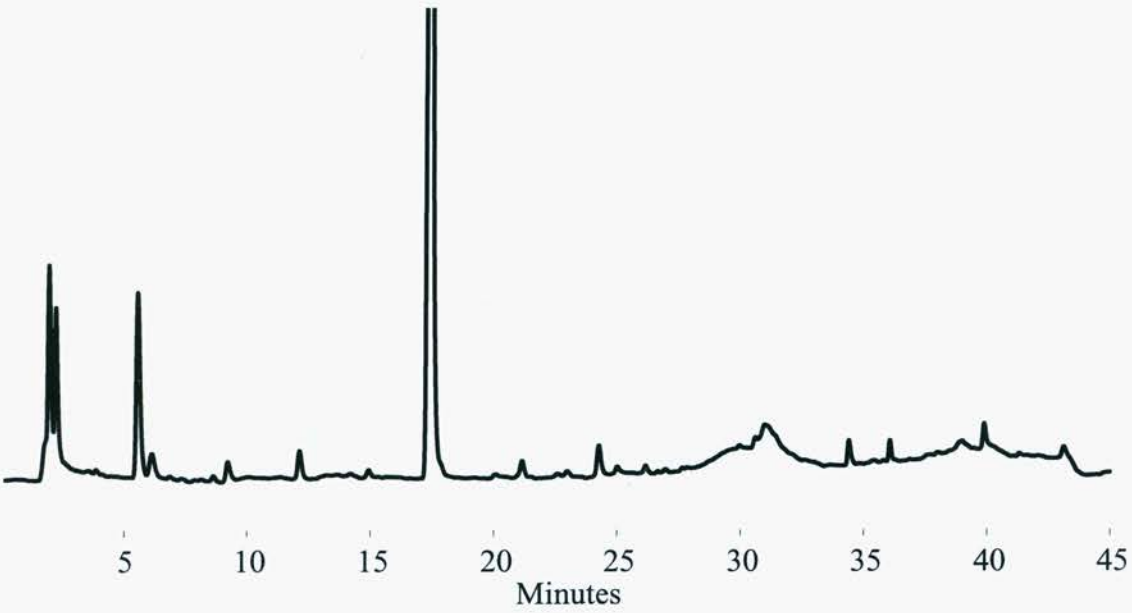

Figure 5.13: HPLC analysis of OPA derivatised, RB photo-oxidised, hydrolysed *N*-acetyl Tyr. HPLC was performed using a Supelco C18 column, which was eluted at a flow rate of 1 mL min^{-1} with methanol, tetrahydrofuran and 20 mM sodium acetate in 20:2.5:77.5 ratio for mobile phase A, and 80:2.5:17.5 for mobile phase B. The gradient program used is described in the text. The peak at 16.5 min is due to Tyr and the peak at 5.5 min is due to (5.9). Peaks were identified using fluorescence detection (λ_{ex} 340 nm, λ_{em} 440 nm).

The analysis of a mixture of the purified sample and a commercially available amino acid mixture showed that the new product eluted close to Ser which eluted at 6 min.

These results were extended by analysing RB photo-oxidised insulin using both the previous UV detection method and the OPA derivatisation method. The respective new peaks could be observed in both analyses (Figure 5.14).

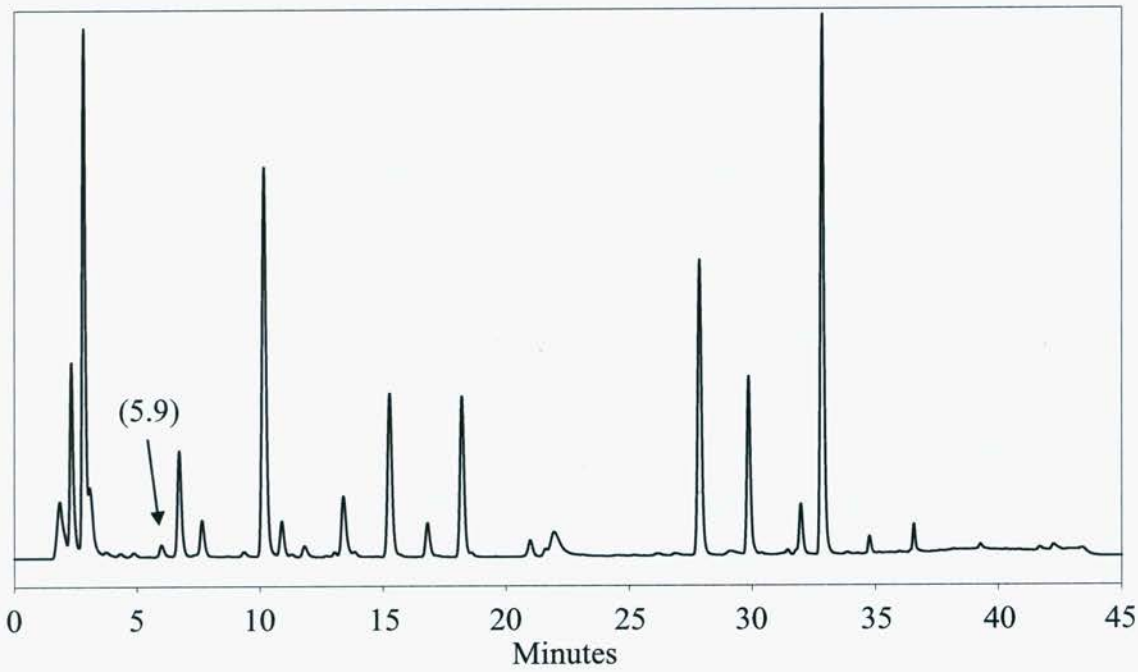

Figure 5.14: HPLC analysis of RB photo-oxidised, hydrolysed, OPA derivatised insulin. Insulin was photo-oxidised and hydrolysed as in Figure 5.12 and OPA HPLC was performed as in Figure 5.13

Despite numerous attempts to obtain clean separation of the OPA-derivatised sample of (5.9) from the various parent amino acids present in the standard sample this was never achieved satisfactorily. This was likely to be particularly problematic with the high ratio of parent to marker that is likely to be found in biological samples, hence other methods of detecting (5.9) were explored.

5.3.3a.ii Investigations of fluorescent tagging with 2-naphthalenethiol

Section 5.3.3 demonstrated that the $^1O_2$-mediated oxidation products of Tyr react with thiol nucleophiles. Thus it was speculated that these oxidation products might react with other thiols and thereby allow a fluorescent tag to be introduced into the product. Previously 2-naphthalenethiol was used by Hara *et al.*,[253] to form fluorescent derivatives of busulfan, an alkylating agent used in the treatment of some leukaemias.

2-naphthalenethiol was used in the hydrolysis reaction in place of 2-mercaptoacetic acid, by adding a solution of 2-napthalenethiol in acetone to the reaction chambers (167 mM final concentration). This resulted in the formation of a

white precipitate, but as the temperature increased this precipitate disappeared. The melting point of 2-naphthalene thiol is 80 °C (Sigma Catalogue) and thus it is expected to be a liquid during the 110 °C incubation.

Unfortunately, no peaks, apart from the peak corresponding to unoxidised Tyr, were observed on HPLC analysis of RB photo-oxidised Tyr hydrolysed using 2-naphthalenethiol (Figure 5.15). This may be due to the lack of volatility of this thiol, meaning that it cannot access the samples (which are contained within the smaller amber vials) during the gas phase hydrolysis procedure. Few thiol containing derivatives are commercially available and so the chance of finding one with higher volatility was slim. Due to this unsuccessful result, and lack of commercially available alternatives, this avenue was not investigated further and attention was switched to the potential detection of (5.9) by electrochemical methods.

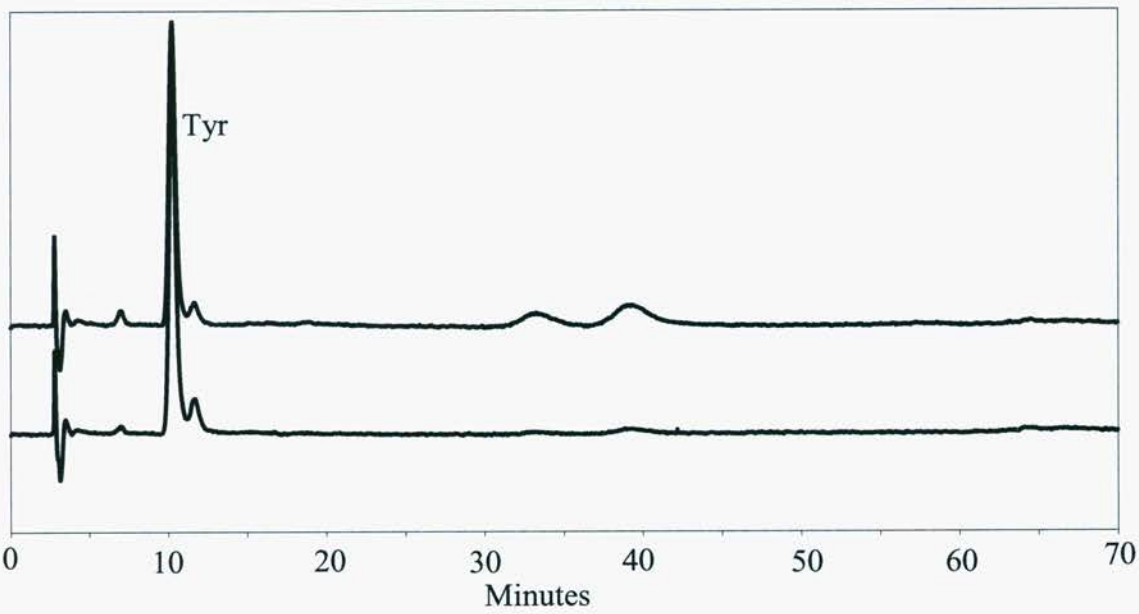

Figure 5.15: HPLC analysis of RB photo-oxidised Tyr hydrolysed in the presence of 2-naphthalenethiol. RB photo-oxidation of Tyr was performed as described in Figure 5.1. Acid catalysed gas phase hydrolysis was performed as described in figure 5.4, except for the addition of 2-naphthalenethiol (167 μM) in place of the 2-mercaptoacetic acid used previously (top), or with no thiol added (bottom). HPLC was performed using the same stationary and mobile phases as described in figure 5.4, however, the eluent was monitored by fluorescence (λ_{ex} 255 nm, λ_{em} 370 nm).

5.3.3a.iii Investigation of electrochemical detection of Tyr oxidation products

Phenolic compounds are generally easily oxidised due to the presence of the electron rich aromatic ring. This property has been utilised in the HPLC detection of Tyr and oxidation products of Tyr (e.g. DOPA, 3-chloro- and 3-nitro-Tyr) derived from HO•, HOCl and nitrating agents [254, 255]. As sulfur-containing compounds are also generally very readily oxidised it was envisaged that electrochemical detection would be suitable for the analysis of the thioacetate derivative of Tyr (5.9) observed above.

Initial experiments were carried out using a purified sample (from HPLC fraction collection) and a 12-channel electrochemical diode array detector to determine what electrochemical potential might be required to oxidised this material. Chromatograms obtained when the potentials were set between + 50 and + 480 mV did not exhibit any peaks. However the 550, 620 and 690 mV chromatogram channels showed increasing amounts of a peak that eluted at 39 min. This RT was different to that previously observed for this compound due to the use of a different mobile and stationary phase combination, which was routinely employed on the electrochemical array instrument. Chromatograms obtained at higher voltages did not contain any peaks, suggesting that the compound was completely oxidised by the 690 mV cell (Figure 5.16).

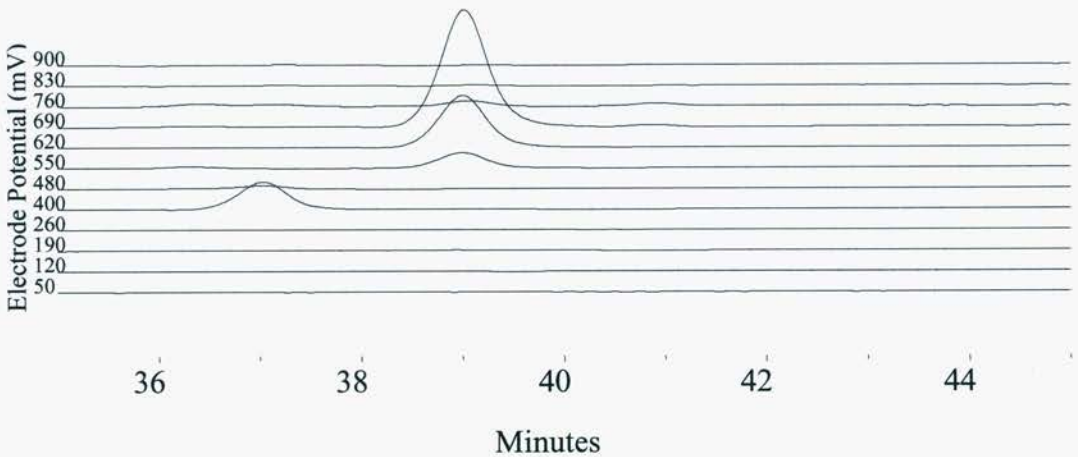

Figure 5.16: HPLC analysis of purified (5.9) with electrochemical array detection. HPLC was performed using a Zorbax ODS column (250 x 4.6 mm, 5 μm pore size) eluted at a rate of 1 mL min^{-1} with a mobile phase consisting of 50 mM phosphoric acid, 2 % acetonitrile, at pH 2.

This knowledge of the electrochemical properties of (5.9) allowed the configuration of a less sophisticated dual channel electrochemical detector (ESA inc., CouloChem II model), which was to be used for routine analysis of (5.9). Subsequent analyses of (5.9) were performed using this dual channel electrochemical detector, with the electrode potentials set to +400 mV and +760 mV, in series with the standard UV detector. These potentials were chosen so to allow the detection of DOPA (+ 400 mV) and (5.9), which was completely oxidised by this potential (see above). This dual channel system allows the detection of markers of both radical- (e.g. DOPA) and $^1O_2$-mediated (i.e. (5.9)) Tyr oxidation simultaneously.

In order to establish the operating parameters for the electrochemical detection system, preliminary experiments were conducted at a qualitative level only, attempts at quantitative analysis are described below.

The same mobile phases and time program as that used for the analysis of (5.9), with UV detection only, was used initially. Using this detection system the RT of Tyr was 10 min and that of (5.9) was 27.5 min. However, the use of the gradient led to significant drifting of the electrochemical detector's baseline, which was especially noticeable with lower concentrations of (5.9) and as it is expected that the concentrations of this material formed on biological samples would be low, this drifting was undesirable.

Thus, it was decided to attempt an isocratic elution method. The mobile phase was designed to make use of the advantageous aspects of the previous results, thus 100 mM sodium perchlorate in 10 mM phosphate buffer, 1 % methanol at pH 2 was used. The RT of DOPA, Tyr, and (5.9) under these conditions were 8, 13, and 51 min respectively (Figure 5.17). Using these conditions it was found that the detection limit of (5.9) was approximately 0.1 nmol, compared to the UV detection (210 nm), which had a sensitivity limit of approximately 1 nmol.

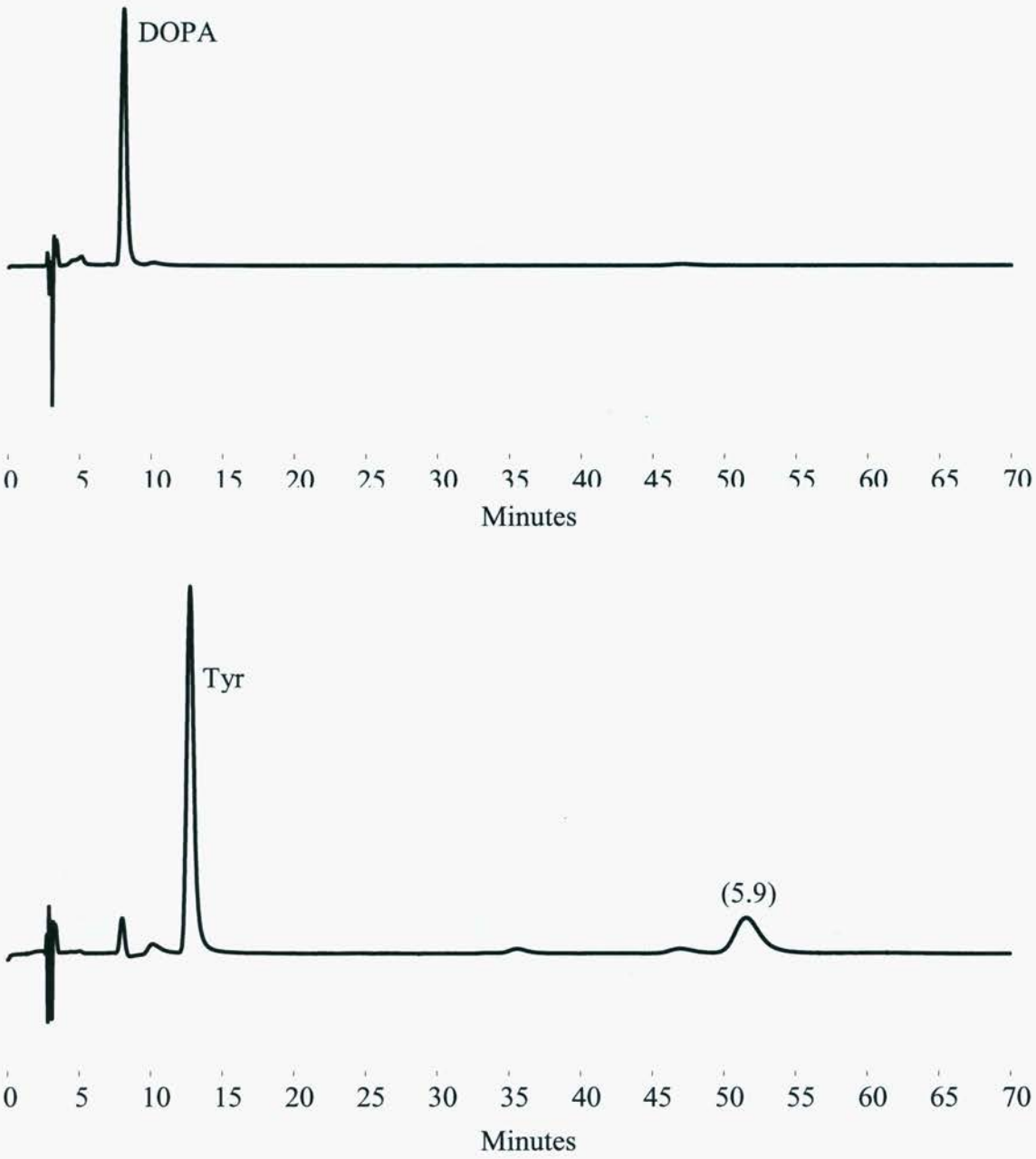

Figure 5.17: Isocratic elution (1 mL min^{-1}) of a mixture of DOPA, Tyr and (5.9). The Zorbax ODS column was used and was eluted with a mobile phase consisting of 100 mM sodium perchlorate, 10 mM phosphate buffer, and 1 % (v/v) methanol at pH 2. The eluent was monitored with a dual channel electrochemical detector with electrode potentials set at +400 mV (top) and +760 mV (bottom).

On the basis of this favourable separation of these compounds this methodology was employed in further investigations.

5.3.3a.iv Quantification of 2-amino-3-(2-carboxymethylsulfanyl-4-hydroxyphenyl)propionic acid by HPLC

The qualitative results presented in the previous section demonstrate that (5.9) has potential as a marker for $^1O_2$-mediated protein oxidation in complex biological samples. Although qualitative information can be useful, it is important to be able to quantify the extent to which particular processes are occurring. Thus, the experiments reported in this section were designed to develop methods of quantifying the formation of (5.9).

Previously the detection of the three analytes of primary interest (i.e. DOPA, Tyr and (5.9)) has been carried out with these compounds present at similar concentrations within runs. However, it is unlikely that this will be the case in tissue samples, as Tyr, being a natural amino acid, is likley to be present at a much greater concentration. This has been observed in studies of DOPA formation *in vivo*, where the results are often expressed as μmol DOPA per mole of parent Tyr or as number of oxidised amino acids per 10 000 parent amino acids. The Tyr peaks were consistently off-scale in chromatograms using electrochemical detection, and were very large when UV detection at 210 nm was employed suggesting that the integration of these peaks might not be reliable. To achieve reliable quantification of Tyr a second run of the same sample that had been diluted by a known amount could be analysed.

Standard curves for each of DOPA, Tyr and (5.9) were constructed using the three detectors (i.e. UV at 210 nm, electrochemical detector at + 400 mV, and electrochemical detector at + 760 mV) (Figure 5.18).

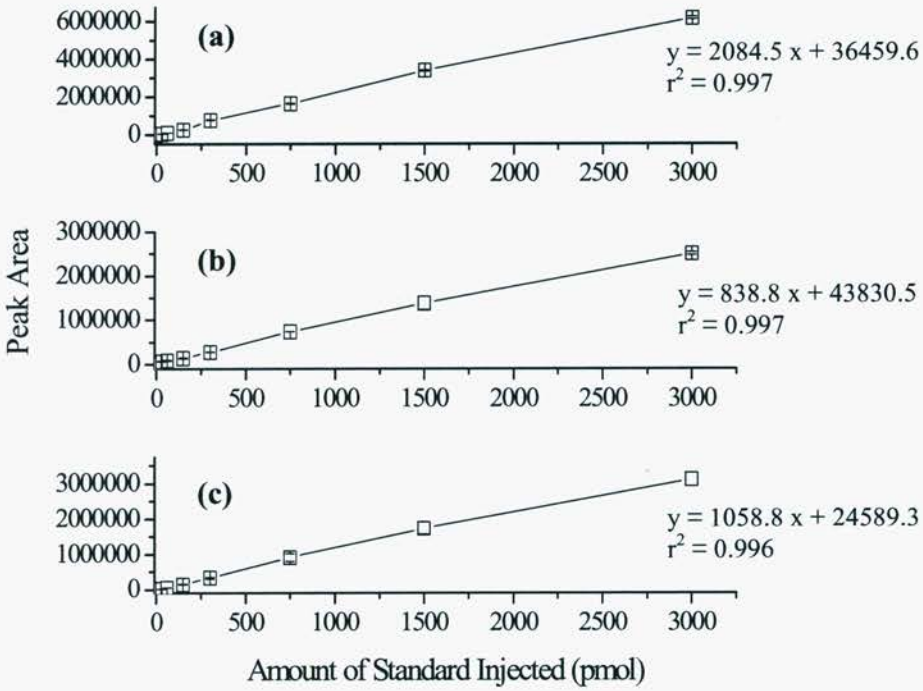

Figure 5.18: Standard curves obtained for (a) DOPA (electrochemical detection at +400 mV), (b) Tyr (electrochemical detection at +760 mV and (c) (5.9) (electrochemical detection at +760 mV). Data are represented as means ± SD (n = 2).

5.3.3b Detection of (5.9) in biological samples

5.3.3b.i Detection in photo-oxidised THP-1 cells

As (5.9) was detected on RB photo-oxidation of isolated proteins the possibility that this compound could be detected in living cells, that contained RB and had been exposed to a visible light source, was investigated.

THP-1 cells were loaded with RB (5 μM in Hank's balanced salt solution (HBSS)) for 30 min in a similar fashion to that described by Chan *et al.* [256]. After loading the extracellular RB was removed by washing in PBS, subsequently the cells were re-suspended in HBSS at a concentration of 4×10^6 cells mL^{-1} and aliquoted into 6-well tissue culture plates for photolysis, as described in Chapter 2. After photolysis using visible light ($\lambda > 345$ nm) from a 40 W tungsten filament bulb, at a distance of 5 cm, for 20 min, the proteins were extracted from the cells by TCA precipitation, resuspension in water, followed by de-lipidation with sodium deoxycholate and re-precipitation with TCA. This procedure was repeated and the resulting pellet was

washed with acetone and diethylether prior to hydrolysis. Analysis of the hydrolysate by HPLC with electrochemical detection revealed the formation of (5.9). However no such peak was observed in the (simultaneously run) chromatogram with UV detection, this is likely to be due to the enhanced sensitivity of the electrochemical detection system (Figure 5.19).

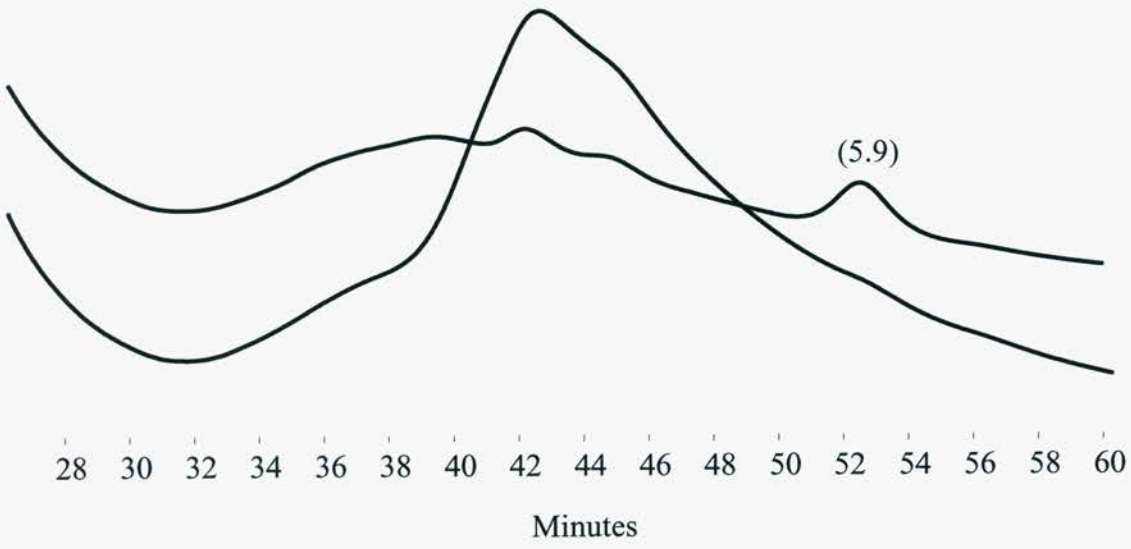

Figure 5.19: HPLC analysis, with electrochemical detection, of proteins obtained from THP-1 cells that had been subjected to intracellular $^1O_2$ generation. THP-1 cells were loaded with RB by incubation in HBSS containing RB (5 μM) at 37 °C for 30 min. Extracellular RB was removed by washing with PBS and the loaded cells were resuspended in HBSS (4 x 10^6 cells mL^{-1}). The cells were then photolysed using visible light ($\lambda > 345$ nm) from a 40 W tungsten filament bulb, at a distance of 5 cm, for 20 min. Subsequently the proteins were extracted form the cells by treatment with TCA, sodium deoxycholate and re-precipitation with TCA. This procedure was repeated and the resulting pellet was washed with acetone and diethylether. The resulting protein sample was then hydrolysed as described in Figure 5.4 and analysed by HPLC with electrochemical detection as described in Figure 5.17.

5.3.3b.ii Detection of (5.9) in human lenses

Further analyses were performed on samples of proteins human lens, which were supplied by Assoc Prof R. Truscott (University of Wollongong). These samples were total protein isolated from the cortex of non-cataractous lenses of donors aged

16, 38, 50, 67, 75 years. These samples were not artificially oxidised (e.g. by RB photo-oxidation), but were subjected to the 2-mercaptoacetic acid hydrolysis procedure. On HPLC examination of these samples a peak corresponding to the putative marker of $^1O_2$-mediated protein oxidation (5.9) was observed in all cases (Figure 5.20), suggesting that the chromatography conditions were well suited to the analysis of complex biological samples and that $^1O_2$-protein oxidation is occurring in the eye lens and can be detected in non-cataractous lenses.

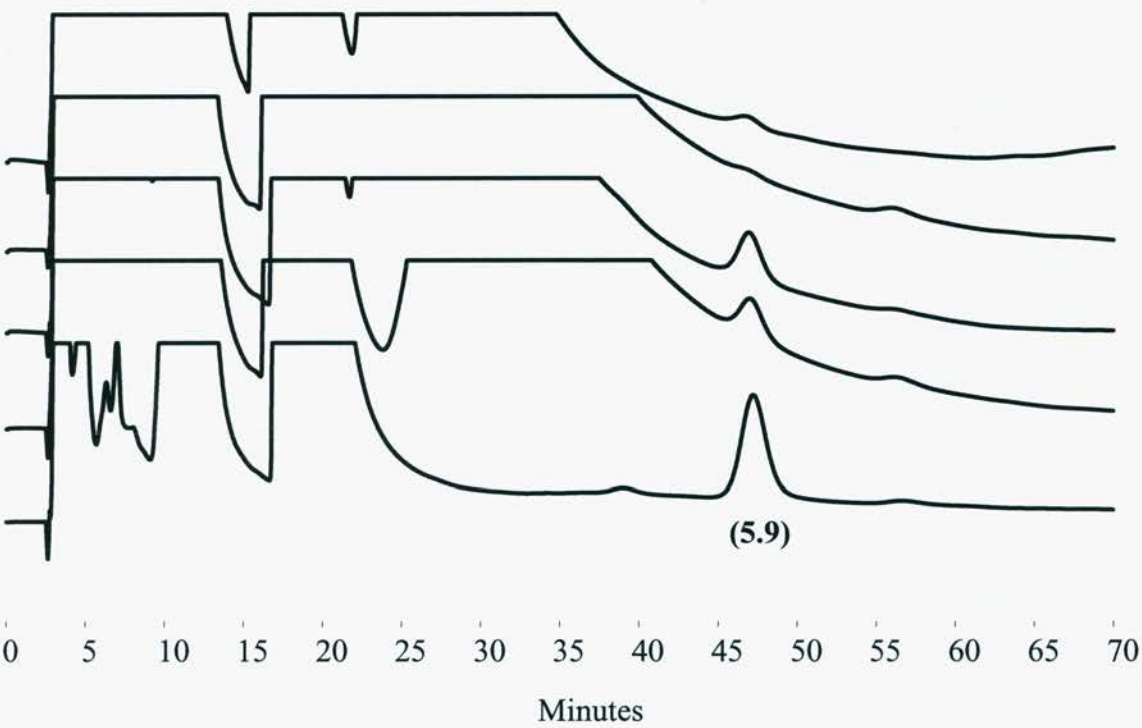

Figure 5.20: HPLC analysis of proteins obtained from the cortex of human lenses. The analyses were performed as described in Figure 5.17. Donors were aged 16 (bottom chromatogram), 38, 50, 67, 75 (top chromatogram) years.

The peak area of (5.9) appears to decrease as the age of the donor increases (Figure 5.20). Further investigation of this was attempted using quantitative analysis of (5.9) in these samples, by integration of the (5.9) peak and comparison to the standard curves obtained previously. Unfortunately due to various restrictions of sample availability and time, reliable, and sensible, results were not obtained. The improvement of the quantification aspects of the (5.9) assay is an obvious avenue for

further research as discussed in Chapter 8.

The results obtained in this section indicate that the previously identified compound (5.9) is electrochemically active, and that this property can be used for its detection after HPLC separation. Further it was demonstrated that the developed methodology could be useful for the detection of this compound on hydrolysis of complex biological samples, and hence $^1O_2$-mediated protein damage in such samples.

5.3.3c Conclusions

It has been shown that (5.9) is a potential marker for the $^1O_2$-mediated oxidation of proteins. This product was observed on isolated proteins that had been oxidised by $^1O_2$ by monitoring the UV absorbance of the HPLC eluent. However, the peaks observed were quite small and it is likely that only low levels of this product would be observed in biological samples. Thus a method that offered enhanced sensitivity of detection for this product was required.

Initial attempts used fluorescent derivatisation with OPA, an agent that is frequently used for the analysis of amino acids. Purified samples of (5.9), which had been previously isolated by HPLC, were used and could be detected by OPA. However, the RT of the OPA- (5.9) adduct was very similar to that of Ser and despite variation in the chromatography conditions, this was not possible to resolve satisfactorily.

Previous sections have demonstrated that thiols such as 2-mercaptoacetic acid and 3-mercaptopropionic acid will derivatise $^1O_2$-oxidised Tyr. It was thought that it might be possible to derivatise these intermediates during the hydrolysis procedure using a fluorescent thiol compound. 2-naphthalenethiol is a known fluorescent compound that has previously been used for the derivatisation of other substances prior to HPLC detection. Thus it was decided to investigate its utility for the derivatisation of the intermediates of Tyr oxidation by $^1O_2$. However this was not successful, probably because of the lack of volatility of this compound.

Electrochemical detection can also be a selective and sensitive method for the detection of some aromatic compounds. The potential marker (5.9) was found to be electrochemically active, using HPLC and an electrochemical array detector. This illustrated that (5.9) was completely oxidised by a potential of + 690 mV. It was then possible to configure a more conventional dual channel electrochemical detector to analyse for (5.9) and DOPA, when the potentials across the electrodes were set at +

760 mV and + 400 mV respectively. After optimising the chromatography conditions this method was found suitable for the detection of (5.9), with an approximate detection limit of 0.1 nmol. Under these conditions UV detection (210 nm) had a sensitivity limit for detection of (5.9) of approximately 1 nmol.

Using the method for detection of (5.9) developed it was possible to identify this product in proteins isolated from RB photo-oxidised THP-1 cells and normal human lenses.

Unfortunately these promising results could not be developed further due to lack of time and availability of samples.

5.4 CONCLUSIONS

The products of $^1O_2$-mediated Tyr oxidation were previously found to contain α,β-unsaturated moieties. Thus it was expected that these compounds would be susceptible to nucleophilic attack. The effect of incubation of peroxides with Lys and AHA on Tyr-derived peroxide decay was studied as an indirect measure of this reaction. It was observed (Chapter 3 and 4) that peroxide decay was more rapid when the peroxides were generated on Tyr, compared to Tyr models that lacked the (free) amino group. This was interpreted to mean that the ring-closed peroxide (analogous to (5.3)) formed on free Tyr is less stable than the non-cyclised form (5.2) due to reduced electron density in the peroxide bond. Thus the formation of any bond at the ring C(2) position is likely to lead to reduced stability of the peroxides. This is what was observed to occur when Tyr peroxides were incubated with Lys or AHA, suggesting that an intermolecular reaction between oxidised Tyr and Lys is occurring. AHA was found to be as effective as Lys in decreasing peroxide stability, suggesting that the α-amino group of Lys was not necessary for the reaction, further suggesting that similar reactions might occur with Lys residues in intact proteins. The reaction of proteins with Tyr-derived peroxides was investigated using the Lys-rich protein histone H1 and a model protein, BSA. Reaction of both of these proteins with Tyr-derived proteins led to enhanced decay of peroxides. Experiments using ^{14}C-labelled Tyr peroxides demonstrated that radiolabel became associated with the protein, suggesting that Tyr was covalently bound to the protein by similar Michael reactions.

Nucleophilic addition to the ring C(2) position was also observed with thiol nucleophiles. The reaction of 2-mercaptoacetic acid with intermediates of $^1O_2$-mediated Tyr oxidation yielded 2-amino-3-(2-carboxymethylsulfanyl-4-

hydroxyphenyl)propionic acid (5.9) as evidenced by ESI-MS and NMR analysis.

The detection of this substance using HPLC and electrochemical detection was developed into an assay for the detection of $^1O_2$-modified Tyr residues within protein. This methodology was used to demonstrate the presence of material likely to be formed as a result of $^1O_2$-mediated oxidation in the cortex of the human lens. The levels of (5.9) detected in these samples appeared to have an inverse relationship to the age of the donor, although reliable quantification was not achieved. This may suggest that the product derivatised to yield (5.9) is not stable for extended time periods *in vivo*, or it may reflect competition with other processes e.g., catabolism of proteins, further oxidation or the crosslinking process mediated by the attack of amine nucleophiles on the electrophilic carbons of Tyr oxidation intermediates. Crosslinked proteins have previously been observed in photo-oxidised lens proteins, supporting this hypothesis [123, 124, 249, 250].

CHAPTER 6 - INTRACELLULAR $^1O_2$ GENERATION AND THE FORMATION OF PROTEIN-DERIVED PEROXIDES

6.1 INTRODUCTION

$^1O_2$ production is likely to occur *in vivo* and it is believed to be an important oxidant generated by the reaction of hypochlorous acid and H_2O_2, which are produced by activated cells of the immune system [99, 257]. $^1O_2$ is known to be a potent bactericidal and virucidal agent [103, 104, 106, 108, 109, 258], with some studies suggesting that it may be the key oxidant produced in the oxidative burst phase of the immune response [100, 101, 103, 104, 106].

Proteins are known to have high rate constants for reaction with $^1O_2$. This fact, coupled with the high intracellular abundance of proteins, suggests that they are major targets for $^1O_2$-induced oxidation. However, $^1O_2$ also oxidises a number of other biological molecules, as discussed in Chapter 1.

The oxidation of DNA, lipids and cholesterol, by $^1O_2$, are all known to yield peroxide species. DNA is oxidised by $^1O_2$ primarily *via* reaction with the guanine base [59]. The oxidation of isolated DNA is well documented and the initial endoperoxidic intermediates of guanosine have been characterised [63, 64]. Recently proof that intracellularly generated $^1O_2$ oxidises specifically guanine bases in cellular DNA was obtained by Ravanat *et al.*,[259] although the efficiency of this process was found to be low. The biological consequences of $^1O_2$-mediated DNA oxidation include, loss of transformation efficiency, partial inhibition of DNA replication, G-T transversions, sister chromatid exchanges and DNA stand breakages [260, 261].

Unsaturated lipids, including phospholipids and cholesterol, are also targets for $^1O_2$-mediated oxidation. These substrates are generally oxidised by $^1O_2$ via the ene reaction, yielding hydroperoxides [69, 155, 262]. Lipid and cholesterol hydroperoxides have cytotoxic properties [155, 262]. This cytotoxicity may be due to the disruption of membrane structure, and thus function. Alternatively these peroxide species may undergo reduction to give radicals, which in turn can trigger further oxidative events [155, 262]. The oxidation of cholesterol by $^1O_2$ yields a specific product, the 5α-hydroperoxide, and has been used as a mechanistic reporter in isolated and cellular systems [36, 69].

$^1O_2$ also has effects on cellular signalling pathways. A recent review by Ryter and Tyrell [136] lists thirteen genes and eight signal transduction intermediates whose activity is known to be affected by $^1O_2$. The biological significance of such regulation is not yet clear in all cases, but one important consequence of $^1O_2$-mediated gene

regulation is the induction of apoptosis [147, 256, 263]. Recently the destruction of bcl-2, an important anti-apoptotic protein, but not bax, an important pro-apoptotic protein, upon intracellular $^1O_2$ generation has been observed [147, 263]. This changes the balance of pro- and anti-apoptotic factors and may ultimately lead to apoptotic cell death.

Thus $^1O_2$ has a number of biological roles, although those mediated by reactions with proteins are not well characterised, at a functional or mechanistic level.

Previous chapters have demonstrated that the $^1O_2$-mediated oxidation of free Tyr and Tyr residues in peptides, results in the formation of peroxide species. Proteins were also oxidised by $^1O_2$ to yield protein-bound peroxide species and evidence that Tyr residues are important targets in such oxidation was presented.

The studies in this chapter were performed to further investigate the formation of similar protein-derived peroxides, and the radicals produced from them, upon intracellular $^1O_2$ production, and to study that fate of these peroxides after $^1O_2$ production has ceased.

6.2 INTRACELLULAR OXIDANT GENERATION AND PROTEIN PEROXIDE FORMATION

Exposure of cells to UV light is known to have deleterious consequences for the cell. The UVB component (λ 280-320 nm) is directly absorbed by DNA and protein leading to DNA photodamage and mutagenesis. However, UVA (λ 320-400 nm) is weakly absorbed by most biological molecules but can generate oxidative species by interaction with intracellular chromophores [145]. Both radical and non-radical species are produced by exposure of cells to UVA, although there is persuasive evidence suggesting that the biological effects of UVA are mainly mediated by $^1O_2$ [140, 141, 144, 145, 264-267].

As described above there is direct evidence for the formation of peroxide species on intracellular $^1O_2$-mediated oxidation of cholesterol and other lipids, as well as on DNA. The rate constants for reaction of these molecules with $^1O_2$ are generally lower than that of $^1O_2$-mediated protein oxidation. In combination with the high levels of proteins found in cells, it is expected that protein-derived peroxide species should be formed as a result of intracellular $^1O_2$ generation. However, this has not been previously studied.

Gieseg *et al.*, [180] have observed protein peroxide formation previously in U937 cells (5 x 10^6 cells mL^{-1}) exposed to the peroxyl radical generator 2,2'-azobis(amidinopropane)dihydrochloride (AAPH). A time dependant increase in protein-derived peroxides was observed which reached approximately 1.2 μM after 22 h. The viability of these cells was not determined and so it is not possible to define whether the peroxides were formed in intact cells, or on released components after cell death. Over this time period it is likely that many peroxides had formed and decayed, but this work does provide the first direct evidence that protein-derived peroxides are formed upon intracellular oxidant generation.

The production of $^1O_2$ intracellularly for experimental purposes has been accomplished previously, generally using two different methods. Firstly thermal $^1O_2$ generating compounds, such as naphthalene endoperoxides, have been widely used [104, 105, 141]. Protein peroxide formation by this system was investigated in Chapter 4. No protein peroxides could be detected in these experiments, possibly due to the high temperature required. The second method involves photo-oxidation of an intracellular photosensitiser; a number of such exogenous sensitisers have been employed included the one used in these studies - rose bengal (RB) [141, 147, 263, 268, 269].

6.3 AIMS

The aim of the series of experiments reported here was to investigate the formation of protein-derived peroxides by $^1O_2$ derived from photo-oxidation of intracellular RB in intact cells. However, prior to this, photo-oxidation conditions that would ensure that the cells remained viable had to be established. Once such conditions had been determined, the formation of protein peroxides was examined. The generation of peroxides, and their stability, was monitored by the ferric / xylenol orange (FOX) method. Radical formation promoted by transition metal ion reduction of these peroxides was studied using electron paramagnetic resonance spectroscopy (EPR) with spin trapping.

Cellular viability was investigated using both lactate dehydrogenase (LDH) release and ethidium bromide assay. Effects on cellular viability of intracellular $^1O_2$ production, peroxide production and decay on were also investigated.

6.4 RESULTS

6.4.1 VIABILITY OF THP-1 CELLS UPON INTRACELLULAR $^1O_2$ GENERATION

$^1O_2$ is known to have cytotoxic properties, possibly due to the induction of apoptosis [144, 145, 147, 263, 270-272]. Therefore a series of experiments was performed to investigate the viability of THP-1 cells undergoing intracellular $^1O_2$ production.

To investigate changes to cellular viability upon intracellular $^1O_2$ generation, THP-1 cells, a human monocyte cell line, were loaded with RB (5 μM in Hank's balanced salt solution (HBSS)) for 30 min in a similar fashion to that described by Chan *et al.* [256]. After loading the extracellular RB was removed by washing in PBS, subsequently the cells were re-suspended in HBSS at a concentration of 4×10^6 cells mL^{-1} and aliquoted into 6-well tissue culture plates for photolysis. The light source used consisted of a 40 W tungsten filament lamp filtered through a 345 nm cut-off filter, as described in Chapter 2.

6.4.1a Results

6.4.1a.i Preliminary experiments with the LDH assay

The LDH assay is commonly employed to measure cell lysis and has been used previously for the determination of viability of human umbilical vein endothelial cells (HUVEC) that had been exposed to low levels of $^1O_2$ [104, 105].

LDH is a cytosolic enzyme that converts pyruvate to lactate using nicotinamide adenine dinucleotide (NADH) as a reducing co-factor. The assay works on the assumption that as a cell dies it will lyse, releasing its intracellular contents, including LDH, into the surrounding media. LDH activity in the media can be quantified spectrophotometrically following the loss of absorbance at 340 nm, corresponding to the loss of NADH. The proportion of intact cells can be calculated by expressing the amount of LDH released in to the media as a percentage of total LDH activity in the system, which is determined after lysing the cells with a surfactant, such as Triton X-100. When measuring cell viability in this way the total LDH activity in the system should remain approximately constant, however this was not observed in these experiments. The total LDH activity was observed to decrease in RB loaded cells that were exposed to light, in contrast to photolysed non-RB loaded

cells (Figure 6.1) indicating that LDH was directly inactivated by this treatment. Therefore this assay could not be used as a reliable measure of cell viability in these experiments.

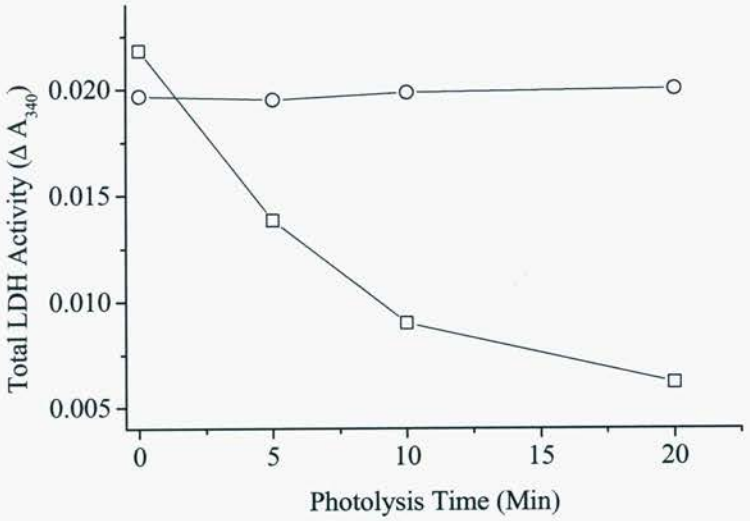

Figure 6.1: Preliminary experiments using the LDH viability assay. Cells were incubated at 37 °C in the dark with (□) and without (○) RB (5 μM) in HBSS for 30 min prior to photolysis. Extracellular RB was removed by centrifugation and washing with PBS. Cells were resuspended at a concentration of 4 x 10^6 cells mL^{-1} in HBSS and photolysed using visible light ($\lambda > 345$ nm) from a 40 W tungsten filament lamp positioned 5 cm above the 6-well plate. The cells were pelleted by centrifugation (800 g, 5 min). Cells were then lysed by treatment with Triton X-100 (0.1 %) and incubation at 4 °C on a rocking platform. 10 μL cell lysate samples were incubated with pyruvate (2.5 mM) and NADH (0.15 mg mL^{-1}). LDH activity was determined by monitoring the change in absorbance at 340 nm over 30 min. Activity was then calculated as described in Chapter 2. Data are from a single experiment with triplicate determinations at the indicated photolysis times.

6.4.1a.ii The effect of intracellular $^1O_2$ generation on cellular viability as determined by ethidium bromide assay

Due to the unsuitability of the LDH assay, an alternative viability assay was employed. Standard assays such as trypan blue exclusion were considered, but not thought likely to be suitable, as this assay relies on rather subjective judgments, which in the presence of another brightly coloured dye (i.e. RB) would be difficult to use

accurately. Thus a non-dye based assay was investigated. The assay employed uses ethidium bromide, a DNA intercalator with very high affinity for double stranded DNA, to measure the release of DNA from lysed cells. The ethidium bromide DNA complex is fluorescent, and so the DNA released in to the media can be estimated spectrofluorometrically. Similarly to the LDH assay, the proportion of intact cells can be calculated by expressing the amount of DNA released into the media to the total amount of DNA in the system after lysis with a suitable agent.

THP-1 cells were approximately 95 % viable prior to photolysis, regardless of whether they were RB loaded or not. After 20 min photolysis the cell viability was generally 90 – 95 % except for the cells that had been both RB loaded and exposed to light, which had viability of 79 ± 1% (Figure 6.2). Statistical analysis (2-way analysis of variance (ANOVA) with Tukey's post-hoc testing) of these results revealed that light alone or RB alone did not have an effect on viability, however the combination of the two produced a statistically significant difference.

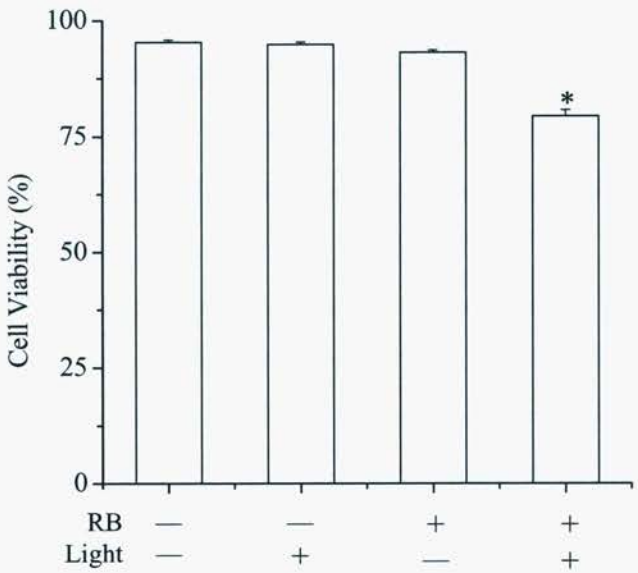

Figure 6.2: Viability of THP-1 cells after 20 min photolysis. Cells were prepared and photolysed as outlined in Figure 6.1. Viability was estimated using the ethidium bromide method as described in Chapter 2 and reference [185]. Data are expressed as means (n=8) ± SEM. (*) indicates statistically significant decrease in cell viability (2-way ANOVA with Tukey's post-hoc testing).

The role of $^1O_2$ in this change in cell viability was examined using D_2O and azide. Experiments with azide alone (i.e. performed on cells which were not RB loaded or exposed to light) were also performed to investigate the effect of this agent on cell viability, as it is known to be cytotoxic under some conditions.

Although there was not a statistically-significant difference (1-way ANOVA) in the viability of cells photolysed in D_2O compared to control (RB loaded cells photolysed in normal HBSS), there was a trend to lower viability (control 91.2 ± 0.5 %, D_2O containing HBSS 86 ± 5 %, n=2, mean ± SEM) in the D_2O photolysed cells. This was protected against with azide containing buffers (94 ± 1 %, n=2, mean ± SEM).

As it was intended to examine protein peroxide formation in cells and the effects of glucose and ascorbate in these processes, further cell viability studies were performed to investigate the potential protective effects of intracellular ascorbate. The viability of cells loaded with RB and ascorbate (as determined in Chapter 2, 10 nmol ascorbate mg cell protein^{-1}) was investigated and displayed a similar loss of viability on photolysis. After 20 min photolysis the viability of RB and ascorbate loaded cells was found to be 85 ± 1 %, which was not significantly different ($p = 0.76$, two-tailed t-test) to the viability of photolysed control cells (i.e. RB loaded only) of 85 ± 2 % (n=6, mean ± SEM).

As glucose is an important molecule for the production of energy within the cell, the effect of depleting cell growth media of glucose was also investigated. No differences (two-tailed t-test, $p = 0.29$) in viability between RB loaded cells photolysed in 5 mM glucose (87 ± 1 %, n=9, mean ± SEM) and non-glucose containing PBS was observed (84 ± 2 %, n=9, mean ± SEM).

6.4.1b Conclusions

Control experiments demonstrated that cells were tolerant of RB loading, incubation at 4 °C for short periods of time (20 min) and photolysis in the absence of RB. The latter result suggests that endogenous molecules are not acting as photosensitisers under these conditions.

Cells that had been both RB loaded and photolysed for 20 min were approximately 10-15 % less viable than the control cells. Previous work using RB to generate $^1O_2$ in human epidermal carcinoma (A431) cells, demonstrated that there was

no significant loss in viability, using a trypan blue exclusion assay [256]. Similar findings have been reported by Nakano *et al.*, who used HUVEC exposed to $^1O_2$ generated by thermal decomposition of a naphthalene endoperoxide and monitored cell death using the LDH assay [104, 105]. These differences may be due to the different cell types used, different methods used to generate $^1O_2$, the presence of different media components, the efficiency of $^1O_2$ production or different techniques for the estimation of cellular viability. These differences were not explored further.

The effect on cellular viability of the amount of $^1O_2$ produced was investigated using D_2O, which enhances the lifetime of $^1O_2$, and azide, which is a potent $^1O_2$ scavenger. The viability of cells photolysed in D_2O was decreased, however this was not significantly different from controls. Azide itself did not lead to significant cell death in accord with the short period of time the cells were exposed to azide (maximum 20 min) and previous reports, which state that cultured cells easily tolerate concentrations of 40 mM [273]. Azide concentrations of 100 mM have also been used previously with no adverse effect on cultured human fibroblast viability over 2 h [22]. The inclusion of azide inhibited the small increase in cell death seen with D_2O photolysed cells, suggesting that $^1O_2$-mediated processes may be involved in this loss of viability.

6.4.2 Formation of Protein-Derived Peroxides as a Result of Intracellular $^1O_2$ Generation

The production of $^1O_2$ by RB photo-oxidation was used successfully for the oxidation of free Tyr (Section 3.4.1), and Tyr containing peptides and proteins (Section 4.3.1). Previous workers (e.g. Chan *et al* [256]) have also used RB photo-oxidation to generate $^1O_2$ intracellularly. Therefore the photolysis of intracellular RB is likely to be a suitable method for the generation of $^1O_2$ in the following experiments.

To investigate the formation of intracellular protein-derived peroxides, THP-1 cells were loaded with RB (5 μM in Hank's balanced salt solution (HBSS)) for 30 min as described above. After loading the extracellular RB was removed by washing with PBS, subsequently the cells were re-suspended in HBSS at a concentration of 4 x 10^6 cells mL^{-1} and aliquoted into 6-well tissue culture plates for photolysis, as described in Chapter 2.

Loaded THP-1 cells were photolysed for set time periods and then the protein peroxides were quantified on trichloroacetic acid (TCA) precipitates of the cell suspension using a modified FOX assay as described by Gieseg *et al.* [180]. The nature of any peroxide species formed was further investigated by washing the TCA precipitates with methanol/hexane, as previously described by Gieseg *et al.* [180]. This procedure is commonly used to extract samples for lipid analysis and has been reported to remove > 99% of lipid components [274].

6.4.2a Results

Visible light ($\lambda > 345$ nm) photolysis of RB loaded THP-1 cells (4×10^6 cell mL^{-1}) in the presence of oxygen lead to the formation of peroxides in a time-dependant manner as determined by FOX assay of TCA cell precipitates (Figure 6.3). The TCA treatment used is a common procedure for the isolation of proteins, however to ensure that only protein peroxides were quantified using this method, the precipitates were extracted with methanol and hexane prior to FOX assay. Similar peroxide levels were observed in both TCA precipitates (7.3 ± 0.1 μM n=8) and TCA precipitates that had been extracted with methanol and hexane (7 ± 1 μM n=8), no significant difference was found between these results ($p = 0.48$, two tailed t-test) indicating that any lipids present in the pellets do not contribute to the concentration of peroxides. Subsequent experiments were performed on TCA precipitates, without methanol and hexane extraction, and the peroxides detected on these pellets are referred to as protein peroxides.

Protein peroxide formation increased in a photolysis time dependant manner over 20 min. Peroxide concentrations of ≤ 1 μM were generally observed in control experiments where either light or RB or both were absent. These results illustrate that the formation of these protein peroxides is not mediated by direct photo-oxidation of proteins or other endogenous sensitisers, nor is it mediated by a non-photolytic reactions involving RB.

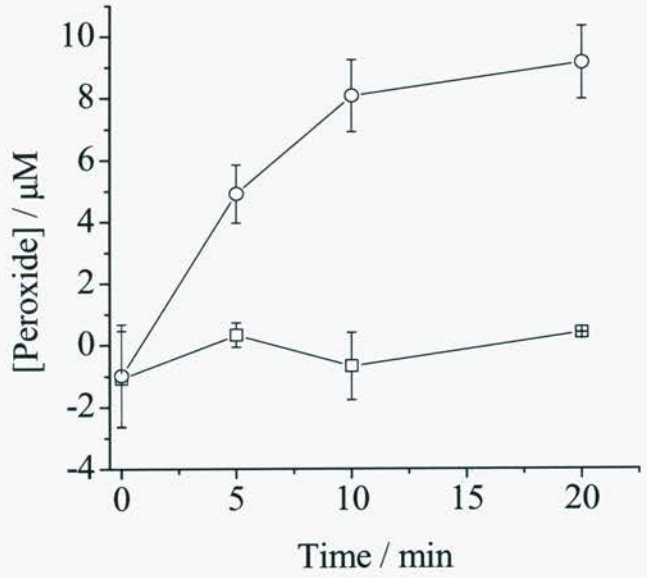

Figure 6.3: The formation of protein-derived peroxides on RB photo-oxidation of THP-1 cells. Cells were loaded with (○) and without (□) RB and otherwise prepared as outlined in Figure 6.1. After cessation of photolysis cells were precipitated with TCA, washed with TCA and then analysed for peroxides using the FOX assay with H_2O_2 standards. Data are expressed as means (n=6 from 2 separate experiments) ± SD.

As the formation of these peroxides might involve either intracellular radicals or $^1O_2$, the effect of D_2O and azide on peroxide yields was investigated. These agents prolong and diminish the lifetime of $^1O_2$ in solution respectively (see Chapters 3 and 4), and thus any process mediated by $^1O_2$ is likely to be exaggerated in the presence of D_2O and inhibited by azide.

The involvement of $^1O_2$ in the formation of intracellular protein peroxides was investigated using buffers that were constituted in D_2O, or contained 5 mM sodium azide. When photolysis experiments were carried out in an identical manner to that described above using these altered buffers, it was found that peroxide formation was increased with D_2O-containing buffers and was inhibited when azide was included (Figure 6.4), indicating that $^1O_2$ mediated reactions led to the formation of these peroxides.

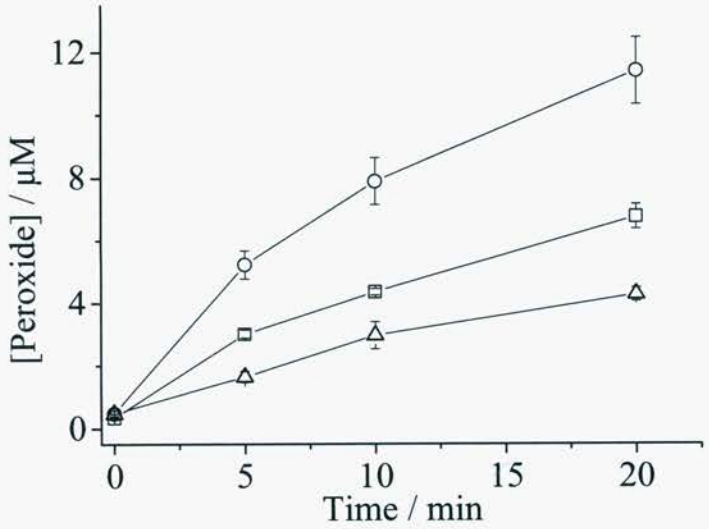

Figure 6.4: The formation of protein-derived peroxides on RB photo-oxidation of THP-1 cells in the presence of D_2O-HBSS (○), HBSS (□), or 5 mM azide (△). Cells were prepared, photolysed and peroxides quantified as in Figure 6.1. Data are presented as means (n=4) ± SD.

6.4.2a.i Effect of cellular integrity on protein peroxide formation

To investigate the ability of cellular reducing/antioxidant systems to limit protein peroxide formation, the effect of cellular integrity on protein peroxide formation was examined. These experiments were carried out in an identical fashion to the experiments described above, except that the cells were lysed (by repeated freeze/thawing cycles) prior to photolysis.

Protein peroxide formation was observed in lysates of cells that had been loaded with RB and photolysed, but not in control cells that had been photolysed but were not RB loaded. This result indicates that molecules endogenous to the cell are not acting as photosensitisers under these conditions. At short photolysis times (≤ 5 min), the yield of protein peroxides was similar between lysed and intact cells (Figure 6.5). However, after 20 min photolysis higher yields of peroxides were obtained with lysed cells suggesting that there are factors that limit the accumulation of high-yields of protein peroxides in intact cells. The similarity in the yield of protein peroxides at early timepoints suggests that the difference observed at later times may not be due to a simple loss of low-molecular weight scavengers. Rather, the difference may be attributable to the loss of functional enzymatic removal or repair systems, or the

reducing equivalents required for such systems. Evidence supporting this hypothesis has been obtained in other studies carried out within the research group, which show that $^1O_2$-derived protein peroxides can inhibit cellular enzymes such as glyceraldehyde-3-phosphate dehydrogenase (GAPDH) and glutathione reductase, both of which are important for the maintenance of reducing equivalents within the cell [175].

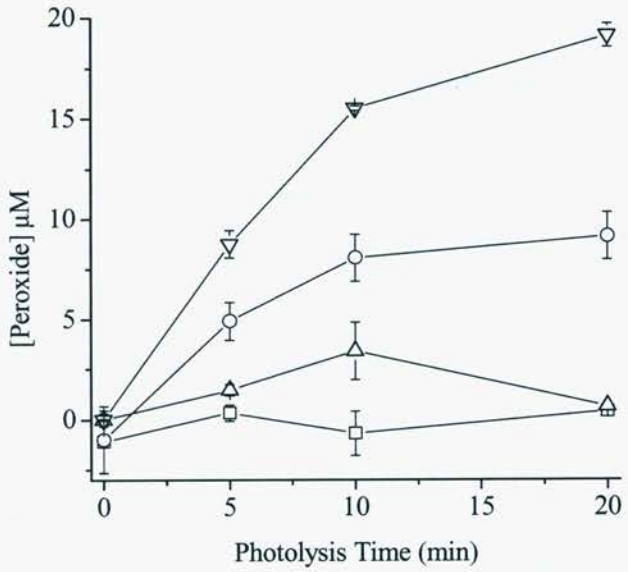

Figure 6.5: The formation of protein peroxides on photo-oxidation of intact (○,□) and lysed (△,▽) THP-1 cells (4 x10^6 cells mL^{-1}) in the presence (▽,○) and absence (△,□) of RB. Intact cells were prepared and photolysed as described in Figure 6.1. Lysed cells were prepared similarly, except that cells were lysed by 3 cycles of freeze thawing prior to photolysis. Peroxide concentrations were determined as described in Figure 6.1.

6.4.2a.ii The effect of cellular ascorbate levels on protein peroxide formation

Many cultured cell lines are known to be ascorbate deficient [275] and this substance is known to react rapidly with $^1O_2$ (k 8.3 x 10^6 M^{-1} s^{-1}) [276], thus the presence of ascorbate may effect the formation of protein peroxides. In order to investigate this possibility cells were pre-loaded with ascorbate by pre-incubation with dehydroascorbate for 30 min. This resulted in the intracellular ascorbate concentration increasing from undetectable levels (sensitivity limit approximately 1

pmol) to 10 nmol (mg cell protein)$^{-1}$ when loading was performed in the presence of RB, and to 13 nmol (mg cell protein)$^{-1}$ in the absence of RB, as measured using HPLC with electrochemical detection (Chapter 2).

When ascorbate and RB loaded cells were photolysed 7.7 ± 0.3 μM (n=9, ± SEM) protein peroxides were detected, which was not significantly different to the non-DHA loaded control (7.2 ± 0.4 μM, n=9, ± SEM) (two-tailed t-test, p=0.35).

6.4.2a.iii The effect of cellular glucose levels on protein peroxide formation

As glucose is a key energy source within cells its absence might be expected to result in a more rapid depletion of reducing equivalents, and possible enhanced build up of peroxides when cells are exposed to an oxidative stress, the effect of glucose deprivation on the formation of protein peroxides was also investigated.

Cells photolysed in glucose-containing media (PBS with the addition of 5 mM glucose) were found to contain 14 ± 3 μM protein peroxide (n=3, mean ± SEM) which was not significantly different to the control level of 13 ± 5 μM (n=3, mean ± SEM) (two-tailed t-test, p=0.95).

6.4.2b Conclusions

Photo-oxidation of RB-loaded cells led to the oxidation of proteins to form peroxidic products. The FOX assay used to quantify peroxides was performed on thoroughly washed TCA precipitates from THP-1 cells. These peroxides therefore are not due to photo-generated H_2O_2 and are assigned as protein-derived peroxide species.

In order to strengthen this assignment, TCA precipitates were extracted with methanol/hexane [180]. This procedure is widely used for extraction of lipids for analysis, and it has been reported that this method removes 99 % of lipids from treated samples [274]. No significant difference between the peroxide levels detected on extracted and non-extracted precipitates was observed suggesting that the observed peroxides are not due to oxidised lipids brought down by, or bound to, the precipitated proteins.

The formation of protein peroxides was shown to be $^1O_2$-dependant by the use of D_2O and sodium azide, which are known to enhance and inhibit $^1O_2$ lifetime in solution, respectively.

Overall, these results are similar to the observed peroxide formation on free Tyr, and on Tyr containing peptides and proteins, however this is the first finding of protein-derived peroxide species upon intracellular $^1O_2$ generation.

The levels of peroxides formed were not influenced by manipulation of either cellular ascorbate or glucose levels. This was initially somewhat surprising as ascorbate has been shown to reduce γ-irradiation-derived as well as $^1O_2$-derived protein peroxides [180, 198]. However it is known that the rate constant for the quenching of $^1O_2$ by ascorbate is similar to that reported for proteins [97, 276] and proteins are present at much higher concentration in the cell and thus it may be that the level of ascorbate enrichment achieved is insufficient to compete with quenching by proteins. Furthermore, it is known that $^1O_2$ can directly oxidise ascorbate [277]. If the entire amount of ascorbate taken up by the cells was directly oxidised by $^1O_2$, it is unlikely that an observable difference in protein peroxide concentration would be noticed due to the nmol amounts of ascorbate present, compared to the μM level of peroxides formed. An alternative explanation for the lack of effect of ascorbate is the intracellular localisation of RB. This photosensitiser is known to localise in the plasma membrane of mammalian cells, although the presence of an anionic group prevents deep penetration in to the lipid bilayer [269]. This is likely to result in the production of $^1O_2$ in close proximity to membrane associated proteins, which may make reaction with ascorbate, which will be present within the cytosol, unfavourable.

Glucose should maintain the cells reductive capacity and thus prevent oxidative damage to some extent. However, the presence or absence of glucose had no detectable effect on the formation of protein peroxides. It may be that the photolysis period is too brief for noticeable levels of depletion of the (unknown) anti-oxidant mechanisms, which may operate to protect the cells against $^1O_2$-mediated oxidation, to occur and thus the ability to regenerate these systems using glucose cannot be observed. Alternatively it is possible that these cells do not have any anti-oxidant defence systems that are effective over this time frame.

6.4.3 $^1O_2$-Derived Protein Peroxide Decay and its Effects on Cell Viability

Previously (Chapter 3 and 4) it was shown that the peroxides formed on free Tyr and on isolated proteins decay at elevated temperatures. The further reactions of these peroxides might damage other cellular components and thus have potentially deleterious consequences for the cell.

In order to examine the loss of protein peroxides within intact cells, and the effects of this process on cellular viability, THP-1 cells that were loaded with RB and photolysed for 20 min, were subsequently incubated at 37 °C for 0, 2 and 4 h and analysed for residual protein peroxide concentrations by FOX assay and cell viability by ethidium bromide. These incubations were done in the absence of light to ensure that $^1O_2$ generation had ceased and under 5 % CO_2 atmosphere to maintain pH control.

6.4.3a Results

Protein peroxides that were generated in RB loaded THP-1 cells were found to decay over a 4-hour incubation period at 37 °C (Figure 6.6). The difference was found to be significantly different to control cells at the 4-hour time point (2-way ANOVA, with Tukey's post-hoc test). Over this same time period a concomitant decrease in cell viability was observed (Figure 6.6), which was found to be significant after 2 and 4 hours (compared to control, 2-way ANOVA, Tukey's post-hoc test). This decrease in viability was only observed when the cells were treated with both RB and light, in other cases the viability remained at baseline levels (Figure 6.6), suggesting that a product of RB photo-oxidation may be responsible for the increase in cell death, as assessed using ethidium bromide binding to released DNA.

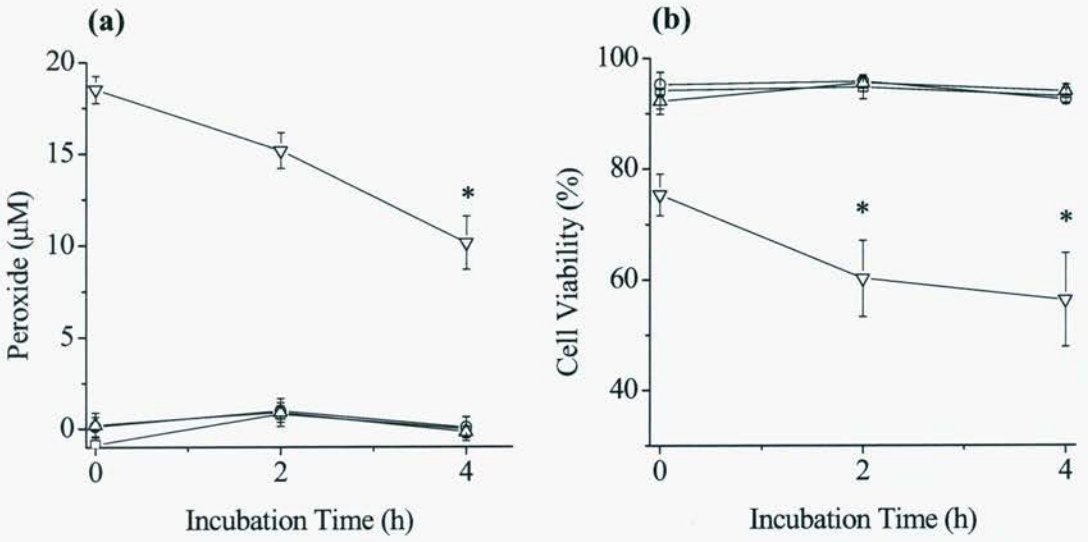

Figure 6.6: The decay of protein peroxides (a) and decrease in THP-1 cell viability (b) upon incubation at 37 °C. THP-1 cells were prepared as described in Figure 6.1. Cells were loaded with RB (▽, △) or sham loaded (□,○) and either photolysed (▽,○) or incubated in the dark at 4 °C (△,□) for 20 min. After photolysis cell suspensions were incubated at 37 °C, in the absence of light under a 5 % CO_2 atmosphere for the indicated time periods. Protein peroxide concentration was then measured using the FOX assay as described in Figure 6.3. Cellular viability was determined using the ethidium bromide release assay as described in Figure 6.5. Data are expressed as means ± SEM (n=8). * indicates statistically significant difference from control (2-way ANOVA with Tukey's post-hoc testing).

The alteration of intracellular ascorbate and glucose levels did not effect the formation of protein peroxides (Section 6.4.1) or cellular viability during the intracellular generation of $^1O_2$. It was thought that these factors might require extended time periods before their effects become noticeable. Thus the alteration of intracellular ascorbate or glucose levels over the post-photolysis incubation period was examined. No differences between control cells that were not loaded with either ascorbate or glucose (32 ± 7 % loss of peroxides and 29 ± 2 % loss of viability, mean ± SEM n=3) in the rates of peroxide decay or the levels of cell death, between ascorbate-loaded cells (24 ± 6 % loss of peroxides, 30 ± 3 % loss of viability), or cells photolysed and subsequently incubated in glucose-deficient media (39 ± 7 % loss of peroxides, 30 ± 5 % loss of viability), were observed.

6.4.3b Conclusions

The loss of cell viability observed with RB loaded, and subsequently illuminated, THP-1 cells is in accord with a previous study [256]. These researchers used intracellular RB photo-oxidation to study $^1O_2$-mediated apoptosis. Although different cell lines and cellular viability estimation techniques were used, a similar post-photolysis loss of cell viability was observed after 4 h incubation at 37 °C.

Cell viability decreased slightly during intracellular $^1O_2$ generation, and decreased further on subsequent incubation. As $^1O_2$ production will cease when the light source is removed, this suggests that the loss of cell viability observed on incubation after photolysis is due to either the products of $^1O_2$-mediated oxidation, or a chain of events initiated during the photolysis period. These two possibilities cannot be separated using the current data. One possible mechanism for decreasing cellular viability is the decay of protein peroxides, which was observed over the incubation period examined.

The thermal decay of protein peroxides, along with reduction by intracellular metal ions, may yield radical species. Similar radical species are suspected of being cytotoxic via a number of processes [2]. $^1O_2$-derived amino acid peroxides were shown to transfer damage to proteins (Section 4.3.4b) and have also been shown to cause inactivation of important cellular enzymes such as GAPDH [175]. Reactions of related peroxides, such as γ-irradiation derived amino acid and protein peroxides, are known lead to the formation of mutagenic DNA base oxidation products, and to the formation of DNA-protein crosslinks, both of which could be detrimental to the cell [193, 217].

The direct inactivation of enzymes by $^1O_2$, or the protein peroxides, is another possible mechanism for the decreased viability. This possibility was demonstrated with the direct inactivation of LDH observed in section 6.4.2a.i and in previous studies [175]. Other enzymes vital to the cells function may also be directly inactivated by $^1O_2$ [175].

Intracellular $^1O_2$ production is also known to induce apoptosis. One study [256] used an epidermal carcinoma cell line (A431), which was RB loaded and irradiated for 30 min, to study apoptosis. This study proposed a mechanism for the RB / light induced apoptosis, which involved rapid activation of the JNK pathway of apoptotic cell death. Whether apoptosis is occurring in the experiments reported in

this thesis is unknown and needs further study. Furthermore it is unclear, if this is the pathway involved, whether this is initiated during the photolysis period, or whether it is initiated after the cessation of photolysis. Recently studies have demonstrated a direct link between the $^1O_2$-mediated oxidation of an important anti-apoptotic protein, bcl-2, and cell death by apoptosis [147, 263] supporting the proposition that $^1O_2$-mediated oxidation of proteins is an important event in the onset of apoptosis.

It has been recently demonstrated that intracellular generation of $^1O_2$ (using thermal decomposition of an ^{18}O-labelled naphthalene endoperoxide) in THP-1 cells leads to the direct oxidation of DNA [259], and many other publications have suggested that intracellular $^1O_2$ production leads to the oxidation of DNA (reviewed in [59, 60, 260, 261]). Lipid oxidation is also suspected to occur upon intracellular $^1O_2$ generation with both cholesterol and membrane lipids as proposed targets [68, 156]. Thus it is possible that the oxidation of other cellular components is responsible for the loss of cellular viability observed in these experiments.

6.4.4 Quantification of Oxygen Consumption and Protein Peroxide Formation in THP-1 Cells

In order to examine the quantitative significance of protein oxidation versus other forms of oxidation the relative rates of these reactions needs to be addressed and quantified. In order to provide a first step in this direction the proportion of cellular oxygen uptake converted in to protein peroxides was investigated using RB loaded THP-1 cells. These loaded cells (4×10^6 cells mL^{-1}) were photolysed over a period of 20 min at 22°C inside the sealed sample chamber of a Clark-style oxygen electrode. The modified FOX assay was then used, as previously, to quantify peroxides in TCA precipitates of photolysed THP-1 cells. Oxygen consumption was monitored by manual recording of the electrode readings every 30 sec over the 20 min photolysis period and peroxide determinations made after 0 min, 5 min, 10 min and 20 min. It should be noted that these experiments were carried out at 22 °C, which is a considerably higher temperature than that employed in section 6.4.2 (4 °C).

6.4.4a Results

Photolysis of RB loaded THP-1 cells with visible light in the sample chamber of the oxygen electrode lead to the formation of peroxides on TCA cell precipitates in a similar manner to that observed previously. Concurrent oxygen depletion was also

observed in these cells (Figure 6.7). Photolysed, non-RB loaded cells did not give rise to significant peroxide formation and only low levels of oxygen consumption, indicating that endogenous molecules were not acting as photosensitisers under these conditions.

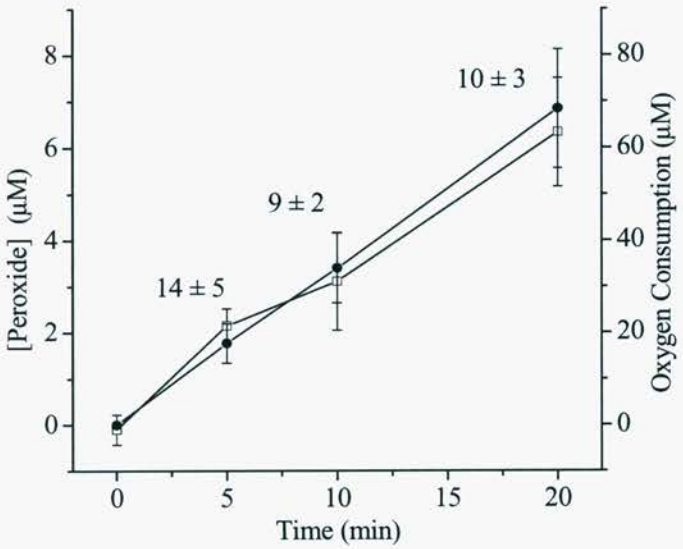

Figure 6.7: The formation of protein peroxides (□) and depletion of oxygen (●) when rose bengal loaded THP-1 are exposed to light. Cells were loaded with RB as described in Figure 6.1 and placed in a Clark-type oxygen electrode at 22°C. The suspension (4×10^6 cells mL^{-1}, 5.5 mL) was stirred slowly and allowed to equilibrate with atmospheric oxygen. The chamber was sealed when steady state readings were observed and the sample photolysed through the water-jacket of the electrode, using a 40 W tungsten filament lamp positioned 5 cm distant from the electrode. At the indicated timepoints samples were taken from the electrode for protein peroxide analysis as described in Figure 6.1. The electrode readings were converted to concentrations as described in Chapter 2. Inset values represent the percentage of oxygen converted to protein peroxide at each time point. Data are represented as means (n=3, from 3 separate experiments) ± SEM.

After 20 min photo-oxidation of RB loaded cells, 70 ± 12 μM (n = 3, ± SEM) oxygen was consumed and this resulted in the generation of 6 ± 2 μM protein peroxides (Figure 6.7). Over the entire time course of photolysis the proportion of oxygen converted through to protein peroxide was ≈ 10%, though this was slightly higher at the earliest time point examined.

6.4.4b Conclusions

Protein peroxide formation was observed, with similar photolysis time dependence, as described in section 6.4.2, despite the different experimental set up and temperature conditions. Comparison of the rates and extents of protein peroxide formation and oxygen depletion indicate that there is efficient conversion of oxygen to protein peroxides especially at early timepoints, where the proportion of oxygen converted to protein peroxides is 14 ± 5 %. The absolute levels of peroxide formation observed were slightly lower than those observed in previous experiments (Section 6.4.2), and this may be due to the photolysis being performed at higher temperatures than previously (22 °C vs. 4 °C used previously) leading to decay of peroxides prior to analysis, or a lower light flux due to absorbance or scattering of the light by the electrode casing. If the former explanation is the case then the proportion of conversion through to peroxides is likely to be underestimated in these experiments. However, the design of the oxygen electrode meant that the effects of the temperature discrepancy and potential change in light flux could not easily be distinguished.

6.4.5 Radical Formation as a Result of Metal Ion Reduction of Cellular Protein Peroxides

Previous chapters have demonstrated that peroxides derived from $^1O_2$-oxidation of proteins can be reduced by metal ions to yield radical species. These radicals were detected by EPR with spin trapping and showed similarities to the spectra obtained from free Tyr-derived peroxides. The formation of radicals after intracellular oxidation has been observed previously, for example the formation of nitrogen-centred radicals from the reduction of chloramines derived from HOCl treatment [185].

The aims of this section, therefore, are to generate peroxides on cellular proteins using RB photo-oxidation and examine the formation of radicals derived from the metal ion catalysed reduction of these peroxides, using EPR spectroscopy with spin trapping.

6.4.5a Results

In order to investigate the formation of radicals on cellular proteins it was decided to first ensure that peroxide formation and radical production could occur on isolated bulk cell proteins. Thus, initial experiments were performed with proteins isolated from THP-1 cells (non-RB loaded, 4 x 10^6 cells mL^{-1}) by TCA (5 %) precipitation and resuspended in urea (6 M). To maximise the yield of peroxides and thus the chances of observing radical formation these isolated proteins were photolysed in the presence of RB (10 μM) with the slide projector illumination system as used in Chapters 3 and 4. Photo-oxidation of these cell proteins (1.5 mg mL^{-1}) for 60 min yielded peroxides (~ 130 μM), which could be detected using the FOX assay. When these peroxides were incubated with Fe^{2+}/EDTA (176 μM) in the presence of MNP (11.8 mM), radical adducts were detected by EPR (Figure 6.8). The major EPR signals observed were assigned as two triplet of doublets assigned to two carbon-centred radicals of partial structure •CHR'R'' [a(N) 1.54 mT, a(H) 0.16 mT and a(N) 1.67 mT, a(H) 0.15 mT]; these parameters were confirmed by spectral simulation (Figure 6.8). These signals have parameters similar to the signals observed with $^1O_2$-oxidised free Tyr (Section 3.4.4c). Other signals are also present at lower relative concentrations. One of these signals is analysed in terms of a triplet of doublets [a(N) 1.52 mT, a(H) 0.38 mT] and may be due to a further carbon-centred radical with partial structure •CHR'R''. The remaining signals appear to be the spin trap decomposition product di-*tert*-butyl nitroxide [(^{t}Bu)$_2$NO•, a(N) 1.70 mT] and the reduced form of the spin trap ^{t}BuNHO• [a(N) 1.44 mT, a(H) 1.44 mT].

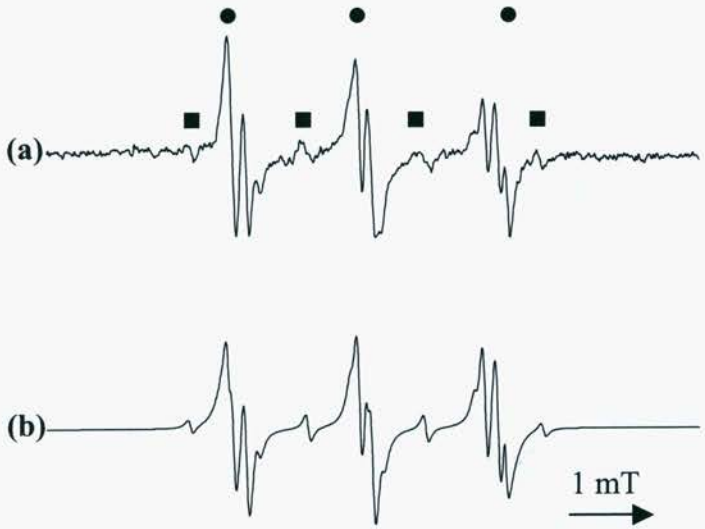

Figure 6.8: (a) EPR spectra observed on reaction of bulk cell protein-derived peroxides (~90 μM peroxide) with Fe^{2+}/EDTA (176 μM) in the presence of MNP (11.8 mM). Peroxides were generated using cell protein isolated by TCA precipitation. The precipitates were resuspended in urea (6 M) and adjusted to pH 7.4 prior to RB (10 μM) photo-oxidation at 4 °C, using the slide projector illumination system (as described in Chapter 2, 250 W bulb, $\lambda > 345$ nm). Signals marked (●) are assigned to $(^tBu)_2NO\bullet$ [a(N) 1.70 mT] and are those marked (■) are assigned to $^tBuNHO\bullet$ [a(N) 1.44 mT, a(H) 1.44 mT]. (b) Computer simulation of the spectrum in (a) using the parameters reported in the text.

Previously, the possibility that these signals arose from reactions involving H_2O_2 has been investigated using catalase treatment. This was considered unlikely to be suitable in this case as it was expected that the high concentration of urea used to redissolve the cell proteins would lead to the denaturing of this enzyme. In order to investigate this further, authentic H_2O_2 (900 μM, final concentration) was added to non-photolysed samples of cell protein and treated with Fe^{2+}/EDTA in the presence of MNP. This treatment resulted in the detection of only spin trap decomposition products, thus no signals analogous to those observed in the untreated experiments were detected. This suggests that the cell-protein signals are not mediated by reactions of H_2O_2 with Fe^{2+}/EDTA, as an increase in radical concentration and hence signal intensity would be expected if this were the case.

These results suggest that the RB photolysis of bulk cell proteins results in the formation of peroxide species that can be reduced to yield radical species, in a similar manner to the reactions observed with homogenous protein solutions (Section 4.3.4a.i).

In order to investigate the reduction of peroxides formed inside cells, similar EPR experiments were performed on RB loaded and photolysed cells.

Cells were loaded with RB then photolysed, as described above, to generate peroxides. Subsequently these cells were incubated with Fe^{2+}/EDTA in the presence of MNP. Examination of these mixtures by EPR led to the detection of spin trap artefacts only. This may be due to an inability of the iron complex to reduce the peroxides due to net charge on the Fe^{2+}/EDTA complex, which prevents it crossing cellular membranes.

To investigate whether this was the correct explanation for the above negative results, further studies were carried out where the RB loaded, photolysed cells were subjected to lysis by resuspension in water and repetitive freeze thaw cycles, before being incubated with Fe^{2+}/EDTA and MNP. In this case broad EPR signals were observed (Figure 6.9). Upon longer incubation a further signal assigned to the MNP reduction product (^{t}BuNHO•) was also observed and increased in intensity with time. The species which gives rise to the broad signal appears to be long-lived and after 60 min incubation at 22 °C little loss of signal intensity was observed. Control experiments, in which cells were RB loaded but not photolysed, exhibited small amounts of spin trap-derived artefact signals only. The broad EPR signals were not observed with cells that had been photolysed but not RB loaded, nor with cells that were neither RB loaded nor photolysed (Figure 6.9), suggesting that these radical adducts are arising as a result of RB-induced photo-oxidative damage, possibly as a result of protein peroxide decomposition. However the contribution from other photo-products such as lipid and cholesterol peroxides to these signals cannot be discounted with this data. Thus broad, anisotropic signals may be observed with radical adducts that are immobilised on other classes of biomolecules, such as DNA and polysaccharides. To investigate the hypothesis that the radicals observed in these experiments are derived from the reduction of protein-derived peroxides, pronase, a non-specific mixture of protease enzymes, was added to solutions of pre-formed radical adducts, in a similar fashion to the experiments performed with BSA in

Chapter 4 (Section 4.3.4a.ii). However, after this treatment the observed signals remained broad, possibly due to the relatively large amount of different proteins present.

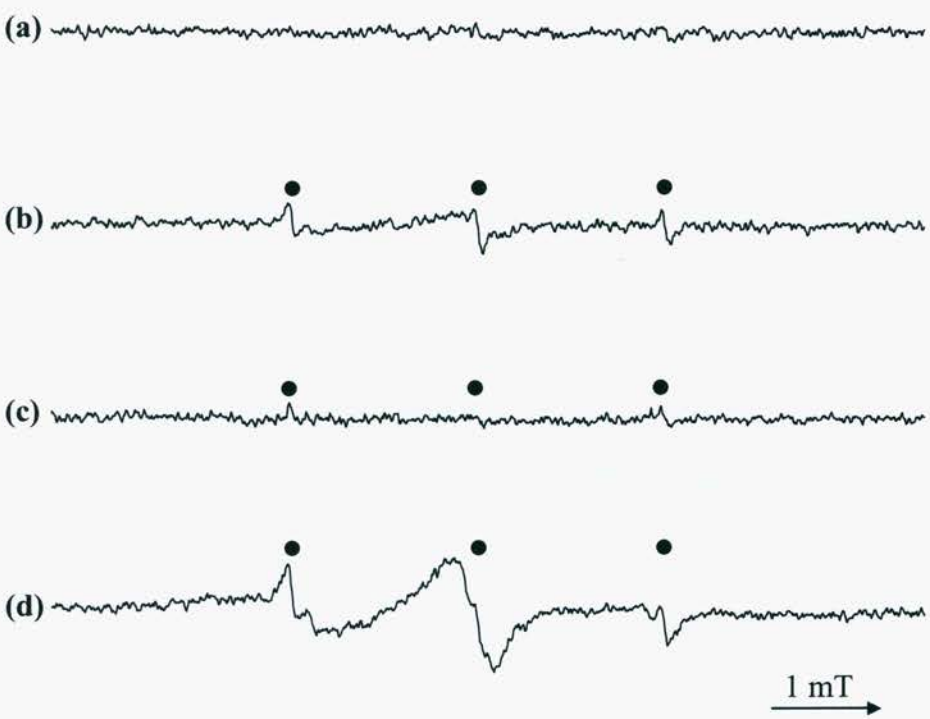

Figure 6.9: EPR spectra derived from RB photo-oxidised THP-1 cells. (a) – (c) are control experiments in which cells were (a) not loaded with RB and not photolysed, (b) RB loaded, but not photolysed, and (c) not RB loaded, photolysed. (d) shows EPR spectra derived from THP-1 cell-derived peroxides (~ 10 μM peroxide, generated using RB photo-oxidation as described in Figure 6.1). All samples were treated with catalase (12320 units mL^{-1}) and Fe^{2+}/EDTA (91 μM) in the presence of MNP (9.1 mM). Cells were concentrated to 40 x 10^6 cells / mL and lysed before treatment, by resuspension in water and freeze/thawing, to allow Fe^{2+}/EDTA access to intracellular peroxides. Signals marked (●) are assigned to $(^tBu)_2NO\cdot$ [a(N) 1.70 mT]. The remaining broad signals are assigned to protein-derived radicals.

The nature of the observed broad signals was further examined using TCA precipitation of the cell lysates, in conjunction with methanol/hexane extraction (as used in Section 6.4.2a) of the TCA pellets. This treatment is reported to remove

greater than 99 % of lipids from such precipitates [274]. It was expected that if the radicals were protein-derived, the observed spectra would be similar to those observed in the non-extracted samples.

EPR spectra observed on treatment of the TCA precipitates with Fe^{2+}/EDTA (91 μM) in the presence of MNP (9.1 mM) consisted of broad, anisotropic signals, similar to those observed with the cell lysates (Figure 6.10). When the precipitates were extracted with methanol and hexane prior to treatment with Fe2+/EDTA and MNP, remnants of the broad signal remained, however the signal was not as intense as those observed with non-extracted samples. This may be due to losses of peroxides due the extraction procedure or may indicate that the radicals are not protein-derived.

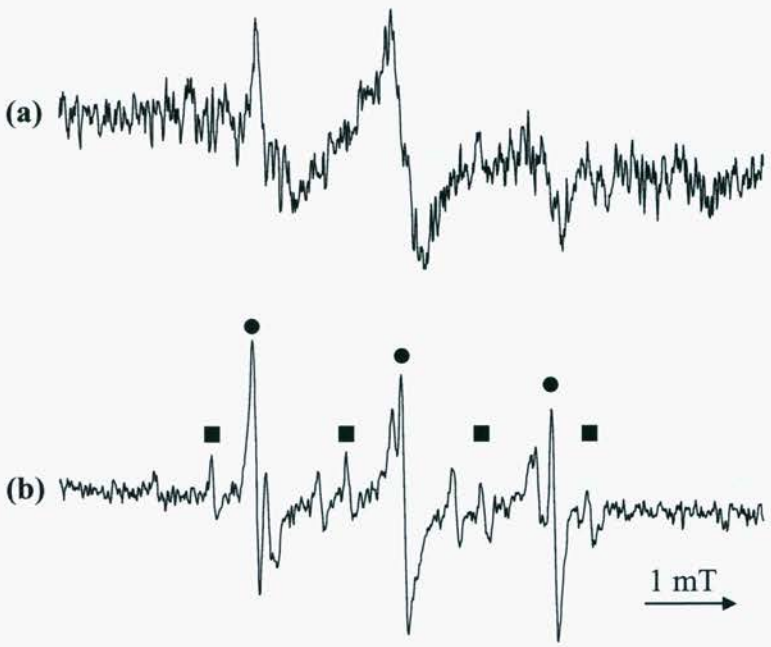

Figure 6.10: EPR spectra derived from THP-1 cell-derived peroxides (~ 10 μM peroxide). Peroxides were generated using RB photo-oxidation as described in Figure 6.1. After cessation of photolysis cells were concentrated to 40 x 10^6 cells / mL, precipitated with TCA (10 % w/v), washed with (TCA 10 % w/v) and (a) resuspended in urea (6 M) or (b) extracted with methanol / hexane and then resuspended in urea. The urea solutions were treated with Fe^{2+}/EDTA (91 μM) in the presence of MNP (9.1 mM) and analysed with EPR spectroscopy. Signals marked (●) are assigned to $(^tBu)_2NO\cdot$ [a(N) 1.70 mT] and those marked (■) are assigned to $^tBuNO\cdot$ [a(N) 1.44 mT, a(H) 1.44 mT].

Further investigation into the nature of these signal was sought by separation of the pre-formed radical adducts by gel filtration. This approach has been used successfully in previous studies to remove low molecular weight adducts from samples of protein radical adducts [278]. It was anticipated that EPR analysis of high molecular weight fractions from this separation would yield similar anisotropic signals, and that protease digestion of these fractions would lead to the observation of more resolved EPR spectra. However, no signals were observed from the high molecular weight fractions. This is likely to be due to overloading/blocking of the column by the crude lysates. This approach was not developed further, as dilution of the samples, which already contained only low peroxide levels, would be likely to result in signals which are too weak to detect by EPR.

6.4.5b Conclusions

EPR spectra characteristic of carbon-centred radical adducts were observed when Fe^{2+}/EDTA was used to reduce peroxides, derived from isolated total cell protein, in the presence of MNP. These signals were quite well resolved, which is unusual, but not unknown, for a protein-derived radical (see Section 4.3.4a.ii). This mobility, which suggests that the adducts are tumbling rapidly in solution, may be due to the fact that urea (6 M) was used to redissolve the protein after TCA precipitation. This treatment is likely to completely denature the secondary and tertiary structure of the protein and therefore result in increased motion of the backbone and side chains. The spectra observed are very similar to those observed with peroxides derived from Tyr, Tyr-containing peptides and BSA after pronase digestion (Section 3.4.4 and Section 4.3.4). Therefore this result further strengthens the hypothesis that Tyr-mediated oxidation may be a key event in $^1O_2$-mediated protein oxidation.

The lack of signals observed upon Fe^{2+}/EDTA treatment of the intact cells is probably due to the charge of this complex, which means that it cannot pass through the hydrophobic cell membrane. Therefore these experiments suggest that the site of peroxide formation is inside the cell, which is to be expected, as $^1O_2$ production is intracellular and $^1O_2$ is thought to travel very short distances in a cellular environment ($\leq$100 nm [51, 279]).

When the cells are lysed, the peroxides are more likely to be available for reaction with Fe^{2+}/EDTA. Thus, EPR signals are observed with RB loaded, photolysed and lysed cells treated with Fe^{2+}/EDTA in the presence of MNP. Cells

that were photolysed but not RB loaded gave only spin trap artefacts. The signals observed with the complete system are very broad, characteristic of a large, slowly-tumbling radical adduct, similar to that seen in experiments with BSA-derived peroxides (Section 4.3.4a.ii). These broad signals are partly overlaid by artefacts generated by decomposition of the spin trap, which increased in intensity over time. The major artefact observed in this case was the reduction product of MNP, which is a 1:2:2:1 quartet with hyperfine coupling constants of a(N) 1.44 mT, a(H) 1.44 mT. This increasing formation of reduced MNP species is likely to be due to the release of intracellular reducing species reacting directly with MNP. As these interfering signals are suspected to be due to low molecular weight species, fractionation of pre-formed lysate adducts with gel filtration chromatography was used in an attempt to remove these contaminating signals. However, this approach was not successful.

EPR spectra obtained from the TCA precipitates of cell lysates showed a broad signal similar to that observed with the lysates, suggesting that the signal may be protein-derived. However, experiments that used methanol and hexane to extract these precipitates did not convincingly demonstrate that the broad signals were protein-derived.

6.5 CONCLUSIONS

The results presented in this chapter demonstrate that photolysis of intracellular RB leads to the formation of protein-derived peroxide species. The formation of these protein peroxides was enhanced by D_2O and inhibited by azide, suggesting a $^1O_2$-dependant mechanism. Formation of protein peroxides has been previously observed in serum and mouse myeloma cells exposed to γ-irradiation [280] and a peroxyl radical generating system (AAPH) [180], however $^1O_2$-mediated protein peroxide formation has not previously been observed inside viable cells.

The absolute levels of peroxide generation detected in these experiments are much greater than those detected in other cell types exposed to either γ-irradiation or AAPH. These treatments yielded protein peroxide concentrations in the order of 1 – 2 μM for similar cell numbers of mouse myeloma cells [280] and U937 cells [180]. This may be due to the cell lines used, the higher temperatures and longer incubation times that were used in these previous experiments and differences in the cellular detoxification mechanisms for the types of peroxides formed. In addition, the data reported by Gieseg *et al.*, [180] suggests that one peroxide is yielded for every 200

peroxyl radicals generated, thus it seems as though this is a rather inefficient method of protein peroxide production. This decreased efficiency of protein peroxide production mirrors the situation observed in isolated proteins. From the data reported in Chapter 4 and comparisons with literature data on the formation of protein peroxides by other oxidants (e.g. [192, 198]) it can be seen that RB photo-oxidation can be an efficient method of producing protein peroxides. Thus, it appears more likely that it is the oxidant generating system, rather then the particular cell type, that governs, at least in part, the level of peroxides detected. The lack of effect of glucose, which is expected to maintain cellular reducing capacity, on $^1O_2$-mediated protein peroxide formation is consistent with this hypothesis.

Cellular viability was decreased by approximately 10-15 % by the photolysis system employed. This is contrary to previous results which have suggested that HUVEC [104, 105] or A341 [256] cells are tolerant of intracellular $^1O_2$ generation. This discrepancy may be due to the different cell lines used, the $^1O_2$ generation method used, the efficiency of $^1O_2$ generation and the levels of intracellular antioxidants or defensive enzymes. The differences in $^1O_2$ production were quite pronounced, Nakano *et al.*, [104, 105] used a naphthalene endoperoxide to generate $^1O_2$ and measured the amount of $^1O_2$ produced to be approximately 10 μM. The yield of protein peroxides obtained in these experiments was always ≥ 10 μM and due to various other $^1O_2$ quenching reactions which are likely to take place within the cell, the $^1O_2$ produced will undoubtedly yield much less than one protein peroxide molecule per $^1O_2$ formed. This assumption is supported by the experiments that quantified the consumption of oxygen by cells undergoing photolysis where only 10-15 % of the O_2 consumed was converted to protein peroxides. Thus, it is likely that much greater amounts of $^1O_2$ are generated in the experiments presented in this chapter, compared to those reported by Nakano *et al.* [104, 105]. Comparison with the data of Chan *et al.*, [256] is not as straightforward. These authors also used RB photo-oxidation to generate $^1O_2$, although they performed their experiments with suspensions of cells in media (DMEM) supplemented with 10 % foetal bovine serum, which contains components that are known to scavenge $^1O_2$. The light source used was a 120 W lamp positioned 30 cm from the surface of the cultures, compared to the 40 W lamp, 5 cm distant, used in this study. This greater distance from the cultures may lead to a significant proportion of the light escaping from the system, but as no

quantification of $^1O_2$ or its reaction products was reported, such comparisons may not be valid.

THP-1 cells are a human monocyte cell line. Monocytes are capable of differentiation to form macrophages, which are thought to be able to produce $^1O_2$ as part of the immune response [101]. The low amount of cell death observed upon generation of $^1O_2$ within THP-1 cells may be due to evolution of mechanisms to protect themselves from $^1O_2$-induced injury. Nakano *et al.*, [104, 105] demonstrated that bacteria are very susceptible to $^1O_2$, with 34 % of wild type *Escherichia coli* killed after exposure to a total of 7 μM $^1O_2$ generated over a period of 5 min. Thus it may be that cells of the human immune system have evolved mechanisms for the killing of potential pathogens (such as bacteria) but have endogenous defence mechanisms against this oxidant. In light of this it would be interesting to examine the ability of $^1O_2$ to induce cell death in different types of human cells.

$^1O_2$-derived protein peroxides were found to decay when incubated at elevated temperatures, although whether this was due to cellular metabolism or thermal decay was not further elucidated. Over the same time period cellular viability decreased. There was only a small loss in viability over the photolysis period, and this decrease in viability continued after the generation of $^1O_2$ had ceased. These results suggest that some product of $^1O_2$ generation may be responsible for the continued loss of viability. There are many possible explanations for this delayed effect on cell viability, including direct inactivation of enzymes by $^1O_2$, the functions performed by which may not be immediately necessary for the cells, but whose loss may lead to cell death after a time lag. The further reactions of these protein peroxides may also be a possible route to cell death. Protein derived radical species have previously been shown to damage other proteins (Section 4.3.4b) and DNA [193, 217] and could therefore have detrimental effects on the cell. However, the results obtained in these experiments cannot exclude the possibility that oxidation of other essential bio-molecules may also be involved in the loss of cell viability. Thus, it is possible that oxidation of nucleic acid or lipid components of the cell which are known to occur under these conditions [36, 69, 259] are contributing factors.

It was observed that peroxides formed on isolated proteins were reduced by metal ions to yield radical species that could be detected by EPR spin trapping (Section 4.3.4a.ii). Therefore the reduction of protein peroxides, formed by

intracellular $^1O_2$ generation, by metal ions was investigated. EPR signals were not observed when intact RB loaded and photolysed cells were treated with Fe^{2+}/EDTA in the presence of MNP. This is thought to be due to the intracellular location of the peroxides and the inability of the Fe^{2+}/EDTA complex to cross cellular membranes. However, when RB photo-oxidised cells were lysed prior to the addition of Fe^{2+}/EDTA and MNP, radicals were observed using EPR spectroscopy. These EPR spectra contained a broad signal, similar to those observed with RB photo-oxidised BSA. Attempts to confirm that these broad EPR signals were derived from proteins, rather than from other cellular macromolecules, included the use of gel filtration, protease treatment, TCA precipitation and extraction. TCA precipitates of cell lysates showed the same signals as observed in the lysates, however none of the other experiments yielded conclusive data.

The oxidation of bulk cell proteins, isolated by TCA precipitation, by RB photolysis has also been investigated, and this has been shown to result in the formation of high yield of protein peroxides. The peroxides yielded were also reduced with Fe^{2+}/EDTA in the presence of MNP. EPR spectra of these reaction mixtures contained one major signal, which has been analysed in terms of a broadened triplet of doublets, characteristic of a carbon-centred radical with couplings to a nearby proton. The parameters of this signal are similar to those found for radicals formed on RB photo-oxidised free Tyr, Tyr containing peptides, and also BSA, after pronase treatment, and histone H1. This suggests that similar species may be formed in cells and that Tyr may be a target for peroxide formation and radical generation.

In conclusion, these results demonstrate that photolysis of cells containing RB leads to the formation of protein-derived peroxide species. This process was shown to be mediated by $^1O_2$ using buffers containing D_2O and azide. The generation of $^1O_2$ inside the cells lead to a small decrease in viability, which further decreased upon incubation of the cells after the cessation of photolysis. As $^1O_2$ production does not occur in the absence of light, this result suggested that the products of $^1O_2$-mediated oxidation were responsible for the increasing cell death observed.

Over the same time period the decay of protein peroxides was observed, suggesting that this process might be involved in the loss of cell viability, although it was not possible to rule out other products of $^1O_2$ reactions with biomolecules such as

DNA or lipids. The reduction of these peroxides by Fe^{2+} was found to yield radical species. However, cell lysis (after photolysis) was required before EPR signals could be observed. This is likely to be due to the intracellular location of the protein peroxides and the inability of the Fe^{2+}/EDTA complex to cross cellular membranes. The radicals observed have been assigned as protein-derived based on their similarity to previous isolated protein experiments and experiments on isolated bulk cell proteins. The formation of such radicals on decay of intracellular protein peroxides may lead to the loss of cell viability.

CHAPTER 7 - PRELIMINARY STUDIES OF $^1O_2$-MEDIATED OXIDATION OF HIS

7.1 INTRODUCTION

Chapters 3 and 4 focused on various aspects of the $^1O_2$-mediated oxidation of Tyr as both the free amino acid (Chapter 3) and as a residue of a peptide or protein (Chapter 4). It was found that peroxide species were the primary products of these reactions, and these species could be detected using the ferric xylenol orange (FOX) method. The peroxides were further characterised by high performance liquid chromatography (HPLC), electrospray ionisation mass spectrometry (ESI-MS) and nuclear magnetic resonance (NMR) spectroscopy.

Amino acids other than Tyr are also known to react with $^1O_2$, including His, Trp Cys and Met, as discussed in Chapter 1. The amino acid with the greatest rate constant for reaction with $^1O_2$ is His ($k \sim 3.2 \times 10^7$ M^{-1} s^{-1} at pH 7.1) [97].

Studies of the photosensitised oxidation of His (7.1) have demonstrated that the reaction proceeds predominantly via a $^1O_2$-dependant (Type II) mechanism [97]. When this reaction is performed at pH 7 and 2 °C, the oxidation of free His occurred with the consumption of one mole equivalent of oxygen [281]. In 1969 Tomita *et al.*, [85] found that His was photo-oxidised (at pH 11) to give aspartic acid via a complex mixture of unstable intermediate products and suggested that the initial reaction was a 1,4-cycloaddition yielding two endoperoxide species (7.2) and (7.3) (Scheme 7.1).

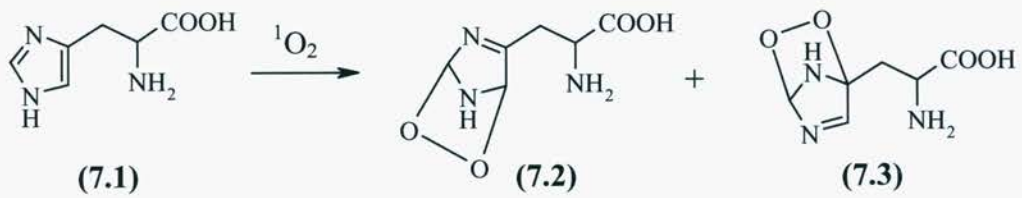

Scheme 7.1: Proposed endoperoxide formation on $^1O_2$-mediated oxidation of His [85].

More recently, low temperature photo-oxygenation in organic solvents and subsequent NMR analysis has led to the direct observation of 2,5-endoperoxides, analogous to (7.2), of various imidazole derivatives including His [82]. These endoperoxides were found to be very unstable, decaying at temperatures above – 88 °C, to yield a complex mixture of products that has not been fully elucidated [83].

Protein His residues generally have pKa values very close to physiological pH (typically ~6.5) [1]. Many enzymes take advantage of this property and have His residues fulfilling vital roles in their catalytic cycle. It is also known that products formed during the $^1O_2$-mediated oxidation of His can form cross-linked species, by reaction with non-oxidised His or Lys residues and thus chemical alteration of His is likely to have important biological consequences [126].

In chapters 3 and 4 (Sections 3.4.4 and 4.3.4) it was shown that the one-electron reduction of Tyr peroxides led to the formation of radical species that could be detected by electron paramagnetic resonance (EPR) spectroscopy with spin trapping. It is therefore possible that similar radical intermediates may also be generated on decomposition of His-derived peroxides.

7.2 AIMS

The aim of the studies presented in this chapter were to investigate the reaction of $^1O_2$ with His and Gly-His-Gly. $^1O_2$ was generated using RB photo-oxidation, as previously, and the products of these reactions were monitored by FOX assay, HPLC and ESI-MS. The formation of radicals generated by one-electron reduction of peroxides, and the transfer of radicals from these species to other peptides and proteins, was investigated using EPR spectroscopy with spin trapping.

7.3 RESULTS

7.3.1 FORMATION AND STABILITY OF HIS-DERIVED PEROXIDES AS A RESULT OF $^1O_2$-MEDIATED OXIDATION

As discussed previously (Chapter 3) RB photo-oxidation was found to be an ideal method for investigating peroxide formation, as the experimental conditions lacked agents that are likely to cause peroxide decomposition, such as, transition metal ions, heat and UV light. This method was also used for the generation of $^1O_2$ in the following experiments.

7.3.1a Peroxide Formation

Photolysis of His and Gly-His-Gly (2.5 mM, pH 7) with visible light ($\lambda > 345$ nm) in the presence of RB (10 μM) and oxygen resulted in the formation of peroxides as detected by the FOX assay. Samples were treated with catalase (3150 units mL^{-1}, 10 min, 22 °C) prior to peroxide determination to ensure that any photo-generated

H_2O_2 was removed. The peroxide concentration increased very rapidly and maximal concentrations were achieved after ~ 20 min reaction time. Peroxide levels then remained approximately constant over 60 min photolysis (Figure 7.1).

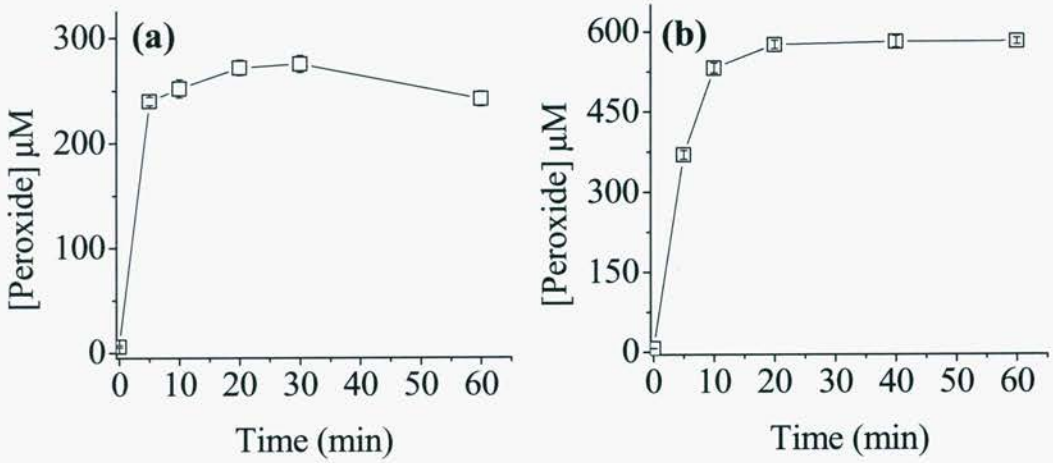

Figure 7.1: The formation of peroxides on (a) His and (b) Gly-His-Gly (both 2.5 mM, pH 7) by visible light (λ > 345 nm) in the presence of oxygen and the photosensitiser RB (10 µM), at 4 °C. Peroxide concentrations were measured using the FOX assay with H_2O_2 standards as described in Chapter 2. Data are the means (± SD) of triplicate determinations from a single experiment, representative of several, as absolute peroxide yields varied between experiments due to slight differences in oxygenation rates.

7.3.1b Peroxide Stability

Studies with Tyr-derived peroxides demonstrated that these were unstable at elevated temperatures. In order to examine whether this was also the case for His-derived peroxides, the stability of these species was examined at a range of temperatures. This was investigated by incubation of reaction mixtures containing the peroxide, RB and residual Gly-His-Gly, in the absence of light at 4 °C, 22 °C and 37 °C. Samples were removed after various times and residual peroxide concentration was determined with the FOX assay.

The Gly-His-Gly peroxides were found to be relatively stable at 4 °C, with 85 ± 1 % peroxides remaining after 24 h (Figure 7.2). The rate of peroxide loss was greater at 22 °C (66 ± 2 % peroxide remaining) and at 37 °C (43 ± 2%).

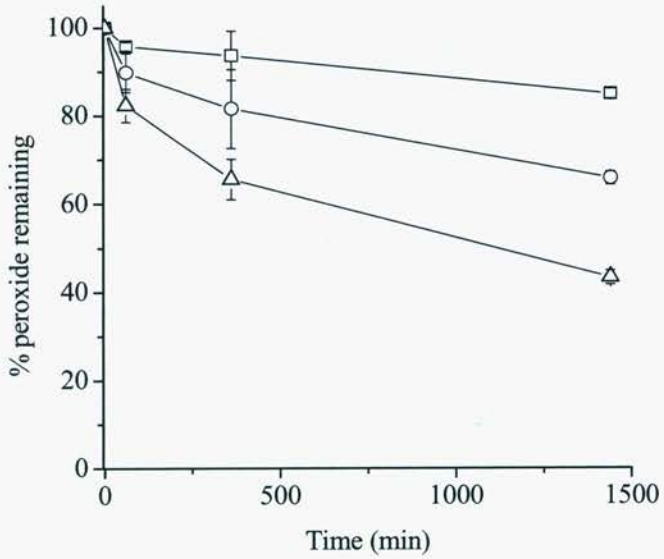

Figure 7.2: Stability of Gly-His-Gly peroxides at elevated temperatures. Peroxides were generated as described in Figure 7.1. Reaction mixtures, which contain RB and unreacted Gly-His-Gly as well as Gly-His-Gly peroxides, were incubated in the absence of light at 4 °C (□), 26 °C (○), and 37 °C (△) for the indicted time periods before residual peroxide levels were determined as in Figure 7.1. Data are expressed as means of percentage initial peroxide concentration (n = 6, from 2 separate experiments) ± SD.

7.3.1c Conclusions

Peroxide formation was observed on the RB photolysis of His and Gly-His-Gly. The reaction was found to be much more rapid than that observed with Tyr (see Section 3.4.1a), in accord with previous studies, which demonstrated that the reaction of $^1O_2$ with His is approximately four-times more rapid than that of Tyr (rate constants 3.2 x 10^7 and 0.8 x 10^7 M^{-1} s^{-1} for His and Tyr respectively [97]).

Peroxides derived from Gly-His-Gly were found to decay at elevated temperatures similar to those derived from Tyr. Previous studies have suggested that peroxides formed on imidazole derivatives similar to His are very unstable, decaying at temperatures above –88 °C [82, 83]. This may indicate that the peroxides measured in these experiments are not the initial endoperoxides, rather that they may be peroxidic breakdown products of these initial species.

7.3.2 Characterisation of His-Derived Peroxides

The previous sections have demonstrated the formation of peroxides on $^1O_2$-mediated oxidation of His. The studies reported in this section are preliminary investigations into the structural characterisation of the peroxides and further products, using ESI-MS and HPLC.

7.3.2a Analysis of $^1O_2$ oxidised His and Gly-His-Gly by HPLC

In chapter 3 it was reported that HPLC analysis of RB photo-oxidised Tyr using a Zorbax ODS column and water as the mobile phase allowed the separation of both the final stable product HOHICA and two intermediate peroxides (Section 3.4.3a). The studies reported in this section aimed to use similar methodology to characterise the products of free His and Gly-His-Gly oxidation.

Initial experiments were carried out at low pH using 0.1 % TFA (pH 2.2) as the mobile phase in order to avoid the presence of both the protonated and deprotonated forms of His (free His pKa 6.04) [282]. The absorption maximum of His occurs at 211 nm, thus initial chromatograms were recorded at 210 nm. At this wavelength, some peaks were observed in the photolysed samples that were not present in the RB containing, non-photolysed control. However these peaks did not change over time, suggesting that they are not peroxidic in nature.

When the eluent was analysed at 280 nm, at least five new peaks were observed in photolysed samples (Figure 7. 3). The peak with retention time (RT) of 2.9 min was observed in non-photo-oxidised controls and is assigned as unmodified His. This peak was found to decrease in intensity during the photolysis reaction. Two peaks eluting before the parent amino acid were observed to increase in intensity initially (up to 30 min) and then decrease, suggesting that these peaks are due to unstable intermediates formed early in the reaction, which either subsequently decay or become further oxidised.

A peak at 3.1 min is observed at short photolysis times (5 min), which is not present in the non-photolysed samples. Over the photolysis period this peak decreases in intensity. A peak at 3.5 min displays similar behaviour, except its decay is at a slower rate. The peak eluting at 5.4 min increased in intensity over the first 30 min photolysis and then remained approximately constant suggesting that this may be a stable product (Figure 7.3).

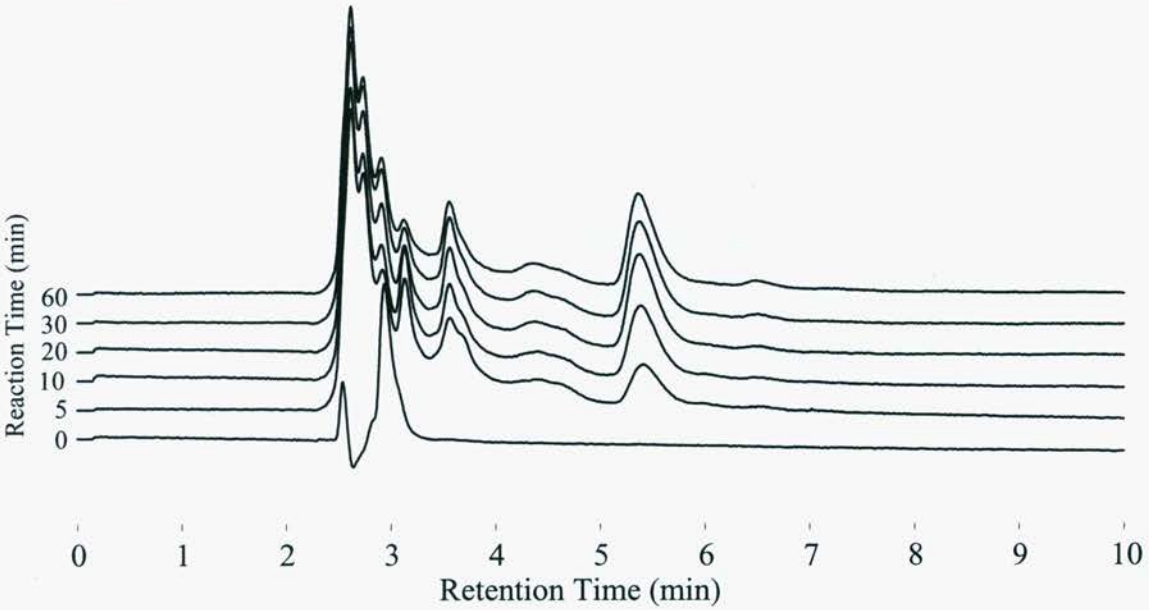

Figure 7.3: HPLC analysis of His oxidation products generated by RB (10 μM) photo-oxidation of free His (2.5 mM in water at pH 7) in the presence of oxygen with visible light ($\lambda > 345$ nm) at 4 °C. Samples were removed from the photo-oxidation reaction at the indicated times and injected (10 μL) on to a Zorbax ODS HPLC column. The mobile phase used was 0.1 % TFA, which was eluted at a rate of 1 mL min^{-1} and the UV absorbance of the eluent, was monitored at 280 nm.

The effect of incubation at 37 °C on the nature of these species was also investigated. His was photo-oxidised with RB as above for 30 min, and the crude reaction mixture then incubated at 37 °C for upto 210 min in the dark. Samples were removed after various incubations periods and analysed by HPLC. The intensity of the peak at 5.4 min increased over this period, whereas the intensities of most other peaks decreased (Figure 7.4).

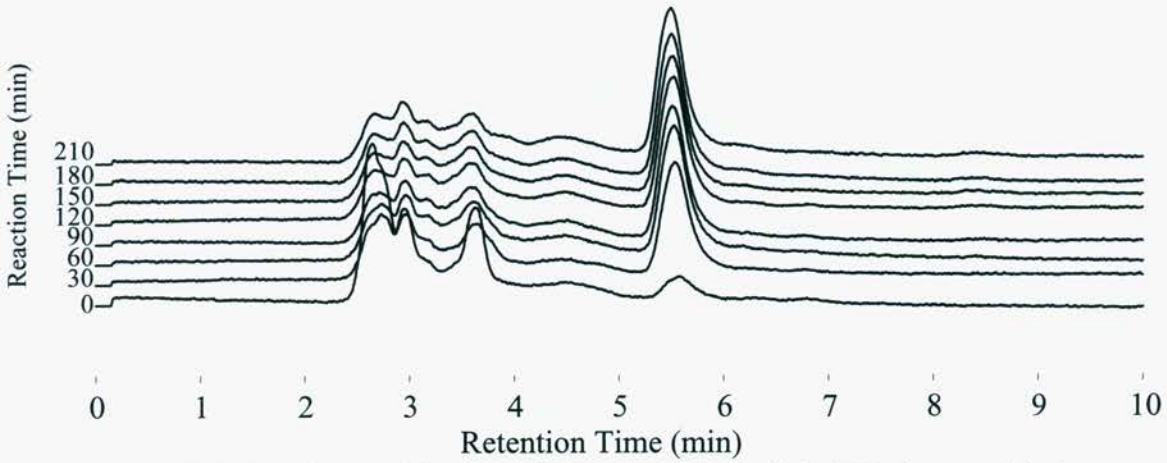

Figure 7.4: HPLC analyses of the time-dependant decay of the RB photo-oxidation products of free His. Samples of His were photo-oxidised for 30 min prior to incubation at 37 °C for the indicted times. Photo-oxidation and HPLC analysis were performed as described in Figure 7.3.

Fractions of the peaks eluting at 3.5 and 5.4 min were collected and analysed by FOX assay. This demonstrated that only the earlier of these peaks contained a peroxide. The relationship between these two peaks was investigated by incubating the collected fractions in the absence of light, at 37 °C. Re-analysis of the 3.5 min fraction after 150 min incubation revealed the almost complete decay of this peak and the appearance of the peak eluting at 5.4 min, whereas no significant change in the nature of the 5.4 min fraction was observed. This suggests that the material responsible for the earlier peak decomposes to yield the latter product (Figure 7.5).

Similar experiments were carried out using Gly-His-Gly as the substrate. Thus RB photo-oxidised Gly-His-Gly was analysed under the same conditions as for free His, except that the eluent was monitored at 210 nm. The parent peptide was found to elute at 4.7 min, and its peak area rapidly decreased over the reaction time. At least 4 new peaks were formed during the photolysis reaction (Figure 7.6), all of which eluted earlier than the parent material.

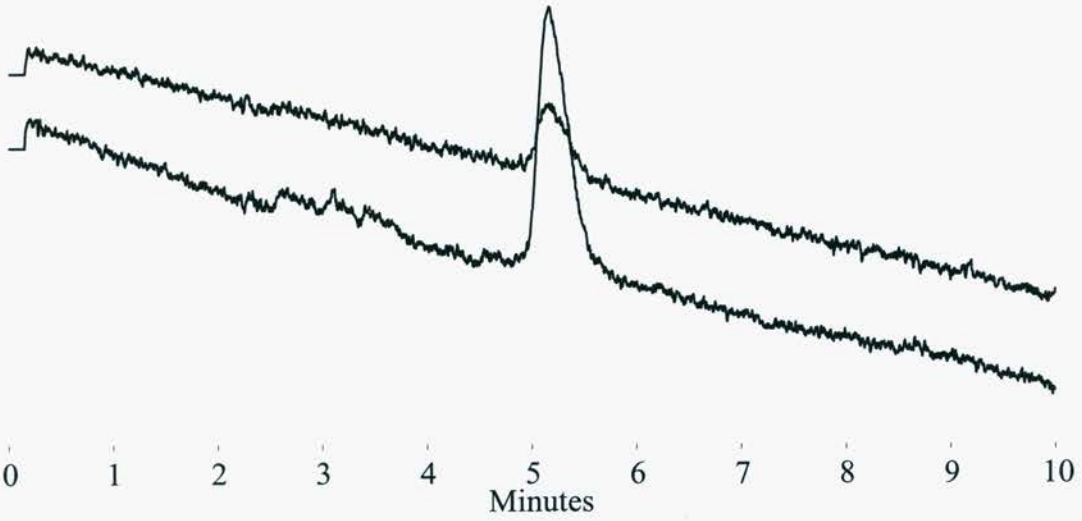

Figure 7.5: HPLC analysis of HPLC fractions eluting at 3.5 min and 5.4 min. The fractions were collected form HPLC, as described in Figure 7.3, immediately following photo-oxidation. Chromatograms obtained after incubation of the 3.5 min fraction (bottom) and 5.4 min (top) fractions at 37 °C for 150 min are shown.

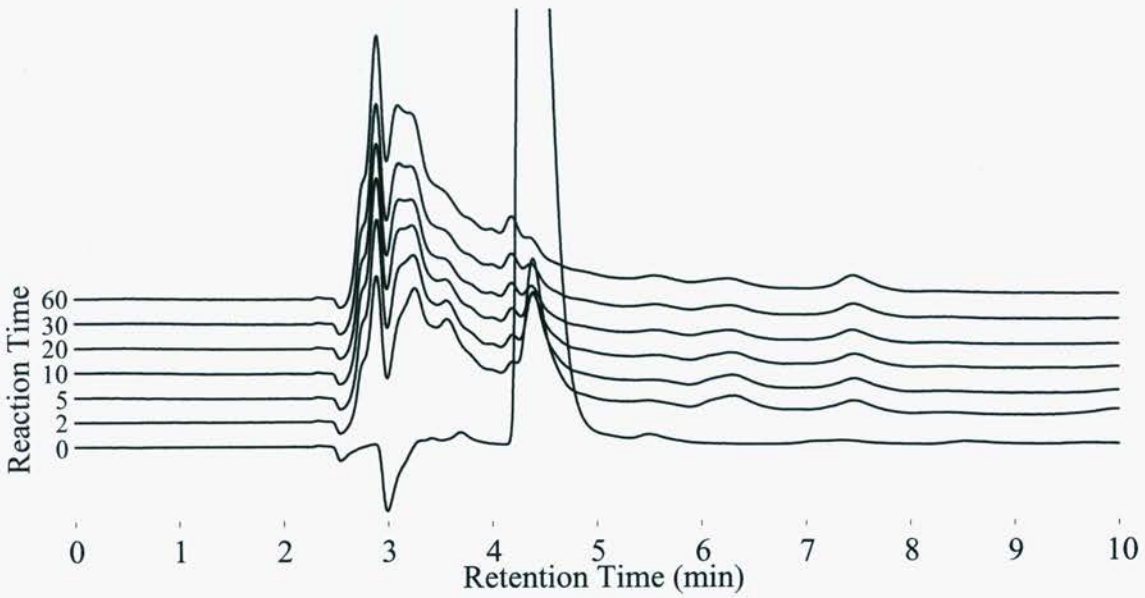

Figure 7.6: HPLC analysis of Gly-His-Gly oxidation products. Gly-His-Gly (2.5 mM in water at pH 7) was RB (10 μM) photo-oxidised, in the presence of oxygen, with visible light ($\lambda > 345$ nm), at 4 °C. Samples were removed from the photo-oxidation reaction at the indicated times and injected (10 μL) on to a Zorbax ODS HPLC column. The mobile phase used was 0.1 % TFA, which was eluted at a rate of 1 mL min^{-1}. The UV absorbance of the eluent was monitored at 210 nm.

On incubation of the unseparated reaction mixture at 37 °C in the absence of light, the peaks that eluted at 2.8 and 4.2 min were found to increase in intensity and a peak eluting at 3.2 min decreased. The latest eluting peak at 4.9 min, was not present immediately after photolysis or after 24 h incubation at 37 °C, but was observed in the intervening samples (Figure 7.7), suggesting that it is a transitory, intermediate species.

The separation in the above chromatograms (Figures 7.3-7.7) is not ideal. The materials are not sufficiently resolved for accurate fractionation and further structural characterisation. Despite the use of various combinations of mobile phases and reverse phase columns better resolution was not achieved. It may be possible to use normal phase chromatography in the future to satisfactorily separate these mixtures.

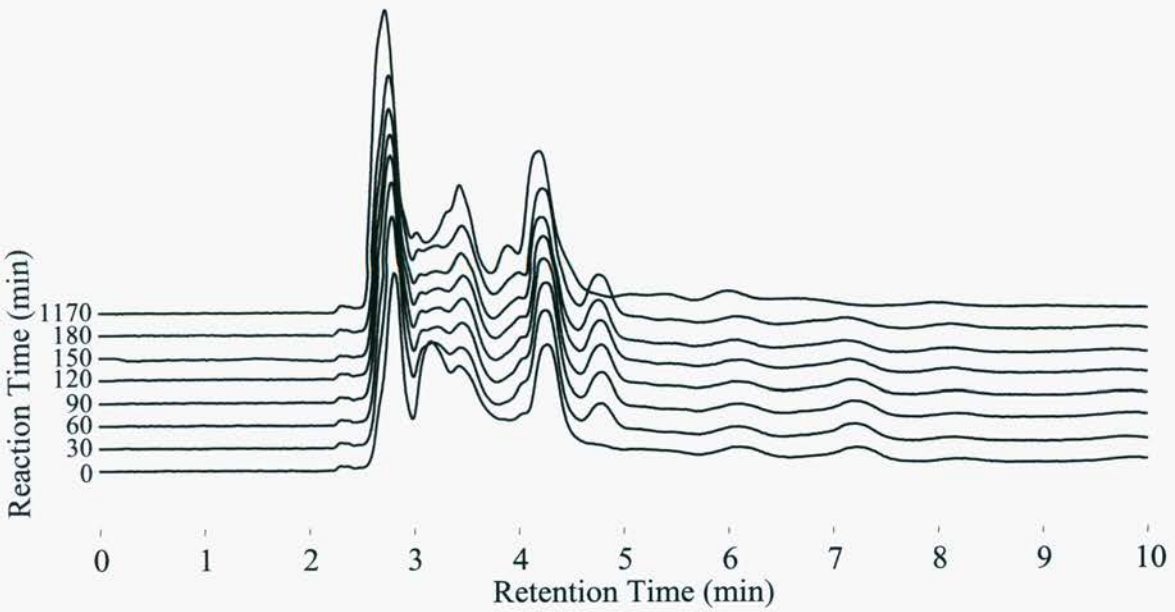

Figure 7.7: HPLC analyses of the time-dependant decay of the RB photo-oxidation products of Gly-His-Gly. Samples of Gly-His-Gly were photo-oxidised for 30 min prior to incubation at 37 °C for the indicted times. Photo-oxidation and HPLC analysis were performed as described in Figure 7.6.

7.3.2b Analysis of $^1O_2$-oxidised His and Gly-His-Gly by ESI-MS

Further investigations into the nature of the species formed on RB photo-oxidation of His and Gly-His-Gly were performed using ESI-MS.

Analysis of His using a cone voltage of 25 V led to the detection of an ion with m/z of 156, corresponding to unmodified His. When the cone voltage was

increased to 50 V, fragmentation occurred resulting in the detection of a peak of m/z 110. This corresponds to the loss of –COOH (m/z 46) and is thus likely to be the immonium ion of His, similar to that observed with free Tyr.

Non-oxidised Gly-His-Gly yielded similar results, with the molecular ion observed at m/z 270 when the sampling cone was set at 25 V. The His immonium ion at m/z 110 and a further fragment at m/z 195 (corresponding to the loss of -$NHCH_2COOH$, i.e., Gly) were observed when a cone voltage of 50 V was used.

ESI-MS analysis of Gly-His-Gly (2.5 mM) that had been photo-oxidised with visible light ($\lambda > 345$ nm) in the presence of RB (10 μM), yielded an ion of m/z M+32, suggesting that two atoms of oxygen have been incorporated into this molecule, consistent with peroxide formation (Figure 7.8).

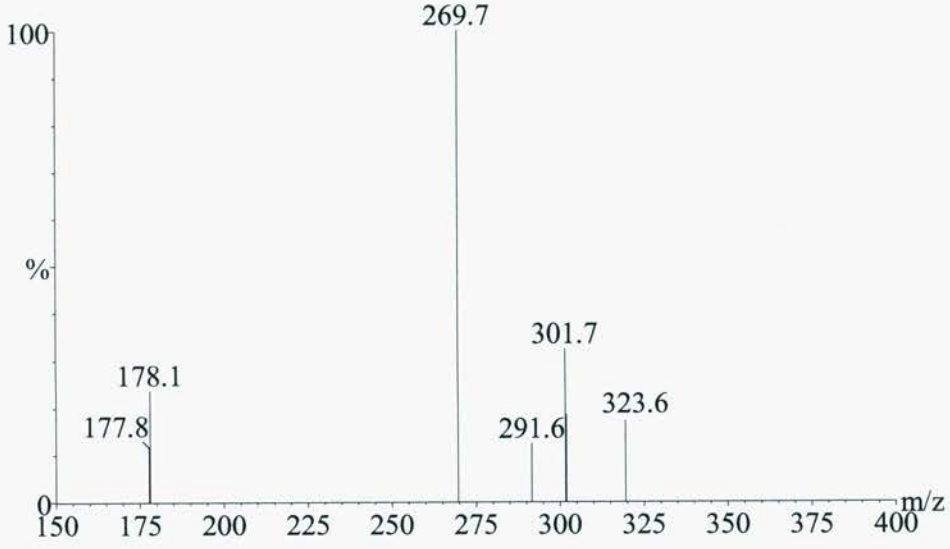

Figure 7.8: ESI-MS analysis of Gly-His-Gly oxidation products generated on photo-oxidation of Gly-His-Gly (2.5 mM) in the presence of oxygen and RB (10 μM) for 1 h. Samples were diluted with 2 % formic acid in methanol to give final concentrations of 50 % methanol and 1 % formic acid to assist ionisation of the sample. Solvent was delivered at 10 μL min^{-1} and 2 x 25 μL injections were made for each analysis. The probe tip was set at 3.5 kV with 0.5 kV on the chicane counter electrode. The sampling cone was set at 25 V. The peak at 269.7 is due to un-modified Gly-His-Gly, the peak at 301.7 is due to M+ 32 consistent with the addition of 2 oxygen atoms to Gly-His-Gly. The peaks at 291.6 and 323.6 are sodium adducts of Gly-His-Gly and the M + 32 species respectively.

7.3.2c Radical Formation on Reduction of His-derived peroxides

The one-electron reduction of Tyr-derived peroxides was shown to yield carbon-centred radicals in Chapters 3 and 4 (Sections 3.4.4 and 4.3.4). To investigate whether similar reactions occur with His-derived peroxides, RB photo-oxidised His and Gly-His-Gly were treated with Fe^{2+}/EDTA in the presence of the spin trap MNP and subsequently analysed by EPR spectroscopy.

The reduction of both His and Gly-His-Gly peroxides (generated by RB photo-oxidation, approximately 300 μM in peroxide) by Fe^{2+}/EDTA (185.5 μM) in the presence of the spin traps DMPO (187.5 mM) or MNP (18.75 mM) led to the detection of complex radical signals by EPR spectroscopy (Figure 7.9).

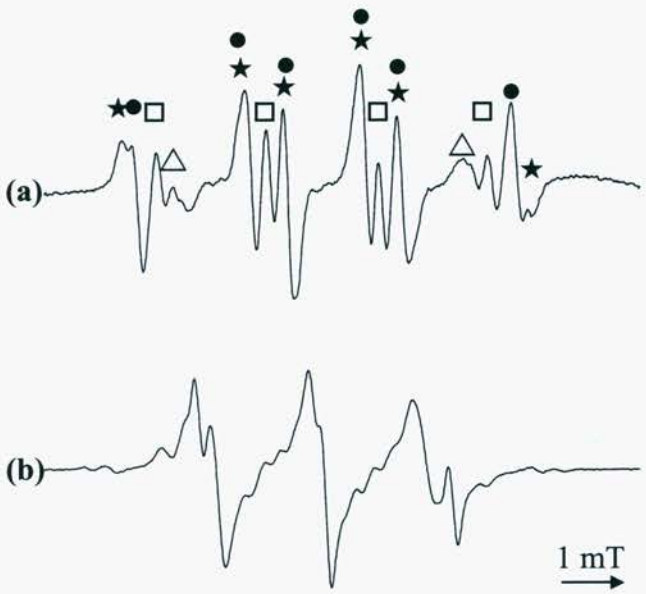

Figure 7.9: EPR spectra detected on reaction of Gly-His-Gly-derived peroxides (~ 300 μM peroxide generated as described in Figure 7.1) with Fe^{2+}/EDTA (187.5 μM) in the presence of (a) DMPO (187.5 mM) and (b) MNP (18.75 mM).

The overlapping features make it difficult to assign these peaks to individual species, however the signals obtained with DMPO appear to be a mixture of 2 carbon-centred radicals (★ and ●), an oxygen-centred species, possibly the $O_2^{-\bullet}$ adduct (△) and the DMPO-OH adduct (□), which is a well-characterised spin trap artefact. The signals obtained from the MNP experiments are likely to be carbon-centred, as MNP adducts of other radicals are generally unstable, however no further assignment is possible with these data. Recent experiments by Hawkins *et al.*, (unpublished data)

using $^1O_2$-oxidised His models and isotope labelled compounds have demonstrated that these radicals are derived from the imidazole ring as well as from the side-chain methylene group.

7.3.2d Transfer of radical damage from Gly-His-Gly to other peptides and proteins

In chapter 4 (Section 4.3.4b) it was demonstrated that radicals formed from Tyr-derived peroxides could transfer damage to other peptides and proteins. In order to investigate the ability of His peroxides to undergo the same reactions, Gly-His-Gly peroxides were generated using RB photochemistry and subsequently reduced by treatment with Cu^+ (generated *in situ* by sequential addition of deoxygenated solutions of Ti^{3+} and Cu^{2+} to give final concentrations of 150 and 100 μM respectively) in the presence of *N*-acetyl Ala methyl ester (230 μL of saturated solution in 500 μL final volume) or bovine γ-globulins (184 mg mL^{-1}) and the spin trap DBNBS (1.15 mM), in accord with earlier experiments carried out with Tyr. However the spectra obtained from RB photo-oxidised Gly-His-Gly alone were of quite low intensity. This may be due to the chelation of Cu^{2+} by His forming a redox inactive complex. In order to alleviate this problem, the order of addition of Cu^{2+} and Ti^{3+} was reversed, this allowed slightly more intense spectra to be observed.

Control reactions with non-photolysed Gly-His-Gly and *N*-acetyl Ala resulted in the detection of a triplet signal, which had parameters identical to the previously observed Ala α-carbon-derived radical [237]. These signals were not completely suppressed by extended de-oxygenation of the solutions. Similar, but more intense, signals were observed when the reaction was performed with RB photo-oxidised Gly-His-Gly. This suggests that radicals formed on decomposition of Gly-His-Gly peroxides can mediate damage to *N*-acetyl-Ala (Figure 7.10).

Figure 7.10: EPR spectra observed on the treatment of (a) non-photo-oxidised and (b) photo-oxidised Gly-His-Gly (~ 300 μM peroxide, generated as described in Figure 7.1) with Cu^{+} (generated in situ by addition of Ti^{3+} (100 μM) and Cu^{2+} (150 μM)) in the presence of *N*-acetyl Ala methyl ester (230 μL of saturated solution in 500 μL final volume) and DBNBS (2 mM).

No radical signals were observed on treatment of non-photo-oxidised Gly-His-Gly with Cu^{+} in the presence of bovine γ-globulins and DBNBS (Figure 7.11). When the reaction was performed using RB photo-oxidised Gly-His-Gly a broad anisotropic signal was observed with some sharp features overlaid. The parameters of the sharper features are similar to those observed when Gly-His-Gly alone. The broad features are attributed to a protein-derived radical. This suggests that radical damage has been transferred from the peptide to the protein (Figure 7.11). To further demonstrate that the broad signals were protein-derived, the low molecular weight components of a the reaction mixture were separated by gel filtration using a PD-10 column. EPR analysis of the high molecular weight, protein-containing fraction, gave a broad, anisotropic signal characteristic of a protein-derived radical. This provides further evidence that radical transfer has occurred from Gly-His-Gly radicals to the protein (Figure 7.11).

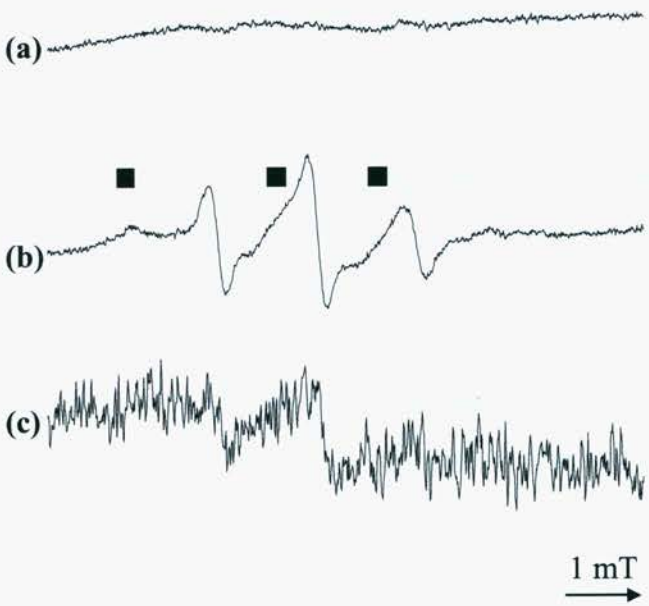

Figure 7.11: EPR spectra observed on treatment of (a) Gly-His-Gly and (b) Gly-His-Gly peroxides (generated as described in Figure 7.1) in the presence of bovine γ-globulins (184 mg mL^{-1}) and DBNBS (2 mM). Features marked (■) are assigned to protein-derived species. (c) EPR spectrum observed on analysis of the major protein containing fraction from gel filtration chromatography (PD-10 column) of an identical reaction mixture to (b). Note that (a) and (b) are presented at the same gain, however (c) is not, due to dilution during gel filtration.

7.4 CONCLUSIONS

Previous chapters have characterised the reactions of Tyr with $^1O_2$ in detail. His is also readily oxidised by $^1O_2$, with a reported rate constant at physiological pH of approximately four times greater than that of Tyr [97]. The reaction of His with $^1O_2$ has been reported to yield a complex product spectrum [84, 85] and the actual mechanism and intermediates have not been conclusively elucidated. The results presented in this chapter are preliminary studies that aimed to investigate the $^1O_2$-mediated oxidation of His using similar methods to those used for the investigation of the reactions of Tyr.

Very rapid peroxide formation was observed on RB photo-oxidation of both free His and Gly-His-Gly, in accord with its high rate constant of reaction with $^1O_2$.

These peroxides were found to be reasonably stable at 4 °C, but decayed more rapidly on incubation at higher temperatures. M + 32 ions were detected on ESI-MS analysis of RB photo-oxidised Gly-His-Gly, further suggesting that peroxide intermediates are formed during this reaction.

HPLC analysis of both His and Gly-His-Gly demonstrated rapid loss of the parent compounds and the formation of a complicated range of products. Generally these product peaks were poorly resolved, however with free His two peaks were sufficiently well resolved to allow further investigation. One of these peaks (RT 3.5 min) was shown to be peroxidic, and the decay of collected fractions of this species led to the formation of a peak at 5.4 min. The characterisation of this more stable substance was not investigated further. Similar complex chromatograms were obtained with RB photo-oxidised Gly-His-Gly.

It was observed previously (Chapters 3 and 4) that one-electron reduction of Tyr-derived peroxides in the presence of a spin-trapping agent led to the formation of radical species that could be detected by EPR spectroscopy. Similar experiments on RB photo-oxidised His and Gly-His-Gly demonstrated that radicals are also formed on reduction of His-derived peroxides. Complicated spectra were observed using both MNP and DMPO spin traps. These could not be assigned fully, although the signals obtained have parameters characteristic of carbon-centred radicals. EPR experiments with $^1O_2$-oxidised imidazole derivatives have been performed recently by Hawkins *et al.*, (unpublished data). These demonstrate that these signals are derived from both the imidazole ring of His and the side-chain methylene group.

Generation of these radicals in the presence of Ala and γ-globulins resulted in the detection of radical adducts characteristic of the Ala-derived α-carbon radical, and anisotropic spectra characteristic of protein-derived radical species. These results are similar to those observed using Tyr-derived radicals and suggest that $^1O_2$-mediated oxidation of these residues in proteins may lead to subsequent damage to other residues. The His-derived radicals also reacted with γ-globulins to yield EPR spectra characteristic of protein-derived radicals. The site of radical formation is not certain, however these species are unlikely to be backbone (i.e. α-carbon) derived due to the large degree of steric hindrance associated with the protein tertiary structure.

In summary, this chapter has reported the results of preliminary studies into His oxidation by $^1O_2$. The results obtained show that similar processes occur to those observed with Tyr, however the initial reaction is at a much higher rate and thus it is likely that His residues are the initial target of $^1O_2$-mediated protein oxidation. This fact coupled with the interesting array of products obtained from $^1O_2$-mediated oxidation of His suggests that this system is worthy of further study.

CHAPTER 8 - GENERAL DISCUSSION

8.1 GENERAL OVERVIEW

The research presented in this thesis has been undertaken to investigate amino acid and protein oxidation by $^1O_2$, with the further aim of discovering a product of such reactions that would be suitable as a marker of $^1O_2$-mediated protein oxidation *in vivo*.

It has been previously reported that under physiological pH conditions only five amino acids - Tyr, His, Trp, Cys and Met - are susceptible to $^1O_2$-mediated oxidation. Met residues are oxidised by $^1O_2$ to give sulfoxide species and the reaction of Cys with $^1O_2$ yields disulfides and sulfonic acids [97]. However, these oxidation products are not unique to $^1O_2$-mediated oxidation and thus are not suitable markers for this process. The oxidation of Trp by both $^1O_2$ and radicals is reasonably well understood. Both processes yield kynurenine and derivatives (reviewed in [3, 72]), thus it was considered unlikely that a $^1O_2$-specific product of Trp oxidation would be identified. Of the remaining two amino acids, initial experiments demonstrated that Tyr (Chapter 3) yielded a much less complicated product spectrum than His (Chapter 7) on $^1O_2$-mediated oxidation and was thus considered more likely to yield an identifiable, specific $^1O_2$-marker.

8.2 THE FORMATION OF TYR- AND PROTEIN-DERIVED PEROXIDES

Initial experiments aimed to determine the intermediates and products formed on $^1O_2$-mediated oxidation of free Tyr (Chapter 3) and peptide bound Tyr (Chapter 4). These investigations showed that peroxides were formed on free Tyr in a dose-dependant manner, by reaction with $^1O_2$ generated using two different systems (Chapter 3). Experiments using the Tyr model compounds 3-(4-hydroxyphenyl)propionic acid (HPPA), *N*-acetyl Tyr and the peptide Gly-Tyr-Gly displayed similar reactivity towards $^1O_2$. Peroxides were also detected on proteins that had been exposed to $^1O_2$ (Chapter 4).

These peroxides were relatively stable at temperatures less than 4 °C, however at higher temperatures significant decay was observed. The peroxides were also susceptible to decomposition by UV light and reduction by both one- (transition metal ions) and two-electron reductants (sodium borohydride). This peroxide stability is similar to that published previously for amino acid and protein-derived peroxides, formed by γ-irradiation [193, 198, 217, 252].

8.3 RADICAL FORMATION ON TRANSITION METAL ION-CATALYSED REDUCTION OF PEROXIDES

It is known that one-electron reduction of peroxides leads to the formation of radicals [225, 226], however radical formation from $^1O_2$-derived peroxides has not previously been investigated in depth. Experiments using EPR spectroscopy showed that radicals were formed on reduction of free Tyr-derived peroxides. These radicals had EPR parameters characteristic of carbon-centred radicals and experiments with isotope labelled Tyr derivatives allowed the assignment of the radicals to carbon-centred species positioned at position C(3) on the Tyr ring (Chapter 3). Similar species were observed on the Tyr model compounds and were assigned as carbon-centred radicals derived form the same ring position (Chapter 4).

EPR experiments with $^1O_2$-oxidised Histone H1 and BSA were also performed (Chapter 4). Histone H1 was chosen for these experiments as it has no Trp or His residues, and thus only Tyr peroxides are likely to be present. Conversely, BSA contains all of the common amino acids and thus was used as a general protein model. The metal ion reduction of histone H1-derived peroxides led to the observation of EPR signals similar to those observed in the experiments with free Tyr, indicating that Tyr may be an important target for $^1O_2$ in this protein. EPR spectra obtained from the reduction of BSA-derived peroxides showed broad anisotropic EPR spectra characteristic of immobilised radical adducts. However, when these radical adducts were digested using the non-specific protease, pronase, spectra were observed that contained signals with similar parameters to those observed with free Tyr and histone H1, again indicating that Tyr residues may be an important target for $^1O_2$-mediated protein oxidation (Chapter 4). Other signals were observed with BSA that may be due to His-derived radicals.

8.4 CHARACTERISATION OF THE PRODUCTS OF $^1O_2$-MEDIATED TYR OXIDATION

NMR spectroscopy was used to characterise the $^1O_2$-mediated oxidation of free Tyr, HPPA and Gly-Tyr-Gly. In experiments with free Tyr it was possible to identify one of the peroxide intermediates as well as the final product of this reaction. The final product was identified as 3a-hydroxy-6-oxo-2,3,3a,6,7,7a-hexahydro-1*H*-indol-2-carboxylic acid (HOHICA) consistent with previous reports [95, 96]. The peroxide observed using NMR was the corresponding indolic hydroperoxide.

These findings were extended with NMR analysis of $^1O_2$ oxidised HPPA and Gly-Tyr-Gly. Unlike Tyr, HPPA does not have an α-amino group and thus cannot form indolic peroxides or alcohols. Examination of $^1O_2$ oxidised HPPA by NMR revealed the formation of a cyclohexadieneone derivative with a hydroperoxide group positioned at the ring C(1) position, which decayed over time to yield the analogous alcohol (Chapter 4). This is a similar result to previous findings by Saito and co-workers who studied this compound at high pH [233, 234]. $^1O_2$-mediated oxidation of Gly-Tyr-Gly was found to yield similar hydroperoxides and alcohols located at the ring C(1) position. These species have not been observed previously and suggest that the reaction of $^1O_2$ with Tyr residues in whole proteins may yield similar species. The use of NMR to investigate such reactions on intact proteins was not attempted as it was expected that the combination of signal broadening, due to the restricted rate of rotation of these large molecules, and the similarity of chemical shifts of multiple residues would make such spectra very complex and difficult to assign accurately. However it may be possible to choose a protein that is sufficiently mobile in solution and, ideally, does not posses any of the other $^1O_2$-reactive residues, to investigate the formation of similar products on an intact protein.

8.5 THE FURTHER REACTIONS OF TYR OXIDATION INTERMEDIATES

The results of chapter 4 showed that the major species formed on HPPA and Gly-Tyr-Gly reaction with $^1O_2$ illustrated that α,β-unsaturated carbonyl species (the cyclohexadieneone derivatives) are formed and therefore these products were expected to be susceptible to attack by nucleophilic species. This was investigated using amine and thiol nucleophiles.

Experiments described in chapters 3 and 4 show that the peroxides on free Tyr decay more rapidly than those on the compounds the either lack the amino group, or have it derivatised e.g. with an amide function. It was found that incubation of $^1O_2$-derived peroxides formed on Tyr, *N*-acetyl Tyr and HPPA with Lys and 6-aminohexanoic acid (AHA; a lysine model compound lacking the α-amino group) accelerated peroxide decomposition (Chapter 5). This suggests that a carbon-nitrogen bond was formed between the Tyr model and Lys, at the C(2) position of the Tyr ring, resulting in accelerated loss of peroxides. Lys residues are often found at the surface of a protein's globular structure and are therefore available for reaction with oxidised

Tyr residues on another protein molecule. If such a reaction occurs cross-link formation and protein dimerisation would result. Protein dimers and higher aggregates have been observed in *in vitro* studies [123, 124, 249] and have been isolated from diseased tissues, such as cataractous lenses (reviewed in [72]). A range of $^1O_2$-mediated cross-links have been characterised by Shen *et al.* [126-128]. These researchers have elucidated the structure of His-His, His-Lys and Tyr-Tyr crosslinks, but the potential Tyr-Lys cross-links described above have not been reported previously. Chemical characterisation of these species would be an interesting avenue for further research.

8.6 DEVELOPMENT OF A MARKER FOR $^1O_2$-MEDIATED TYR OXIDATION

Products similar to HOHICA, the final product of $^1O_2$-mediated free Tyr oxidation, do not appear to be formed on oxidised Tyr residues in peptides. Therefore this product is unlikely to be a suitable marker for $^1O_2$-mediated protein oxidation. The instability of the peroxidic products also makes them unsuitable for this purpose

A potentially useful marker was found in studies of the reaction of Tyr oxidation intermediates / products with sulfur nucleophiles (Chapter 5). In these reactions $^1O_2$-oxidised Tyr was incubated with 2-mercaptoacetic acid under conditions usually used for gas phase protein hydrolysis. The product of this reaction was found to be a Tyr derivative that contained a thioacetate group at ring position C(2). This compound was also produced by gas phase hydrolysis of a range of $^1O_2$-oxidised Tyr derivatives (although not the model compound HPPA) as well as on isolated proteins that had been oxidised by $^1O_2$, proteins extracted from THP-1 cells that were subjected to photo-oxidation of intracellular RB and also on proteins isolated from non-cataractous human lenses. These results suggest that this new material may be suitable as a marker for $^1O_2$-protein oxidation *in vivo*. Further studies attempted to follow up these novel qualitative results by quantifying the amount of this product formed in normal human lenses of different ages, however this was thwarted by a lack of samples.

Markers of protein oxidation have been reported previously, such as 3,4-dihydroxyphenylalanine (for HO•), 3-chloro Tyr (HOCl), and alcohols of Leu, Val and Lys (HO•), however no markers of $^1O_2$-mediated protein oxidation have been reported previously. Therefore, the discovery of this product will expand the set of

diagnostic markers available for investigations of protein oxidative damage in various diseased tissues and will allow simultaneous measurement of the products of radical- and $^1O_2$-mediated Tyr oxidation on *in vivo* samples.

One avenue of further investigation that is likely to yield positive results is investigation of eye lens proteins. There is a large amount of indirect evidence for the participation of $^1O_2$ in the formation of cataract (e.g. [121, 123, 124, 249, 265, 266, 283, 284]) and the initial results reported in chapter 5 demonstrate that $^1O_2$-mediated protein oxidation is occurring in normal lenses. Comparison of normal lenses to cataractous samples and further normal lenses of different ages, should yield interesting information about the role of $^1O_2$ in this disease. Many other biologically relevant processes are also thought to involve $^1O_2$. These include the killing of pathogenic organisms by neutrophils [103-106]. A range of oxidising species are produced by these activated cells and it would be interesting to compare radical and $^1O_2$ mediated oxidation in this environment, which may now be possible using the assay developed in Chapter 5. Further avenues include investigating the mode of action of photodynamic therapy, which is becoming increasingly employed for the treatment of various malignancies, and the effects of solar radiation, including UV radiation, on the skin and eyes.

8.7 INTRACELLULAR GENERATION OF $^1O_2$ –CELL VIABILITY AND PROTEIN PEROXIDE FORMATION

The formation of protein-derived peroxides in a cellular system has been reported recently. Gieseg and co-workers [180] generated peroxyl radicals within cells using a thermal source and found that peroxides could be detected on proteins isolated from these cells. Intracellular $^1O_2$ production has been used previously, mainly in studies of $^1O_2$-induced apoptosis [147, 263]. In the experiments reported in chapter 6 the effect of intracellular $^1O_2$ formation on cell viability and the formation of protein peroxides by this process were investigated. It was found that the $^1O_2$ generation system used lead to a slight increase in cell death (approximately 10 % less viable than the controls), and over the time course of $^1O_2$ production, increasing amounts of protein-derived peroxides were detected. These peroxides were not due to lipid oxidation, as shown by peroxide determination of de-lipidated TCA precipitates. When cells containing protein peroxides were incubated at 37 °C for extended periods of time after $^1O_2$ production had ceased, the levels of protein peroxide decreased, with

a concomitant decrease in cell viability. The relationship between these two processes was not investigated further due to a lack of time, and this could be an interesting area for further study. Investigations into the type of cell death, i.e. necrosis or apoptosis, which occurs during the initial $^1O_2$ generation and the post-$^1O_2$-exposure incubation phase were not performed but would also be an interesting extension to the results obtained in this study.

The effect of ascorbate and glucose on both protein peroxide formation and cellular viability was studied, neither of which had any significant effect. Further studies in this area might include investigation of the role of cellular thiols in peroxide formation and cell viability. Previous work has shown that thiols can scavenge $^1O_2$-derived protein peroxides and that the reaction of peroxides with thiols located in the active site of important cellular enzymes can lead to the inactivation of the enzyme [175]. Total cellular thiols can be blocked by treatment with *N*-ethylmaleimide and butamine sulfoxide can be used to deplete cells of glutathione. Experiments using these treatments should yield interesting information about cellular defence mechanisms involved in protection against $^1O_2$-mediated damage.

Chapter 4 showed that protein-derived peroxides could be reduced to yield radicals observable by EPR spectroscopy. The finding that similar peroxides were formed on cellular proteins suggested that radical formation might also occur intracellularly. Initial experiments on isolated bulk cell protein demonstrated both peroxide and radical formation could take place on these proteins. The use of urea in these experiments caused the secondary and tertiary structure of the proteins to become disrupted and allowed the observation of isotropic EPR spectra. The major signal observed was found to have similar parameters to the signals observed on free Tyr, again suggesting that Tyr residues may be an important target for $^1O_2$-mediated protein oxidation.

Further experiments were carried out in which $^1O_2$ was generated intracellularly, leading to protein-peroxide formation. On treatment of the intact cells with Fe^{2+}/EDTA in the presence of a spin trap, no EPR signals could be observed. However, when the cells were lysed prior to metal ion treatment and EPR analysis, radical adduct signals could be observed. Radicals are not observed with intact cells presumably due to the inability of the charged Fe^{2+}/EDTA complex to cross the plasma membrane, suggesting that the peroxides were located inside the cell. This is

consistent with intracellular $^1O_2$ production, as the migration distance of $^1O_2$ is expected to be < 100 nm [51, 279].

The EPR signals observed were broad in character, similar to those observed on $^1O_2$-oxidised BSA, suggesting that they may be protein-derived. In order to confirm the assignment of these signals to protein-derived species, it was attempted to separate the high molecular weight proteins by gel-filtration with PD-10 columns, however this was not successful due to column blockage. Other methods attempted included incubation with pronase, a non-specific protease that was used earlier to digest protein-bound spin adducts and release more mobile fragments, which yield isotropic spectra. Unfortunately this approach was also unsuccessful. Finally lipid extraction from the TCA precipitates was attempted. The yields of peroxides on extracted samples were not significantly different from the non-extracted samples, however the results of EPR experiments on de-lipidated TCA precipitates were not as convincing.

8.8 FUTURE DIRECTIONS

The reactions of Tyr and Tyr-containing peptides with $^1O_2$ have been characterised in this study. However, chemical characterisation of the peroxides formed on the $^1O_2$-mediated oxidation of proteins was not performed. It may be possible to observe NMR signals characteristic of Tyr oxidation intermediates / products if there are sufficiently few interfering resonances. Hence a small protein likely to tumble rapidly in solution, with few, non-Tyr, aromatic residues would need to be chosen. One possibility is aprotinin, which has 4 Tyr and no His or Trp residues.

The reactions of the intermediates and products of $^1O_2$-mediated Tyr oxidation is also a potential avenue for further research. It was shown that radicals derived from $^1O_2$-oxidised Tyr could be transferred to other peptides and proteins. This work could be extended to investigate the transfer of radicals to other biologically important targets. For example Luxford *et al.*, have recently demonstrated the transfer of radical damage, derived from γ-irradiated proteins, to nucleic acids [193, 217]. Similar experiments could be performed with $^1O_2$-oxidised proteins, and may reveal interesting differences between the types of initial radicals.

The potential cross-linking reaction between $^1O_2$-oxidised Tyr and Lys residues could be further studied by structural elucidation of the cross-linked species.

This would involve performing the reaction as described in this study, followed by MS and NMR characterisation. It may be possible to perform these analyses on crude reaction mixtures, or it might prove advantageous to first separate unreacted substrates from the cross-linked material. This could be accomplished by HPLC with either UV or fluorescence detection, or if the radiolabelled Tyr peroxides were used, by radiometric detection. Development of such an HPLC method may allow the development of an analytical protocol for the detection of this cross-link.

The discovery of a specific marker compound for $^1O_2$-mediated protein oxidation was interesting and could be expanded by enhancing the quantitative aspects of the work presented in this thesis. This may involve some 'fine-tuning' of the electrochemical detection methodology, or the use of a different detection system such as fluorescence. The fluorescence spectrum of the marker compound was not fully examined and it may be that this substance has characteristic absorbance and emission maxima.

Intracellular generation of $^1O_2$ provided interesting results demonstrating that protein peroxides were formed and that the decay of these peroxides on incubation correlated with decreasing cell viability. There are many aspects of this study that could be investigated further. These include the effect of intracellular $^1O_2$ generation on intracellular thiols. Thiols are known to be able to reduce peroxide species and it would be interesting to compare the formation and decay of protein peroxides, as well as changes in cell viability, in cells that have had all thiols blocked, cells with depleted glutathione levels, and normal cells.

The experiments reported in this study do not differentiate between necrotic and apoptotic cell death. It has been suggested previously that intracellular $^1O_2$ generation leads to apoptotic cell death (e.g. [146, 147, 263]) and thus it would be interesting to examine the type of cell death observed in both the initial $^1O_2$ generation phase and also during post-oxidation incubation.

The final set of experiments, the $^1O_2$-mediated oxidation of His, were intended as preliminary studies and offer many starting points for future investigation. Previous product identification studies have not been conclusive and it would be interesting to follow-up these initial experiments in order to obtain a full characterisation of $^1O_2$-mediated His oxidation products.

In conclusion the results presented in this study provide important information about the oxidation of proteins by $^1O_2$ and the effects of such oxidation on living cells. Methodology for the analysis of such reactions *in vivo* has also been developed and this could provide important insights into the role of $^1O_2$ and protein oxidation in the development of disease.

REFERENCES

1. Stryer, L., *Biochemistry*. 4th ed. 1995, New York: W.H. Freeman and Co.
2. Halliwell, B. and Gutteridge, J.M.C., *Free Radicals in Biology and Medicine*. 3rd ed. 1999, Oxford: Clarendon Press.
3. Davies, M.J. and Dean, R.T., *Radical Mediated Protein Oxidation*. 1997, Oxford: Oxford Science Publications.
4. Davies, M.J., Fu, S., Wang, H., and Dean, R.T., Stable Markers of Oxidant Damage to Proteins and Their Application in the Study of Human Disease. *Free Radical Biology and Medicine*, 1999. **27**: 1151-1163.
5. Priestley, J., *Experiments and Observations on Different Kinds of Air*. Vol. II. 1775, London.
6. Ihde, A.J., *Priestley and Lavoisier*, in *Joseph Priestley, Scientist, Theologian and Metaphysician; a Symposium Celebrating the 200th Anniversary of the Discovery of Oxygen by Joseph Priestly in 1774*, L. Kieft and B.R. Willeford Jr, Editors. 1980, Bucknell University Press: Lewisberg, Pa. p. 62-91.
7. Francis, A.W., *Oxygen*, in *Mcgraw-Hill Encyclopedia of Science and Technology*. 1997, McGraw-Hill: New York. p. 678-682.
8. Ho, R.Y.N., Liebman, J.F., and Valentine, J.S., *Overview of the Energetics and Reactivity of Oxygen*, in *Active Oxygen in Chemistry*, C.S. Foote, J.S. Valentine, A. Greenberg, and J.F. Liebman, Editors. 1995, Blackie Academic and Professional: New York. p. 1-23.
9. Gerschman, R., Gilbert, D.L., Nye, S.W., Dwyer, P., and Fenn, W.O., Oxygen Poisoning and X-Irradiation; a Mechanism in Common. *Science*, 1954. **119**: 623-626.
10. Bensasson, R.V., Land, E.J., and Truscott, T.G., *Excited States and Free Radicals in Biology and Medicine*. 1993, Oxford: Oxford Science Publications.
11. Ingold, K.U., Paul, T., Young, M.J., and Doiron, L., Invention of the First Azo Compound to Serve as a Superoxide Thermal Source under Physiological Conditions: Concept, Synthesis and Chemical Properties. *Journal of the American Chemical Society*, 1997. **119**: 12364-12365.
12. Bielski, B.H.J. and Cabelli, D.E., *Superoxide and Hydroxyl Radical Chemistry in Aqueous Solution*, in *Active Oxygen in Chemistry*, C.S. Foote, J.S. Valentine, A. Greenberg, and J.F. Liebman, Editors. 1995, Blackie Academic and Professional: New York. p. 66-104.
13. Fenton, H.J.H., Oxidation of Tartaric Acid in the Presence of Iron. *Journal of the Chemical Society*, 1894. **75**: 1-11.
14. Haber, F. and Weiss, J., The Catalytic Decomposition of Hydrogen Peroxide by Iron Salts. *Proceedings of the Royal Society (London)*, 1934. **A147**: 322-352.
15. von Sonntag, C., *The Chemical Basis of Radiation Biology*. 1987, London: Taylor and Francis.
16. Singh, A., Chemical and Biochemical Aspects of Superoxide Radicals and Related Species of Activated Oxygen. *Canadian Journal of Physiology and Pharmacology*, 1981. **60**: 1330-1345.
17. Bennett, J.E., Kinetic Electron Paramagnetic Resonance Study of the Reactions of *t*-Butyl Peroxyl Radicals in Aqueous Solution. *Journal of the Chemical Society, Faraday Transactions*, 1990. **86**: 3247-3252.

18. Russell, G.A., Deuterium Isotope Effects in the Autoxidation of Aralkyl Hydrocarbons. Mechanism of the Interaction of Peroxy Radicals. *Journal of the American Chemical Society*, 1957. **79**: 3871-3877.
19. Wong, P.C., Griller, D., and Scaiano, J.C., A Kinetic Study of the Reactions of *Tert*-Butoxyl with Alkenes: Hydrogen Abstraction vs Addition. *Journal of the American Chemical Society*, 1982. **104**: 5106-5108.
20. Alberts, B., Bray, D., Lewis, J., Raff, D., Roberts, K., and Watson, J.D., *Molecular Biology of the Cell*. 3rd ed. 1994, New York: Garland Publishing.
21. Grether-Beck, S., Buettner, R., and Krutmann, J., Ultraviolet A Radiation-Induced Expression of Human Genes: Molecular and Photobiological Mechanisms. *Biological Chemistry*, 1997. **378**: 1231-1236.
22. Tyrrell, R.M., Role for Singlet Oxygen in Biological Effects of Ultraviolet A Radiation. *Methods in Enzymology*, 2000. **319**: 290-296.
23. Harrison, M.D., Jones, C.E., Solioz, I., and Dameron, C.T., Intracellular Copper Routing: The Role of Copper Chaperones. *Trends in Biochemical Sciences*, 2000. **25**: 29-33.
24. Breuer, W., Epsztejn, S., and Cabantchik, Z.I., Dynamics of the Cytosolic Chelatable Iron Pool of K562 Cells. *FEBS Letters*, 1996. **382**: 304-308.
25. Hampton, M.B., Kettle, A.J., and Winterbourne, C.C., Inside the Neutrophil Phagosome: Oxidants, Myeloperoxidase, and Bacterial Killing. *Blood*, 1998. **92**: 3007-3017.
26. Winterbourn, C.C. and Kettle, A.J., Reactions of Myeloperoxidase with Superoxide and Hydrogen Peroxide: Significance for Its Function in the Neutrophil. *Basic Life Sciences*, 1988. **49**: 823-827.
27. Henderson, L.M. and Chappell, J.B., NADPH Oxidase of Neutrophils. *Biochimica et Biophysica Acta*, 1996. **1273**: 87-107.
28. Nelson, M.J. and Seitz, S.P., *The Mechanism of Lipoxygenases*, in *Active Oxygen in Biochemistry*, J.S. Valentine, C.S. Foote, A. Greenberg, and J.F. Liebman, Editors. 1995, Blackie Academic and Professional: New York. p. 276-312.
29. Canas, P.E., The Role of Xanthine Oxidase and the Effects of Antioxidants in Ischemia Reperfusion Cell Injury. *Acta Physiologica, Pharmacolgica et Therapeutica Latinoamericana*, 1999. **49**: 13-20.
30. Zhai, X. and Asraf, M., Direct Detection and Quantification of Singlet Oxygen During Ischemia and Reperfusion in Rat Hearts. *American Journal of Physiology*, 1995. **269**: H1229-H1236.
31. Gute, D.C., Ishida, T., Yarimizu, K., and Korthuis, R.J., Inflammatory Responses to Ischemia and Reperfusion in Skeletal Muscle. *Molecular and Cellular Biochemistry*, 1998. **179**: 169-187.
32. Dizdaroglu, M., Chemical Determination of Free Radical-Induced Damage to DNA. *Free Radical Biology and Medicine*, 1991. **10**: 225-242.
33. Marnett, L.J., Oxyradicals and DNA Damage. *Carcinogenesis*, 2000. **21**: 361-370.
34. Dizdaroglu, M., *Oxidative DNA Damage: Mechanisms of Product Formation and Repair by Base-Excision Pathway*, in *Free Radicals in Chemistry, Biology and Medicine*, T. Yoshikawa, S. Toyokuni, Y. Yamamoto, and Y. Naito, Editors. 2000, OICA International (UK): London. p. 58-76.
35. de Zwart, L.L., Meerman, J.H.N., Commandeur, J.N.M., and Vermeulen, N.P.E., Biomarkers of Free Radical Damage; Applications in Experimental

Animals and in Humans. *Free Radical Biology and Medicine*, 1999. **26**: 202-226.
36. Girotti, A.W. and Korytowski, W., Cholesterol as a Singlet Oxygen Detector in Biological Systems. *Methods in Enzymology*, 2000. **319**: 85-100.
37. Dean, R.T., Fu, S., Stocker, R., and Davies, M.J., Biochemistry and Pathology of Radical-Mediated Protein Oxidation. *Biochemical Journal*, 1997. **324**: 1-18.
38. Gieseg, S., Simpson, J.A., Charlton, T.S., Duncan, M.W., and Dean, R.T., Protein-Bound 3,4-Dihydroxyphenylalanine Is a Major Reductant Formed During Hydroxyl Radical Damage to Proteins. *Biochemistry*, 1993. **32**: 4780-4786.
39. Listzt, F., Schnittker-Schulze, K., Stuhlsatz, H.W., and Greiling, H., Composition of Proteoglycan Fragments from Hyaline Cartilage Produced by Granulocytes in a Model of Frustrated Phagocytosis. *European Journal of Clinical Chemistry and Clinical Biochemistry*, 1991. **29**: 123-130.
40. Chance, B., Sies, H., and Boveris, A., Hydroperoxide Metabolism in Mammalian Organs. *Physiological Reviews*, 1979. **59**: 527-605.
41. Bowry, V.W. and Stocker, R., Tocopherol Mediated Peroxidation. The Pro-Oxidant Effect of Vitamin E on the Radical-Initiated Oxidation of Human Low Density Lipoprotein. *Journal of the American Chemical Society*, 1993. **115**: 6029-6044.
42. Briviba, K. and Sies, H., Biological Singlet Oxygen Quenchers Assessed by Monomol Light Emission. *Methods in Enzymology*, 2000. **319**: 222-226.
43. Clennan, E.L., New Mechanistic and Synthetic Aspects of Singlet Oxygen Chemistry. *Tetrahedron*, 2000. **56**: 9151-9179.
44. Wasserman, B.H. and Larsen, D.L., Reactions of Singlet Oxygen with Heterocyclic Systems. *Journal of the Chemical Society, Chemical Communications*, 1972. **253**: 429-509.
45. Kautsky, H., Quenching of Luminescence by Oxygen. *Transactions of the Faraday Society*, 1939. **35**: 216-219.
46. Foote, C.S. and Clennan, E.L., *Properties and Reactions of Singlet Dioxygen*, in *Active Oxygen in Chemistry*, C.S. Foote, J.S. Valentine, A. Greenberg, and J.F. Liebman, Editors. 1995, Blackie Academic and Professional: New York. p. 105-140.
47. Aubry, J.M., Cazin, B., and Duprat, F., Chemical Sources of Singlet Oxygen. 3. Peroxidation of Water Soluble Singlet Oxygen Carriers with the Hydrogen Peroxide-Molybdate System. *Journal of Organic Chemistry*, 1989. **54**: 726-728.
48. Aubry, J.-M. and Bouttemy, S., Preparative Oxidation of Organic Compounds in Microemulsions with Singlet Oxygen Generated Chemically by the Sodium Molybdate/Hydrogen Peroxide System. *Journal of the American Chemical Society*, 1997. **119**: 5286-5294.
49. Saito, I., Matsuura, T., and Inoue, K., Formation of Superoxide Ion from Singlet Oxygen. On the Use of a Water-Soluble Singlet Oxygen Source. *Journal of the American Chemical Society*, 1981. **103**: 188-190.
50. Pierlot, C., Aubry, J.-M., Briviba, K., Sies, H., and Di Mascio, P., Naphthalene Endoperoxides as Generators of Singlet Oxygen in Biological Media. *Methods in Enzymology*, 2000. **319**: 3-20.
51. Kochevar, I.E. and Redmond, R.W., Photosensitised Production of Singlet Oxygen. *Methods in Enzymology*, 2000. **319**: 20-28.

52. Griesbeck, A.G., *Ene Reactions with Singlet Oxygen*, in *CRC Handbook of Organic Photochemistry and Photobiology*, W.M. Horspool and P.-S. Song, Editors. 1995, CRC Press: New York. p. 301-310.
53. Orfanopoulos, M. and Stephenson, L.M., Stereochemistry of the Singlet Oxygen Olefin-Ene Reaction. *Journal of the American Chemical Society*, 1980. **102**: 1417-1418.
54. Orfanopoulos, M., Grdina, S.M., and Stephenson, L.M., Site Specificity in the Singlet Oxygen-Trisubstituted Olefin Reaction. *Journal of the American Chemical Society*, 1979. **101**: 275-276.
55. Schulte-Elte, K.H. and Rautenstrauch, V., Preference for the Syn Ene Additions of $^1O_2$ to 1-Methylcycloalkenes. Correlation with Ground-State Geometry. *Journal of the American Chemical Society*, 1980. **102**: 1738-1740.
56. Gollnick, K. and Griesbeck, A.G., [4+2]-Cycloaddition of Singlet Oxygen to Conjugated Acyclic Hexadienes: Evidence of Singlet Oxygen Induced Cis-Trans Isomerism. *Tetrahedron Letters*, 1983. **24**: 3303-3306.
57. Adam, W. and Griesbeck, A.G., *Photooxygenation of 1,3-Dienes*, in *CRC Handbook of Organic Photochemistry and Photobiology*, W.M. Horspool and P.-S. Song, Editors. 1995, CRC Press: New York. p. 311-324.
58. Baumstark, A.L., *The 1,2-Dioxetane Ring System: Preparation, Thermolysis and Insertion Reactions*, in *Singlet O_2*, A.A. Frimer, Editor. 1985, CRC Press: Boca Raton, Fl. p. 1-35.
59. Lutgerink, J.T., van der Akker, E., Smeets, I., Pachen, D., van Dijk, P., Aubry, J.-M., Joenje, H., Lafleur, M.V.M., and Retel, J., Interaction of Singlet Oxygen with DNA and Biological Consequences. *Mutation Research*, 1992. **275**: 377-386.
60. Piette, J., Biological Consequences Associated with DNA Oxidation Mediated by Singlet Oxygen. *Journal of Photochemistry and Photobiology B:Biology*, 1991. **11**: 241-260.
61. Devasagayam, T.P.A., Steenken, S., Obendorf, M.S.W., Schultz, W.A., and Sies, H., Formation of 8-Hydroxy(Deoxy)Guanosine and Generation of Strand Breaks at Guanine Residues in DNA by Singlet Oxygen. *Biochemistry*, 1991. **30**: 6238-6289.
62. Cadet, J., Decarroz, C., Wang, S.Y., and Midden, W.R., Mechanisms and Products of Photosensitised Degradation of Nucleic Acids and Related Model Compounds. *Israeli Journal of Chemistry*, 1983. **23**: 420-429.
63. Cadet, J., Berger, M., Decarroz, C., Wagner, J.R., Van Lier, J.E., Ginot, Y.M., and Vigny, P., Photosensitised Reactions of Nucleic Acids. *Biochemie*, 1986. **68**: 813-834.
64. Sheu, C. and Foote, C.S., Endoperoxide Formation in a Guanosine Derivative. *Journal of the American Chemical Society*, 1993. **115**: 10446-10447.
65. Sheu, C. and Foote, C.S., Reactivity toward Singlet Oxygen of 7,8-Dihydro-8-Oxoguanosine (8-Hydroxyguanosine) Formed by Photooxidation of a Guanosine Derivative. *Journal of the American Chemical Society*, 1995. **117**: 6439-6442.
66. Cadet, J. and Teoule, R., Comparative Study of Oxidation of Nucleic Acid Components by Hydroxyl Radical, Singlet Oxygen, and Superoxide Anion Radicals. *Photochemistry and Photobiology*, 1978. **28**: 661-667.
67. Sies, H. and Menck, C.F.M., Singlet Oxygen Induced DNA Damage. *Mutation Research*, 1992. **275**: 367-375.

68. Valenzeno, D.P., Photomodification of Biological Membranes with Emphasis on Singlet Oxygen Mechanisms. *Photochemistry and Photobiology*, 1987. **46**: 147-160.
69. Girotti, A.W., Photosensitised Oxidation of Membrane Lipids: Reaction Pathways, Cytotoxic Effects, and Cytoprotective Mechanisms. *Journal of Photochemistry and Photobiology B: Biology*, 2001. **63**: 103-113.
70. Stratton, S.P. and Liebler, D.C., Determination of Singlet Oxygen-Specific Versus Radical-Mediated Lipid Peroxidation in Photosensitised Oxidation of Lipid Bilayers: Effect of B-Carotene and α-Tocopherol. *Biochemistry*, 1997. **36**: 12911-12920.
71. Doleiden, F.H., Fahrenholtz, S.R., Lamola, A.A., and Trozzolo, A.M., Reactivity of Cholesterol and Some Fatty Acids toward Singlet Oxygen. *Photochemistry and Photobiology*, 1974. **20**: 519-521.
72. Davies, M.J. and Truscott, R.J.W., Photo-Oxidation of Proteins and Its Role in Cataractogenesis. *Journal of Photochemistry and Photobiology B: Biology*, 2001. **63**: 114-125.
73. Wilkinson, F., Helman, W.P., and Ross, A.B., Rate Constants for the Decay and Reactions of the Lowest Electronically Excited State of Singlet Molecular Oxygen in Solution. An Expanded and Revised Compilation. *Journal of Physical Chemistry Reference Data*, 1995. **24**: 663-1021.
74. Monroe, B., *Singlet Oxygen in Solution: Lifetimes and Reaction Rate Constants.*, in *Singlet O_2*, A.A. Frimer, Editor. 1985, CRC Press: Boca Raton. p. 177-224.
75. Matheson, I.B.C., Etheridge, R.D., Kratowich, N.R., and Lee, J., The Quenching of Singlet Oxygen by Amino Acids and Proteins. *Photochemistry and Photobiology*, 1974. **21**: 165-171.
76. Matheson, I.B.C. and Lee, J., Chemical Reaction Rates of Amino Acids with Singlet Oxygen. *Photochemistry and Photobiology*, 1978. **29**: 879-881.
77. Lindig, B.A. and Rodgers, M.A.J., Rate Parameters for the Quenching of Singlet Oxygen by Water-Soluble and Lipid-Soluble Substrates in Aqueous and Micellar Systems. *Photochemistry and Photobiology*, 1981. **33**: 627-6634.
78. Palumbo, M.C., Garcia, G.A., and Arguello, G.A., The Interaction of Singlet Molecular Oxygen O_2 ($^1\Delta_g$) with Indolic Derivatives. Distinction between Physical and Reactive Quenching. *Journal of Photochemistry and Photobiology B: Biology*, 1990. **7**: 485-489.
79. Michaeli, A. and Feitelson, J., Reactivity of Singlet Oxygen toward Amino Acids and Peptides. *Photochemistry and Photobiology*, 1994. **59**: 284-289.
80. Rougee, M., Bensasson, R.V., Land, E.J., and Pariente, R., Deactivation of Singlet Molecular Oxygen by Thiols and Related Compounds. *Photochemistry and Photobiology*, 1988. **47**: 485-489.
81. Papeschi, G., Monici, M., and Pinzauti, S., pH Effect on Dye Sensitised Photooxidation of Amino Acids and Albumins. *Medecine Biologie Environnement*, 1982. **10**: 245-250.
82. Ryang, H.-S. and Foote, C.S., Chemistry of Singlet Oxygen. 31. Low-Temperature Nuclear Magnetic Resonance Studies of Dye-Sensitised Photooxygenation of Imidazoles: Direct Observation of Unstable 2,5-Endoperoxide Intermediates. *Journal of the American Chemical Society*, 1979. **101**: 6683-6687.

83. Kang, P. and Foote, C.S., Synthesis of a ^{13}C, ^{15}N Labelled Imidazole and Characterisation of the 2,5-Endoperoxide and Its Decomposition. *Tetrahedron Letters*, 2000. **41**: 9623-9626.
84. Johns, R.B. and Jaskewycz, T., Photolysis of L-Histidine. *Nature*, 1965: 1140.
85. Tomita, M., Irie, M., and Ukita, T., Sensitized Photooxidation of Histidine and Its Derivatives. Products and Mechanism of the Reaction. *Biochemistry*, 1969. **8**: 5149-5160.
86. Inoue, K., Matsuura, T., and Saito, I., Mechanism of the Dye-Sensitised Photooxidation of Tryptophan, Tryptamine and Their Derivatives. Singlet Oxygen Process in Competition with Type I Process. *Bulletin of the Chemical Society of Japan*, 1982. **55**: 2959-5964.
87. Nakagawa, M., Okajima, H., and Hino, T., Photosensitised Oxygenation of Nβ-Methoxycarbonyltryptophan Methyl Ester. Isolation and Novel Transformation of a 3a-Hydroperoxypyrroloindole. *Journal of the American Chemical Society*, 1976. **98**: 635-637.
88. Nakagawa, M., Okajima, H., and Hino, T., Photosensitised Oxygenation of Nβ-Methoxycarbonyltryptamines. A New Pathway to Kynurenine Derivatives. *Journal of the American Chemical Society*, 1977. **99**: 4424-4429.
89. Nakagawa, M., Watanabe, H., Kodato, S., Okajima, H., Hino, T., Flippen, J.L., and Witkop, B., A Valid Model for the Mechanism of Oxidation of Tryptophan to Formylkynurenine - 25 Years Later. *Proceedings of the National Academy of Science of the USA*, 1977. **74**: 4730-4733.
90. Nakagawa, M., Yosikawa, K., and Hino, T., The Photosensitised Oxygenation of Nβ-Methyltryptophan. *Journal of the American Chemical Society*, 1975. **97**: 6496-6501.
91. Saito, I., Matsuura, T., Nakagawa, M., and Hino, T., Peroxidic Intermediates in the Photosensitised Oxygenation of Tryptophan Derivatives. *Accounts of Chemical Research*, 1977. **10**: 346-352.
92. Walrant, P. and Santus, R., *N*-Formylkynurenine, a Tryptophan Photooxidation Product, as a Photodynamic Sensitizer. *Photochemistry and Photobiology*, 1974. **19**: 411-417.
93. Pileni, M.-P., Giraud, M., and Santus, R., Kynurenic Acid. II. Photosensitising Properties. *Photochemistry and Photobiology*, 1979. **30**: 257-261.
94. Pileni, M.-P. and Santus, R., On the Photosensitising Properties of *N*-Formylkynurenine and Related Compounds. *Photochemistry and Photobiology*, 1978. **28**: 525-529.
95. Jin, F., Leitich, J., and von Sonntag, C., The Photolysis ($\lambda = 254$ nm) of Tyrosine in the Absence and Presence of Oxygen. The Reaction of Tyrosine with Singlet Oxygen. *Journal of Photochemistry and Photobiology A:Chemistry*, 1995. **92**: 147-153.
96. Endo, K., Seya, K., and Hikino, H., Photo-Oxidation of L-Tyrosine, an Efficient 1,4-Chirality Transfer Reaction. *Journal of the Chemical Society, Chemical Communications*, 1988: 934-935.
97. Straight, R.C. and Spikes, J.D., *Photosensitised Oxidation of Biomolecules*, in *Singlet O_2*, A.A. Frimer, Editor. 1985, CRC Press: Boca Raton. p. 91-143.
98. Sysak, P.K., Foote, C.S., and Ching, T.-Y., Chemistry of Singlet Oxygen - XXV. Photooxygenation of Methionine. *Photochemistry and Photobiology*, 1977. **27**: 19-27.

99. Rosen, H. and Klebanoff, S.J., Formation of Singlet Molecular Oxygen by the Myeloperoxidase-Mediated Antimicrobial System. *Journal of Biological Chemistry*, 1977. **252**: 4803-4810.
100. Steinbeck, M.J., Khan, A.U., and Karnovsky, M.J., Intracellular Singlet Oxygen Generation by Phagocytosing Neutrophils in Response to Particles Coated with a Chemical Trap. *Journal of Biological Chemistry*, 1992. **267**: 13425-13433.
101. Steinbeck, M.J., Khan, A.U., and Karnovsky, M.J., Extracellular Production of Singlet Oxygen by Stimulated Macrophages Quantified Using 9,10-Diphenylanthracene and Perylene in a Polystyrene Film. *Journal of Biological Chemistry*, 1993. **268**: 15649-15854.
102. Kanofsky, J.R., Hoogland, H., Wever, R., and Weiss, S.J., Singlet Oxygen Production by Human Eosinophils. *Journal of Biological Chemistry*, 1988. **20**: 9692-9696.
103. Tatsuzawa, H., Maruyama, T., Hori, K., Sano, Y., and Nakano, M., Singlet Oxygen ($^1\Delta_g$ O_2) as the Principal Oxidant in Myeloperoxidase-Mediated Bacterial Killing in Neutrophil Phagosome. *Biochemical Biophysical Research Communications*, 1999. **262**: 647-650.
104. Nakano, M., Kambayashi, Y., Tatsuzawa, H., Komiyama, T., and Fujimori, K., Useful $^1O_2$ ($^1\Delta_g$) Generator, 3-(4'-Methyl-1'-Naphthyl)-Propionic Acid, 1',4'-Endoperoxide (NEPO), for Dioxygenation of Squalene (a Skin Surface Lipid) in an Organic Solvent and Bacterial Killing in Aqueous Medium. *FEBS Letters*, 1998. **432**: 9-12.
105. Nakano, M., Kambayashi, Y., and Tatsuzawa, H., 3-(4'-Methyl-1'-Naphthyl)Propionic Acid, 1',4'-Endoperoxide for Dioxygenation of Squalene and for Bacterial Killing. *Methods in Enzymology*, 2000. **319**: 216-222.
106. Tatsuzawa, H., Maruyama, T., Misawa, N., Fujimori, K., Hori, K., Sano, Y., Kambayashi, Y., and Nakano, M., Inactivation of Bacterial Respiratory Chain Enzymes by Singlet Oxygen. *FEBS Letters*, 1998. **439**: 329-333.
107. Lenard, J. and Vanderoef, R., Photoinactivation of Influenza Virus Fusion and Infectivity by Rose Bengal. *Photochemistry and Photobiology*, 1993. **58**: 527-531.
108. Dewilde, A., Pellieux, C., Pierlot, C., Wattre, P., and Aubry, J.-M., Inactivation of Intracellular and Non-Enveloped Viruses by a Non-Ionic Naphthalene Endoperoxide. *Biological Chemistry*, 1998. **379**: 1377-1379.
109. Dewilde, A., Pellieux, C., Hajjam, S., Wattre, P., Pierlot, C., Hober, D., and Aubry, J.-M., Virucidal Activity of Pure Singlet Oxygen Generated by Thermolysis of a Water-Soluble Naphthalene Endoperoxide. *Journal of Photochemistry and Photobiology B:Biology*, 1996. **36**: 23-29.
110. Lenard, J., Rabson, A., and Vanderoef, R., Photodynamic Inactivation of Infectivity of Human Immunodeficiency Virus and Other Enveloped Viruses Using Hypericin and Rose Bengal: Inhibition of Fusion and Syncytia Formation. *Proceedings of the National Academy of Science of the USA*, 1993. **90**: 158-162.
111. Wentworth Jr, P., Jones, L.H., Wentworth, A.D., Zhu, X., Larsen, N.A., Wilson, I.A., Xu, X., Godard III, W.A., Janda, K.D., Eschenmoser, A., and Lerner, R.A., Antibody Catalysis of the Oxidation of Water. *Science*, 2001. **293**: 1806-1811.
112. Wentworth, A.D., Jones, L.H., Wentworth Jr, P., Janda, K.D., and Lerner, R.A., Antibodies Have the Intrinsic Capacity to Destroy Antigens.

Proceedings of the National Academy of Science of the USA, 2000. **97**: 10930-10935.

113. Dougherty, T.J., Gomer, C.J., Henderson, B.W., Jori, G., Kessel, D., Korbelik, M., Moan, J., and Peng, Q., Photodynamic Therapy. *Journal of the National Cancer Institute*, 1998. **90**: 889-905.
114. Ackroyd, R., Kelty, C., Brown, N., and Reed, M., The History of Photodetection and Photodynamic Therapy. *Photochemistry and Photobiology*, 2001. **74**: 656-669.
115. Kelly, J.F., Snell, M.E., and Berenbaum, M.C., Photochemical Destruction of Human Bladder Carcinoma. *British Journal of Cancer*, 1975. **31**: 237-244.
116. Kelly, J.F. and Snell, M.E., Hematoporphyrin Derivative: A Possible Aid in the Diagnosis and Treatment of Carcinoma in the Bladder. *Journal of Urology*, 1976. **115**: 150-151.
117. Sibata, C.H., Colussi, V.C., Oleinick, N.L., and Kinsella, T.J., Photodynamic Therapy: A New Concept in Medical Treatment. *Brazilian Journal of Medical and Biological Research*, 2000. **33**: 869-880.
118. Rockson, S.G., Lorenz, D.P., Cheong, W.-F., and Woodburn, K.W., Photoangioplasty; an Emerging Clinical Cardiovascular Role for Photodynamic Therapy. *Circulation*, 2000. **102**: 591-596.
119. Hayase, M., Woodburn, K.W., Perlroth, J., Miller, R.A., Baumgardner, W., Yock, P.G., and Yeung, A., Photoangioplasty with Local Motexafin Lutetium Delivery Reduces Macrophages in a Rabbit Post-Balloon Injury Model. *Cardiovascular Research*, 2001. **49**: 449-455.
120. Carbonare, M.D. and Pathak, M.A., Skin Photosensitising Agents and the Role of Reactive Oxygen Species in Photoaging. *Journal of Photochemistry and Photobiology B: Biology*, 1992. **14**: 105-124.
121. Zigler Jr, J.S. and Goosey, J.D., Photosensitised Oxidation in the Ocular Lens: Evidence for Photosensitisers Endogenous to the Human Lens. *Photochemistry and Photobiology*, 1981. **33**: 869-874.
122. Roberts, J.E., Finley, E.L., Patat, S.A., and Schey, K.L., Photooxidation of Lens Proteins with Xanthurenic Acid: A Putative Chromophore for Cataractogenesis. *Photochemistry and Photobiology*, 2001. **74**: 740-744.
123. Goosey, J.D., Zigler Jr, J.S., and Kinoshita, J.H., Cross-Linking of Lens Crystallins in a Photodynamic System: A Process Mediated by Singlet Oxygen. *Science*, 1980. **208**: 1278-1280.
124. Balasubramanian, D., Du, X., and Zigler Jr, J.S., The Reaction of Singlet Oxygen with Proteins, with Special Reference to Crystallins. *Photochemistry and Photobiology*, 1990. **52**: 761-768.
125. Shen, H.-R., Spikes, J.D., Kopeckova, P., and Kopecek, J., Photodynamic Crosslinking of Proteins II. Photocrosslinking of a Model Protein - Ribonuclease A. *Journal of Photochemistry and Photobiology B: Biology*, 1996. **35**: 1996.
126. Shen, H.-R., Spikes, J.D., Kopeckova, P., and Kopecek, J., Photodynamic Crosslinking of Proteins. I. Model Studies Using Histidine- and Lysine-Containing *N*-(2-Hydroxypropyl)Methacrylamide Copolymers. *Journal of Photochemistry and Photobiology B: Biology*, 1996. **34**: 203-210.
127. Shen, H.-R., Spikes, J.D., Smith, C.J., and Kopecek, J., Photodynamic Cross-Linking of Proteins V. Nature of the Tyrosine-Tyrosine Bonds Formed in the Fmn-Sensitized Intermolecular Cross-Linking of *N*-Acetyl-L-Tyrosine.

Journal of Photochemistry and Photobiology A:Chemistry, 2000. **133**: 115-122.
128. Shen, H.-R., Spikes, J.D., Smith, C.J., and Kopecek, J., Photodynamic Cross-Linking of Proteins IV. Nature of the His-His Bond(S) Formed in the Rose Bengal-Photosensitised Cross-Linking of *N*-Benzoyl-L-Histidine. *Journal of Photochemistry and Photobiology A:Chemistry*, 2000. **130**: 1-6.
129. Spikes, J.D., Shen, H.-R., Kopeckova, P., and Kopecek, J., Photodynamic Crosslinking of Proteins. III. Kinetics of the FMN- and Rose Bengal-Sensitised Photooxidation and Intermolecular Crosslinking of Model Tyrosine-Containing *N*-(2-Hydroxypropyl)Methacrylamide Copolymers. *Photochemistry and Photobiology*, 1999. **70**: 130-137.
130. Ortwerth, B.J., Casserly, T.A., and Olesen, P.R., Singlet Oxygen Production Correlates with His and Trp Destruction in Brunescent Cataract Water-Insoluble Proteins. *Experimental Eye Research*, 1998. **67**: 377-380.
131. Yamazaki, S., Ozawa, N., Hiratsuka, T., and Watanabe, T., Photogeneration of 3-Hydroxy-5-Cholest-6-Ene-5-Hydroperoxide in Rat Skin: Evidence for Occurrence of Singlet Oxygen *in vivo*. *Free Radical Biology and Medicine*, 1999. **27**: 301-308.
132. Lindquist, S., The Heat Shock Response. *Annual Review of Biochemistry*, 1986. **55**: 1151-1191.
133. Gomer, C.J., Ryter, S.W., Ferrario, A., Rucker, N., Wong, S., and Fisher, A., Photodynamic Therapy-Mediated Oxidative Stress Can Induce Expression of Heat Shock Proteins. *Cancer Research*, 1996. **56**: 2355-2360.
134. Munro, S. and Pelham, H., An Hsp-Like Protein in the ER, Identity with the 78 Kd Glucose Regulated Protein and Immunoglobulin Heavy Chain Binding Protein. *Cell*, 1986. **46**: 291-300.
135. Kozutsumi, Y., Segal, M., Normington, K., Gething, M., and Sambrook, J., The Presence of Malfolded Proteins in the Endoplasmic Reticulum Signals the Induction of the Glucose Regulated Proteins. *Nature*, 1988. **332**: 462-464.
136. Ryter, S.W. and Tyrrell, R.M., Singlet Molecular Oxygen ($^1O_2$): A Possible Effector of Eukaryotic Gene Expression. *Free Radical Biology and Medicine*, 1998. **24**: 1520-1534.
137. Basu-Modak, S. and Tyrell, R.M., Singlet Oxygen: A Primary Effector in the Ultraviolet A/near Visible Light Induction of the Human Heme Oxygenase Gene. *Cancer Research*, 1993. **53**: 4505-4510.
138. Kick, G., Messer, G., Plewig, G., and Goetz, A., A Strong and Prolonged Induction of c-Jun and c-Fos Protooncogenes by Photodynamic Therapy. *British Journal of Cancer*, 1996. **74**: 30-36.
139. Luna, M., Wong, S., and Gomer, C.J., Photodynamic Therapy Mediated Induction of Early Response Genes. *Cancer Research*, 1994. **54**: 1374-1380.
140. Grether-Beck, S., Olaizola-Horn, S., Schmitt, H., Grewe, M., Jahnke, A., Johnson, J.P., Briviba, K., Sies, H., and Krutmann, J., Activation of Transcription Factor AP-2 Mediates UVA Radiation- and Singlet Oxygen-Induced Expression of the Human Intercellular Adhesion Molecule 1 Gene. *Proceedings of the National Academy of Sciences USA*, 1996. **93**: 14586-14591.
141. Klotz, L.-O., Pellieux, C., Briviba, K., Pierlot, C., Aubry, J.-M., and Sies, H., Mitogen Activated Protein Kinase (p38-, Jnk-, Erk-) Activation Pattern Induced by Extracellular and Intracellular Singlet Oxygen and UVA. *European Journal of Biochemistry*, 1999. **260**: 917-922.

142. Klotz, L.-O., Briviba, K., and Sies, H., Mitogen-Activated Protein Kinase Activation by Singlet Oxygen and Ultraviolet A. *Methods in Enzymology*, 2000. **319**: 130-143.
143. Wlaschek, M., Heinen, G., Poswig, A., Schwartz, A., Krieg, T., and Scharffetter-Kochanek, K., UVA-Induced Autocrine Stimulation of Fibroblast-Derived Collagenase/MMP-1 by Interrelated Loops of Interlukin-1 and Interlukin-6. *Photochemistry and Photobiology*, 1994. **59**: 550-556.
144. Tyrrell, R.M. and Pidoux, M., Singlet Oxygen Involvement in the Inactivation of Cultured Human Fibroblasts by UVA (334 nm, 365 nm) and near Visible (405 nm) Radiations. *Photochemistry and Photobiology*, 1989. **49**: 407-412.
145. Pourzand, C. and Tyrrell, R.M., Apoptosis, the Role of Oxidative Stress and the Example of Solar UV Radiation. *Photochemistry and Photobiology*, 1999. **70**: 380-390.
146. Kessel, D. and Luo, Y., Photodynamic Therapy: A Mitochondrial Inducer of Apoptosis. *Cell Death and Differentiation*, 1999. **6**: 28-35.
147. Xue, L.-Y., Chiu, S.-M., and Oleinick, N.L., Photochemical Destruction of the Bcl-2 Oncoprotein During Photodynamic Therapy with the Phthalocyanine Photosensitizer Pc 4. *Oncogene*, 2001. **20**: 3420-3427.
148. Frank, H., Hintze, T., Bimboes, D., and Remmer, H., Monitoring Lipid Peroxidation by Breath Analysis: Endogenous Hydrocarbons and Their Metabolic Elimination. *Toxicology and Applied Pharmacology*, 1981. **56**: 337-344.
149. Lynch, S.M., Morrow, J.D., Robertson, L.J., and Frei, B., Formation of Non-Cylcooxygenase-Derived Prostanoids (F_2-Isoprostanes) in Plasma and Low Density Lipoprotein Exposed to Oxidative Stress *in Vitro*. *Journal of Clinical Investigation*, 1994. **93**: 998-1004.
150. Gopaul, N.K., Nourooz-Zadeh, J., Mallet, A.I., and Änggård, E.E., Formation of F_2-Isoprostanes During Aortic Endothelial Cell-Mediated Oxidation of Low Density Lipoprotein. *FEBS Letters*, 1994. **348**: 297-300.
151. Gopaul, N.K., Nourooz-Zadeh, J., Mallet, A.I., and Änggård, E.E., Formation of PGF_2-Isoprostanes During the Oxidative Modification of Low Density Lipoprotein. *Biochemical and Biophysical Research Communications*, 1994. **200**: 338-343.
152. Morrow, J.D., Frei, B., Longmire, A.W., Gaciano, J.M., Lynch, S.M., Shyr, Y., Strauss, W.E., Oats, J.A., and Robertson, L.J., Increase in Circulating Products of Lipid Peroxidation (F_2-Isoprostanes) in Smokers. Smoking as a Cause of Oxidative Damage. *New England Journal of Medicine*, 1995. **332**: 1198-1203.
153. Bird, R.P., Silas, S., Hung, O., Hadley, M., and Draper, H.H., Determination of Malondialdehyde in Biological Materials by High-Pressure Liquid Chromatography. *Analytical Biochemistry*, 1983. **128**: 240-244.
154. Draper, H.H., Polensek, L., Hadley, M., and McGirr, L.G., Urinary Malondialdehyde as an Indicator of Lipid Peroxidation in the Diet and in the Tissues. *Lipids*, 1984. **19**: 836-843.
155. Girotti, A.W., Lipid Hydroperoxide Generation, Turnover, and Effector Action in Biological Systems. *Journal of Lipid Research*, 1998. **39**: 1529-1542.
156. Korytowski, W. and Girotti, A.W., Singlet Adducts of Cholesterol: Photogeneration and Reductive Turnover in Membrane Systems. *Photochemistry and Photobiology*, 1999. **70**: 484-489.

157. Shigenaga, M.K., Gimeno, C.J., and Ames, B.N., Urinary 8-Hydroxy-2'-Deoxyguanosine as a Biological Marker of *in vivo* Oxidative DNA Damage. *Proceedings of the National Academy of Science of the USA*, 1989. **86**: 9697-9701.
158. Cheng, K.C., Cahill, D.S., Kasai, H., Nishimura, S., and Loeb, L.A., 8-Hydroxyguanine, an Abundant Form of DNA Oxidative Damage, Causes G-T and A-C Substitutions. *Journal of Biological Chemistry*, 1992. **267**: 166-172.
159. Shacter, E., Williams, J.A., and Levine, R.L., Oxidative Modification of Fibrinogen Inhibits Thrombin-Catalyzed Clot Formation. *Free Radical Biology and Medicine*, 1995. **18**: 815-821.
160. Amici, A., Levine, R.L., Tsai, L., and Stadtman, E.R., Conversion of Amino Acid Residues in Proteins and Amino Acid Homopolymers to Carbonyl Derivatives by Metal-Catalyzed Oxidation Reactions. *Journal of Biological Chemistry*, 1989. **264**: 3341-3346.
161. Silvester, J.A., Timmins, G.S., and Davies, M.J., Protein Hydroperoxides and Carbonyl Groups Generated by Porphyrin-Induced Photo-Oxidation of Bovine Serum Albumin. *Archives of Biochemistry and Biophysics*, 1998. **350**: 249-258.
162. Cross, C.E., Reznik, A.Z., Packer, L., Davis, P.A., Suzuki, Y.J., and Halliwell, B., Oxidative Damage to Human Plasma Proteins by Ozone. *Free Radical Research Communications*, 1992. **15**: 347-52.
163. Shacter, E., Williams, J.A., Lim, M., and Levine, R.L., Differential Susceptibility of Plasma Proteins to Oxidative Modification - Examination by Western Blot Immunoassay. *Free Radical Biology and Medicine*, 1994. **17**: 429-437.
164. Buss, H., Chan, T.P., Sluis, K.B., Domigan, N.M., and Winterbourn, C.C., Protein Carbonyl Measurement by a Sensitive ELISA Method. *Free Radical Biology and Medicine*, 1997. **23**: 361-366.
165. Fu, S. and Dean, R.T., Structural Characterisation of the Products of Hydroxyl Radical-Damage to Leucine and Their Detection on Proteins. *Biochemical Journal*, 1997. **324**: 41-48.
166. Fu, S., Hick, L.A., Sheil, M.M., and Dean, R.T., Structural Identification of Valine Hydroperoxides and Hydroxides on Radical Damaged Amino Acid, Peptide and Protein Molecules. *Free Radical Biology and Medicine*, 1995. **19**: 281-292.
167. Morin, B., Bubb, W.A., Davies, M.J., Dean, R.T., and Fu, S., 3-Hydroxylysine, a Potential Marker for Studying Radical-Induced Protein Oxidation. 1998.
168. Wells-Knecht, M.C., Huggins, T.G., Dyer, D.G., Thorpe, S.R., and Baynes, J.W., Oxidised Amino Acids in Lens Protein with Age. Measurement of *o*-Tyrosine and Di-Tyrosine in the Aging Human Lens. *Journal of Biological Chemistry*, 1993. **268**: 12348-12352.
169. Hazen, S.L. and Heinecke, J.W., 3-Chlorotyrosine, a Specific Marker of Myeloperoxidase-Catalysed Oxidation, Is Markedly Elevated in Low Density Lipoprotein Isolated from Human Intima. *Journal of Clinical Investigation*, 1997. **99**: 2075-2081.
170. Fu, S., Davies, M.J., Stocker, R., and Dean, R.T., Evidence for Roles of Radicals in Protein Oxidation in Advanced Human Atherosclerotic Plaque. *Biochemical Journal*, 1998. **333**: 519-525.

171. Fu, S., Dean, R.T., Southan, M., and Truscott, R.J.W., The Hydroxyl Radical in Lens Nuclear Cataractogenesis. *Journal of Biological Chemistry*, 1998. **273**: 28603-28609.
172. Lledias, F. and Hansberg, W., Catalase as a Marker for Singlet Oxygen. *Methods in Enzymology*, 2000. **319**: 110-119.
173. Lledias, F., Rangel, P., and Hansberg, W., Oxidation of Catalase by Singlet Oxygen. *Journal of Biological Chemistry*, 1998. **273**: 10630-10637.
174. Kaur, H., Leungk, H.W., and Perkins, M.J., A Water Soluble Nitroso-Aromatic Spin Trap. *Journal of the Chemical Society Chemical Communications*, 1981: 142-143.
175. Morgan, P.E., Dean, R.T., and Davies, M.J., *European Journal of Biochemistry*, 2002. **in press**.
176. Fieser, L.F. and Gates Jr, M.D., Synthetic Experiments Utilizing 7-Perinaphthanone. *Journal of the American Chemical Society*, 1940. **62**: 2335-2341.
177. Gay, C., Collins, J., and Gebicki, J.M., Hydroperoxide Assay with the Ferric-Xylenol Orange Complex. *Analytical Biochemistry*, 1999. **273**: 149-155.
178. Gay, C. and Gebicki, J.M., A Critical Evaluation of the Effect of Sorbitol on the Ferric-Xylenol Orange Hydroperoxide Assay. *Analytical Biochemistry*, 2000. **284**: 217-220.
179. Gay, C., Collins, J., and Gebicki, J.M., Determination of Iron in Solutions with the Ferric-Xylenol Orange Complex. *Analytical Biochemistry*, 1999. **273**: 143-148.
180. Gieseg, S., Duggan, S., and Gebicki, J.M., Peroxidation of Proteins before Lipids in U937 Cells Exposed to Peroxyl Radicals. *Biochemical Journal*, 2000. **350**: 215-218.
181. Jessup, W., Dean, R.T., and Gebicki, J.M., Iodometric Determination of Hydroperoxides in Lipids and Proteins. *Methods in Enzymology*, 1994. **233**: 289-303.
182. Smith, P.K., Krohn, R.I., Hermanson, G.T., Mallia, A.K., Gartner, F.H., Provenzano, M.D., Fujimoto, E.K., Goeke, N.M., Olson, B.J., and Klenk, D.C., Measurement of Protein Using Bicinchoninic Acid [Published Erratum Appears in Analytical Biochemistry (1987) **163**,279]. *Analytical Biochemistry*, 1985. **150**: 76-85.
183. Walker, J.M., The Bicinchoninic Acid (BCA) Assay for Protein Quantification. *Methods in Molecular Biology*, 1994. **32**: 5-8.
184. Means, G.E. and Feeny, R.E., *Chemical Modifications of Proteins*. 1971, San Francisco: Holden-Day Inc.
185. Hawkins, C.L., Brown, B.E., and Davies, M.J., Hypochlorite- and Hypobromite-Mediated Radical Formation and Its Role in Cell Lysis. *Archives of Biochemistry & Biophysics*, 2001. **395**: 137-145.
186. Laggner, H., Besau, V., and Goldenberg, H., Preferential Uptake and Accumulation of Oxidised Vitamin C by THP-1 Monocytic Cells. *European Journal of Biochemistry*, 1999. **262**: 659-665.
187. Mohr, D. and Stocker, R., *Sensitive and Selective Measures of Vitamin C, Ubiquniol-10 and Other Low Molecular Weight Antioxidants*, in *Free Radicals; Practical Approach*, N. Punchard and F. Kelly, Editors. 1996, Oxford Press: Oxford. p. 271-285.
188. Mitra, S., Finlay, J.C., McNeill, D., Conover, D.L., and Foster, T.H., Photochemical Oxygen Consumption, Oxygen Evolution and Spectral

Changes During UVA Irradiation of EMT6 Spheroids. *Photochemistry and Photobiology*, 2001. **73**: 703-708.
189. Duling, D.R., Simulation of Multiple Isotropic Spin-Trap EPR Spectra. *Journal of Magnetic Resonance B*, 1994. **104**: 105-110.
190. Fu, S., Fu, M.-X., Baynes, J.W., Thorpe, S.R., and Dean, R.T., Presence of Dopa and Amino Acid Hydroperoxides in Proteins Modified with Advanced Glycation End Products (Ages): Amino Acid Oxidation Products as a Possible Source of Oxidative Stress Induced by Age Proteins. *Biochemical Journal*, 1998. **330**: 233-239.
191. Latarjet, R. and Loiseleur, J., Modalites De La Fixation De L'oxygene En Radiobiologie. *Societe de Biologie Comptes Rendue*, 1942. **136**: 60-63.
192. Gebicki, S. and Gebicki, J.M., Formation of Peroxides in Amino Acids and Proteins Exposed to Oxygen Free Radicals. *Biochemical Journal*, 1993. **289**: 743-749.
193. Luxford, C., Morin, B.S., Dean, R.T., and Davies, M.J., Histone H1- and Other Protein- and Amino Acid-Hydroperoxides Can Give Rise to Free Radicals Which Oxidise DNA. *Biochemical Journal*, 1999. **344**: 125-134.
194. Stadtman, E.R., Oxidation of Free Amino Acids and Amino Acid Residues in Proteins by Radiolysis and by Metal-Catalysed Reactions. *Annual Review of Biochemistry*, 1993. **62**: 797-821.
195. Garrison, W.M., Radiation Induced Reactions of Amino Acids and Peptides. *Radiation Research Reviews*, 1972. **3**: 305-326.
196. Carless, H.A.J., Atkins, R., and Fekarurhobo, G.K., Thermal and Photochemical Reactions of Unsaturated Bicyclic Endoperoxides. *Tetrahedron Letters*, 1985. **26**: 803-806.
197. Gardner, H.W. and Jursinic, P.A., Degradation of Linoleic Acid Hydroperoxides by a Cysteine $FeCl_3$ Catalyst as a Model for Similar Biochemical Reactions. I. Study of Oxygen Requirement, Catalyst and Effect of pH. *Biochimica et Biophysica Acta*, 1981. **665**: 100-112.
198. Simpson, J.A., Narita, S., Gieseg, S., Gebicki, S., Gebicki, J.M., and Dean, R.T., Long-Lived Reactive Species on Free-Radical-Damaged Proteins. *Biochemical Journal*, 1992. **282**: 621-624.
199. Hiatt, R., Irwin, K.C., and Gould, C.W., Homolytic Decompositions of Hydroperoxides. IV. Metal-Catalysed Decompositions. *Journal of Organic Chemistry*, 1968. **33**: 1430-1435.
200. Symons, M.C.R. and Gutteridge, J.M.C., *Free Radicals and Iron: Chemistry Biology and Medicine*. 1998, New York, USA: Oxford University Press, Inc.
201. Hiatt, R., in *Organic Peroxides*, D. Swern, Editor. 1971, John Wiley and Sons: New York. p. 1-151.
202. Jin, F., Leitich, J., and von Sonntag, C., The Superoxide Radical Reacts with Tyrosine-Derived Phenoxyl Radicals by Addition Rather Than Electron Transfer. *Journal of the Chemical Society Perkins Transactions 2*, 1993: 1583-1588.
203. Winterbourn, C.C., Pichorner, H., and Kettle, A.J., Myeloperoxidase Dependent Generation of a Tyrosine Peroxide by Neutrophils. *Archives of Biochemistry and Biophysics*, 1997. **338**: 15-21.
204. Tratnyek, P.G. and Holgne, J., Oxidation of Substituted Phenols in the Environment: A QSAR Analysis of Rate Constants for Reaction with Singlet Oxygen. *Environmental Science and Technology*, 1991. **25**: 1596-1604.

205. Okamoto, K.-I., Hondo, F., Itaya, A., and Kusabayashi, S., Kinetics of Dye-Sensitized Photo-Degradation of Aqueous Phenol. *Journal of Chemical Engineering of Japan*, 1982. **15**: 368-375.
206. Briviba, K., Devasagayam, T.P.A., Sies, H., and Steenken, S., Selective Parahydroxylation of Phenol and Aniline by Singlet Molecular Oxygen. *Chemical Research in Toxicology*, 1993. **6**: 548-553.
207. Pagliero, D. and Arguello, G.A., Mechanism of Oxidation of Phenol and 2,6-Dimethylphenol in the Presence of $Cr(Phen)_3^{3+}$ Excited State: The Role of O_2. *Journal of Photochemistry and Photobiology A:Chemistry*, 2001. **138**: 207-211.
208. Li, C. and Hoffman, M.Z., Oxidation of Phenol by Singlet Oxygen Photosensitised by the Tris(2,2'-Bipyridine)Ruthenium(II) Ion. *Journal of Physical Chemistry A*, 2000: 5998-6002.
209. d'Alessandro, N., Bianchi, G., Fang, X., Jin, F., Schuchmann, H., and von Sonntag, C., Reaction of Superoxide with Phenoxyl-Type Radicals. *Journal of the Chemical Society Perkins Transactions 2*, 2000: 1862-1867.
210. Saito, I., Kato, S., and Matsuura, T., Photoinduced Reactions-XL. Addition of Singlet Oxygen to Monocyclic Aromatic Ring. *Tetrahedron Letters*, 1970. **3**: 239-242.
211. Saito, I., Yoshimura, N., Arai, T., Omura, K., Nishinaga, A., and Matsuura, T., Photoinduced Reactions-LVIII. Addition of Singlet Oxygen to 4,6-Di-*t*-Butylresorcinol and Its Derivatives. *Tetrahedron*, 1972. **28**: 5131-5137.
212. Jesen, F. and Foote, C.S., Chemistry of Singlet Oxygen-48. Isolation and Structure of the Primary Product of Photooxygenation of 3,5-Di-*t*-Butyl Catechol. *Photochemistry and Photobiology*, 1987. **46**: 325-330.
213. Seely, G.R. and Hart, R.L., The Photosensitized Oxidation of Tyrosine Derivatives in the Presence of Alginate-I: Reaction under Homogenous Conditions. *Photochemistry and Photobiology*, 1976. **23**: 1-6.
214. Wilkinson, F., Helman, W.P., and Ross, A.B., Quantum Yields for the Photosensitised Formation of the Lowest Electronically Excited State of Molecular Oxygen in Solution. *Journal of Physical Chemistry Reference Data*, 1993. **22**: 113-262.
215. Gorman, A.A. and Rodgers, M.A.J., *Singlet Oxygen*, in *Crc Handbook of Organic Photochemistry*, J.C. Scaiano, Editor. 1989, CRC Press: Boca Raton. p. 229-247.
216. Haag, W.R. and Mill, T., Rate Constants for Interaction of $^1O_2$ ($^1\Delta_g$) with Azide Ion in Water. *Photochemistry and Photobiology*, 1987. **45**: 317-321.
217. Luxford, C., Dean, R.T., and Davies, M.J., Radicals Derived from Histone Hydroperoxides Damage Nucleobases in RNA and DNA. *Chemical Research in Toxicology*, 2000. **13**: 665-672.
218. Fossey, J., Lefort, D., and Sorba, J., *Free Radicals in Organic Chemistry*. 1995, Chichester: John Wiley and Sons.
219. Rogalewicz, F., Hoppilliard, Y., and Ohanessian, G., Fragmentation Mechanisms of Alpha-Amino Acids Protonated under Electrospray Ionization: A Collisional Activation and Ab Initio Theoretical Study. *International Journal of Mass Spectrometry*, 2000. **196**: 565-590.
220. McDonald, C.C. and Phillips, W.D., Proton Magnetic Resonance Spectra of Proteins in Random-Coli Configurations. *Journal of the American Chemical Society*, 1969. **91**: 1513-1521.

221. Sy, L.-K., Hui, S.-M., Cheung, K.-K., and Brown, G.D., A Rearranged Hydroperoxide from the Reduction of Artemisinin. *Tetrahedron*, 1997. **53**: 7493-7500.
222. Fessenden, R.J. and Fessenden, J.S., *Organic Chemistry*. 1990, Pacific Grove, California: Brooks/Cole Publishing Company.
223. Takabatake, T., Miyazawa, T., Hasegawa, M., and Foote, C.S., Reaction of 4,7-Dimethylbenzofurazan with Singlet Oxygen. *Tetrahedron Letters*, 2001. **42**: 987-989.
224. Gilbert, B.C., Applications of Electron Spin Resonance Spectroscopy to the Study of Free Radicals. *Essays in Chemistry*, 1972. **4**: 61-89.
225. Rustgi, S.N., Joshi, A., Moss, H., and Riesz, P., ESR of Spin-Trapped Radicals in Aqueous Solutions of Amino Acids. Reactions of the Hydroxyl Radical. *International Journal of Radiation Biology and Related Studies on Physical Chemistry and Medicine*, 1977. **31**: 415-440.
226. Davies, M.J., Fu, S., and Dean, R.T., Protein Hydroperoxides Can Give Rise to Reactive Free Radicals. *Biochemical Journal*, 1995. **305**: 643-649.
227. Buettner, G.R., Spin Trapping: ESR Parameters of Spin Adducts. *Free Radical Biology and Medicine*, 1987. **3**: 259-303.
228. Weil, J.A., Bolton, J.R., and Wertz, J.E., *Electron Paramagnetic Resonance; Elementary Theory and Practical Application*. 1994, New York: John Wiley and Sons.
229. Wilcox, A.L. and Marnett, L.J., Polyunsaturated Fatty Acid Alkoxyl Radicals Exist as Carbon Centred Epoxyallylic Radicals: A Key Step in Hydroperoxide-Amplified Lipid Peroxidation. *Chemical Research in Toxicology*, 1993. **6**: 413-416.
230. Craido, S., Soltermann, A.T., Marioloi, J.M., and Garcia, N.A., Sensitised Photooxidation of Di- and Tripeptides of Tyrosine. *Photochemistry and Photobiology*, 1998. **68**: 453-458.
231. Michaeli, M. and Feitelson, J., Reactivity of Singlet Oxygen toward Large Peptides. *Photochemistry and Photobiology*, 1995. **61**: 255-260.
232. Gebicki, S. and Gebicki, J.M., Crosslinking of DNA and Proteins Induced by Protein Hydroperoxides. *Biochemical Journal*, 1999. **338**: 629-636.
233. Saito, I., Yamane, M., Shimazu, H., Matsuura, T., and Cahnmann, H.J., Biogenic Type Conversion of *p*-Hydroxyphenylpyruvic Acid into Homogentisic Acid. *Tetrahedron Letters*, 1975. **9**: 641-644.
234. Saito, I., Chujo, Y., Shimazu, H., Yamane, M., Matsuura, T., and Cahnmann, H.J., Nonenzymatic Oxidation of *p*-Hydroxyphenylpyruvic Acid with Singlet Oxygen to Homogentisic Acid. A Model for the Action of *p*-Hydroxyphenylpyruvate Hydroxylase. *Journal of the American Chemical Society*, 1975. **97**: 5272-5277.
235. Davies, M.J., Detection and Identification of Macromolecule-Derived Radicals by EPR Spin Trapping. *Research in Chemical Intermediates*, 1993. **19**: 669-679.
236. Hawkins, C.L. and Davies, M.J., Hypochlorite-Induced Damage to Proteins - Formation of Nitrogen-Centred Radicals from Lysine Residues and Their Role in Protein Fragmentation. *Biochemical Journal*, 1998. **332**: 617-625.
237. Hawkins, C.L. and Davies, M.J., Oxidative Damage to Collagen and Related Substrates by Metal Ion/Hydrogen Peroxide Systems: Random Attack or Site-Specific Damage. *Biochimica et Biophysica Acta*, 1997. **1360**: 84-96.

238. Yurkova, I.L., Schumann, H.-Z., and von Sonntag, C., Production of Oh Radicals in the Autoxidation of the Fe(II)-Edta System. *Journal of the Chemical Society Perkins Transactions 2*, 1999: 2049-2052.
239. Luxford, C., *Investigation of the Formation of Amino Acid and Protein Hydroperoxides, and the Reactions of These Species with Nucleic Acids*, in *Heart Research Institute*. 2000, The University of Sydney: Sydney. p. 315.
240. Easton, C.J., Free-Radical Reactions in the Synthesis of Alpha-Amino Acids and Derivatives. *Chemical Reviews*, 1997. **97**: 53-82.
241. Davies, K.J., Lin, S.W., and Pacifici, R.E., Protein Damage and Degradation by Oxygen Radicals. IV. Degradation of Denatured Protein. *Journal of Biological Chemistry*, 1987. **262**: 9914-9920.
242. Dean, R.T., Thomas, S.M., Vince, G., and Wolff, S.P., Oxidation Induced Proteolysis and Its Possible Restriction by Some Secondary Protein Modifications. *Biomedica et Biochimica Acta*, 1986. **45**: 1563-1573.
243. Refsgaard, H.H.F., Tsai, L., and Stadtman, E.R., Modifications of Proteins by Polyunsaturated Fatty Acid Peroxidation Products. *Proceedings of the National Academy of Science of the USA*, 2000. **97**: 611-616.
244. Requena, J.R., Fu, M.-X., Ahmed, M.U., Jenkins, A.J., Lyons, T.J., Baynes, J.W., and Thorpe, S.R., Quantification of Malondialdehyde and 4-Hydroxynonenal Adducts to Lysine Residues in Native and Oxidized Human Low-Density Lipoprotein. *Biochemical Journal*, 1997. **322**: 317-325.
245. Esterbauer, H., Schaur, R.J., and Zollner, H., Chemistry and Biochemistry of 4-Hydroxynonenal, Malonaldehyde and Related Aldehydes. *Free Radical Biology and Medicine*, 1991. **11**: 81-128.
246. Suzuki, M., Mori, M., Niwa, T., Hirata, R., Furuta, K., Ishikawa, T., and Noyori, R., Chemical Implications for Antitumor and Antiviral Prostaglandins - Reaction of Delta(7)-Prostaglandin a(1) and Prostaglandin a(1) Methyl Esters with Thiols. *Journal of the American Chemical Society*, 1997. **119**: 2376-2385.
247. Uchida, K., Kanematsu, M., Morimitsu, Y., Osawa, T., Noguchi, N., and Niki, E., Acrolein Is a Product of Lipid Peroxidation Reaction: Formation of Free Acrolein and Its Conjugate with Lysine Residues in Oxidised Low Density Lipoproteins. *Journal of Biological Chemistry*, 1998. **273**: 16058-16066.
248. Uchida, K., Kanematsu, M., Sakai, K., Matsuda, T., Hattori, N., Mizuno, Y., Suzuki, D., Miyata, T., Noguchi, N., Niki, E., and Osawa, T., Protein-Bound Acrolein: Potential Markers for Oxidative Stress. *Proceedings of the Chemical Society*, 1998. **95**: 4882-4887.
249. Goosey, J.D., Zigler Jr., J.S., Matheson, I.B.C., and Kinoshita, J.H., Effects of Singlet Oxygen on Human Lens Crystallins *in vitro*. *Investigative Ophthalmology & Visual Science*, 1981. **20**: 679-683.
250. Verweij, H. and van Stevenick, J., Model Studies on Photodynamic Cross-Linking. *Photochemistry and Photobiology*, 1982. **35**: 265-267.
251. Stadtman, E.R., Protein Modification in Aging. *Journal of Gerontology*, 1988. **43**: B112-B120.
252. Fu, S., Gebicki, S., Jessup, W., Gebicki, J.M., and Dean, R.T., Biological Fate of Amino Acid, Peptide and Protein Hydroperoxides. *Biochemical Journal*, 1995. **311**: 821-827.
253. Hara, S., Tsuchie, M., Tsujioka, R., Kimura, M., Fujii, M., Kuroda, T., and Ono, N., High-Performance Liquid Chromatographic Quantification of

Busulfan in Human Serum after Fluorescence Derivatization by 2-Naphthalenethiol. *Analytical Sciences*, 2000. **16**: 287-291.
254. Hensley, K., Maidt, M.L., Pye, Q.N., Stewart, C.A., Wack, M., Tabatabaie, T., and Floyd, R.A., Quantitation of Protein Bound 3-Nitrotyrosine and 3,4-Dihydroxyphenylalanine by High Performance Liquid Chromatography with Electrochemical Array Detection. *Analytical Biochemistry*, 1997. **251**: 187-195.
255. Hensley, K., Williamson, K.S., and Floyd, R.A., Measurement of 3-Nitrotyrosine and 5-Nitro-γ-Tocopherol by High-Performance Liquid Chromatography with Electrochemical Detection. *Free Radical Biology and Medicine*, 2000. **28**: 520-528.
256. Chan, W.-H., Yu, Y.-S., and Yang, S.-D., Apoptotic Signalling Cascade in Photosensitised Human Epidermal Carcinoma A431 Cells: Involvement of Singlet Oxygen, c-Jun N-Terminal Kinase, Caspase-3 and P21-Activated Kinase. *Biochemical Journal*, 2000. **351**: 221-232.
257. Kiryu, C., Makiuchi, M., Miyazaki, J., Fujinaga, T., and Kakinuma, K., Physiological Production of Singlet Molecular Oxygen in the Myeloperoxidase-H_2O_2-Chloride System. *FEBS Letters*, 1999. **443**: 154-158.
258. Nagano, T., Tanaka, T., Mizuki, H., and Hirobe, M., Toxicity of Singlet Oxygen Generated Thermolytically in *Escherichia Coli*. *Chemical and Pharmaceutical Bulletin*, 1994. **42**: 883-887.
259. Ravanat, J.-L., Di Mascio, P., Martinez, G.R., Meeiros, M.H.G., and Cadet, J., Singlet Oxygen Induces Oxidation of Cellular DNA. *Journal of Biological Chemistry*, 2000. **275**: 40601-40604.
260. Epe, B., Genotoxicity of Singlet Oxygen. *Chemico-Biological Interactions*, 1991. **80**: 239-260.
261. Piette, J., Mutagenic and Genotoxic Properties of Singlet Oxygen. *Journal of Photochemistry and Photobiology, B:Biology*, 1990. **4**: 335-342.
262. Girotti, A.W., Photosensitized Oxidation of Cholesterol in Biological Systems: Reaction Pathways, Cytotoxic Effects and Defence Mechanisms. *Journal of Photochemistry and Photobiology B:Biology*, 1992. **13**: 105-118.
263. Kessel, D. and Castelli, M., Evidence That Bcl-2 Is the Target of Three Photosensitizers That Induce a Rapid Apoptotic Response. *Photochemistry and Photobiology*, 2001. **74**: 318-322.
264. Berneburg, M., Grether-Beck, S., Kurten, V., Ruzicka, T., Briviba, K., Sies, H., and Krutman, J., Singlet Oxygen Mediates the UVA-Induced Generation of the Photoaging Associated Mitochondrial Common Deletion. *Journal of Biological Chemistry*, 1999. **274**: 15345-15349.
265. Linetsky, M. and Ortwerth, B.J., Quantitation of the Reactive Oxygen Species Generated by the UVA Irradiation of Ascorbic Acid-Glycated Lens Proteins. *Photochemistry and Photobiology*, 1996. **63**: 649-655.
266. Linetsky, M. and Ortwerth, B.J., Quantitation of the Singlet Oxygen Produced by UVA Irradiation of Human Lens Proteins. *Photochemistry and Photobiology*, 1997. **65**: 522-529.
267. Vile, G.F. and Tyrrell, R.M., UVA Radiation-Induced Oxidative Damage to Lipids and Proteins in Vitro and in Human Skin Fibroblasts Is Dependent on Iron and Singlet Oxygen. *Free Radical Biology and Medicine*, 1995. **18**: 721-730.
268. Bilski, P., Kukielczak, B.M., and Chignell, C.F., Photoproduction and Direct Spectral Detection of Singlet Molecular Oxygen ($^1O_2$) in Keratinocytes

Stained with Rose Bengal. *Photochemistry and Photobiology*, 1998. **68**: 675-678.
269. Kochevar, I.E., Bouvier, J., Lynch, M., and Lin, C.-W., Influence of Dye and Protein Location on the Photosensitization of the Plasma Membrane. *Biochimica et Biophysica Acta*, 1994. **1196**: 172-180.
270. Morita, A., Werfel, T., Stege, H., Ahrens, C., Karmann, K., Grewe, M., Grether-Beck, S., Ruzicka, T., Kapp, A., Klotz, J.-O., Sies, H., and Krutmann, J., Evidence That Singlet Oxygen-Induced Human T Helper Cell Apoptosis Is the Basic Mechanism of Ultraviolet-a Radiation Phototherapy. *Journal of Experimental Medicine*, 1997. **186**: 1763-1768.
271. Chen, Z., Woodburn, K.W., Shi, C., Adelman, D.C., Rogers, C., and Simon, D.I., Photodynamic Therapy with Motexafin Lutetium Induces Redox-Sensitive Apoptosis of Vascular Cells. *Arteriosclerosis Thrombosis and Vascular Biology*, 2001. **21**: 759-764.
272. Zhuang, S., Demirs, J.T., and Kochevar, I.E., p38 Mitogen-Activated Protein Kinase Mediates bib Cleavage, Mitochondrial Dysfunction, and Caspase-3 Activation During Apoptosis Induced by Singlet Oxygen but Not by Hydrogen Peroxide. *Journal of Biological Chemistry*, 2000. **275**: 25939-25948.
273. Scharffetter-Kochanek, K., Wlaschek, M., Bribiva, K., and Sies, H., Singlet Oxygen Induces Collagenase Expression in Human Skin Fibroblasts. *FEBS Letters*, 1993. **331**: 304-306.
274. Baoutina, A., Macrophages Can Decrease the Level of Cholesteryl Ester Hydroperoxides in Low Density Lipoprotein. *Journal of Biological Chemistry*, 2000. **275**: 1635-1644.
275. Baoutina, A., Dean, R.T., and Jessup, W., Trans-Plasma Membrane Electron Transport Induces Macrophage-Mediated Low-Density Lipoprotein Oxidation. *FASEB Journal*, 2001: Express article 10.1096/fj.00-0704fje.
276. Chou, P.T. and Khan, A.U., L-Ascorbic Acid Quenching of Singlet Delta Molecular Oxygen in Aqueous Media: Generalized Antioxidant Property of Vitamin C. *Biochemical and Biophysical Research Communications*, 1983. **115**: 932-937.
277. Kwon, B.M. and Foote, C.S., Chemistry of Singlet Oxygen. 50. Hydroperoxide Intermediates in the Photooxygenation of Ascorbic Acid. *Journal of the American Chemical Society*, 1988. **110**: 6852-6853.
278. Inanami, O., Kuwabara, M., Hayashi, M., Yoshii, G., Syuto, B., and Sato, F., Reaction of the Hydrated Electron with Histone H1 and Related Compounds Studied by E.S.R and Spin-Trapping. International Journal of Radiation *Biology*, 1986. **49**: 47-56.
279. Moan, J., On the Diffusion Length of Singlet Oxygen in Cells and Tissues. *Journal of Photochemistry and Photobiology B: Biology*, 1990. **6**: 343-347.
280. Gebicki, J.M., Du, J., Collins, J., and Tweeddale, H., Peroxidation of Proteins and Lipids in Suspensions of Liposomes, in Blood Serum, and in Mouse Myeloma Cells. *Acta Biochimica Polonica*, 2000. **47**: 901-911.
281. Weil, L., On the Mechanism of the Photo-Oxidation of Amino Acids Sensitized by Methylene Blue. *Archives of Biochemistry and Biophysics*, 1965. **110**: 57-68.
282. Dawson, R.M.C., Elliot, D.C., Elliot, W.H., and Jones, K.M., *Data for Biochemical Research*. 3rd ed. 1994, Oxford: Clarendon Press.
283. Linetsky, M., Ranson, N., and Ortwerth, B.J., The Aggregation in Human Lens Proteins Blocks the Scavenging of UVA-Generated Singlet Oxygen by

Ascorbic Acid and Glutathione. *Archives of Biochemistry and Biophysics*, 1998. **351**: 180-188.

284. Ortwerth, B.J., Coots, A., James, H.L., and Linetsky, M., UVA Irradiation of Human Lens Proteins Produces Residual Oxidation of Ascorbic Acid Even in the Presence of High Levels of Glutathione. *Archives of Biochemsitry and Biophysics*, 1998. **351**: 189-196.